TOP STRAND EFFECT AND EVALUATION OF EFFECTIVE PRESTRESS IN PRESTRESSED CONCRETE BEAMS

by

Hunter T. Hodges

Thesis submitted to the Faculty of the Virginia Polytechnic Institute and State University in partial fulfillment of the requirements for the degree of

MASTER OF SCIENCE

in

CIVIL ENGINEERING

APPROVED:

Thomas E. Cousins, Chairperson

Carin L. Roberts-Wollmann, Chairperson

C. Dale Buckner

December 7, 2006

Blacksburg, Virginia

Keywords: prestressed concrete, prestress losses, transfer length, development length

TOP STRAND EFFECT AND EVALUATION OF EFFECTIVE PRESTRESS IN PRESTRESSED CONCRETE BEAMS

Hunter T. Hodges

ABSTRACT

The first objective of this thesis was to assess the effect of casting orientation on bond strength in pretensioned prestressed concrete members. The "top strand effect" was evaluated through transfer and development length tests of prestressed concrete beams. Eight beams were cast with normal orientation, while four beams were cast with inverted orientation so that a significant depth of fresh concrete was placed below prestressing strands. Discrete transfer lengths were determined at the ends of each beam by measuring concrete surface strains. Inverted casting orientation caused an average 70 percent increase in transfer length. Some transfer lengths in beams with inverted casting orientation exceed current ACI and AASHTO code provisions. All measured transfer lengths were less than 90 strand diameters (45 in. for 0.5 in. diameter strands). Ranges of development length were determined through iterative load testing. The top strand effect on development length was more qualitative than quantitative. Ranges of development length in normal beams were conservatively less than code provisions. Ranges of development length in beams with inverted casting orientation were much closer to and sometimes exceeded code provisions. It is recommended that ACI and AASHTO code provisions for the development length of prestressing strand be modified to include the same magnification factors that are specified for the development length of deformed bars with twelve or more inches of fresh concrete placed below.

The second objective of this thesis was to compare experimentally measured prestress losses to theoretical calculations. Theoretical prestress losses were calculated according to PCI and AASHTO Refined methods. These methods produced similar results. Prestress losses were experimentally measured by vibrating wire gages and flexural load testing. Vibrating wire gages were used to monitor internal concrete strains. Two methods were used to reduce vibrating wire gage data: an upper/lower bound method and a basic method. The upper/lower bound method produced distorted data that was unreasonable in some cases. The basic method was more reasonable, but resulted in some prestress loss measurements that were greater than theoretical predictions. Flexural load testing was used to back calculate prestress losses from crack initiation and crack reopening loads. Prestress losses measured by crack initiation loads were generally greater than theoretical values. Losses measured by crack reopening loads were distorted. The distortion was attributed to difficulty in isolation of the correct crack reopening load. Large measurements of prestress losses by the basic vibrating wire gage and crack initiation methods suggested that losses occurred between the time when concrete was poured and prestress transfer occurred. Such losses are not accounted for in current code provisions. More research is recommended to determine the magnitude of these additional losses and their effect on design.

ACKNOWLEDGEMENTS

I must first thank the Charles E. Via, Jr. Department of Civil and Environmental Engineering at Virginia Tech for the opportunity to pursue a Master's degree. I extend my deepest gratitude to the Via family for their generous scholarship program of which I was a part. I must also thank the Virginia Transportation Research Council for funding for this project and StrandTech Martin, Inc. for providing prestressing strand. It was an honor to be selected by my co-advisors, Dr. Thomas E. Cousins and Dr. Carin L. Roberts-Wollmann, to work on this research project. Their advice and direction, as well as physical help in the lab, were greatly appreciated. I would also like to thank my other committee member, Col. C. Dale Buckner of the Virginia Military Institute. His expertise in prestressed concrete and suggestion of the top strand effect played a large role in this project.

Now I must thank those who assisted me with the physical portion of this research project in the Structures and Materials Laboratory at Virginia Tech. I deeply appreciate the help of doctoral student J. Chris Carroll, who worked alongside me throughout this project. The project would not have been possible without his knowledge and experience, as well as his invention, the "girder inverter". Special thanks go to lab technicians Brett Farmer and Dennis Huffman who had a significant role in the fabrication of test beams. I would also like to thank the numerous other graduate students who assisted me in the lab.

Finally, I thank my family and friends. They supported me through phone calls, emails, and occasional visits while at Virginia Tech.

TABLE OF CONTENTS

LIST OF FIGURES

LIST OF TABLES

1. INTRODUCTION

1.1 Background

Prestressed concrete is an application of structural concrete design in which members are preloaded to counter the effects of service loads. The benefits of prestressed concrete were identified by French engineer Eugene Freyssinet in the early twentieth century. His studies and designs came to fruition by the completion of a bridge over the river Marne in Luzancy, France. This 180 ft single span bridge was completed in 1941 and is recognized as one of the first utilizations of prestressed concrete. While prestressed concrete is primarily used in bridges, it is also implemented in buildings, foundations, and pavements.

Prestressed concrete has several advantages over conventionally reinforced concrete. One advantage is that the number and width of cracks can be limited or even eliminated. Another benefit is that camber can be used to offset and reduce deflections from loads. In addition to these serviceability advantages, prestressed concrete allows for the effective use of high strength steel reinforcement and high strength concrete. Longer span lengths can be achieved, and precast construction is possible.

Prestressed concrete also has some disadvantages. Prestressing strand is more expensive than mild steel reinforcement, and the use of higher strength concretes can add to costs. The design of prestressed concrete members is more rigorous than that for normal reinforced concrete. Prestressed concrete members are subjected to significantly higher stresses during fabrication and service life. Finally, prestressed members experience losses in prestress force that are difficult to predict.

Prestressed concrete members can be classified by the manner in which prestress is applied. Pretensioned concrete members are fabricated by initially stressing strands with anchorage and jacking devices. Forms are assembled and concrete is cast around the strands. The concrete is allowed to cure until a desired compressive strength is attained and then the strands are cut, transferring the prestress force to the members. Post-tensioned members are made by casting concrete with hollow ducts where the prestressing strands will be placed. When the members are in place, strands are threaded through the ducts and then stressed with jacking and anchorage devices. These ducts are sometimes filled with grout to ensure that the strands have strain compatibility with the concrete around them (Nilson 1987).

1.2 Objectives

This thesis documents a portion of a research project sponsored by the Virginia Department of Transportation (VDOT) and the Virginia Transportation Research Council (VTRC). The project was conducted in the Structures and Materials Laboratory at Virginia Polytechnic Institute and State University. While the overall goal of the project was to test the properties of the new grade 300 prestressing strand, this thesis pertains to two specific objectives. The first is an experimental assessment of the top strand effect. The second is to compare experimentally determined values of effective prestress to theoretical models for computing prestress losses.

1.2.1 Top Strand Effect

The first objective is to investigate the effect of casting orientation on bond strength between prestressing strands and concrete. The top bar effect is a phenomenon of conventional reinforced concrete in which steel reinforcement bars at the top of a section experience less bond strength than those at the bottom. The American Concrete Institute (ACI) accounts for this effect by increasing the development length equation by 30 percent when twelve or more inches of fresh concrete are cast below a horizontal reinforcement bar (ACI 2005). The American Association of State Highway and Transportation Officials (AASHTO) recommends a 40 percent increase in development length when a top horizontal or nearly horizontal bar has twelve or more inches of fresh concrete cast below (AASHTO 2006). However, neither ACI nor AASHTO recommend a similar increase for the development length of prestressing strands.

Twelve pretensioned prestressed concrete beams were cast in four pours for this project. In two of the pours, two beams were cast in a normal orientation while two other specimens with identical cross sections were cast in an inverted orientation. Transfer lengths at the end of each beam were measured when the prestress force was released, and development lengths were iteratively determined during flexural testing. The top strand effect is assessed by comparing values of transfer and development length for the two different casting orientations.

1.2.2 Evaluation of Effective Prestress

The second objective is to compare experimentally determined values of effective prestress to theoretical predictions from prestress loss models. Effective prestress, an important parameter for the design engineer, is the stress that exists in prestress strands after losses have occurred. While not so crucial for ultimate flexural strength calculations, an accurate estimation of effective prestress is necessary for determining deflections, cracking loads, and crack widths. An overestimation of prestress losses may lead to over prestressing, which causes excessive camber and high concrete stresses. An underestimation of prestress losses results in a low effective prestress and low cracking loads (Nilson 1987). Prestress losses are not easily predicted, nor can they be readily measured, so this subject is addressed in this thesis.

Two methods were used to experimentally determine effective prestress in this project. One method involved the use of vibrating wire gages embedded in the concrete beams at the level of the prestress strands. These gages were assumed to be compatible with the concrete and thus the strands, allowing for continual measurement of strain in the beams. The other method was to determine the loads required to first crack the beams and then reopen those cracks. The effective prestress was then back calculated using basic theory of mechanics. These experimental values of effective prestress are compared to theoretical predictions from prestress loss models prescribed by the Precast Prestressed Concrete Institute Committee on Prestress Losses (PCI 1975) and the American Association of State and Highway Transportation Officials (AASHTO 2006).

1.3 Thesis Organization

This thesis is organized into five chapters. Chapter 1 is an introduction that provides a brief background and outlines the objectives of the thesis. Chapter 2 presents a literature review that includes code provisions and results of previous studies pertaining to transfer length, development length, and prestress losses. Also included in the literature review are results from studies related to the top strand effect. Chapter 3 explains the details of beam fabrication and testing. It includes information about the concrete mix design and data collection. Chapter 4 presents the test results with accompanying analysis and discussion. Techniques for data reduction and all theoretical calculations are given here. Finally, Chapter 5 provides a summary, conclusions, recommendations for code revisions, and recommendations for further research.

2. LITERATURE REVIEW

2.1 Transfer Length

Pretensioned prestressed concrete members are fabricated by jacking strands, casting concrete around them, and then releasing the force in the strands. When the prestress force in the strands is released, it is applied to the concrete member in the end regions over a distance that is referred to as the transfer length. Immediately after release, the stress in the strands becomes zero at the end of a member, and increases gradually to the effective prestress at the transfer length. Figure 2.1 shows how strand stress is assumed to vary in the end of a member after prestress transfer. Slip usually occurs between the prestressing strands and concrete, but is often restricted to the ends of a member. Factors that affect transfer length include jacking force, initial concrete strength, surface condition of strands, strand spacing and layout, and the rate of prestress transfer (Nilson 1987).

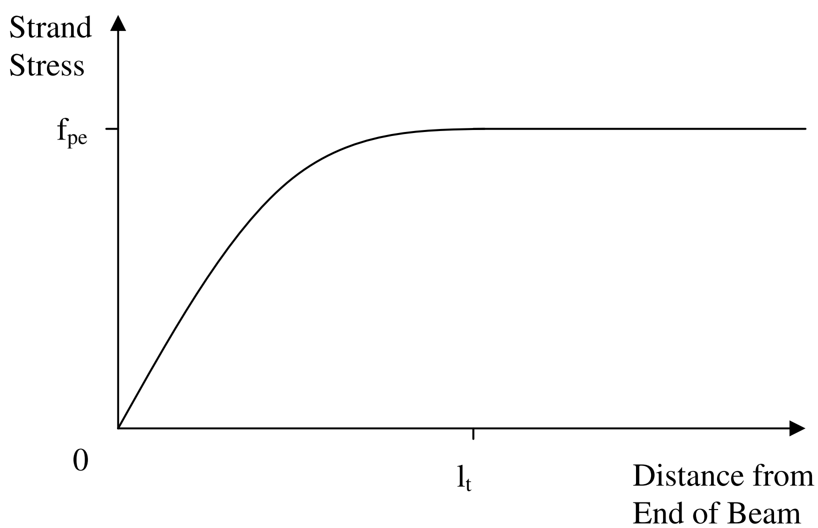

Figure 2.1 Effective Strand Stress vs. Member Length

Bond stresses in pretensioned anchorage/transfer zones are primarily attributed to friction and mechanical resistance. Unlike conventional reinforced concrete, chemical bond has a small effect because the adhesion is broken upon transfer of prestress. Friction is developed between a strand and concrete in the transfer zone as a result of the strand being pulled through the concrete toward the center of the member. When a strand is tensioned along its length, the diameter is reduced by the Poisson Effect. Concrete hardens around this reduced effective diameter. Upon release, the strand tends to return to its original diameter. This increases the normal stress between the strand and concrete, and thus intensifies the frictional bond stresses. This phenomenon is commonly called the Hoyer Effect. Anchorage in the transfer zone is also provided by mechanical resistance. Because of the helical shape of a seven wire prestressing strand, it will tend to twist as it is pulled through the concrete. Mechanical interlock forms between the strand and concrete, resulting in significant bond stresses.

Transfer length is an important parameter in shear design. High levels of shear occur in the end transfer zones of pretensioned beams and girders. An underestimation of transfer length could result in a design that is not conservative. Transfer length is also important for pretensioned anchorage zone design. Anchorage zone reinforcement is determined based on transverse tensile stresses in concrete, which are inversely proportional to transfer length. Finally, the transfer length represents a portion of the development length of a prestressing strand, which will be discussed later (Barnes, et al 2003).

2.1.1 Code Provisions

ACI provides two means for calculating transfer length in a prestressed concrete member. The first is found in Section 11.4.4, which pertains to shear design. When calculating the nominal concrete web shear strength V_{cw} at a section within the transfer length, the prestress force should be reduced according to a linear variation from zero at the end of a member to an effective prestress force at the transfer length. The transfer length is assumed to be 50 strand diameters for this calculation. The second method for calculating transfer length is found in Equation 12-4 of Section 12.9.1, which is shown below.

$$l_d = \left(\frac{f_{se}}{3000}\right)d_b + \left(\frac{f_{ps} - f_{se}}{1000}\right)d_b \qquad 2.1$$

Where:

l_d = development length (in.)

f_{se} = effective stress in prestressing steel (psi)

d_b = strand diameter (in.)

f_{ps} = stress in prestressing steel at nominal flexural strength (psi)

The entire equation represents the calculation of development length, which will be discussed further in subsequent sections. However, Section R12.9 states that the first term in Equation 2.1 represents the transfer length. If grade 270 strands are stressed to 75 percent ultimate tensile strength and approximately 25 percent prestress losses are assumed, then f_{se} will become approximately 150,000 psi, and the transfer length term will simplify to 50 strand diameters (ACI 2005).

AASHTO recommends that transfer length be taken as 60 strand diameters in Article 5.11.4.1 (AASHTO 2006). The increase of ten strand diameters over the ACI recommendation represents higher effective prestress values that are currently employed in design (Nassar 2002).

2.1.2 Barnes, Grove, and Burns

Researchers in this study measured transfer lengths using concrete surface strains on 36 AASHTO Type I girders with 0.6 in. diameter prestressing strands. Two thirds of the test specimens were debonded in the ends, resulting in 192 total transfer zones (184 were measured). The effects of concrete strength, time, surface condition of strand, and type of prestress release were investigated. Each girder was prestressed with eight to twelve strands, depending on whether strands were debonded and the type of debonding pattern used. Strands were spaced on a standard 2 in. grid. Three concrete mixes labeled L, M, and H were used. The target initial concrete strengths were 4000, 7000, and 9000 psi for mixes L, M, and H, respectively. The range of expected 28 day compressive strengths was 5000 to 7000 psi for mix L, 9500 to 11,500 psi for mix M, and 13,000 to 15,000 psi for mix H. Some strands had a clean “bright” finish, while others exhibited some degree of rusting. All strands were flame cut using one of two methods. The first method was to cut each strand simultaneously at both ends of a specimen. The second method was to cut strands at the “live” end of a specimen, resulting in a rapid release at that end and a more gradual release at the other “dead” end.

Researchers found that all transfer lengths were less than the AASHTO LRFD stipulation of 60 strand diameters, and only three transfer lengths were greater than the ACI recommendation of 50 strand diameters. The following equation was used to normalize the data.

$$l_t = \alpha \frac{f_{pt}}{\sqrt{f'_{ci}}} d_b \qquad 2.2$$

Where:

l_t = transfer length (in.)

α = proportionality constant ($ksi^{-.5}$)

f_{pt} = tendon stress after release (ksi)

f'_{ci} = initial concrete compressive strength (ksi)

d_b = strand diameter (in.)

Equation 2.2 shows that transfer length must be inversely proportional to concrete strength. With α set equal to 0.57, Equation 2.2 provided an upper bound for all long-term transfer lengths measured. The long term transfer lengths were generally 10 to 20 percent greater than initial transfer lengths. Most of the increase in transfer length occurred within the first few weeks after prestress release. The average transfer length of rusted strands in lower strength concrete was approximately 13 percent less than the transfer length of bright strands. In higher strength concrete, the rusted strand transfer length values were widely dispersed and were sometimes greater than the bright strand transfer lengths. This effect was attributed to the fact that concrete bonds to rust rather than strand. The dynamic release of prestress caused the rust to break free from the strand, resulting in less friction at the bond interface than a bright strand would possess. The researchers recommended that strand weathering not be used to decrease transfer lengths. There was no apparent difference in transfer length for bright strands subjected to sudden vs. gradual prestress release. However, the transfer length of rusted strands in live ends was 30 to 50 percent greater than the transfer length in dead ends. A final recommendation from this study was to use a lower bound estimate of transfer length when checking allowable stresses. For the transfer lengths measured in this study, an α value of 0.17 in Equation 2.2 gave a lower bound estimate of transfer length (Barns, et al. 2003).

2.1.3 Russell and Burns

The researchers in this study measured transfer lengths on 44 pretensioned prestressed concrete members. Twelve of these specimens were scale models of AASHTO type cross sections, while the other specimens were rectangular with one, three, or five concentric prestressing strands. Several variables were examined, including number of strands, size of strands, debonding, confinement reinforcement, and type of cross section. The fabrication of specimens was conducted in a manner similar to the practice of prestressed concrete plants.

Initial concrete compressive strengths ranged from 3850 to 5580 psi with an average of 4460 psi. Final concrete compressive strengths varied from 5110 to 7530 psi with an average of 6500 psi. Strands with 0.5 and 0.6 in. diameters were tensioned to 75 percent of ultimate tensile strength (270 ksi). The strand spacing was 2 in. in all specimens except for three of the AASHTO type members with 0.6 in. diameter strands, which had 2.25 in. spacing. Cover was 2, 2.25, or 2.5 in., depending on cross section type. The prestress was released by flame-cutting the strands. Some of the strands in the rectangular sections were gradually detensioned to 70 percent of their original tension before flame cutting.

Three parameters were measured in this study: concrete surface strain, end slip, and steel strain. Concrete strain was measured using a demountable mechanical strain gage. End slip was measured with dial gages and steel rules. However, some dial gages were damaged during flame cutting. Electrical resistance strain gages were attached to strands, but were deemed ineffective due to differences in individual strand wires, destruction during transfer, and localized debonding.

The average measured transfer length for bonded 0.5 in. diameter strands was 29.5 in. with a standard deviation of 6.85 in. The average transfer length for bonded 0.6 in. diameter strands was 40.0 in. with a standard deviation of 6.80 in. While the linear relation between transfer length and strand diameter in current code provisions would suggest a 20 percent increase in transfer length for 0.6 in. diameter strands, a 36 percent increase was actually measured. The authors proposed the following nonlinear relation between transfer length and strand diameter.

$$l_t = K d_b^{\alpha} \qquad 2.3$$

Where:

l_t = transfer length (in.)

K = constant

d_b = strand diameter (in.)

α = constant

A value of 1.68 for α in Equation 2.3 was found to fit the test data in this study. The researchers also normalized the data and found that the average transfer lengths were 59 strand diameters and 67 strand diameters for the 0.5 and 0.6 in. diameter strands, respectively. The authors resolved the strand diameter issue by recommending the following equation as a conservative estimate of transfer length.

$$l_t = \frac{f_{se}}{2} d_b \qquad 2.4$$

Where:
l_t = transfer length (in.)
f_{se} = effective prestress (ksi)
d_b = strand diameter (in.)

Equation 2.4 reduces to 80 strand diameters for an effective prestress of 160 ksi.

End slip refers to the sliding action occurring between prestressing strands and concrete in the end regions of members. The researchers used the following equation to compare transfer length and end slip values. This equation was first proposed by Guyon (1960).

$$l_t = \frac{2E_{ps}}{f_{si}} L_{es} \qquad 2.5$$

Where:
l_t = transfer length (in.)
E_{ps} = prestressing strand modulus of elasticity (ksi)
f_{si} = strand stress immediately prior to release (ksi)
L_{es} = end slip (in.)

Using experimental values of E_{ps} and f_{si}, the researchers predicted that transfer lengths would be approximately 290 times the end slip. Regression analysis of test data showed that the measured transfer lengths were approximately 295 times the measured end slips. Researchers concluded that end slip may be an accurate predictor of transfer length, but its measurement is not trivial and can be adversely affected by sudden prestress release.

Strand spacing was a concern for 0.6 in. diameter strands since 2 in. spacing violated the rule of thumb that center to center spacing should be no less than four diameters. The average transfer length of the three specimens with 0.6 in. diameter strands at 2.25 in. spacing was 43.3 in. The average transfer length for all 0.6 in. diameter specimens was 40.1 in., which disproves the notion that 0.6 in. diameter strands need spacing larger than 2 in. The researchers concluded that 0.6 in. diameter strand at 2.0 in. spacing was acceptable for use in pretensioned members.

Several other parameters were assessed. Transfer lengths for debonded strands were approximately 16 percent shorter than fully bonded strands. The average debonded transfer length was 25.8 and 32.7 in. for the 0.5 and 0.6 in. diameter strands, respectively. The effect of cross sectional shape was significant. The transfer lengths measured from the scale AASHTO beams were 25 percent less than the values from rectangular prisms. Finally, confinement reinforcement appeared to have no major effect on transfer length (Russell & Burns 1996).

2.1.4 C. Dale Buckner

The Federal Highway Administration (FHWA) issued a memorandum in 1988 prohibiting the use of 0.6 in. diameter strand in pretensioning applications and requiring minimum strand spacing to be four times the strand diameter. This was a response to very long transfer lengths measured by Cousins, et al. at North Carolina State University (1990). Numerous studies with conflicting recommendations were conducted in the years following the memorandum. Buckner conducted an extensive literature review, re-analyzed data from recent studies and addressed differences in the conclusions in each study, and recommended new design criteria.

Buckner recommended the following transfer length equation based on results from several different studies.

$$l_t = \frac{1250 f_{si} d_b}{E_c} \tag{2.6}$$

Where:

l_t = transfer length (in.)

f_{si} = initial strand stress (ksi)

d_b = strand diameter (in.)

E_c = elastic modulus (ksi)

This transfer length equation differs from others because it uses strand stress at the time of transfer rather than effective prestress, and it incorporates the modulus of elasticity. This idea was first proposed by the Florida Department of Transportation Structures Research Center (Shahawy 2001). Buckner simplified Equation 2.6 to the following expression for normal weight concrete with initial compressive strength greater than 3500 psi.

$$l_t = \frac{f_{si} d_b}{3} \qquad 2.7$$

This formulation is similar to code provisions with the exception that initial prestress force is substituted for effective prestress. This is more fitting since transfer length is established just after release and varies little with time. Buckner also suggested that Equation 2.7 be multiplied by 1.3 for strands in the upper third of a section and strands with 12 in. or more concrete below (1994).

2.1.5 Robert Kolozs

This researcher examined transfer length in high performance lightweight concrete. Eight pretensioned fully bonded AASHTO Type I beams were fabricated. One beam was cast with normal weight concrete with 6000 psi target strength. The other beams were cast with lightweight concrete with target strengths of either 6000 or 8000 psi. Two 20 ft beams were used to introduce the prestressing plant to lightweight concrete. These beams were prestressed with 16 strands. The other six beams were 40 ft long and had twelve strands. Two of these strands were placed in the top of the section to prevent tension cracking. All beams had a minimum cover of 2 in., and used a standard 2 in. strand spacing pattern. A gradual release was used to transfer prestress force in most strands (a few of the top strands were flame cut). Transfer lengths were determined from concrete surface strains.

The average measured transfer length of the normal weight concrete beam with an initial compressive strength of 3849 psi was 18.2 in. The transfer lengths of the 6000 psi lightweight concrete beams ranged from 18.3 to 37.8 in., but were concentrated at the upper end of this range with an average of 35.8 in. The transfer lengths of the 8000 psi lightweight concrete beams ranged from 24.8 to 40.7 in., with an average of 34.4 in. The initial concrete compressive strengths of the 6000 and 8000 psi lightweight concrete mixes were 4902 and 5563 psi, respectively. The normal weight concrete strain profile was typical of a fully bonded specimen. However, the strain profiles of the lightweight concrete beams had two strain plateaus and resembled debonded strain profiles. The measured transfer lengths of the normal weight beam were conservatively estimated by code provisions. However, most of the measured lightweight concrete transfer lengths exceeded code provisions. The researcher concluded that code provisions and other models for predicting transfer length in normal weight concrete were not applicable to lightweight concrete. However, Buckner's model (Equation 2.6) could be applied to both normal and lightweight prestressed concrete members (Kolozs 2000).

2.2 Development Length

Development length is the embedded length of strand required to attain the necessary stress in prestressing steel (f_{ps}) for nominal flexural strength. The development length is the sum of the transfer length (previously discussed) and the flexural bond length. Figure 2.2 shows the generally accepted variation of strand stress near the end of a member, as presented by Nilson (1987). Flexural bond stresses differ from transfer bond stresses in that they result from increases in strand tension caused by variation of bending moment along the length of an externally loaded member. Flexural bond stresses are proportional to the rate of change of bending moment at a section, which is equal to the shear force at that same section. These stresses are typically low before cracking occurs, but increase significantly after crack initiation. High stresses may occur on one side of a crack while lower stresses (possibly in the opposite direction) exist on the other side. While local bond failure may take place, a general failure can be prevented if strands have the necessary embedment length (Nilson 1987).

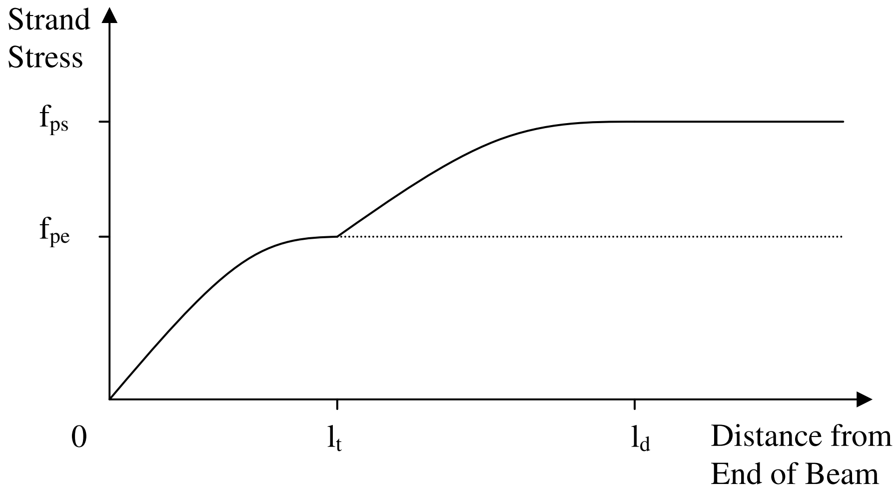

Figure 2.2 Nominal Strand Stress vs. Member Length

Hanson and Kaar elaborated on the issue of flexural bond stresses. Upon crack initiation, bond stress near the crack rises to a nominal stress. This causes slip near the crack and a subsequent decrease in bond stress. As more load is applied, a wave of high bond stress progresses from the crack to the beam ends. When the high bond stress enters the transfer zone, bond slip causes an increase in strand stress. This results in a decrease in strand diameter due to the Poisson Effect, and a general bond failure occurs because of loss of frictional resistance. Hanson and Kaar state that the strand's helical shape offers mechanical resistance and allows the member to support additional load after slip occurs at the member ends (1959).

2.2.1 Code Provisions

The ACI recommendation for calculating development length is given in Equation 2.1, where the second term of this equation represents the flexural bond length. Section 12.9.1 states that a seven wire strand must have an embedment length (beyond the critical section) that is greater than or equal to the development length calculated by Equation 2.1. On the corollary, Section 12.9.1.1 permits embedment lengths less than the calculated development length only if the design strand stress is less than the value predicted by the bilinear relationship of Equation 2.1 (ACI 2005).

AASHTO recommends a similar method for calculating development length in Equation 5.11.4.2-1 of Article 5.11.4.2, which is shown below.

$$l_d \geq \kappa\left(f_{ps} - \frac{2}{3} f_{pe}\right)d_b \qquad 2.8$$

Where:

l_d = development length (in.)

d_b = nominal strand diameter (in.)

f_{ps} = average stress in prestressing steel required for nominal resistance (ksi)

f_{pe} = effective stress in prestressing steel after losses (ksi)

κ = 1.0 for pretensioned members with depth less than or equal to 24.0 in.

κ = 1.6 for pretensioned members with depth greater than 24.0 in.

If κ is equal to one, Equation 2.8 is functionally equivalent to the ACI recommendation for development length. AASHTO also recommends a bilinear relationship for determining maximum strand stress for sections within the transfer or development length. Equation 5.11.4.2-3 states than within the recommended transfer length of 60 strand diameters, the strand stress varies linearly from zero to the effective prestress. Equation 5.11.4.2-4 states that strand stress varies from the f_{pe} to f_{ps} at sections that fall between 60 strand diameters and the development length (AASHTO 2006).

2.2.2 C. Dale Buckner

In reference to large measured development lengths in a North Carolina State University Study, the FHWA issued a memorandum in 1988 that included the following restrictions: 1) the use of 0.6 in. diameter strands for pretensioning is prohibited, 2) strand spacing must be at least four strand diameters, and 3) the AASHTO development length equation should be multiplied by 1.6 for strand diameters less than or equal to 9/16 in. This caused concern for designers and the precast/prestressed concrete industry. Several experimental studies were conducted, but individual results were conflicting. Buckner addressed the issue by reviewing the studies and analyzing the discrepancies.

Buckner recommended the following equation for calculation of development length.

$$l_d = \frac{f_{si} d_b}{3} + \lambda\left(f_{ps} - f_{se}\right)d_b \qquad 2.9$$

Where:

l_d = development length (in.)

f_{si} = strand stress immediately after release (ksi)

d_b = strand diameter (in.)

$\lambda = [0.6 + 0.4\varepsilon_{ps}]$ (ε_{ps} is the strain corresponding to f_{ps})

f_{ps} = stress in strands at nominal capacity (ksi)

f_{se} = effective prestress

One difference between Equation 2.9 and the AASHTO equation is that f_{si} replaces f_{se} in the transfer length term, which was discussed previously. The other difference is the use of a λ multiplier for the flexural bond length term. The lower and upper limits of λ are 1.0 and 2.0, which correspond to strand strains 0.01 and 0.035, respectively. These are reasonable strain limits for flexural design.

Buckner also noted that the effect of strand position on development length was not considered in the studies under review. Settlement of wet concrete and deposits of bleed water can decrease bond stress. A 30 percent increase was recommended for Equation 2.9 when 12 in. or more concrete is placed below horizontal strands or strands are draped to the top third of a section (Buckner 1995).

2.2.3 Mohsen Shahawy

This researcher analyzed results from extensive tests of prestressed slabs, piles, and girders at the Florida Department of Transportation (FDOT) Structures Research Center (FSRC). Twelve AASHTO Type II girders were cast with concrete designed for initial and 28 day compressive strengths of 4000 and 5000 psi, respectively. Each girder had a cast in place concrete deck with 28 day strength of 5000 psi. The variables of the study were strand diameter (0.5 in., 0.5 in. special, and 0.6 in.), embedment length, and confinement reinforcement.

The measured transfer lengths of all strand diameters were in agreement with Equation 2.7, which uses initial strand stress rather the effective prestress for calculation of transfer length. Researchers found that confinement reinforcement in the tension flange improved strength and ductility.

Development length tests were normalized by dividing embedment length by strand diameter since different strand diameters were tested. Researchers found that an embedment length equal to 230 strand diameters was necessary to develop the moment capacity calculated by code provisions. Assuming a nominal strand stress of 98 percent ultimate stress (grade 270 strands), initial strand stress of 75 percent ultimate stress, and 20 percent prestress loss, the AASHTO provision at the time of this research (Equation 2.8 above without the κ factor) resulted in a development length estimate of 157 strand diameters, which was not conservative. The current AASHTO provision would have resulted in a conservative development length estimate of 251 strand diameters since the sections were deeper than 24 in. (κ equal to 1.6).

Researchers noticed that initial slippage and the first shear crack occurred almost simultaneously. This suggested an interaction between concrete shear and bond of strands. Researchers observed that piles and girders with depths greater than 24 in. had measured development lengths greater than the AASHTO equation prediction. A new development length equation was proposed for these members that included a flexure term and shear term. The flexure term is shown below.

$$l_{df} = \left(\frac{f_{si}}{3}\right)D + \frac{\left(f_{su}^{*} - f_{se}\right)D}{4u_{ave}} \qquad 2.10$$

Where:

l_{df} = flexural development length (in.)

f_{si} = strand stress immediately after release (ksi)

D = strand diameter (in.)

f_{su}^{*} = strand stress required for ultimate strength (ksi)

f_{se} = effective prestress (ksi)

u_{ave} = average bond stress (ksi)

If the average bond stress is assumed to be 0.3 ksi, the denominator of the second term in Equation 2.10 becomes 1.2. The shear term for the proposed development length equation is shown below.

$$l_{dv} = d\cot\theta \qquad 2.11$$

Where:

l_{dv} = shear development length (in.)

d = distance to critical section (in.)

θ = angle of shear failure

Assuming that the angle of shear failure is 30 degrees and the distance to the critical section is 85 percent of the section height, Equation 2.11 becomes 1.47h. Combining the previous two equations yields Equation 2.12 below. This was the researcher's recommendation for sections deeper than 24 in. (Shahawy 2001).

$$l_d = \left(\frac{f_{si}}{3}\right)D + \frac{\left(f_{su}^{*} - f_{se}\right)D}{1.2} + 1.47h \qquad 2.12$$

2.2.4 Michael Simmons

The primary goal of this study was to determine the effect of strand spacing on transfer length, development length, and flexural behavior. Fourteen tee beams were prestressed with 0.5 in. diameter grade 270 strands. Half of the beams had 2.0 in. strand spacing, while the other half had 1.75 in. spacing. Other variables were concrete strength and presence of confinement steel. The majority of the specimens were unconfined with normal strength concrete. For both 1.75 and 2.0 in. strand spacing, an embedment length of approximately 120 in. was required for flexural failure rather than bond failure. The AASHTO equation at the time of this study (Equation 2.8 without the κ factor) predicted a 71 in. minimum embedment length. The researcher found that strand spacing had no effect on development length. High concrete strength and the presence of confinement steel appeared to decrease the development length. However, sudden prestress release caused dispersion in the data, and the effect of these two parameters was difficult to isolate (Simmons 1995).

2.3 Prestress Losses

Prestressed concrete members experience losses in prestress force throughout their life. These losses are classified as either instantaneous losses or long term/time dependent losses. The sources of instantaneous losses are anchorage slip, friction, and elastic shortening. These losses can be easily determined using basic mechanics. Time dependent losses include creep and shrinkage of concrete and relaxation of prestressing steel. These losses are interdependent and difficult to calculate. Prestress losses have little effect on the ultimate strength of a member.

However, an estimation of effective prestress is necessary for determining deflections and cracking loads.

A pretensioned member is fabricated by tensioning strands to a jacking stress. Strands are tensioned in air, so no frictional losses are incurred. Strands are seated in anchors at the ends of a prestressing bed, and a small amount of slip results in a loss of force. Once concrete is cast and allowed to cure, the strands are cut and the prestress force is transferred to the member. The member shortens and experiences an elastic shortening loss. The stress in strands immediately after transfer is referred to as the initial stress. Now the member will experience long term losses. Creep of concrete is defined as a continual deformation under sustained load. Shrinkage of concrete occurs as excess water not hydrated by cement evaporates from the member. Compressive strains in the concrete from creep and shrinkage cause significant prestress losses. Prestressing steel also experiences relaxation during this time, which is a loss in stress under a constant strain. However, steel relaxation losses are usually small. A large portion of long term losses occur early in a member's life. The stress in strands after all losses have occurred is the effective prestress (Nilson 1987).

2.3.1 Code Provisions

ACI gives no provisions for calculating prestress losses. Instead, the reader is referred to several other sources for these provisions. One of the references is the report completed by the PCI Committee on Prestress Losses (ACI 2005). While the PCI provisions are over 30 years old, they are still recognized by designers as a viable method for determining prestress losses.

PCI approaches the interdependency of long term prestress losses with a general time step method. PCI recommends a minimum of four time steps and suggests the addition of a step whenever substantial load changes are predicted. The first step begins when strands are stressed and ends upon prestress transfer. The second step begins at prestress transfer and lasts 30 days or until a new load is applied, such as a cast in place deck on top of precast pretensioned girders. The third step extends until a member is one year old, and the fourth step concludes at the end of service. Losses due to creep and shrinkage of concrete and relaxation of steel are calculated during each of these time steps using equations and tables provided by PCI, which will be outlined in Chapter 4. The equations and tables are based on a body of research and reflect material properties, section properties, and time effects (PCI 1975).

AASHTO recommends an approximate estimate and a refined time step method for calculating long term prestress losses. The approximate method applies to standard precast, pretensioned members subjected to normal loading and exposure conditions. It is restricted to members made from normal weight concrete which is moist or steam cured. Prestressing strands must have normal or low relaxation properties (AASHTO 2006). The refined method was adopted from NCHRP Report 496. The method in this report is applicable to normal and high strength concrete (Tadros, et al. 2003). This method was developed for pretensioned prestressed concrete girders with cast in place composite decks.

The refined method categorizes prestress losses into four components. The first is the instantaneous loss from elastic shortening at transfer. The second component is time-dependent losses (creep and shrinkage of concrete and relaxation of steel) that occur between prestress transfer and deck placement. The third component is actually a gain in prestress resulting from deck placement and other additional permanent loads. The final component is time dependent losses occurring between deck placement and end of service, including a prestress gain due to shrinkage of deck concrete. Although this method was designed primarily for pretensioned girders with composite toppings, AASHTO allows the equations to be adapted for precast pretensioned girders with non-composite toppings and post-tensioned nonsegmental girders with grouted tendons. Specific details of this method will be given in Chapter 4 (AASHTO 2006).

2.3.2 Ahlborn, French, & Shield

The researchers in this study performed parametric and experimental studies to evaluate the use of high strength concrete (HSC) in bridge design applications. Two Mn/DOT 45M I-girders were cast with 46 0.6 in. diameter grade 270 strands each. Strands were either draped or debonded in the ends to prevent tension cracks at release. The initial compressive strengths of Girders I and II were 9300 and 10400 psi, respectively. The 28 day compressive strengths were 12100 and 11100 psi for Girders I and II, respectively. A composite deck was cast on top of each girder. The researchers measured prestress losses with vibrating wire gages and flexural load testing.

Vibrating wire gages were placed in each girder at a location corresponding to the center of gravity of the strand pattern. Prestress losses were classified as either initial or long term in order to interpret vibrating wire gage readings. The sources of initial prestress losses were elastic shortening and steel relaxation that occurred before transfer. Long term prestress losses resulted from concrete creep and shrinkage. Since long term steel relaxation losses occur at constant strain, they were not reflected by vibrating wire gage strain readings. They were calculated theoretically and added to the creep and shrinkage losses measured with vibrating wire gages. The following equation for prestress force after release was derived by assuming an elastic stress distribution at the center of gravity of the strands.

$$P_i = \left(\frac{1}{\frac{1}{A_n} + \frac{e_n^{\ 2}}{I_n}} \right) \left(\frac{M_o e_n}{I_n} - \Delta \varepsilon_{vw@release} E_{ci} - \sigma_{c,pre-release} \right) \qquad 2.13$$

Where:

P_i = prestress force after release (k)

A_n = net section area (in.^{2})

e_n = net section eccentricity (in.)

I_n = net section moment of inertia (in.^{4})

M_o = self weight moment (k in.)

$\Delta\varepsilon_{vw@release}$ = change in vibrating wire gage strain during release

E_{ci} = initial modulus of elasticity of concrete (ksi)

$\sigma_{\sigma c,pre-release}$ = stress in concrete prior to release (ksi)

The stress in prestressing strands after release may be divided by the total strand area to find the initial prestress, f_{pi}. The $\sigma_{c,pre-release}$ term in Equation 2.13 represents tensile concrete stresses resulting from shrinkage and temperature effects. Once concrete is bonded to strands, any shrinkage will cause the concrete to contract. The tensioned strands restrain this contraction and cause tensile stress in the concrete. Steel has a higher thermal expansion coefficient than concrete, so it will expand at a higher rate when heated. Once concrete and strands are bonded, temperature increases during curing will cause tensile concrete stress and a reduction in strand tensile stress. Shrinkage and temperature effects may cause prestress losses before prestress transfer. A lower bound estimate of initial prestress loss (higher initial prestress force) was calculated by assuming there was no stress in concrete before release. On the corollary, an upper bound estimate of initial prestress loss (lower initial prestress force) was calculated by assuming the stress in concrete before release was equal to the concrete tensile strength, which suggests the existence of pre-release cracks. The formula used for calculating percentage initial prestress loss is shown below.

$$InitialLoss = \left(\frac{f_{pj} - f_{pi}}{f_{pj}} \right) \times 100 \qquad 2.14$$

The term f_{pj} in Equation 2.14 represents the jacking stress. Changes in strand stress after release were calculated with the following equation.

$$\Delta f_p = \Delta \varepsilon_{vw} E_{ps} + \Delta f_{relaxation} \qquad 2.15$$

Where:

Δf_p = change in strand stress (ksi)

$\Delta \varepsilon_{vw}$ = change in vibrating wire gage strain since release

E_{ps} = modulus of elasticity of prestressing steel (ksi)

$\Delta f_{relaxation}$ = change in strand stress due to steel relaxation (ksi)

The formula used for calculating percentage long term prestress loss is shown below.

$$LongTermLoss = \left(\frac{f_{pi} - \Delta f_p}{f_{pj}} \right) \times 100 + InitialLoss \qquad 2.16$$

In addition to measuring prestress losses with vibrating wire gages, the researchers also used flexural load testing to calculate effective prestress, and thus total prestress losses. The loads required to initiate and reopen cracks were used to back calculate effective prestress according to the following elastic stress equation.

$$\sigma = -\frac{P_e}{A_{nc}} - \frac{P_e e_{nc} c_{nc}}{I_{nc}} + \frac{(M_o + M_d) c_{nc}}{I_{nc}} + \frac{M_{applied} c_c}{I_c} \qquad 2.17$$

Where:

σ = stress in concrete (ksi)

P_e = effective prestress force (k)

A_{nc} = non-composite area (in.^{2})

e_{nc} = non-composite eccentricity (in.)

c_{nc} = non-composite distance to extreme tension fiber (in.)

I_{nc} = non-composite moment of inertia (in.^{4})

M_o = self weight moment (k-in.)

M_d = deck moment (k-in.)

$M_{applied}$ = applied moment during load testing (k-in.)

c_c = composite distance to extreme tension fiber (in.)

I_c = composite moment of inertia (in.^{4})

For a crack initiation test, the concrete stress and applied moment are equal to the concrete tensile strength and cracking moment, respectively. Crack initiation and location were detected with Acoustic Emissions (AE) monitoring equipment and visually confirmed. The concrete stress is set equal to zero for a crack reopening test, and the applied moment is the moment at which the crack reopened. Crack reopening was detected with the AE equipment and with Linearly Variable Differential Transducers (LVDTs).

The lower bound initial prestress losses measured with vibrating wire gages for Girders I and II were 15.5 and 18.6 percent, respectively. The upper bound initial losses were 25.9 and 29.3 percent for Girders I and II, respectively. Initial prestress loss predictions from PCI and AASHTO models based on normal strength concrete (NSC) relationships were less than the lower bound measured losses. Researchers found that NSC relationships over predict the modulus of elasticity of HSC. The incorporation of actual measured material properties into prestress loss models resulted in predictions that were closer to the lower bound measured losses. Long term lower bound measured prestress losses were less than predicted losses from models based on NSC relationships. The researchers concluded that NSC creep and shrinkage loss models over predict these same losses in HSC. The total prestress losses measured by flexural crack reopening tests were 7.7 and 12.0 percent higher than the lower bound long term losses measured with vibrating wire gages in Girders I and II, respectively. This validated the assumption that concrete stresses prior to release cause prestress losses (Ahlborn, et al 2000).

2.3.3 Baran, Shield, & French

The researchers in this study investigated three different experimental methods for determining prestress losses. Methods included embedded vibrating wire gages, flexural crack initiation and reopening tests, and destructive testing by severing and exposing gaged strands. Eleven 20 ft long Mn/DOT Type 28 prestressed concrete beams were fabricated and tested. All were instrumented with vibrating wire gages and subjected to load testing, while only two were destructively tested. Eight of the beams had pre-release cracks at midspan. Each beam had four straight 0.6 in. diameter grade 270 strands that were stressed to 54 percent ultimate strength. The low jacking stress was used because the beams were originally designed for 0.5 in. diameter strands. The average concrete strength at the time of testing was 9950 psi.

The following premise governed the reduction of vibrating wire gage data: if perfect bond was assumed, the change in gage strain was equal to change in concrete and strand strain. However, the researchers recognized that vibrating wire gages could not measure concrete strains until the concrete hardened. The following equation was recommended for extrapolating changes in strand stress vibrating wire gage readings.

$$\Delta f_p = E_{ps}\left[B(R_3 - R_2) - \alpha_s (T_2 - T_1)\right] \qquad 2.18$$

Where:

Δf_p = change in strand stress since tensioning strands (ksi)

E_{ps} = modulus of elasticity of prestressing steel (ksi)

B = gage calibration factor

R_3 = gage reading at time of interest

R_2 = gage reading at time when concrete had hardened, but before prestress was released

α_s = coefficient of thermal expansion of steel (1/^{o}C)

T_2 = steel temperature corresponding to R_2 (^{o}C)

T_1 = steel temperature when strands were stressed (^{o}C)

The second portion of Equation 2.18 represents a temperature related strand stress change that occurs between strand tensioning and the first vibrating wire gage reading.

Flexural crack initiation and crack reopening tests were conducted for each specimen. The following elastic stress equation was used to back calculate the effective prestress force.

$$P_e = \left(\frac{M_{crack}}{S_t} + \frac{M_o}{S_t} - f_r \right) / \left(\frac{1}{A_g} + \frac{e_g}{S_g} \right) \qquad 2.19$$

Where:

P_e = effective prestress force (k)

M_{crack} = applied cracking or crack reopening moment (k in.)

S_t = transformed section modulus (in.^{3})

M_o = self weight moment (k in.)

f_r = concrete modulus of rupture (ksi)

A_g = gross section area (in.^{2})

e_g = gross section eccentricity (in.)

S_g = gross section modulus (in.^{3})

Crack initiation was detected using visual observation, crack detection gages, and concrete surface strain gages. Crack reopening was detected using bottom surface strain gages and bottom surface LVDTs. When calculating effective prestress using crack reopening tests, the modulus of rupture becomes zero in Equation 2.19, and the cracking moment is replaced by the moment corresponding to the crack reopening.

The total prestress loss (before load testing) measured by vibrating wire gages ranged from 20.7 to 26.4 ksi for the eleven specimens. Only two beams were subjected to strand cutting tests. These tests resulted in total losses of 34.5 and 34.8 ksi. Researchers found that prestress losses could not be calculated from flexural load tests in beams that exhibited pre-release cracks. The three beams without pre-release cracks had the following average prestress losses measured from the indicated methods: vibrating wire measurements, 21.9 ksi; crack initiation tests, 98.4 ksi; crack reopening tests, 69.2 ksi; PCI theoretical losses after one year, 22.1 ksi; AASHTO theoretical final losses, 24.6 ksi.

The researchers concluded from the results of this study that vibrating wire gages and strand cutting were the most effective methods for measuring prestress losses. The vibrating wire gage measurements were similar to theoretical predictions from PCI and AASHTO. There were large discrepancies between losses predicted by flexural tests and the losses measured by vibrating wire gages. The researchers concluded that traditional mechanics overestimated prestress losses when crack initiation and reopening loads were measured, assuming these loads were accurately determined. As a corollary, crack initiation and reopening loads were overestimated by effective prestress predictions (assuming prestress losses were accurately evaluated). Test data suggested that the equation used to predict crack initiation represented the load at which cracks became visible rather than the load at which the modulus of rupture was exceeded. Similarly, the equation used to estimate crack reopening predicted the load at which crack reopening became visible rather than the load at which decompression occurred in the bottom of a section (Baran, et al 2005).

2.4 Top Bar/Strand Effect

The top bar effect is a generally accepted phenomenon of conventionally reinforced concrete. ACI recommends a 30 percent increase in development length when twelve or more inches of fresh concrete are cast below a horizontal reinforcement bar. AASHTO recommends a 40 percent increase in development length when a top horizontal or nearly horizontal bar has more than 12 in. of fresh concrete cast below (2006). Two studies supporting the effect of casting orientation on development length of reinforcement bars are presented below. Neither ACI nor AASHTO recommend a similar increase for the development length of top cast prestressing strands. Little or no research has been conducted to assess this effect. Another study relating to the effect of casting orientation on transfer length and end slip in prestressed concrete piles is also presented below.

2.4.1 Jirsa and Breen

The researchers in this study investigated the influence of casting position on development of deformed reinforcement bars. Pull out tests were performed on large concrete blocks cast with anchored reinforcement bars at varying depths. Each specimen was 72 in. deep and had eight bars spaced evenly throughout the depth. The concrete used to cast the first two specimens had a 3 in. slump. The slump was increased to 8.5 in. for the third specimen. Steel stress and loaded end slip were measured during each pull out test. A bond efficiency ratio was determined for each test by dividing the ultimate steel stress achieved in the tested bar by the ultimate stress achieved in the bottom bar of the same specimen. A casting position factor for development length was calculated as the reciprocal of the bond efficiency ratio.

The researchers found that the casting position factor increased continually as the depth of concrete below a bar increased. Researchers also concluded that an increase in slump will also increase the casting position factor. Design recommendations were made for three categories of slump. The casting position factor within each range of slump varied according to the depth of fresh concrete below a bar. The development length factor was given in the form of a constant factor supplied for a range of depth, as well as a continuous linear equation. The design recommendations are shown in Table 2.1. The recommendations for concrete with slump less than 4 in. and greater than 6 in. are based on test results from the specimens with 3 in. slump and 8.5 in. slump, respectively. The recommendations for concrete with slump between four and six inches are based on splice length tests performed in a separate portion of the research project. These test specimens had 5.5 in. slump. It is important to note that some of the development length modification factors presented in Table 2.1 are significantly greater than code provisions.

Table 2.1 Top Bar Development Length Factors

z^* (in.)	Slump (in.)		
	< 4	4 to 6	> 6
< 12	1.0	1.0	1.0
12 to 24	1.1	1.2	1.3
24 to 48	1.2	1.4	1.8
> 48	1.3	1.6	2.2
Equation	$1 + 0.005z$	$1 + 0.01z$	$1 + 0.02z$

*Depth of fresh concrete cast below horizontal bar.

2.4.2 Jeanty, Mitchell, & Mirza

The researchers in this study sought to quantify the effect of casting position and transverse reinforcement on development and bond of mild steel reinforcement. Variables in the study were casting position, embedment length of test bars, and the presence of transverse reinforcement. Twelve 9 in. wide by 18 in. deep beams were cast in six pairs. One No. 8 reinforcing bar with 1.5 in. cover was placed with varying but equal embedment lengths (30 to 48 in.) on both sides of the beam centerline. A No. 6 bar running the full 10 ft length of the beam was placed in each corner closest to the No. 8 test bar. Two No. 3 bars were placed in the other corners. No. 3 stirrups were placed at 8 in. spacing throughout the beam. These stirrups were open in four pairs of beams and closed in the other two pairs. Each pair of beams was cast so that the orientation of one reinforcement cage was inverted from the orientation of the other. The yield stress of all bars was approximately 60 ksi, and the average concrete strength was 4170 psi.

Researchers found that top cast bars required an embedment length of 44 in., while bottom cast bars only needed 36 in. This translated to a top bar factor equal to 1.22. Top cast beams cracked at lower loads than bottom cast beams, suggesting that the tensile strength of top cast concrete was lower than that of bottom cast concrete. Transverse reinforcement in locations of potential splitting reduced required development length by 20 percent for both casting orientations (Jeanty, et al 1988).

2.4.3 Wan, Harries, & Petrou

The researchers in this study investigated top cast strand effect in prestressed concrete piles. Although piles are vertical structural elements, they are cast horizontally with strands spaced uniformly in all portions of the cross section. Strand end slip and transfer length were measured for 32 precast prestressed piles. Each pile was 18 ft long and had an 18 in. square cross section. All piles had eight grade 270 strands with 0.375 or 0.5 in. diameter. Two concrete mixes were used. One had minimum initial and 28 day compressive strengths of 3500 and 5000 psi, respectively. The minimum 28 day strength of the other mix was 4000 psi, but wasn't intended for prestressing applications and did not have high early strength. End slip was measured for each strand on both ends of all piles. One pile from each concrete pour was instrumented with electrical resistance strain gages on the top concrete surface to measure transfer length. Five piles were instrumented internally with strain gages attached to No. 3 reinforcement bars. Two of these piles had a single No. 3 bar at the center of the cross section. The other three piles had pairs of the No. 3 bars positioned 4 in. above and below the center.

The average top and bottom strand slips were 0.140 and 0.058 in., respectively. Numerous top strand end slips were greater than the recommended value of 0.1 in. Ratios of top to bottom strand slip (t/b) varied from 1.03 to higher than 3.0. The t/b based on average top and bottom end slips was 2.4. The researchers found that surface strain gages could not be used to accurately predict internal strains. However, they did provide qualitative measurements of top strand transfer length. The transfer lengths of the two piles with a single strain gaged reinforcement bar were 40 and 45 in. The ACI recommended value was 28.5 in. The transfer lengths of the three piles with pairs of strain gaged reinforcement bars were 25, 45, and 25 in. for top strands and 10, 25, and 15 in. for bottom strands. These transfer lengths resulted in top to bottom ratios of 2.5, 1.8, and 1.7. The end slip t/b values for these three beams were 3.36, 2.03, and 1.17. The researchers recommended that a top strand factor be included when determining pile capacities and when performing development length calculations for other types of prestressed members (Wan, et al. 2002).

3. BEAM FABRICATION AND TESTING

3.1 Introduction

This chapter provides details on beam design, reinforcement, casting processes, curing, instrumentation, and testing. Twelve pretensioned prestressed concrete beams were cast and tested in the Virginia Tech Structures and Materials Laboratory. A timeline for a typical specimen follows.

1. A small prestressing bed was built in the lab. The bed consisted of two lines of beams that were approximately 60 ft long.
2. Formwork was built, strands were tensioned, and mild steel reinforcement was installed.
3. A vibrating wire gage was placed in one end of the member at or near the embedment length for load testing.
4. Concrete was poured and subjected to a seven day moist cure.
5. Formwork was stripped as early as the day after pouring, and both sides of each beam end were instrumented with DEMEC gage points.
6. Prestress force was released by flame cutting strands once adequate initial concrete compressive strength was achieved, and transfer lengths were measured.
7. The beam was allowed to cure until the strength required for load testing was attained. Internal strains were continuously monitored with the vibrating wire gage.
8. The beam was loaded until the first flexural crack occurred. The beam was then unloaded and reloaded until the crack reopened.
9. Beam loading was continued until a flexural or bond failure occurred.

3.2 Nomenclature

A unique name was used to describe each specimen. A typical beam designation is shown in Figure 3.1. The first term indicates the pour in which a beam was cast. The second term represents the grade of prestressing strand in the beam (the grade refers to the ultimate strength of the strand). The third term specifies which size strands were used. The first letter of the fourth term indicates the casting orientation and completes an individual beam's classification. The second letter of the fourth term represents the beam end for load testing purposes. Finally, the third letter of the fourth term specifies the side of the beam for transfer length considerations.

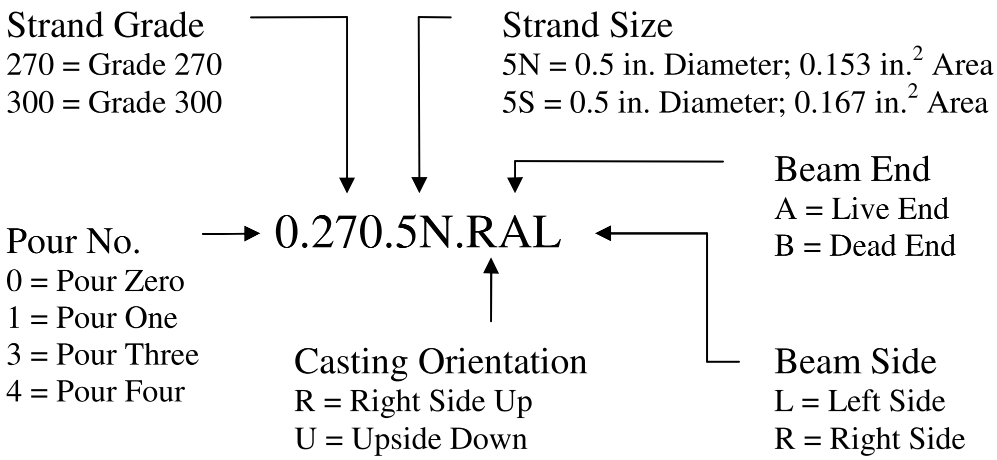

Figure 3.1 Beam Nomenclature

3.3 Prestressed Concrete Beam Fabrication

Twelve pretressed beams were cast in four pours of concrete. Two prestressing lines were used for each pour: one for grade 270 strands and one for grade 300 strands. This allowed a head to head comparison of strand grade among beams from the same pour. The first two sets of beams (pours zero and one) were prestressed with normal 0.5 in. diameter strands. The third and fourth sets of beams had special 0.5 in. diameter strands that have approximately 10 percent more area than a normal strand. Beams in pours three and four also had larger cross sections. The nominal cross sectional areas of normal and special strands are 0.153 and 0.167 in.^{2}, respectively. In pours one and three, two beams were cast right side up and two beams were cast upside down. This permitted a head to head comparison of casting orientation. Only two right side up beams were cast in pours zero and four. Table 3.1 shows the differences in each test beam and further explains the nomenclature mentioned above.

A short explanation is necessary to explain why there is no pour two. The first pour was intended to produce a full set of four beams: grade 270 right side up, grade 270 upside down, grade 300 right side up, and grade 300 upside down. However, the concrete mix had an early set, so only the grade 270 right side up beam and part of the grade 300 right side up beam were cast. This pour was then renamed pour zero, and pour one would be a repeat in which the four previously mentioned beams would be cast. Pour two was reserved for the possible testing of additional beams with normal 0.5 in. diameter strands. Despite complications, three satisfactory load tests were obtained from pour zero, and all eight anticipated load tests were obtained from pour one. Beam fabrication was resumed with special 0.5 in. diameter strands in pour three.

Table 3.1 Test Specimens

Beam Name	Pour No.	Strand Grade	Strand Size	Casting Orientation
0.270.5N.R	0	270 ksi	0.5 in. Regular	Right Side Up
0.300.5N.R	0	300 ksi	0.5 in. Regular	Right Side Up
1.270.5N.R	1	270 ksi	0.5 in. Regular	Right Side Up
1.300.5N.R	1	300 ksi	0.5 in. Regular	Right Side Up
1.270.5N.U	1	270 ksi	0.5 in. Regular	Upside Down
1.300.5N.U	1	300 ksi	0.5 in. Regular	Upside Down
3.270.5S.R	3	270 ksi	0.5 in. Special	Right Side Up
3.300.5S.R	3	300 ksi	0.5 in. Special	Right Side Up
3.270.5S.U	3	270 ksi	0.5 in. Special	Upside Down
3.300.5S.U	3	300 ksi	0.5 in. Special	Upside Down
4.270.5S.R	4	270 ksi	0.5 in. Special	Right Side Up
4.300.5S.R	4	300 ksi	0.5 in. Special	Right Side Up

3.3.1 Prestressing Bed

A small scale prestressing bed was built on a portion of the reaction floor in the Virginia Tech Structures and Materials Lab. As previously mentioned, two separate reaction beams were used for grade 270 strands and grade 300 strands. Each reaction beam, comprised of a 60 ft long wide flange steel section embedded in a concrete floor slab, provided adequate resistance to the eccentric force from the prestressing strands. Four steel abutments were bolted to the ends of each reaction beam. A diagram of the prestressing bed for a typical pour of four beams (pours one and three) is shown in Figure 3.2. In the case of pours zero and four, the set up was similar, but excluded the two upside down beams.

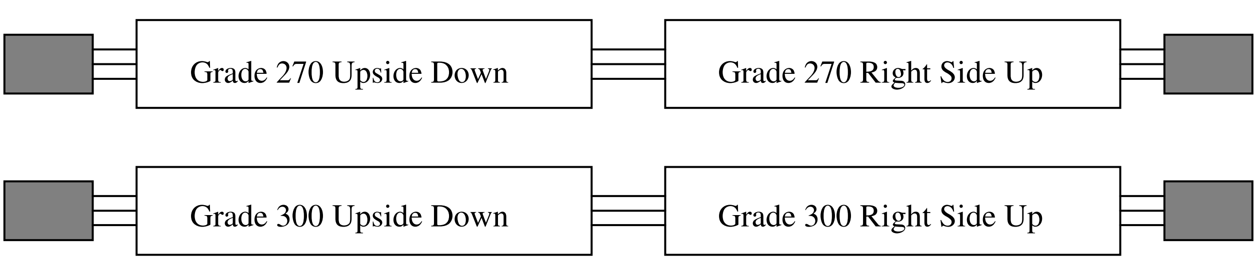

Figure 3.2 Prestressing Bed Layout

3.3.2 Cross Section Design

Different beam cross sections were used for different size strands. The design of the cross sections was influenced by three main factors. First of all, large compressive strains near the beam ends at the level of the strands were desired so that transfer lengths could be accurately measured. The beams were designed so that these large strains could be achieved without exceeding stress limits at the tension face near beam ends and compression face at center span. The second goal of the beam design was to achieve large strains in the prestressing steel at ultimate flexural strength. These strains, which were designed to be approximately 0.04 to 0.05 in./in., ensured that the sections would have adequate ductility. The last goal of the beam design was to minimize differences in cross sections so that few changes to the formwork would be required. A bulb tee shape was determined to be most effective for beam design. A 17 in. deep section was used for the normal strands, while a 19 in. section was used for special strands. A summary of geometric properties is provided in Table 3.2. The transformed section properties are based on the 28 day design concrete modulus of elasticity. Cross sectional drawings for normal and special 0.5 in. diameter strands are shown in Figure 3.3 and Figure 3.4. The only difference between cross-sections is that the top and bottom flanges of the 19 in. section are one inch thicker than the flanges of the 17 in. section. The under sides of the top flange are gently sloped by a rate of 32:1 for concrete placement. The top and bottom chamfers have 1:1 slope.

Table 3.2 Geometric Section Properties

Section Property		Normal Section (17 in. Total Height)	Special Section (19 in. Total Height)
Gross Section Properties	A_g (in.^{2})	134.0	166.0
	I_g (in.^{4})	4513	6664
	e_g (in.)	8.085	9.728
Transformed Section Properties	A_t (in.^{2})	139.4	171.6
	I_t (in.^{4})	4773	7026
	e_t (in.)	8.178	9.697
Net Section Properties	A_n (in.^{2})	132.9	164.9
	I_n (in.^{4})	4485	6620
	e_n (in.)	8.187	9.735

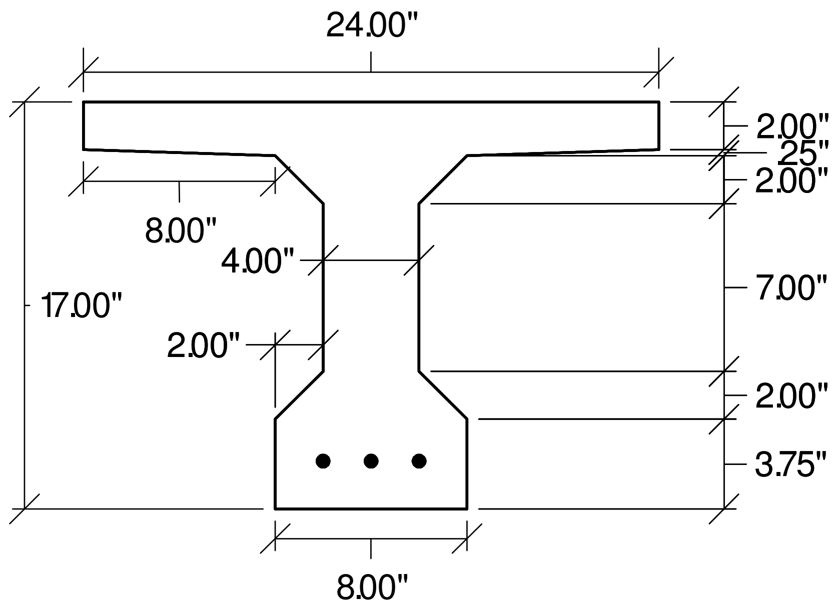

Figure 3.3 Cross section for 0.5 in. Normal Strands

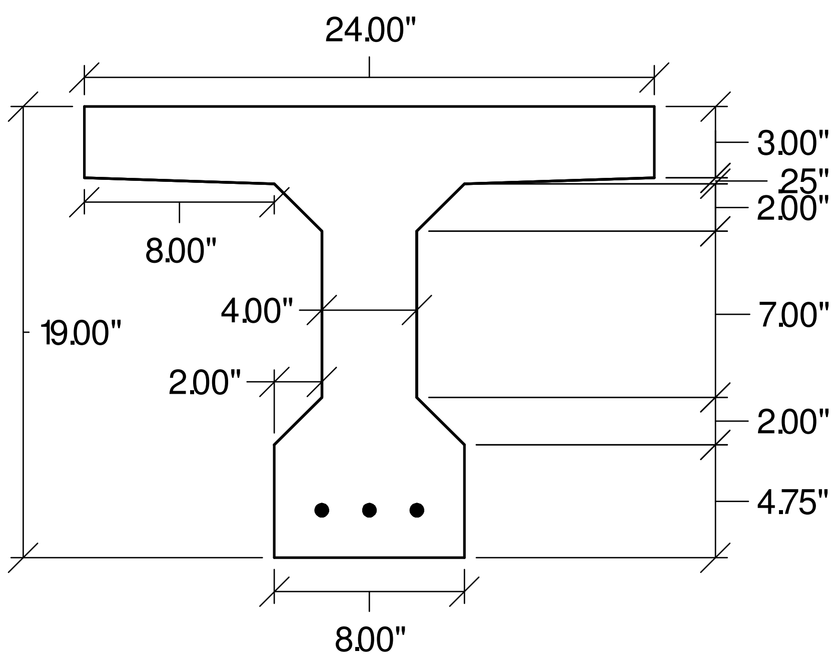

Figure 3.4 Cross section for 0.5 in. Special Strands

3.3.3 Details of Reinforcement

All prestressing strands were obtained from Strand-Tech Martin, Inc. (www.strandtech.com). Material property testing was conducted in the Virginia Tech Structures and Materials Laboratory as part of an earlier phase of this project. Idealized plots of stress vs. strain for grade 270 and grade 300 strands are shown in Figure 3.5. For each strand grade, the yield point was taken as the average strand stress for all tests at 1.0 percent elongation. The stress coordinate of the final point was taken as the average breaking stress for all tests of a given strand grade, while the strain coordinate was taken as the average maximum elongation. The plots in Figure 3.5 show that the tested material properties were generally greater than the requirements of the American Society of Testing and Materials (ASTM). ASTM A416 states that the minimum yield stress of low relaxation strand should be 90 percent of the guaranteed ultimate tensile strength, which is 243 ksi for grade 270 strands and 270 ksi for grade 300 strands. The yield stresses from all tests were greater than this standard. ASTM A416 also states that the breaking stress should be greater than the guaranteed ultimate tensile strength, and the total elongation should be greater than or equal to 3.5 percent (ASTM 2005). With the exception of one grade 270 0.5 in. diameter normal strand test, all breaking stresses were greater than the guaranteed ultimate tensile strength. The total elongation of each tested strand was much larger than the 3.5 percent minimum.

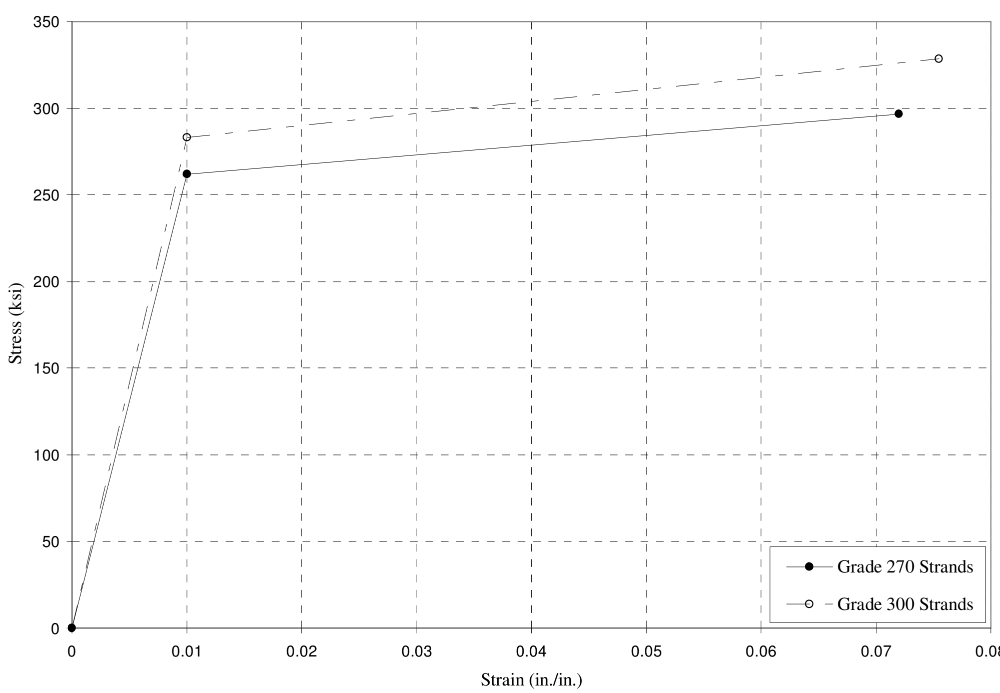

Figure 3.5 Prestressing Strand Stress vs. Strain Plots

The results of yield stress, ultimate stress, and modulus of elasticity tests of 0.5 in. diameter normal and special strands are summarized in Table 3.3. Six tension tests were conducted for each type of strand. In both sets of normal strand specimens, four tests were conducted with aluminum foil grips while the other two tests implemented aluminum inserts with an aluminum oxide grip material. The breaking stresses of tests with aluminum foil grips were significantly lower than those achieved with the aluminum insert and aluminum oxide grip system. All tests of special strands utilized the aluminum insert and aluminum oxide grip system, which was found to be more effective. As mentioned previously, the tested yield and ultimate stresses were generally higher than the minimum specified values. The modulus of elasticity test results were in accord with generally accepted values (Hill 2006).

Table 3.3 Prestressing Steel Material Properties

Strand Type	Average Yield Stress from Six Tests (ksi)	Average Ultimate Stress from Six Tests (ksi)	Average Modulus of Elasticity from Six Tests (ksi)
Grade 270 1/2" Normal	260	320 (four tests w/ al. oxide grips); 273 (two tests w/ al. foil grips)	28400
Grade 300 1/2" Normal	281	351 (four tests w/ al. oxide grips); 305 (two tests w/ al. foil grips)	28600
Grade 270 1/2" Special	264	304	29300
Grade 300 1/2" Special	285	337	29300

Each test beam contained three straight prestressing strands which served as the primary flexural reinforcement. These strands were spaced 2 in. on center, and were located 2 in. from the bottom of the cross section. This strand pattern coincides with standard industry practice and provides adequate concrete cover. The surface condition of the strands was clean and free of rust. Strands were stored inside to prevent exposure to moisture or temperature extremes.

Test beams were also reinforced with mild steel (grade 60) in the form of compression reinforcement, shear reinforcement, confinement steel, and temperature & shrinkage steel. All secondary reinforcement was designed according to *AASHTO LRFD Bridge Design Specifications* (2006). Compression reinforcement consisted of three No. 4 bars located one inch from the top of the cross section. Beams were reinforced for shear by No. 4 stirrups at various spacing. The design shear force was estimated as the shear at the critical section resulting from a load applied at the predicted development length that would cause a moment equal to the nominal moment capacity. This design shear was increased by a load factor of 1.4, and the required reinforcement was determined according to AASHTO Article 5.8.3. Confinement reinforcement was supplied per AASHTO Article 5.10.10.2. Three No. 3 deformed bars were placed around the strands at 2 in. increments beginning 2 in. from the ends of the beam. Temperature and shrinkage steel consisted of No. 3 bars at 16 in. spacing placed transversely in the top flange. This met the requirements of AASHTO Article 5.10.8 for shrinkage and temperature reinforcement (AASTHO 2006). Figure 3.6 shows a typical reinforcement layout near the end of a 17 in. section. In a 19 in. section, the relative location of compression reinforcement and temperature and shrinkage steel with respect to the top of the section did not change. Likewise, the distance between the bottom of the section and the strands and confinement reinforcement was constant. The only difference between sections was that the stirrup length was increased by two inches.

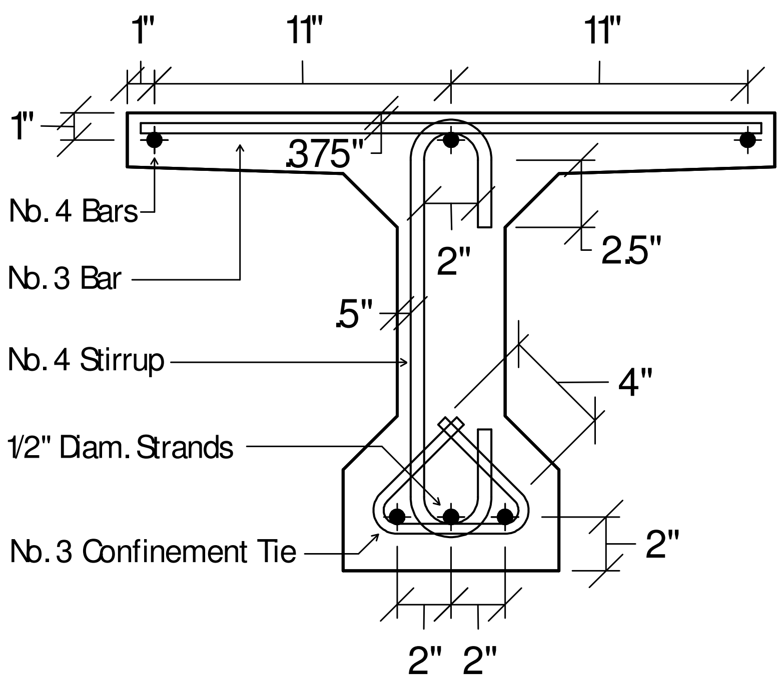

Figure 3.6 Mild Steel Reinforcement Schematic

3.3.4 Concrete Mixture and Properties

The concrete mix used in this project was designed to have lower initial and 28 day compressive strengths than what is normally used in prestressing applications. These lower bound strengths were desired so that any problems associated with the higher strength grade 300 strands would be apparent. The target initial compressive strength was 4500 to 5000 psi. The 28 day design compressive strength was 6000 psi. The concrete had normal weight. A 0.75 in. maximum aggregate size was specified because of tight rebar spacing in the formwork. Concrete was batched at a nearby ready mix plant and then delivered to the lab. An air entraining admixture was added to the mix at the plant. The plant dispatcher dosed the mix with an amount that would produce 3 to 5 percent air content, so this amount varied from pour to pour. A high range water reducing admixture (super plasticizer) was shipped separately and added on site if more workability was needed. As mentioned previously, a flash set occurred during pour zero. The reason could not be isolated, but was most likely due to excessive holding time in the concrete truck. To prevent problems in future pours, the mix was modified by increasing water by two gallons per yard and adding a retarder. The original and modified mix designs are shown in Table 3.4.

Table 3.4 Concrete Mix Design

Component	Initial Mix Design Quantity (per yd^3)	Revised Mix Design Quantity (per yd^3)
No. 78 Stone	1443 lb	1443 lb
Natural Sand	1083 lb	1083 lb
Portland Cement	600 lb	600 lb
Fly Ash	150 lb	150 lb
Water	34 gal	36 gal
Air Entrainment	Target: 3-5 % Air	Target: 3-5 % Air
Super Plasticizer	19 oz	19 oz
Retarder	None	19 oz
W/C Ratio	0.38	0.40

A standard practice at ready mix plants is to withhold water from the mix when batching, and then add a portion or all of the remaining water on site. The addition of water increases the water to cementitious material ratio and can decrease the compressive strength of hardened concrete. When the concrete truck arrived at the lab, water was added to the mix until desired slumps were attained. Table 3.5 documents water additions to each batch of concrete. Super plasticizer was only needed for pour zero. The target water values are based on Table 3.4. The actual water value is the sum of water batched at the plant, water assumed to be in the sand, and water added at the lab. With the exception of pour zero, large slumps were achieved with water amounts significantly less than the full design amount. One possible reason for this is that the plant added more water than the amount that was reported. Another possible explanation is that the actual water content in the sand was greater than the value assumed for calculations.

Table 3.5 On-site Manipulation of Concrete Mix

Parameter	Pour 0	Pour 1	Pour 3	Pour 4
Concrete Volume	4.5 yd^3	4.5 yd^3	5.5 yd^3	3.5 yd^3
Target Water	153 gal	162 gal	198 gal	126 gal
Actual Water	139 gal	139 gal	173 gal	117 gal
Actual W/C Ratio	0.34	0.34	0.35	0.37
Target Super Plasticizer	85.5 oz	85.5 oz	104.5 oz.	66.5 oz.
Actual Super Plasticizer	76 oz	None	None	None
Final Slump	2.75 in.	7.5 in.	6.5 in.	7.5 in.

3.3.5 Formwork, Strand Stressing, and Concrete Placement

Formwork for the beams was built using form board and two by fours. Styrofoam insulation was cut to shape and glued to the forms to create the web block out in the cross section. Forms were built in 8 ft sections and then connected together before concrete was poured. When casting inverted beams, forms were assembled upside down. Figure 3.7 depicts the prestressing bed in the lab. Formwork for the right side up beams is in the foreground, while forms for the upside down beams are in the background. The grade 300 beams are on the left and the grade 270 beams are on the right.

Figure 3.7 Prestressing Bed and Formwork

In a typical prestressing plant, strands are tensioned, rebar is tied, forms are assembled, and concrete is poured in a single day. However, this process was extended over a week for this project because of time and manpower restrictions. Forms were assembled first. Logistics required that mild steel reinforcement for inverted beams be placed before and during form assembly. Rebar for right side up beams was placed after forms were completed. Next, prestressing strands were threaded through the forms and tensioned. Load cells, consisting of hollow aluminum cylinders equipped with full bridge strain gages, were used to monitor strand stress at the dead end of the prestressing bed (this dead end refers to the end of the prestressing bed where strands are not jacked). The load cells were calibrated with a universal testing machine and could accurately measure strand force within about 100 lb. Prestressing chucks provided restraint to tensioned strands. Figure 3.8 shows the steel abutments, load cells, and chucks at the dead end of the prestressing bed.

Figure 3.8 Dead End Anchorage

A hydraulic ram was used to tension each strand at the live end of the prestressing bed. The ram and abutment were separated by a chair that provided space to seat the chuck after a strand was tensioned. While tensioning a strand, the force was monitored by the the load cell at the dead end. An additional load cell was placed between the ram head and jacking chuck so that strand force at the live end could be verified. The stressing operation is depicted in Figure 3.9. Concrete was poured as early as two days and as late as seven days after stressing. During the time between stressing strands and pouring concrete, any remaining rebar was tied and forms were leveled and supported. Just before pouring concrete, the strands were shimmed to compensate for anchorage seating and steel relaxation losses. The shims, which were as thin as 1/16 in., ensured that the stress in strands prior to casting concrete was within about 2.5 ksi of the recommended 75 percent ultimate strand stress.

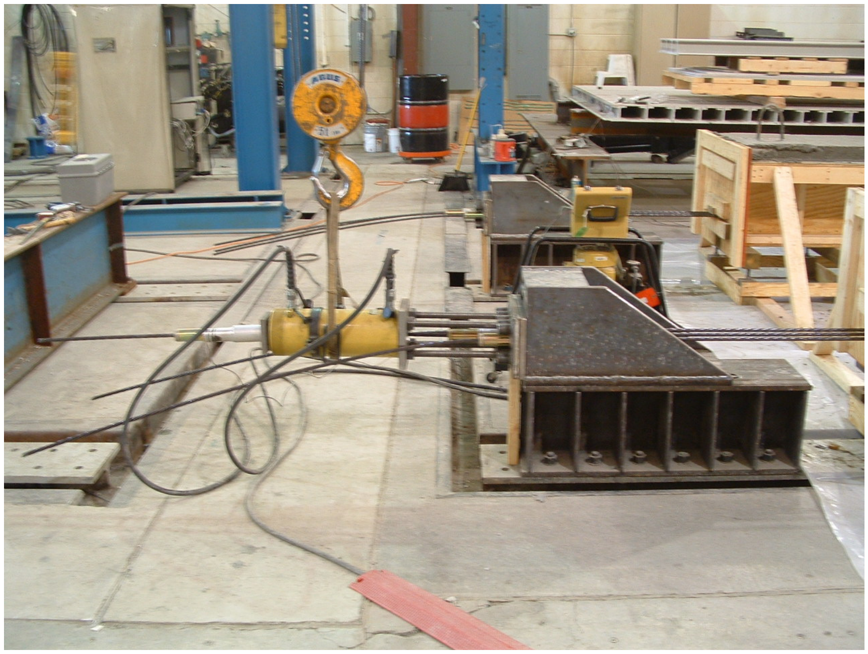

Figure 3.9 Live End Jacking Apparatus

Casting concrete was the final step in the beam fabrication process. Concrete was transported from the ready mix truck to the formwork by an overhead crane. Vibration was used to consolidate the concrete. Once all forms were filled with concrete, exposed surfaces were finished. Then these surfaces, as well as a large portion of the formwork, were covered with water soaked burlap and plastic sheeting. Moist cure was maintained for seven days. Concrete test cylinders were also cast for each pour. These cylinders were subjected to the same cure as the beams, and the molds were stripped at the same time that formwork was removed. Prestress force was transferred as early as three days and as late as twelve days after pouring concrete. The time of transfer was determined by initial concrete strength gain and scheduling issues. Prestress force was transferred by flame cutting the strands with an acetylene torch at the location between right side up and upside down beams.

3.3.6 Rotation of Inverted Beams

Four beams were cast upside down, as indicated previously. These beams had to be lifted and rotated 180 degrees for load testing. In normal prestressing applications, bending moments from prestress force and self weight act in opposite directions. These moments were additive in the inverted beams, so special care was taken to prevent cracking. Lifting hooks were inset from the ends of the beams to reduce the effect of the self weight moment. Two steel frames were used to rotate the beams. Each frame had six conveyor belt rollers that were positioned so that three imaginary lines connecting opposite pairs of rollers would intersect at a common point in the middle of the frame. The frames were mounted on the beams so that the centroid of the beam cross section coincided with this intersection point. The location of the frames relative to the beam's longitudinal axis was determined so that stresses at all points in the cross section would not exceed the tensile strength of the concrete during rotation. The rollers were cradled by slings suspended from overhead cranes. This set up allowed the beams to be manually rotated by two workers. No cracking was observed during or after rotation of inverted beams. The rotation apparatus is illustrated in Figure 3.10.

Figure 3.10 Beam Rotation System

3.4 Testing and Instrumentation

Several types of tests and measurements were performed on each beam. Transfer length tests were conducted at the time of prestress release by measuring concrete surface strains. Development lengths were predicted iteratively by load testing. Prestress losses were measured by vibrating wire gages and load tests. The following sections document the manner in which these tests and measurements were performed, and describe the different types of instrumentation that were used.

3.4.1 Transfer Length

Transfer length is the length required to develop the effective prestress force in the end of a fully bonded pretensioned concrete member. Transfer length was determined by measuring compressive concrete strains that resulted from the release of prestress force. Before release, the strain was assumed to be zero since there were no forces on the member. The application of prestress force caused changes in strain that increased incrementally as the distance from the end of the member increased. This provided a strain profile from which transfer length could be determined.

3.4.1.1 DEMEC Gage and Gage Points

Transfer length was determined by measuring concrete surface strains using a DEmountable MEChanical (DEMEC) strain gage and surface mounted gage points. The DEMEC strain gage, manufactured by Mayes Instruments Limited of the United Kingdom (www.mayes.co.uk), had a gage length of 200 mm and could measure strains with an accuracy of approximately +/- five microstrains. The DEMEC gage was comprised of a rigid metallic bar, fixed contact point, pivot point, and digital dial gage (see Figure 3.11). The gage points were small metallic discs with contact points in the center. These were attached to both sides of each beam end at the level of the prestressing strands. Quick setting epoxy was used to affix gage points to the concrete. Gage point spacing was either 50 or 100 mm. Each individual strain reading was based on the total gage length of 200 mm, so adjacent strain readings overlapped each other. True strain was calculated as the gage extension (or contraction) divided by the gage length. The gage extension/contraction was found by multiplying the measured change in gage readings by the nominal pivot lever ratio. The pivot lever ratio, which was 0.8:1, related the actual movement to the movement indicated by the digital dial gage.

A gage point spacing of 100 mm was used near the beginning and end of transfer zones. The smaller 50 mm spacing was used in the middle of the transfer region where strain transitions were expected. The majority of the gage points were spaced 50 mm apart. Beams in pour zero had a gage point layout that allowed strain measurements up to approximately 58 in. from the end. Due to short transfer lengths measured in pour zero, the gage point layout in subsequent pours was altered so that the final strain measurement was at about 48 in., and the reduced 100 mm spacing was only used near this location. This layout was used for all beams in subsequent pours except the upside down beams in pour three. These beams had extended gage points at

100 mm spacing so that the last strain measurement was taken at approximately 60 in. from the ends of the beams.

Figure 3.11 DEMEC Gage

3.4.1.2 Data Collection and Transfer of Prestress

Three sets of initial DEMEC readings were taken before the prestress force was transferred. The gage was zeroed on a reference bar before each set of readings. Two researchers took turns reading the DEMEC gage so that user error could be alleviated. If any of the three readings at a given location were significantly different from the other two readings at that location, an additional reading was taken. A sudden release was used to transfer the prestress force to the beams. An acetylene torch was used to cut each strand at a location between two beams (see Figure 3.2). The two outer strands were cut first, followed by the inner strand. Immediately after transfer, a set of DEMEC readings was taken to determine the strain profile and transfer length. Another set of readings was taken one or two weeks later to determine the effect of time on transfer length.

End slip measurements were also obtained at the time of prestress transfer. This end slip refers to the tendency of prestressing strands to draw into the end of a member upon prestress release. End slip was measured with a depth micrometer at the dead end of each beam. Live end measurements were neglected because of distortion from a sudden release. Small cuts of aluminum channel were mounted to each strand with a hose clamp. Each piece of channel served as a reference point for the micrometer. A thin strip of steel plate was glued to the beam end, providing a smooth contact surface for the depth micrometer rod. The steel plate method was not used for beams in pour zero, so these measurements were not very accurate. Initial and final distances between the aluminum bracket and concrete beam end were recorded before and after prestress transfer. The end slip was calculated as the difference between the two measurements.

3.4.2 Development Length

Development length is the length of embedded strand required to develop a full flexural failure. Development length tests were conducted for each end of each beam. The goal was to determine an estimate of development length for four types of strands: 0.5 in. normal grade 270, 0.5 in. normal grade 300, 0.5 in. special grade 270, and 0.5 in. special grade 300. Development lengths were determined by loading each beam end at embedment lengths that varied from test to test. Deflection and strand slip were monitored during each test. If a test resulted in a flexural failure, the development length was assumed to be less than the embedment length at which the load was applied. If a bond failure occurred, the development length was assumed to be greater than the embedment length.

3.4.2.1 Test Setup

Each beam was 24 ft long. A 16 ft span was used for load tests so that a test at one beam end would not damage the other end. Neoprene bearing pads were used for supports, which is typical in bridge applications. It is possible that bearing pad supports can provide horizontal reactions, representing a pin-pin type support condition. However, significant bearing pad movement was observed during tests, so the support condition was assumed to represent a pin-roller support condition. A simple test was conducted to verify this assumption. A beam from pour zero which had already been tested was reloaded to 40 kips four separate times, twice with bearing pads and twice with pin and roller supports. The load vs. deflection behavior from the two support conditions was very similar. Deflections from the pin/roller supported tests were about six percent greater than deflections from bearing pad tests. Thus, the bearing pad supports added about six percent additional stiffness to the system. Because of this small increase, the bearing pads were deemed acceptable and used in subsequent tests. Each 10 in. by 24 in. bearing pad was positioned so that the beam was supported 10 in. along the longitudinal axis and the full bottom flange width in the transverse direction. A hydraulic actuator was mounted to a steel load frame that was bolted to the reaction floor. This actuator applied a single point load through a 10 in. by 20 in. spreader beam. The actuator was connected to a hand pump that was used to apply load. The test set up is illustrated in Figure 3.12.

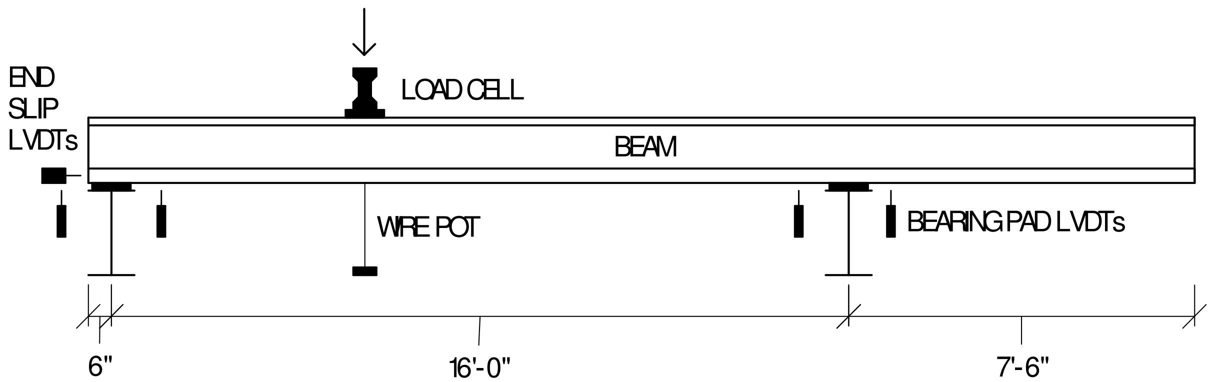

Figure 3.12 Test Setup

3.4.2.2 Instrumentation and Data Acquisition

An array of instrumentation was used to monitor load, deflection, and strand slip during each test. A load cell was used to monitor load. The load cell was calibrated before each set of tests and was accurate to approximately 100 lb. Two types of deflection were measured: apparent deflection and bearing pad deflection. Apparent deflection was measured by a wire pot located immediately below the load point. The wire pot could accurately read deflections as small as 0.01 in. Bearing pad deflection was measured by four linear variable differential transformers (LVDTs). These LVDTs were accurate to 0.001 in. and had a range of about 2 in. LVDTs could not be placed at the centerline of the supports, so two LVDTs were placed at equal distances on both sides of each support centerline. The two LVDT readings at each support were averaged, resulting in a single bearing pad deflection measurement at each support. The ratio of shear span to total span was then used to extrapolate the bearing pad deflection at the load point. The true deflection was calculated by subtracting the bearing pad deflection from the apparent deflection measured by the wire pot. Strand slip was measured for all three strands using LVDTs. These LVDTs had a much smaller range (about 0.1 in.) than those used for bearing pad deflection and could measure movement as small as one millionth of an inch. The LVDTs extended from a bracket mounted to the end of a beam. The spindle contacted one of the seven wires of each strand and detected movement of the strand relative to the end of a beam. The test setup in Figure 3.12 shows where each of these instruments was positioned. Figure 3.13 shows how LVDTs were mounted so that bearing pad deflection and strand slip could be measured.

Figure 3.13 Strand Slip and Deflection Instrumentation

Data was collected with a Vishay Measurements System 5000 scanner and accompanying Strain Smart 5000 data acquisition software. A sample rate of one second was deemed adequate for these load tests. All instruments were directly calibrated within this system. Upon test completion, data files were reduced into Microsoft Excel files for further analysis.

3.4.2.3 Procedure

Each development length test was preceded by flexural crack initiation and reopening tests, which will be discussed in the next section. After these tests, each beam was unloaded and all instruments were zeroed. Load was applied until the previous cracking load was reached, and any unmarked cracks were marked. Load was then increased by two kip increments. Cracks were marked between each increment. Deflection and strand slip were continually monitored during loading. The load was incrementally increased until a flexural or bond failure occurred.

Flexural failures were characterized by concrete crushing and/or fully plastic behavior (increases in deflection without increases in load). Bond failures were classified by 0.01 in. or more strand slip. Some tests also indicated shear failures in the form of web crushing.

3.4.3 Prestress Losses

Prestress losses are decreases in strand stress that occur throughout the life of a prestressed member. The sources of prestress losses relevant to this project were elastic shortening, steel relaxation, concrete creep, and concrete shrinkage. Anchorage seating and early age steel relaxation losses were compensated by shimming strands, as mentioned previously. Prestress losses were experimentally measured using two different methods. One method utilized vibrating wire gages embedded in each beam, permitting continuous measurement of prestress loss. The other method involved flexural crack initiation and crack reopening tests that were performed to determine effective prestress. Prestress losses and effective prestress are directly related. Effective prestress is the stress in strands after prestress losses have occurred. The sum of effective prestress and prestress loss is equal to the initial prestress.

3.4.3.1 Vibrating Wire Gages

Vibrating wire gages were used to experimentally measure prestress losses. One Geokon VCE-4200 vibrating wire gage was placed in each prestressed concrete beam (www.geokon.com). Each gage was comprised of a steel wire stretched between two end blocks and encased by a protective tube. Strain readings were measured as follows. An electronic signal from a data logger interface caused a device inside the gage to pluck the wire. The wire vibrated at a certain frequency, which was measured and reported back to the data logger. The relative location of the two end blocks caused changes in frequency. Strain in the surrounding concrete was therefore determined by the response frequency. Each vibrating wire gage also contained a thermistor for monitoring temperatures.

One vibrating wire gage was placed in each beam at the level of the prestressing strands. The gage was either suspended with plastic cable ties between two of the three strands or tied to one strand with small wooden spacers, as shown in Figure 3.14. The gages were placed 6.5 ft from the live end of the two beams in pour zero. This dimension was reduced to 5.5 ft for all other beams. These locations were in the vicinity of probable embedment lengths for load tests, allowing a logical comparison of vibrating wire gage results and load tests results. Strain readings were recorded with a Campbell Scientific CR3000 Micrologger and an accompanying vibrating wire gage interface. Short recording intervals (one to five minutes) were used from the time of concrete placement to the time of prestress transfer. The recording interval was changed to one hour to monitor strains between prestress transfer and load testing.

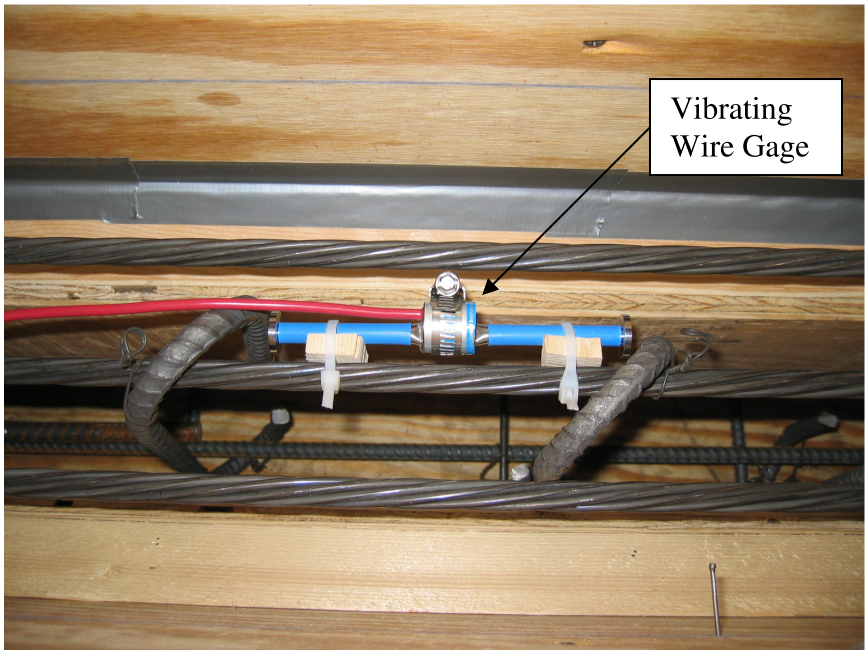

Figure 3.14 Vibrating Wire Gage

3.4.3.2 Flexural Crack Initiation and Reopening Tests

Effective prestress was experimentally determined from the loads required to initiate cracking and reopen the same cracks. These load tests were performed prior to development length load tests. The same instrumentation and procedure that was described for development length tests was used for the crack initiation and reopening tests.

Each crack initiation test was conducted by incrementally loading a beam while measuring concrete surface strains between each increment. Initial load increments were five kips. The increment was reduced to two kips when the applied load approached the anticipated cracking load. Concrete surface strains were measured with a DEMEC strain gage in a manner similar to that used for transfer length tests. Target points were placed on the bottom flange of both sides of each beam so that three strain measurements could be obtained. These points were located near the extreme compression fiber for beams of pour zero. Points were placed at the level of the prestressing strands for all other beams. A plot of load vs. strain was maintained during each test. When the plot became nonlinear, the beam was visually inspected for cracking. If necessary, load was increased until a crack could be visually observed. The crack was marked on the sides and bottom of the beam. The beam was then unloaded for the next test.

Each crack reopening tests was conducted by monitoring strain across a crack while reloading a beam. The strain across a crack was measured with one or two crack detection gages. A crack detection gage, shown in Figure 3.15, was comprised of a metal bracket with an attached strain gage and two contact points that could be affixed to concrete. Crack reopening tests for beams of pours zero and one were conducted with one crack detection gage placed directly over a crack. The beam was loaded at a constant rate, and a plot of load vs. gage strain was monitored. When the plot became nonlinear, the crack was assumed to have reopened. The sampling interval was one second during pour zero tests. Some critical data points were not collected because of the short duration of these tests, so the sampling rate was increased to one tenth of a second for all other tests. A second crack detection gage was used when testing beams of pours three and four. The second gage was placed adjacent to the gage directly over the crack, as shown in Figure 3.16. A plot of load vs. strain from both crack detection gages was monitored during loading. The crack was assumed to have reopened when the strain readings diverged, and the test was considered complete.

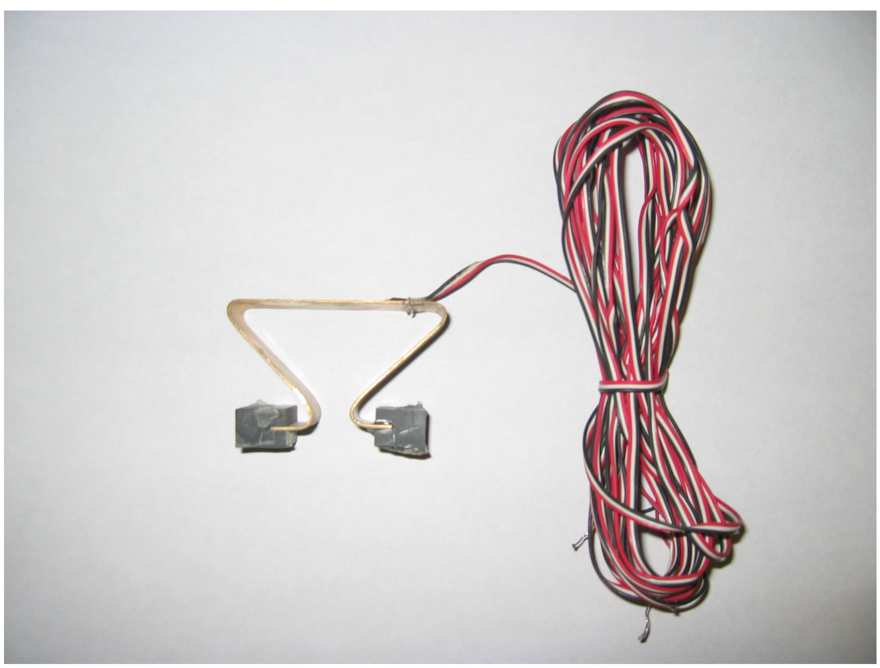

Figure 3.15 Crack Detection Gage

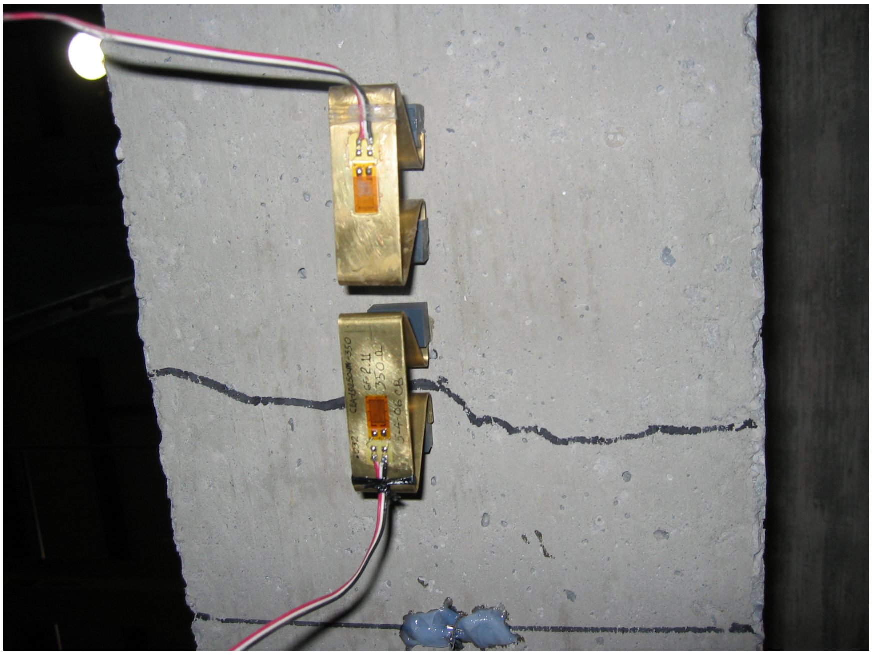

Figure 3.16 Measurement of Crack Reopening

4. TEST RESULTS, ANALYSIS, AND DISCUSSION

4.1 Transfer Length and End Slip

Concrete surface strains in the end regions of each test beam were measured before and after prestress transfer. A total of 23 transfer lengths were determined from the resulting concrete strain profiles. End slips at the dead ends of beams in pours one, three, and four were also measured. Average end slips were obtained at the ends of ten beams.

4.1.1 Material Properties

The prestress was not transferred to concrete beams until a minimum initial compressive strength of 4500 psi was attained. This ensured that concrete stresses in the beams (tensile and compressive) would be less than AASHTO stress limits (2006). Compressive strength was monitored after each concrete pour. Strength gain plots for pours one, three, and four are provided in Appendix A. No strength gain plot was attained for pour zero because of a lack of test cylinders and a holiday break. Once the desired compressive strength was achieved, DEMEC points were mounted, initial gage point distances were recorded, and prestressing strands were cut. Table 4.1 shows the initial concrete compressive strength at the time of transfer for each pour. Modulus of elasticity tests were also performed at transfer for pours three and four. The modulus of elasticity measured for the fourth pour was significantly low. The last column of the table shows the modulus of elasticity that would be calculated according to current code provisions. The unit weight was assumed to be 150 lb/ft^3. Results from all initial concrete material testing are provided in Appendix A.

Table 4.1 Initial Concrete Material Properties

Pour	Concrete Age at Transfer (days)	f'_{ci} (psi)	E_{ci} (ksi)	$33w_c^{1.5}f'^{0.5}_{ci}$ (ksi)
Zero	3	4870	No Data	4230
One	9	5330	No Data	4430
Three	12	5970	4120	4680
Four	6	4850	2960	4220

4.1.2 Data Reduction and Determination of Transfer Length

DEMEC point measurements were taken before and after prestress transfer. The difference between DEMEC gage readings at each location was multiplied by the pivot ratio of the DEMEC extensometer (0.8:1) and divided by the gage length (200 mm) to obtain the strain. Measurement of strain at multiple points along the end of each beam produced a strain profile like the one shown in Figure 4.1. The plot shows initial strain readings on both sides of the beam end, as well as strain readings recorded 15 days after prestress transfer. Most of the strain profiles were smooth and had very few irregular points, so a smoothing function or running average was not necessary.

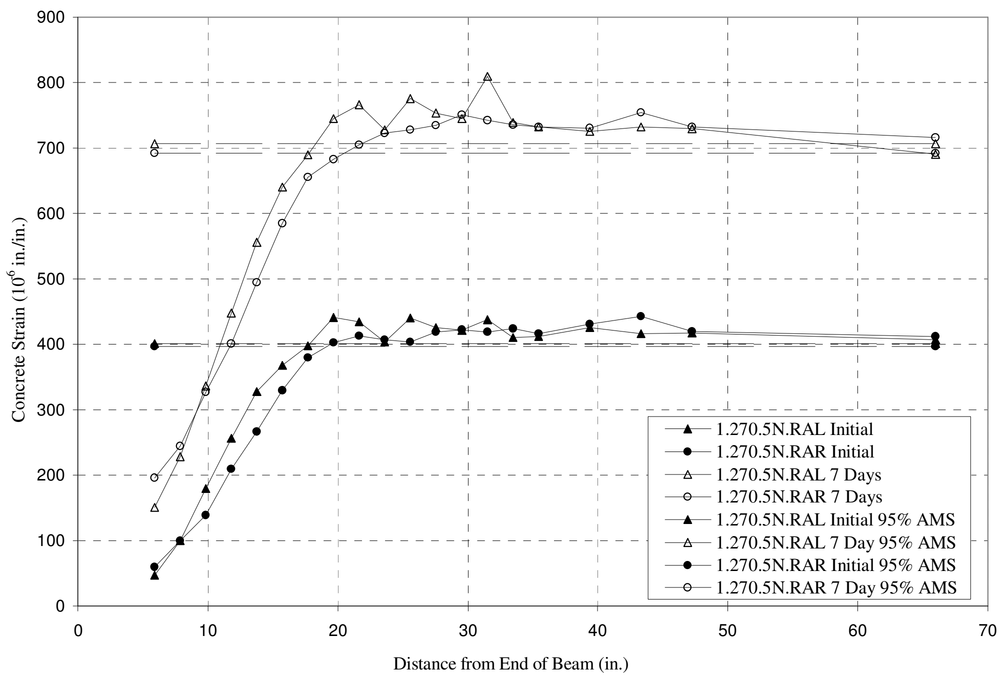

Figure 4.1 Strain Profile for 1.270.5N.RA

Next, a transfer length had to be derived from the strain profile. The 95 percent average maximum strain (95% A.M.S.) technique was chosen to determine transfer length. This generally accepted method was used by Barnes, et al. (2003) and recommended by Buckner (1994). Details of the method are described below.

1. The point at which the strain plateau began is identified.
2. The strain of all points in the plateau are averaged.
3. The average maximum strain plateau is reduced by 5 percent.
4. The intersection of the strain profile and 95 percent strain plateau is determined.

Visual inspection was used to determine the beginning of the strain plateau as well as the intersection of the strain profile and 95 percent average maximum strain. The 95 percent average maximum strain profile is represented by a dashed line in strain profile plots. A transfer length for each side of each beam end was determined in this manner. The transfer lengths of the two sides of each beam end were averaged and reported to the nearest half inch. Strain profiles for all 23 transfer zones are provided in Appendix B.

4.1.3 Initial and Final Transfer Length Results

Results from all initial transfer length measurements are shown in Table 4.2. The measured transfer lengths are compared to three different code provisions for transfer length. The first comparison is the ratio of measured transfer length to the ACI provision in Section 11.4.4, which is 50 strand diameters, or 25 in. for all specimens tested (2005). Only four measured transfer lengths exceeded this stipulation. Next, the measured transfer lengths are compared to the AASHTO Article 5.11.4.1 recommendation of 60 strand diameters, or 30 in. for 0.5 in. diameter strands (2006). Only two measured transfer lengths were greater than 30 in. The final comparison is the ratio of measured transfer length to the expression $f_{si}*d_b/3$, which is similar to the transfer length portion of the ACI development length equation (2005). This provision for transfer length differs from the other two because it incorporates strand stress. The initial prestress (just after transfer) was used to calculate the transfer length instead of the effective prestress, which has been suggested by Shahawy (2001) and Buckner (1994). The initial prestress was calculated by subtracting the theoretical elastic shortening loss from the jacking stress, assumed to be 75 percent of guaranteed ultimate tensile strength. The expression resulted in a transfer length of approximately 32 in. for normal and special grade 270 strands, and approximately 35 in. for normal and special grade 300 strands.

Table 4.2 Initial and Final Transfer Length Measurements

Beam Designation	Casting Orientation	Beam End	Strand Type	Initial l_t (in.)	$l_{t,MEASURED}/l_{t,ACI}$	$l_{t,MEASURED}/l_{t,AASHTO}$	$l_{t,MEASURED}/f_{si}*d_b/3$	Final l_t (in.)	$l_{t,FINAL}/l_{t,INITIAL}$	Time of 2nd Reading
0.270.5N.RA	Normal	Live	270 Norm.	15.0	0.60	0.50	0.47	15.0	1.00	15 Days after Transfer
0.270.5N.RB	Normal	Dead	270 Norm.	12.0	0.48	0.40	0.38	13.5	1.13	
0.300.5N.RB	Inverted	Dead	300 Norm.	14.0	0.56	0.47	0.40	15.0	1.07	
1.270.5N.RA	Normal	Live	270 Norm.	18.5	0.74	0.62	0.58	19.5	1.05	7 Days after Transfer
1.270.5N.RB	Normal	Dead	270 Norm.	11.5	0.46	0.38	0.36	13.0	1.13	
1.300.5N.RA	Normal	Live	300 Norm.	21.0	0.84	0.70	0.60	21.0	1.00	
1.300.5N.RB	Normal	Dead	300 Norm.	14.0	0.56	0.47	0.40	15.0	1.07	
1.270.5N.UA	Inverted	Live	270 Norm.	30.0	1.20	1.00	0.94	30.0	1.00	
1.270.5N.UB	Inverted	Dead	270 Norm.	25.0	1.00	0.83	0.78	27.0	1.08	
1.300.5N.UA	Inverted	Live	300 Norm.	43.0	1.72	1.43	1.23	44.0	1.02	
1.300.5N.UB	Inverted	Dead	300 Norm.	22.0	0.88	0.73	0.63	24.5	1.11	
3.270.5S.RA	Normal	Live	270 Spec.	22.0	0.88	0.73	0.69	22.5	1.02	7 Days after Transfer
3.270.5S.RB	Normal	Dead	270 Spec.	13.5	0.54	0.45	0.42	14.0	1.04	
3.300.5S.RA	Normal	Live	300 Spec.	21.0	0.84	0.70	0.60	23.0	1.10	
3.300.5S.RB	Normal	Dead	300 Spec.	15.0	0.60	0.50	0.43	16.0	1.07	
3.270.5S.UA	Inverted	Live	270 Spec.	28.0	1.12	0.93	0.88	28.5	1.02	
3.270.5S.UB	Inverted	Dead	270 Spec.	21.0	0.84	0.70	0.66	22.0	1.05	
3.300.5S.UA	Inverted	Live	300 Spec.	39.0	1.56	1.30	1.11	41.0	1.05	
3.300.5S.UB	Inverted	Dead	300 Spec.	22.0	0.88	0.73	0.63	23.5	1.07	
4.270.5S.RA	Normal	Live	270 Spec.	18.0	0.72	0.60	0.56	18.5	1.03	12 Days after Transfer
4.270.5S.RB	Normal	Dead	270 Spec.	15.0	0.60	0.50	0.47	19.0	1.27	
4.300.5S.RA	Normal	Live	300 Spec.	18.5	0.74	0.62	0.53	20.0	1.08	
4.300.5S.RB	Normal	Dead	300 Spec.	14.0	0.56	0.47	0.40	16.0	1.14	
Average				20.6	0.82	0.69	0.61	21.8	1.07	

The results from the second set of transfer length measurements are also shown in Table 4.2. The time at which the second set of readings was taken varied from pour to pour. In pour zero, the average increase in transfer length over 15 days was about seven percent. In both pours one and three, transfer lengths increased approximately six percent in seven days. The average increase in pour four was 14 percent in twelve days. Barnes, et al. found that long term transfer lengths generally increase 10 to 20 percent and also noted that the majority of the increase occurred in the first four weeks after prestress transfer (2003). While the final transfer length measurements in this study were taken only one to two weeks after prestress transfer, it is reasonable to assume that the eventual long term increase would only have been between 10 and 20 percent.

Figure 4.2 presents the final measured transfer lengths in a visual manner. The final transfer length of each beam end is shown as its ratio to the strand diameter (0.5 in.). Transfer lengths of normally cast beams are shown above the horizontal dotted line, while inverted beam transfer lengths are below the dotted line. The three bold vertical lines represent 50 strand diameters (ACI provision), 60 strand diameters (AASHTO provision), and 90 strand diameters. The transfer lengths of all beam ends with normal casting orientation were less than the current ACI and AASHTO provisions. However, several of the transfer lengths of beam ends with inverted casting orientation exceeded current code provisions. All measured transfer lengths were less than 90 strand diameters.

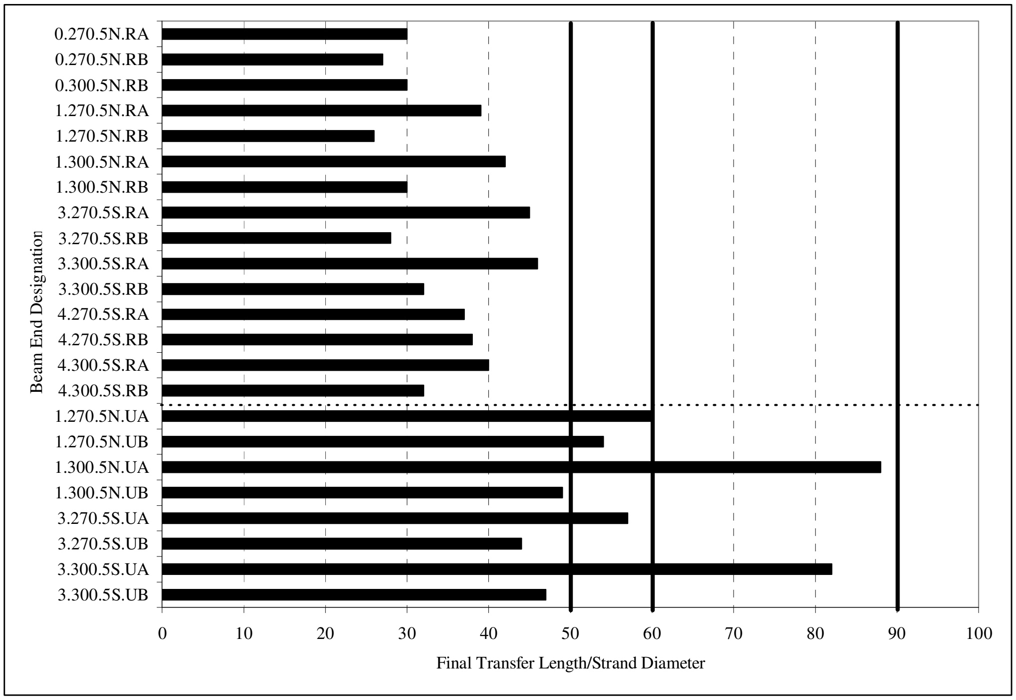

Figure 4.2 Normalized Final Transfer Lengths

4.1.4 Effect of Strand Grade on Transfer Length

Beams were poured in a manner such that each beam with grade 270 prestressing strands would have a partner beam in the same pour with grade 300 prestressing strands and the same casting orientation. This permitted eleven head to head comparisons among 22 of the 23 transfer zones (the transfer length of 0.300.5N.RA could not be measured because of concrete issues previously discussed). These comparisons are provided in Table 4.3. Also shown are comparisons of jacking stress and initial prestress. The initial prestress was the stress in strands just after transfer computed according to the basic vibrating wire gage method. The average increase in transfer length was about 12 percent. Similarly, the average increase in jacking stress and initial prestress was about 10 percent. Large increases in transfer length (40 to 43 percent) were observed in the comparisons of strand grade for live ends of inverted beams. In three of the comparisons, the grade 300 transfer length was shorter than the grade 270 transfer length.

Table 4.3 Effect of Strand Grade on Transfer Length

Beam Designation	Strand Type	Initial l_t (in.)	$l_{t,300}/l_{t,270}$	f_{pj} (ksi)	$f_{pj,300}/f_{pj,270}$	f_{pi} (ksi)	$f_{pi,300}/f_{pi,270}$
0.300.5N.RB 0.270.5N.RB	300 Norm. 270 Norm	14.0 12.0	1.17	223 200	1.11	210 187	1.12
1.300.5N.RA 1.270.5N.RA	300 Norm. 270 Norm	21.0 18.5	1.14	225 207	1.09	212 195	1.09
1.300.5N.RB 1.270.5N.RB	300 Norm. 270 Norm	14.0 11.5	1.22	225 207	1.09	212 195	1.09
1.300.5N.UA 1.270.5N.UA	300 Norm. 270 Norm	43.0 30.0	1.43	225 207	1.09	211 195	1.08
1.300.5N.UB 1.270.5N.UB	300 Norm. 270 Norm	22.0 25.0	0.88	225 207	1.09	211 195	1.08
Average Ratio for Normal Strands			1.17		1.09		1.09
3.300.5S.RA 3.270.5S.RA	300 Spec. 270 Spec.	21.0 22.0	0.95	225 203	1.11	211 190	1.11
3.300.5S.RB 3.270.5S.RB	300 Spec. 270 Spec.	15.0 13.5	1.11	225 203	1.11	211 190	1.11
3.300.5S.UA 3.270.5S.UA	300 Spec. 270 Spec.	39.0 28.0	1.39	225 203	1.11	211 190	1.11
3.300.5S.UB 3.270.5S.UB	300 Spec. 270 Spec.	22.0 21.0	1.05	225 203	1.11	211 190	1.11
4.300.5S.RA 4.270.5S.RA	300 Spec. 270 Spec.	18.5 18.0	1.03	226 202	1.12	210 188	1.12
4.300.5S.RB 4.270.5S.RB	300 Spec. 270 Spec.	14.0 15.0	0.93	226 202	1.12	210 188	1.12
Average Ratio for Special Strands			1.08		1.11		1.11
Average Ratio for All Strands			1.12		1.10		1.10

4.1.5 Effect of Casting Orientation on Transfer Length

In pours one and three, two beams were cast upside down to complement the other two right side up beams. This allowed eight comparisons of casting orientation among 16 transfer zones. The only difference in each comparison was the depth of concrete below prestressing strands. Beams cast in the normal position had 2 in. of fresh concrete below the strands. Beams cast in the inverted position had either 15 or 17 in. of fresh concrete below the strands, depending on whether the overall section height was 17 or 19 in. The comparison of casting orientation is shown in Table 4.4. The inverted section transfer length was greater than the normal transfer length in each case. The increase in transfer length ranged from 26 percent to 120 percent, with an average of 69 percent. The slope of each concrete strain profile was also determined. This slope provided an indication of the bond stress according to the following premise. The plots of prestressing strand strain and concrete strain in the end of a member have a similar shape but different magnitude. Since bond stress is a linear function of the derivative of steel strain with respect to length, the derivative of concrete strain with respect to length must be an indication of the magnitude of bond stress. The slope of the inclined portion of each transfer length plot was determined by linear regression. The average ratio of inverted beam strain profile slope to normal beam strain profile slope was 0.58. This suggested an average 42 percent decrease in bond stress for beams cast in an inverted orientation.

Table 4.4 Top Strand Effect on Transfer Length

Beam Designation	Casting Orientation	Initial l_t (in.)	$l_{t,INVERTED}$/ $l_{t,NORMAL}$	$d\varepsilon_c/dx$ ($\mu\varepsilon$/in.)	$(d\varepsilon_c/dx)_{INV}$/ $(d\varepsilon_c/dx)_{NORM}$
1.270.5N.UA 1.270.5N.RA	Inverted Normal	30.0 18.5	1.62	16.3 27.7	0.59
1.270.5N.UB 1.270.5N.RB	Inverted Normal	25.0 11.5	2.17	13.5 22.4	0.60
1.300.5N.UA 1.300.5N.RA	Inverted Normal	43.0 21.0	2.05	15.3 26.5	0.58
1.300.5N.UB 1.300.5N.RB	Inverted Normal	22.0 14.0	1.57	15.5 29.5	0.53
Average Ratio for Normal Strands			1.85		0.57
3.270.5S.UA 3.270.5S.RA	Inverted Normal	28.0 22.0	1.27	16.9 25.0	0.68
3.270.5S.UB 3.270.5S.RB	Inverted Normal	21.0 13.5	1.56	16.4 25.4	0.65
3.300.5S.UA 3.300.5S.RA	Inverted Normal	39.0 21.0	1.86	15.8 27.9	0.57
3.300.5S.UB 3.300.5S.RB	Inverted Normal	22.0 15.0	1.47	13.1 29.2	0.45
Average Ratio for Special Strands			1.54		0.58
Average Ratio for All Strands			1.70		0.58

Figure 4.3 illustrates the different surface strain behavior exhibited by beams with inverted casting orientation. Initial strain profiles for beam ends 3.300.5S.RA and 3.300.5S.UA are superimposed in this plot. Displayed strain values are the average strains from left and right sides of each beam end. The transfer length of the inverted beam was much longer than the transfer length of the normal beam. Conversely, the slope of the strain profile in the transfer region was less for the inverted beam. The plot for 3.300.5S.UA also exhibited unique bilinear behavior in the transfer region. Concrete strain varied linearly with an initial slope. Then the

slope increased for the remainder of the transfer zone. This behavior was also evident in the strain profile of beam end 1.300.5N.UA.

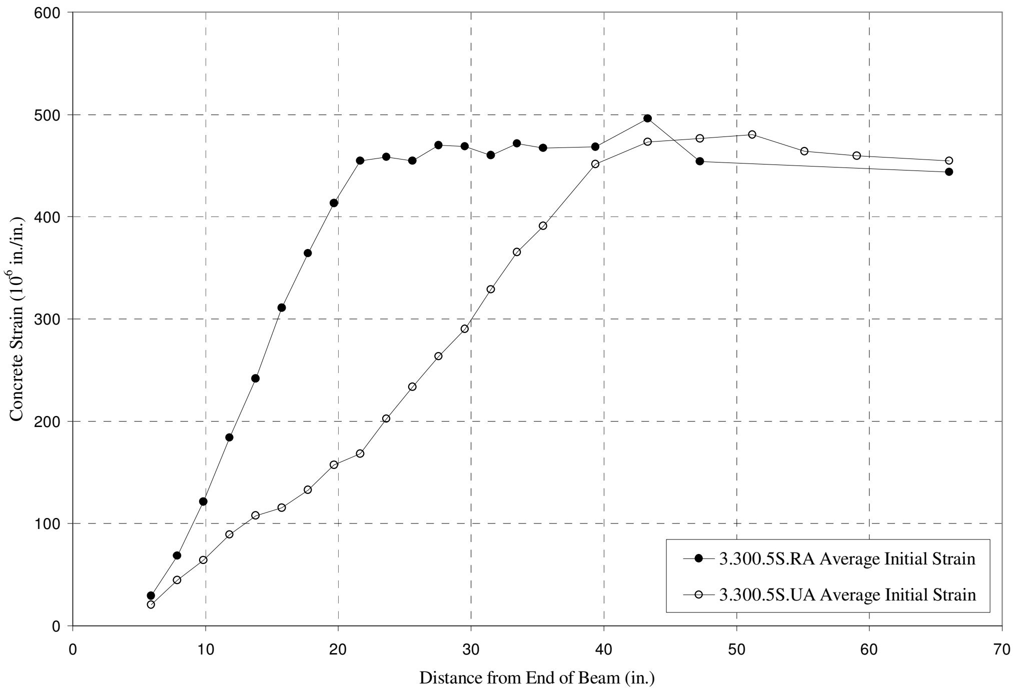

Figure 4.3 Effect of Casting Orientation on Surface Strains in the Transfer Region

4.1.6 End Slip Results and Comparison to Measured Transfer Lengths

End slip was measured for each strand at the dead end of each beam in pours one, three, and four. Table 4.5 shows the end slip for each individual strand, as well as the average end slip for each beam end. The end slip of beam end 1.300.5N.RB was significantly less than other beam ends. Inverted beams exhibited longer end slips than normal beams. It is important to note that the end slip of the center strand in inverted beams was longer than that of the outer strands. This was likely due to a decreased depth of fresh concrete below the outer strands because of the web block out.

Table 4.5 End Slip Measurements

Beam Designation	Casting Orientation	Left Strand End Slip (in.)	Center Strand End Slip (in.)	Right Strand End Slip (in.)	Average End Slip (in.)
1.270.5N.RB	Normal	0.050	0.040	0.040	0.043
1.300.5N.RB	Normal	0.009	0.016	0.017	0.014
1.270.5N.UB	Inverted	0.053	0.081	0.067	0.067
1.300.5N.UB	Inverted	0.106	0.109	0.083	0.099
3.270.5S.RB	Normal	0.048	0.049	0.049	0.049
3.300.5S.RB	Normal	0.061	0.056	0.052	0.056
3.270.5S.UB	Inverted	0.075	0.089	0.038	0.067
3.300.5S.UB	Inverted	0.076	0.106	0.081	0.088
4.270.5S.RB	Normal	0.053	0.066	0.056	0.058
4.300.5S.RB	Normal	0.070	0.071	0.055	0.065

The measured end slips were compared to end slips calculated from measured transfer lengths according to the following model. An idealized plot of prestressing steel strain and concrete strain vs. beam length is shown below. The general shape of the two strain curves is similar, but the magnitude of the steel strain curve is greater.

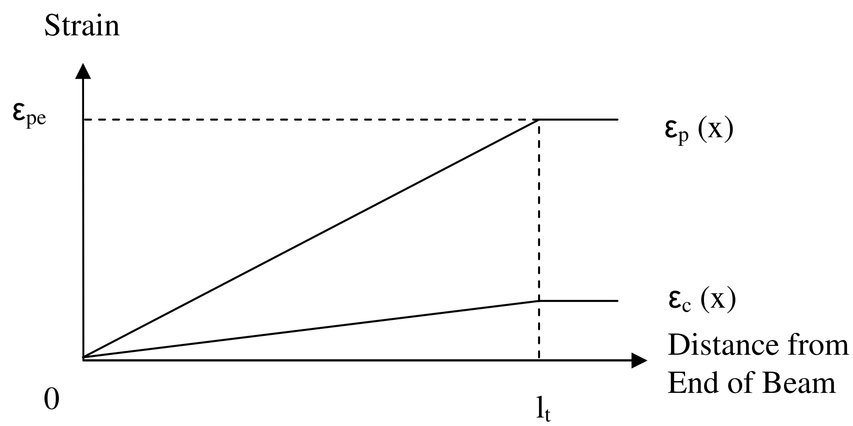

Figure 4.4 Idealized Strain Plot

The elastic shortening of the beam over the transfer region is calculated by Equation 4.1 below. The sum of elastic shortening and end slip is calculated by Equation 4.2 below.

$$ES_{TransferLength} = \int_0^{l_t} \varepsilon_c(x)dx \qquad 4.1$$

$$ES_{TransferLength} + L_{es} = \varepsilon_{pi} l_t - \int_0^{l_t} \varepsilon_p(x)dx \qquad 4.2$$

The two equations above are solved to find end slip. Integration of the end slip expression, assuming linear strain curves, yields Equation 4.3.

$$L_{es} = \frac{l_t}{2}\left(\frac{f_{pi}}{E_{ps}} + \varepsilon_{ci}\right) \qquad 4.3$$

Where:

L_{es} = end slip (in.)

l_t = transfer length (in.)

f_{pi} = stress in prestressing strands immediately after transfer (ksi)

E_{ps} = modulus of elasticity of prestressing steel (ksi)

ε_{ci} = magnitude of concrete strain plateau immediately after transfer (in./in.)

The initial measured transfer lengths and average measured end slips are presented together with the calculated end slips in Table 4.6. The first set of calculated end slips was computed with Equation 4.3. The effective prestress was assumed to be the jacking stress minus the elastic shortening loss measured with the vibrating wire gage. The effective concrete strain was taken from surface strain profiles. The table also shows end slip calculated by Equation 2.5, which is an expression of transfer length as a function of end slip (Guyon 1960). The expression was rearranged so that end slip could be calculated as a function of measured transfer length. If the concrete strain term in Equation 4.3 is neglected and the stress just before transfer is used, the expression is the same as Equation 2.5. The end slips calculated by Equation 2.5 and Equation 4.3 are essentially the same. Most of the calculated end slips correlated well with the measured end slips.

Table 4.6 Comparison of End Slip Measurements and Calculations

Beam Designation	Measured l_t (in.)	Measured End Slip (in.)	Calculated End Slip (in.)	Calculated/ Measured	Guyon End Slip (in.)	Calculated/ Measured
1.270.5N.RB	11.5	0.043	0.042	0.98	0.042	0.98
1.300.5N.RB	14.0	0.014	0.055	3.93	0.055	3.93
1.270.5N.UB	25.0	0.067	0.092	1.37	0.091	1.36
1.300.5N.UB	22.0	0.099	0.087	0.88	0.086	0.87
3.270.5S.RB	13.5	0.049	0.046	0.94	0.047	0.96
3.300.5S.RB	15.0	0.056	0.058	1.04	0.057	1.02
3.270.5S.UB	21.0	0.067	0.073	1.09	0.073	1.09
3.300.5S.UB	22.0	0.088	0.084	0.95	0.084	0.95
4.270.5S.RB	15.0	0.058	0.052	0.90	0.052	0.90
4.300.5S.RB	14.0	0.065	0.054	0.83	0.054	0.83
Average*	17.3	0.066	0.064	1.00	0.064	0.99

*Beam end 1.300.5N.RB is neglected in the averages involving measured end slip.

4.1.7 Additional Transfer Length Discussion

The transfer lengths measured for beams of pour one were significantly longer than those measured in other pours. A large amount of bleed water was observed in the fresh concrete, and was suspected as the reason for the large transfer lengths. Two beams from pour zero and two beams from pour one were cut open to investigate differences in strand/concrete bond interface appearance, if any. Figure 4.5 shows a section of concrete cut from a beam in each pour. These are corner sections of the bottom flange, so the helical impression is from outer strands. No noticeable differences were observed. The bond interface between concrete and strands appeared uniform with no significant air voids. The effect of the bleed water on transfer length was therefore ignored.

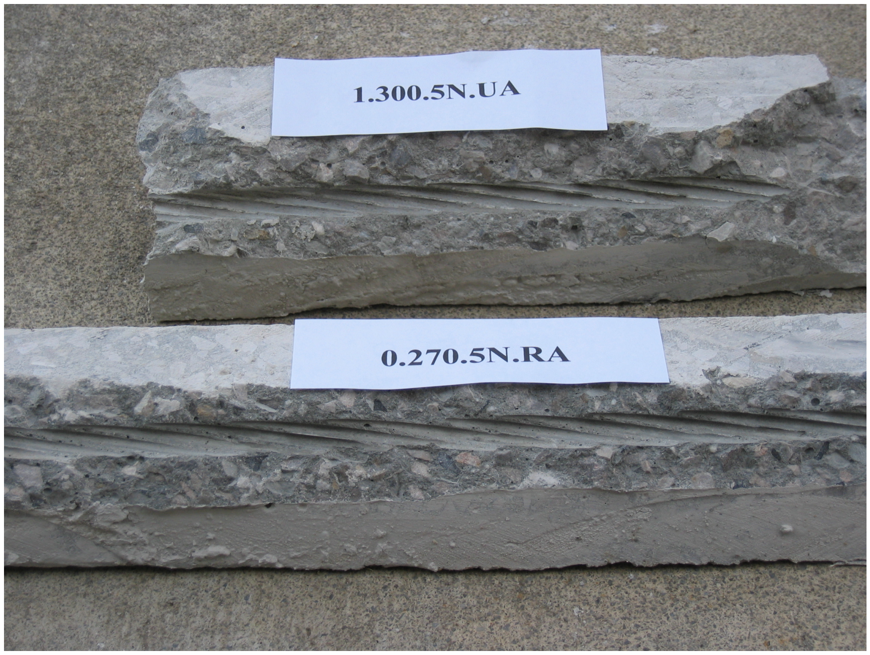

Figure 4.5 Bond Interface between Prestressing Strands and Concrete

In some transfer zones, the strains on opposite sides of a beam end differed by as much as 200 microstrain. Weak axis strand eccentricity was first suspected as the cause for this difference. This eccentricity would result from strands not being exactly centered between the sides of the bottom flange. However, a large tolerance of 0.25 in. eccentricity would have only resulted in a strain difference on the order of ten microstrain. The other possible explanation was that the flame cutting sequence caused differences in strain on opposite sides of a beam. The outer strands were cut one after the other, followed by the inner strand. This may have caused the observed differences in strain.

The increased cross sectional area of special strands suggested a possible increase in transfer length. When comparing similar pairs of beams with normal casting orientation, special strands exhibited larger transfer lengths in some cases, but not others. In comparisons of beams with inverted casting orientation, special strands exhibited transfer lengths that were equal to or shorter than normal strands.

4.2 Development Length

Experimental estimates of development length were determined through iterative load testing. Each end of each beam was tested, with the exception of the live end of the grade 300 beam in pour zero. A total of 23 tests allowed development lengths to be determined for four types of prestressing strand: normal grade 270, normal grade 300, special grade 270, and special grade 300. All strands had 0.5 in. diameter, but the cross sectional area varied between 0.153 and 0.167 in.^{2} for normal and special strands, respectively. For each type of strand, three to four tests were conducted for normally cast beams, while two tests were performed for beams with inverted casting orientation. Therefore, a total of eight development length ranges were obtained.

4.2.1 Material Properties

Beams were tested a minimum of three weeks after being cast. Observation of compressive strength gain plots (shown in Appendix A) indicated that changes in concrete strength after three weeks would be minimal. Neglect of additional compressive or tensile strength gain over the testing period is also supported by comparison of cylinder test data within each pour. Test results exhibited inherent variation with no strength gain trend. At least two compressive strength tests, one splitting tensile strength test, and one modulus of elasticity test were performed each day that flexural load tests were conducted. Results from all cylinder tests are provided in Appendix A.

Concrete material properties at the time of testing are summarized in Table 4.7. The table shows the mean and standard deviation for all tests of compressive strength, tensile strength, and modulus of elasticity within each pour. The average compressive strength achieved in pours zero, one, and three was just above the target strength of 6000 psi, while the average compressive strength in pour three was about 2000 psi greater than the target strength. Code provisions for tensile strength and modulus of elasticity are also included in the table. The tested tensile strengths from split cylinder tests were slightly greater than code provisions in pours one, three, and four. In general, the tested modulus of elasticity was significantly less than the recommended code provision for calculating modulus of elasticity as a function of compressive strength.

Table 4.7 Final Concrete Material Properties

Pour	Average Concrete Age (days)	f'_c (psi)		f_t (psi)			E_c (ksi)		
		Mean	Std. Dev.	Mean	Std. Dev.	$7.5f'_c{}^{0.5}$	Mean	Std. Dev.	$33w_c{}^{1.5}f'_{ci}{}^{0.5}$
Zero	26	6540	130	605	19	607	2900	745	4900
One	21	6420	90	664	30	601	2370	601	4860
Three	45	8190	70	731	16	679	5120	117	5490
Four	30	6250	120	691	17	593	3520	73	4790

4.2.2 Failure Modes and Determination of Development Length

Estimates of development length were determined through iterative load testing. The embedment length (distance from the concentrated load to the nearest beam end) was varied from test to test by 6 in. increments. Tests were divided into eight groups according to strand grade, strand area, and casting orientation. Within each group, beams were loaded at several different embedment lengths. The load points were chosen so that some tests resulted in bond failures (shorter embedment lengths) while other tests resulted in flexural failures (longer embedment lengths). If a bond failure occurred, the embedment length was assumed to be less than the development length. Conversely, a flexural failure indicated that the embedment length was greater than the development length. This iterative process yielded an estimated range of development length for all four strand types in normal and inverted beams.

Several modes of failure were observed. A flexural failure was characterized by crushing of concrete at the extreme compression fiber. In two tests, the prestressing strands ruptured, resulting in complete sudden failures. If concrete crushing or strand rupture occurred, the strands were fully developed and the tested embedment length was greater than the development length. A bond failure was indicated by an average strand slip of 0.01 in. This threshold was used by Simmons (1995). Most test results showed that once strand slip reached 0.01 in., little or no additional load could be resisted. If average strand slip exceeded 0.01 in., the strands were not fully developed and the tested embedment length was less than the development length. In two tests, crushing of concrete in the top of the section occurred after average strand slip exceeded the 0.01 in. threshold. The embedment lengths used in these two tests were assumed to be the same as or near the development length. Three of the tests that resulted in bond failure were also accompanied by shear failure indicated by web crushing.

4.2.3 Moment vs. Deflection and Moment vs. Strand Slip Behavior

Beam deflection and strand slip were monitored and recorded during each flexural test. Plots of bending moment vs. deflection and bending moment vs. strand slip for each load test are provided in Appendix C. Since the load point varied between tests, bending moment was plotted rather than applied load, allowing more meaningful comparisons between different tests. A representative moment vs. deflection plot is shown in Figure 4.6. This beam test exhibited generally tri-linear behavior typical of prestressed concrete beams. The three linear segments of the plot are separated by zero moment, cracking moment, yield moment, and ultimate capacity. Some beam tests exhibited curvilinear behavior between the yield moment and ultimate capacity, and significant additional load was sustained after first yielding. This may be attributed to the fact that the strands had higher ultimate strength and more ductility than minimum specified values (see Figure 3.5 and Table 3.3).

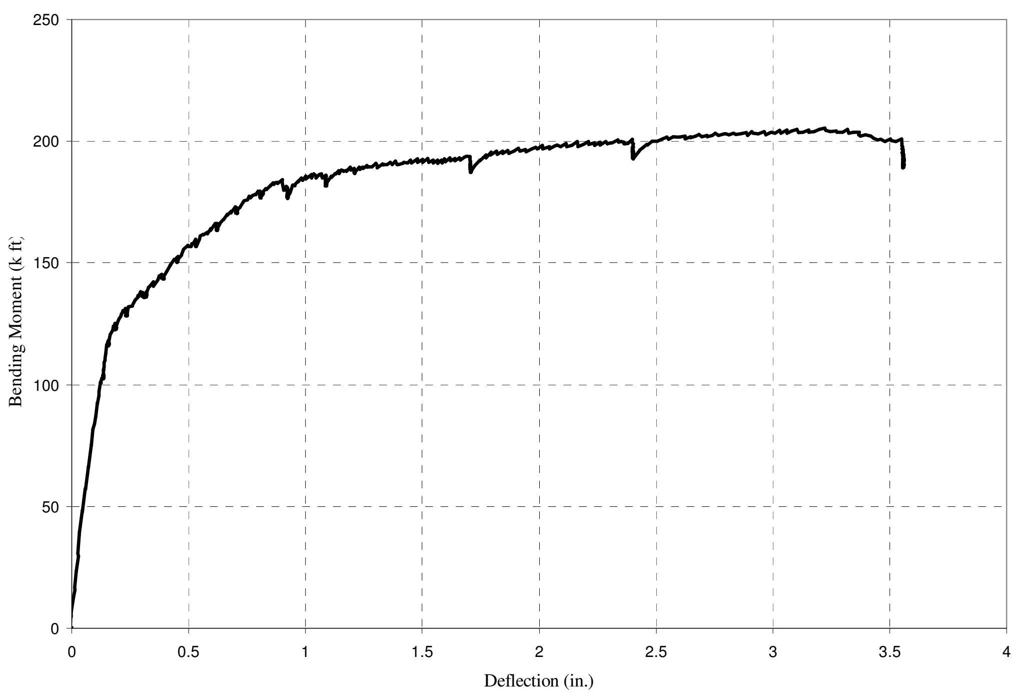

Figure 4.6 Bending Moment vs. Deflection for 1.270.5N.UA

Strand slip for all three strands was plotted for each load test. The bending moment vs. strand slip plot that accompanies the bending moment vs. deflection plot above is shown in Figure 4.7. This is an example of one of the two tests in which concrete crushing occurred after the average strand slip exceeded 0.01 in. This plot supports the bond failure criteria presented previously. Once the average strand slip exceeded 0.01 in., little additional load was resisted. The deflection significantly increased after this threshold, which is evident from the moment vs. deflection plot above. An additional bending moment vs. strand slip plot is shown in Figure 4.8. This test resulted in a flexural failure with no significant strand slip. However, a small scale on the strand slip axis illustrates a behavior pattern characteristic of some of the load tests. Strands initially push away from the beam end (negative slip) before drawing back into the beam end (positive slip). An explanation for this behavior was not determined. However, the strand movement was very small, and therefore ignored.

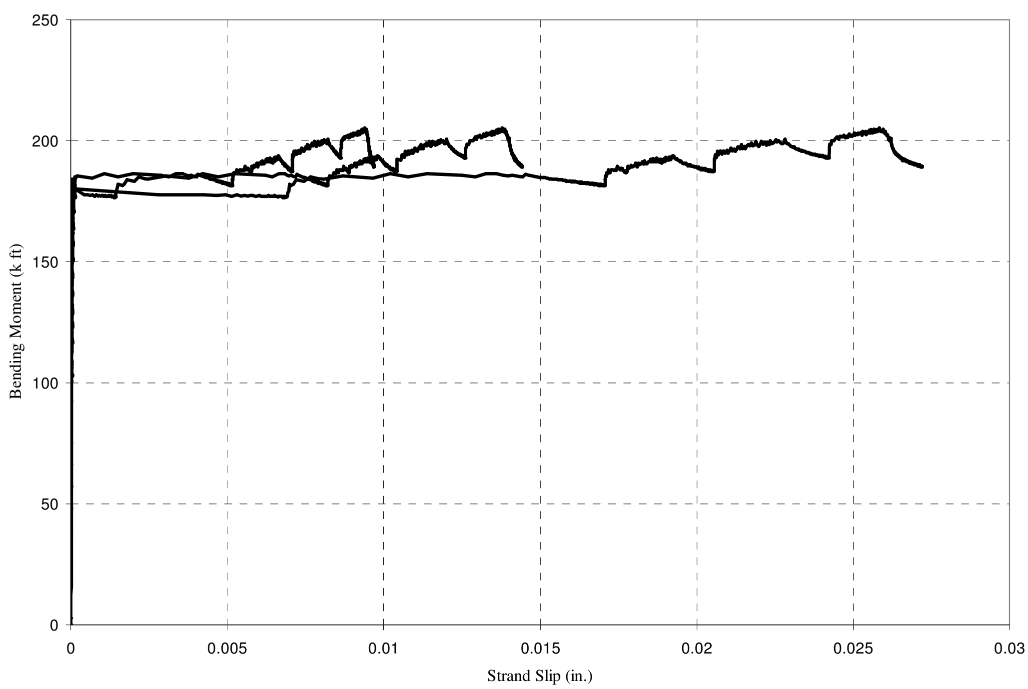

Figure 4.7 Bending Moment vs. Strand Slip for 1.270.5N.UA

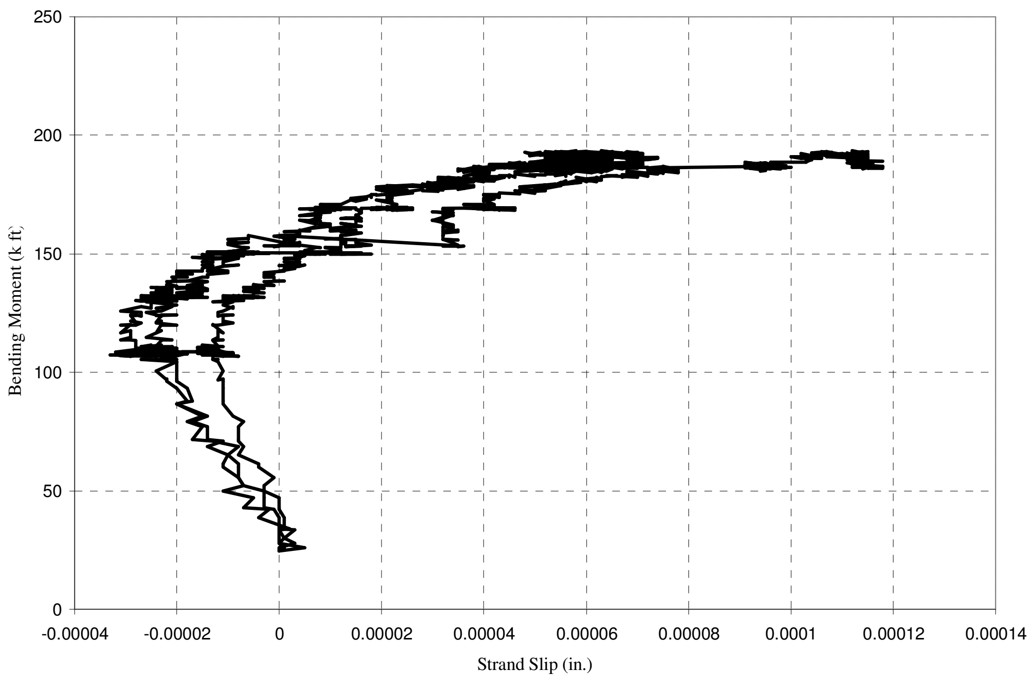

Figure 4.8 Bending Moment vs. Strand Slip for 0.270.5N.RA

4.2.4 Crack Patterns

Beams were loaded incrementally in each load test. The beams were inspected for cracking between each load increment, and any visible cracks were traced with a permanent marker. The corresponding load was recorded at the terminus of each crack. The cracking patterns were typical of flexural beam tests. The first flexural cracks began at the bottom of the section below the load point. As the load increased, additional cracks developed at semi-regular spacing. The propagation of each crack was initially vertical, followed by a turning towards the load point. Flexural cracks near the load point terminated at the location corresponding to the calculated depth of the neutral axis. Figure 4.9 illustrates the flexural cracking behavior that was characteristic of most beam tests. Some beam tests also resulted in web shear cracks. These diagonal cracks formed in the web of the beam between the load point and closest support. Initial strand slip often occurred at the same time that a web shear crack crossed the centroid of the prestressing strands. This type of behavior was also observed by Shahawy (2001). Figure 4.10 shows an example of web shear cracking, with a crack that has extended to the bottom of the section.

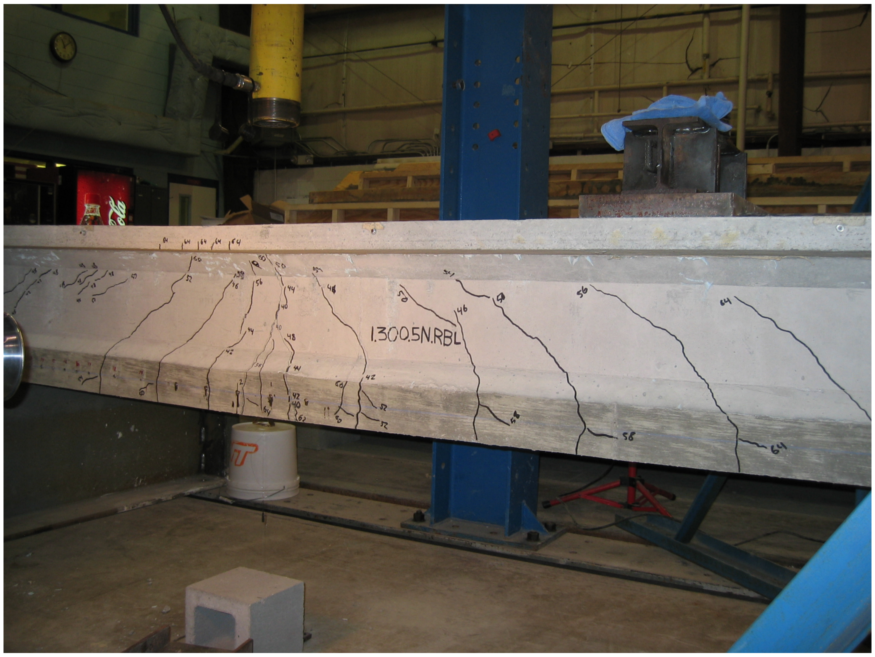

Figure 4.9 Flexural Cracks for 1.300.5N.RB

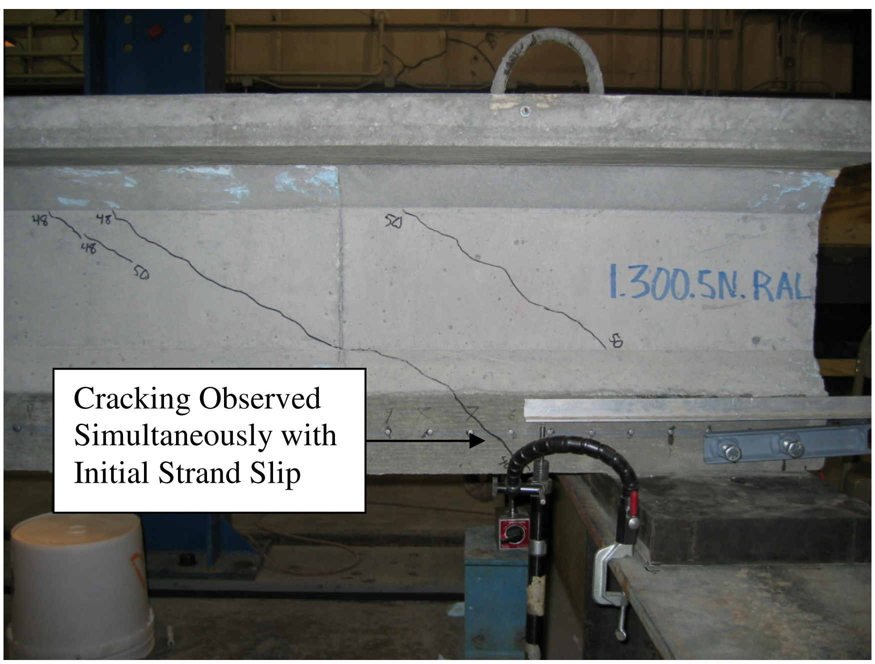

Figure 4.10 Web Shear Cracks for 1.300.5N.RA

4.2.5 Development Length Results

Development length test results are presented in Table 4.8. The data are grouped according to the four tested strand types. The bold line within each strand type separates normal cast beams from those with inverted casting orientation. The final transfer length measurement for each beam end is included. The self weight bending moment was ignored since it was only one to two percent of the maximum applied moment. The maximum applied moment is compared to two theoretical calculations for nominal moment capacity. Both capacities were calculated according to AASHTO Articles 5.7.3.1 and 5.7.3.2 (2006). The first capacity is based on the guaranteed ultimate tensile strength of prestressing strands (270 and 300 ksi for grade 270 and grade 300 strands, respectively). The second moment capacity was calculated with higher values for ultimate strand stress obtained from experimental tests, which are provided in Table 3.3. Average maximum strand slip is provided in the table, as well as the observed mode of failure according to the criteria outlined previously.

A range of development length and flexural bond length was determined for normal and inverted casting position within each type of strand, resulting in eight separate estimates. The upper limit of a development length range corresponded to the shortest embedment length at which a flexural failure occurred, while the lower limit was associated with the longest embedment length resulting in bond failure. Ranges of flexural bond length were estimated by examining the difference in transfer and embedment length for each test. The maximum flexural bond length was taken as the difference in transfer and embedment length for the shortest embedment length test that resulted in flexural failure. The minimum flexural bond length was taken as the difference in transfer and embedment length for the longest embedment length test that resulted in bond failure. These premises were modified for sets of tests in which only one type of failure occurred or the individual beam end transfer lengths were significantly different.

Table 4.8 Development Length Load Test Results

Strand Type	Beam Designation	Final Transfer Length (in.)	Tested Embedment Length (in.)	Maximum Applied Moment (k-ft)	M_{AASHTO} w/ Min. f_{pu} (k-ft)	$M_{APPLIED}/M_{AASHTO}$ (Min. f_{pu})	M_{AASHTO} w/ Exp. f_{pu} (k-ft)	$M_{APPLIED}/M_{AASHTO}$ (Exp. f_{pu})	Average Maximum Strand Slip (in.)	Observed Mode of Failure
0.5 in. Normal Grade 270	0.270.5N.RA	15.0	78	193	147	1.31	173	1.12	8.20E-05	Flexure
	0.270.5N.RB	13.5	66	187	147	1.27	173	1.08	3.60E-05	Flexure
	1.270.5N.RA	19.5	66	205	147	1.39	173	1.18	1.04E-03	Flexure
	1.270.5N.RB	13.0	60	156	147	1.06	173	0.90	2.37E-04	Flexure
	1.270.5N.UA	30.0	66	205	147	1.39	173	1.18	1.71E-02	Flexure/Bond
	1.270.5N.UB	27.0	60	189	147	1.29	173	1.09	6.93E-02	Bond/Shear
0.5 in. Normal Grade 300	0.300.5N.RB	15.0	78	205	162	1.27	188	1.09	0.00E+00	Flexure
	1.300.5N.RA	21.0	48	161	162	0.99	188	0.86	6.39E-02	Bond/Shear
	1.300.5N.RB	15.0	60	212	162	1.31	188	1.13	2.56E-03	Flexure
	1.300.5N.UA	44.0	78	215	162	1.33	188	1.14	7.24E-02	Bond
	1.300.5N.UB	24.5	60	219	162	1.35	188	1.16	5.55E-02	Bond/Shear
0.5 in. Special Grade 270	3.270.5S.RA	22.5	60	227	182	1.25	204	1.11	1.35E-02	Rupture/Bond
	3.270.5S.RB	14.0	72	239	182	1.31	204	1.17	4.80E-05	Flexure
	4.270.5S.RA	18.5	54	199	182	1.09	204	0.98	6.55E-02	Bond
	4.270.5S.RB	19.0	66	233	182	1.28	204	1.14	3.15E-04	Flexure
	3.270.5S.UA	28.5	60	206	182	1.13	204	1.01	3.93E-02	Bond
	3.270.5S.UB	22.0	72	230	182	1.26	204	1.13	5.11E-04	Flexure
0.5 in. Special Grade 300	3.300.5S.RA	23.0	60	255	201	1.27	225	1.13	3.98E-02	Bond
	3.300.5S.RB	16.0	72	260	201	1.29	225	1.16	2.20E-05	Rupture
	4.300.5S.RA	20.0	66	235	201	1.17	225	1.04	7.01E-02	Bond
	4.300.5S.RB	16.0	78	268	201	1.33	225	1.19	5.30E-05	Flexure
	3.300.5S.UA	41.0	60	53	201	0.26	225	0.24	5.03E-02	Bond
	3.300.5S.UB	23.5	72	254	201	1.26	225	1.13	2.93E-04	Flexure
Average Moment Ratio for Tests Resulting in Flexural Failure Only						1.28		1.12		
Average Moment Ratio for Tests Resulting in Bond Failure Only						1.10		0.96		

All tests of normal cast beams with normal grade 270 strands had flexural failures. Test 1.270.5N.RB failed at a moment much lower than the other tests. The results indicated that the maximum experimental development length was 60 in. No bond failures occurred, so a lower bound for development length was not determined. The maximum experimental flexural bond length was 47 in., which was the difference in embedment and transfer length for test 1.270.5N.RB. The normal grade 270 beam with inverted casting orientation had a bond failure at 60 in. and combination of flexural and bond failure at 66 in. This suggested a development length greater than or equal to 66 in. The flexural bond length was greater than or equal to 36 in., based on test 1.270.5N.UA. A maximum flexural bond length was not determined since neither test resulted in a pure flexural failure.

Tests of normal cast beams with normal grade 300 strands resulted in two flexural failures and one bond failure. The bond failure at 48 in. and flexural failure at 60 in. suggested that the development length was between these two embedment lengths. The experimental flexural bond length was between 27 and 45 in. Tests of the beam with inverted casting orientation and normal grade 300 strands resulted in bond failures at 60 and 78 in., which indicated that the development length was at least 78 in. However, the transfer lengths were 24.5 and 44 in. for the 60 and 78 in. embedment length tests, respectively. If the beam end with 24.5 in. transfer length was tested at 78 in. embedment length, a flexural failure may have occurred. The difference between embedment length and transfer length in the 60 in. test indicated a minimum flexural bond length equal to 35.5 in. The minimum development length was taken as the sum of the larger transfer length and the minimum flexural bond length, or 79.5 in.

Tests of normal cast beams with special grade 270 strands resulted in two flexural failures, one bond failure, and one combination failure. A bond failure at 54 in., flexural failure at 66 in., and combination failure between these embedment lengths indicated that the development length was between 54 and 66 in. The experimental flexural bond length was between 35.5 and 47 in. Tests of the inverted beam with special grade 270 strands resulted in a bond failure at 60 in. and flexural failure at 72 in. Therefore, the development length was between these embedment lengths. The flexural bond length was between 31.5 and 50 in.

Tests of normal cast beams with special grade 300 strands resulted in two flexural failures and two bond failures. A bond failure at 66 in. and strand rupture failure at 72 in. suggested that the development length was between 66 and 72 in. The experimental flexural bond length was between 46 and 56 in. The first test of the inverted beam with special grade 300 strands resulted in bond failure at 60 in. with a corresponding 41 in. transfer length. This suggested a 19 in. minimum flexural bond length. A flexural failure occurred at 72 in., but the transfer length at this end was only 23.5 in. This suggested the maximum flexural bond length was 48.5 in. The maximum development length was conservatively taken as the sum of the maximum transfer length and maximum flexural bond length, or 89.5 in. Conversely, the minimum development length was taken as the sum of minimum transfer and minimum flexural bond length, or 42.5 in.

4.2.6 Effect of Strand Grade and Casting Position on Development Length

The effects of strand grade and casting position were not easy to isolate because discrete values of development length and flexural bond length could not be determined. Rather, ranges were estimated for these parameters, and the ranges often overlapped. The experimental estimates of development length and flexural bond length that were determined in the previous section are summarized in Table 4.9. The last column of the table shows the development length that was calculated according to the current AASHTO provision (see Equation 2.8). The nominal strand stress was calculated according to Article 5.7.3.1.1, assuming minimum guaranteed ultimate tensile strength (270 and 300 ksi for grade 270 and 300 strands, respectively). Effective prestress was calculated according to AASHTO refined method. The effective prestress used in the development length equation was the average value for all beams cast with a certain strand type (AASHTO 2006).

Table 4.9 Summary of Development Length Results

Strand Type	Casting Orientation	Development Length (in.)		Final Transfer Length (in.)		Flexural Bond Length (in.)		AASHTO Development Length (in.)
		Minimum	Maximum	Minimum	Maximum	Minimum	Maximum	
Normal Grade 270	Normal	No Data	60	13	19.5	No Data	47	73
	Inverted	66	No Data	27	30	36	No Data	
Normal Grade 300	Normal	48	60	15	21	27	45	80
	Inverted	79.5	No Data	24.5	44	35.5	No Data	
Special Grade 270	Normal	54	66	14	22.5	35.5	47	74
	Inverted	60	72	22	28.5	31.5	50	
Special Grade 300	Normal	66	72	16	20	46	56	82
	Inverted	42.5	89.5	23.5	41	19	48.5	

Strand grade appeared to have a minimal effect on beams with normal strands and normal casting position. Maximum development lengths and flexural bond lengths were quite similar. The distinction between normal grade 300 and normal grade 270 strands with inverted casting position was not clear either. The increase in strand strength caused a 13.5 in. increase in minimum development length and no substantial effect on flexural bond length. Strand grade had a considerable effect on beams with special strands and normal casting position. The range of development length for grade 300 strands was 6 in. greater than the range for grade 270 strands. The upper bound flexural bond length for grade 300 strands was 10.5 in. greater than the range for grade 270 strands. The strand grade distinction was less prevalent for beams with special strands and inverted casting position.

Casting position had a significant effect on beams with normal grade 270 strands. The minimum development length for inverted casting position was 6 in. greater than the maximum development length for normal casting position. The two ranges of flexural bond length overlapped by 14 in., with the inverted beam range being greater. In beams with normal grade 300 strands, the minimum development length for inverted casting position was much greater than the range for normal casting position. A clear comparison of flexural bond length was not possible. In beams with special grade 270 strands, the development length range for inverted casting position was 6 in. greater than the normal range, and had 6 in. of overlap. The range of flexural bond length was similar for inverted and normal casting orientation. Due to dispersion, no clear comparison was made between inverted and normal casting position for special grade 300 strands.

The development length results given in Table 4.9 are illustrated in Figure 4.11. The chart shows eight ranges of development length, representing the different combinations of strand grade (270 or 300), strand size (normal or special), and casting orientation (normal or inverted). A range that only has one end marker represents a set of tests in which a maximum or minimum experimental development length was not determined. Each solid vertical line indicates the average theoretical development length for normal and special strands, calculated according to current AASHTO provisions (2006). Experimental estimates of development length for normally cast beams were less than the theoretical development length. However, the experimental estimates of development length in beams with inverted casting orientation were much closer to theoretical. In particular, the experimental development length of normal grade 270, normal grade 300, and special grade 300 strands were possibly greater than the respective code provisions. A forty percent increase in the theoretical development length (represented by a dotted vertical line) includes a larger portion of the experimental development length ranges for strands placed in inverted beams.

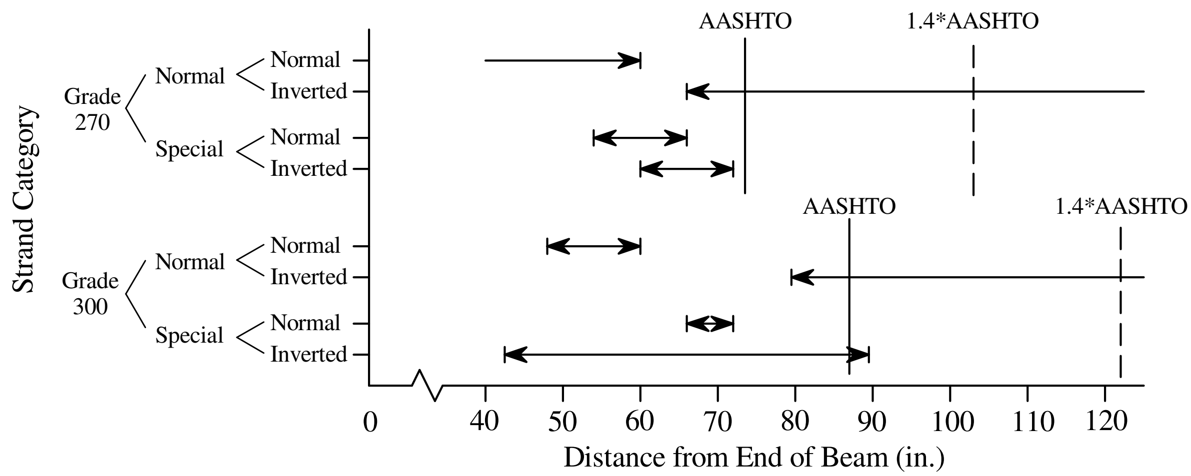

Figure 4.11 Experimental Development Lengths

4.2.7 Additional Development Length Discussion

Establishing experimental ranges of development length through iterative load testing was difficult. While the target variable in each load test was embedment length, several other variables could have distorted the results. For instance, both ends of two beams were tested over a 24 in. range of embedment lengths to determine the development length in normal cast beams with special grade 270 strands (see Table 4.9). However, the transfer lengths of these four beam ends differed by 8 in. Two tests were performed on live ends while the other two tests were on dead ends. In addition, the two beams were cast in different concrete pours. For these reasons, comparisons of strand type and casting orientation were more qualitative than quantitative.

The applied moments at which flexural failures occurred were much higher that theoretical moment capacities. The average ratio of applied moment to the AASHTO capacity based on guaranteed ultimate tensile strength was 1.28 (AASHTO 2006). Even if the actual measured ultimate stresses were used to compute theoretical capacity, the applied moments were still 12 percent greater on average. In addition, several of the tests resulting in bond failure occurred at moments that were higher than either calculated capacity. A possible explanation for high applied moments is the large ductility observed in strand tension tests (see Figure 3.5).

The cross sectional area of prestressing strands had a noticeable effect on experimental development lengths of strands in beams with normal casting orientation. The maximum experimental development length of special grade 270 strands was 6 in. greater than the maximum experimental development length of normal grade 270 strands. The experimental range of development length for special grade 300 strands was considerably larger than the range for normal grade 300 strands. The theoretical development lengths of both grade 270 and grade 300 strands only increased 2 in. for special strands with larger area.

4.3 Prestress Losses

Effective prestress was theoretically predicted and experimentally determined for twelve pretensioned prestressed concrete beams. Effective prestress and prestress losses are directly related, as explained previously. Theoretical prestress losses were estimated according to PCI and AASHTO models. Experimental measurements of prestress loss were obtained by vibrating wire gage strain readings, crack initiation tests, and crack reopening tests.

4.3.1 Theoretical Predictions of Prestress Losses

Prestress losses in each test beam were calculated according to two theoretical models. Each model utilizes a time step method to predict losses for different segments of a prestressed member's service life. Time step methods are effective because they address the interdependency of time dependent prestress losses. Several key assumptions implemented in the calculations are described below.

In order to simulate design prestress loss calculations, design material properties of concrete and prestressing strand were used. The initial and 28 day concrete compressive strengths were assumed to be 4500 and 6000 psi, respectively. The prestressing strand strength was based on guaranteed ultimate tensile strength (270 and 300 ksi for grade 270 and 300 strands, respectively), and the yield stress was assumed to be 90 percent of the ultimate strength when calculated steel relaxation losses. The jacking stress was assumed to be 75 percent of ultimate strength, and modulus of elasticity of prestressing strands was taken as 28500 ksi.

Strands were tensioned between two and seven days before pouring concrete. Anchorage seating losses occurred when chucks were seated on the strands, and steel relaxation losses occurred in the time between tensioning and pouring concrete. However, shims placed between previously seated chucks and steel abutments just before a concrete pour compensated for these losses. Shimming allowed the stress level just before pouring concrete to be very close to 75 percent ultimate tensile strength. In addition, the fact that strands were tensioned several days before casting concrete was reflected in subsequent steel relaxation calculations. The relative "age" of the strands reduced additional relaxation losses.

End of moist cure and transfer of prestress are assumed to occur on the same day in prestress loss models. However, end of cure and prestress transfer occurred on different dates for each set of beams. In pours zero and four, release occurred before the end of the seven day moist cure. In pours one and three, release occurred after curing. Theoretically, a time step could have been assigned to the period between these two events. A small amount of shrinkage would have been calculated for the time between end of cure and prestress transfer, or a small amount of creep would have been calculated for the time between transfer and end of cure. This complication was avoided by using only one time step to calculate time dependent concrete creep and shrinkage losses. The difference in concrete age at end of cure and transfer of prestress was accounted for by using different time periods for individual creep and shrinkage calculations. The effect this assumption had on final effective prestress was negligible.

Prestress losses were calculated at mid span of each beam, and therefore incorporated the mid span self weight bending moment. However, experimental measurements of prestress losses were based on sections near quarter span that corresponded to the location of vibrating wire gages and embedment length of load tests. The bending moment at quarter span of normally cast beams was three fourths of the mid span moment, based on a simple support condition. This produced a negligible difference in prestress loss calculations. The bending moment at quarter span of an inverted beam was 12.5 percent of the mid span moment. This was based on a single unstable mid span support resulting from the bending moment of eccentric prestressing strands. Theoretically, this decrease in self weight moment would increase elastic shortening prestress losses by approximately one ksi for the beams in question. However, this effect was ignored so that prestress loss calculations would be consistent. In addition, the calculation of creep losses in inverted beams could have been divided into a time step before rotation, instantaneous prestress gain during rotation, and another time step after rotation. The prestress gain was associated with the increase in self weight moment induced by rotation of a beam from inverted to normal position. This alteration to calculations produced minimal changes in effective prestress, so it was ignored as well.

4.3.1.1 PCI Recommendations for Prestress Losses

Recommendations from the PCI Committee on Prestress Losses were used to predict effective prestress in test beams (PCI 1975). While this method is over thirty years old, it is still recognized as a viable method for the calculation of prestress losses, and is referenced by ACI (2005). The types of losses applicable to the beams tested in this project were elastic shortening, creep and shrinkage of concrete, and steel relaxation. Elastic shortening losses were instantaneous, while the other losses were time dependent. PCI recommends a minimum of four time steps for the calculation of time dependent losses: 1) anchorage of prestressing steel to transfer of prestress 2) prestress transfer to 30 days or application of load other than self weight 3) end of step two to one year 4) one year to end of service. Only the first two time steps were applicable to this project. The first time step began after strands were shimmed and ended at prestress transfer. The second time step resumed at transfer and ended at load testing.

Elastic shortening losses were calculated by Equation 4.4.

$$ES = f_{cr}\left(E_s / E_{ci}\right) \qquad 4.4$$

Where:

ES = elastic shortening loss (ksi)

f_{cr} = concrete stress at centroid of prestressing steel just after transfer (ksi)

E_s = modulus of elasticity of prestressing steel (ksi)

E_{ci} = initial modulus of elasticity of concrete (ksi)

When computing f_{cr} above, the steel stress after transfer was unknown, so the jacking stress was applied to the transformed section and the elastic shortening loss was computed without iteration. Creep losses were calculated according to Equation 4.5.

$$CR = f_c(UCR)(PCR)(SCF)(MCF) \qquad 4.5$$

Where:

CR = creep loss (ksi)

f_c = net concrete stress at centroid of prestressing steel at beginning of time step (ksi)

$UCR = 95 - 20E_c/1000 \geq 11$ (E_c is the concrete modulus of elasticity in ksi)

$PCR = AUC_{\text{end of step}} - AUC_{\text{beginning of step}}$

SCF, MCF, and AUC are presented in Table 4.10, Table 4.11, and Table 4.12.

Table 4.10 PCI Creep factors for Member Size and Shape

Volume to Surface Ratio (in.)	SCF
1	1.05
2	0.96
3	0.87
4	0.77
5	0.68
>5	0.68

Table 4.11 PCI Creep Factors for Age at Prestress and Length of Cure

Age of Prestress Transfer (days)	Period of Cure (days)	MCF
3	3	1.14
5	5	1.07
7	7	1.00
10	7	0.96
20	7	0.84
30	7	0.72
40	7	0.60

Table 4.12 PCI Creep Factors for Time

Time After Prestress Transfer (days)	AUC
1	0.08
2	0.15
5	0.18
7	0.23
10	0.24
20	0.30
30	0.35
60	0.45
90	0.51
180	0.61
365	0.74
End of Service	1.00

Shrinkage losses were calculated according to Equation 4.6.

$$SH = (USH)(PSH)(SSF) \tag{4.6}$$

Where:

SH = shrinkage loss (ksi)

USH = 27 - 3E_c/1000 ≥ 12 (units of USH are ksi if units of E_c are also ksi)

PSH = $AUS_{\text{end of step}} - AUS_{\text{beginning of step}}$

SSF and AUS are presented in Table 4.13 and Table 4.14.

Table 4.13 PCI Shrinkage Factors for Member Size and Shape

Volume to Surface Ratio (in.)	SSF
1	1.04
2	0.96
3	0.86
4	0.77
5	0.69
6	0.60

Table 4.14 PCI Shrinkage Factors for Time

Time After End of Cure (days)	AUS
1	0.08
3	0.15
5	0.20
7	0.22
10	0.27
20	0.36
30	0.42
60	0.55
90	0.62
180	0.68
365	0.86
End of Service	1.00

Steel relaxation losses were calculated according to Equation 4.7. The last term in Equation 4.7 was taken no less than 0.05 (PCI 1975).

$$RET = \frac{f_{st}}{45}\log\left(\frac{24t_{end}}{24t_{begin}}\right)\left(\frac{f_{st}}{f_{py}} - 0.55\right) \qquad 4.7$$

Where:

RET = steel relaxation loss (ksi)

f_{st} = stress in prestressing steel at beginning of time step (ksi)

t_{end} = time at end of time step (days)

t_{begin} = time at beginning of time step (days)

f_{py} = yield stress of prestressing steel (ksi)

The PCI model was used to predict prestress losses in each test beam. The results are shown in Table 4.15. The jacking stress was assumed to be 75 percent of the ultimate tensile stress, as mentioned previously. The initial prestress f_{pi} is the strand stress just after transfer. The tabulated steel relaxation loss (Σ RET) is the sum of the losses between shimming and transfer and between transfer and load testing. Shrinkage and creep losses were only calculated for the second time step. The time shown in the last column is the time that was used to mark the end of the second time step. This time corresponds to the last vibrating wire gage reading for each beam, and is near the time of load testing for each beam.

Table 4.15 PCI Prestress Loss Predictions

Beam Name	f_{pj} (ksi)	ES (ksi)	f_{pi} (ksi)	Σ RET (ksi)	SH (ksi)	CR (ksi)	f_{pe} (ksi)	End Time (days)
0.270.5N.R	203	12.3	190	0.736	4.27	7.56	178	24
0.300.5N.R	225	13.9	211	0.815	4.27	8.50	198	24
1.270.5N.R	203	12.3	190	0.679	3.81	5.63	180	20
1.300.5N.R	225	13.9	211	0.771	3.26	6.48	201	21
1.270.5N.U	203	12.3	190	0.694	3.93	5.77	180	21
1.300.5N.U	225	13.9	211	0.771	3.26	6.48	201	21
3.270.5S.R	203	12.2	190	0.936	5.43	7.20	177	40
3.300.5S.R	225	13.7	211	1.06	5.53	8.34	196	42
3.270.5S.U	203	12.2	190	0.962	5.59	7.49	176	43
3.300.5S.U	225	13.7	211	1.10	5.81	8.74	196	47
4.270.5S.R	203	12.2	190	1.31	4.51	6.99	178	27
4.300.5S.R	225	13.7	211	1.47	4.59	7.99	197	28

4.3.1.2 AASHTO Recommendations for Prestress Losses

Prestress losses in test beams were also predicted by the refined method outlined in *AASHTO LRFD Bridge Design Specifications* (AASHTO 2006). Losses were divided into initial losses (elastic shortening) and long term losses (creep and shrinkage of concrete and relaxation of steel). Elastic shortening losses were calculated according to Article 5.9.5.2.3a, which is similar to the PCI recommendation. Long term losses were calculated according to Article 5.9.5.4.2, which is intended for determining prestress losses between transfer and time of composite deck placement. The test beams had no topping, so the time of deck placement was taken as the time of load testing. This assumption was permitted by Article 5.9.5.4.4.

Estimates of creep and shrinkage were calculated according to Articles 5.4.2.3.2 and 5.4.2.3.3. The creep coefficient was found by Equation 4.8.

$$\psi(t,t_i) = 1.9 k_{vs} k_{hc} k_f k_{td} t_i^{-0.118} \qquad 4.8$$

Where:

ψ = creep coefficient

k_{vs} = 1.45 – 0.13*(volume to surface ratio) ≥ 0.0

k_{hc} = 1.56 – 0.008*(relative humidity)

k_f = 5/(1+f'_{ci}) (f'_{ci} is the initial concrete compressive strength in ksi)

k_{td} = t/(61 – 4*f'_{ci} + t)

t = time between prestress transfer and load testing (days)

t_i = age of concrete at prestress transfer (days)

The shrinkage strain was found by Equation 4.9.

$$\varepsilon_{sh} = k_{vs} k_{hs} k_f k_{td} (480 \times 10^{-6}) \qquad 4.9$$

Where:

ε_{sh} = shrinkage strain

k_{hs} = 2.0 – 0.014*(relative humidity)

The factors k_{vs}, k_f, and k_{td} were common to both creep and shrinkage models. The relative humidity was assumed to be 70 percent since beams were cast, cured, and tested in an enclosed laboratory. The time used in the factor k_{td} for shrinkage was taken as the time between end of cure and load testing because the end of cure did not coincide with prestress transfer. An additional parameter required for calculation of long term creep and shrinkage losses is the transformed section coefficient shown in Equation 4.10. A time of ten years was used to calculate the ultimate creep coefficient.

$$K_{id} = \frac{1}{1 + \frac{E_p}{E_{ci}} \frac{A_{ps}}{A_g} \left(1 + \frac{A_g e_g^{\,2}}{I_g}\right) \left[1 + 0.7 \psi_b (t_f, t_i)\right]} \qquad 4.10$$

Where:

K_{id} = transformed section coefficient for time between transfer and deck placement

E_p = modulus of elasticity of prestressing strand (ksi)

E_{ci} = initial modulus of elasticity of concrete (ksi)

A_{ps} = area of prestressing steel (in.^{2})

A_g = gross section area (in.^{2})

e_g = gross section strand eccentricity (in.)

I_g = gross section moment of inertia (in.^{4})

$\psi_b(t_f,t_i)$ = creep coefficient at final time

Time dependent prestress losses due to shrinkage and creep of concrete and relaxation of prestressing strands were calculated according to Articles 5.9.5.4.2a, 5.9.5.4.2b, and 5.9.5.4.2c, respectively. Equation 4.11 was used to determine shrinkage losses.

$$\Delta f_{pSR} = \varepsilon_{bid} E_p K_{id} \qquad 4.11$$

Where:

Δf_{pSR} = prestress loss due to shrinkage (ksi)

ε_{bid} = concrete shrinkage strain in beam between end of cure and load testing

E_p = modulus of elasticity of prestressing strand (ksi)

K_{id} = transformed section coefficient for time between transfer and deck placement

Creep losses were calculated by Equation 4.12.

$$\Delta f_{pCR} = \frac{E_p}{E_{ci}} f_{cgp} \psi_b \left(t_d . t_i\right) K_{id} \qquad 4.12$$

Where:

Δf_{pCR} = prestress loss due to creep (ksi)

E_p = modulus of elasticity of prestressing strand (ksi)

E_{ci} = initial modulus of elasticity of concrete (ksi)

f_{cgp} = concrete stress at centriod of prestressing strands just after transfer (ksi)

$\psi_b(t_d,t_i)$ = creep coefficient for time between transfer and load testing

K_{id} = transformed section coefficient for time between transfer and deck placement

Finally, steel relaxation losses were computed with Equation 4.13. A note in Article 5.9.5.4.2c indicates that steel relaxation losses in low relaxation strands may be assumed to equal 1.2 ksi (AASHTO 2006).

$$\Delta f_{pR1} = \frac{f_{pt}}{K_L}\left(\frac{f_{pt}}{f_{py}} - 0.55\right) \qquad 4.13$$

Where:

Δf_{pR1} = prestress loss due to relaxation (ksi)

f_{pt} = stress in prestressing strands just after transfer (ksi)

K_L = 30 for low relaxation strands

f_{py} = yield stress of prestressing strands (ksi)

The AASHTO refined estimate of prestress loss was used to predict losses in each test beam. The results are shown in Table 4.16. The jacking stress and time corresponding to effective prestress are the same as the values used in Table 4.15. In general, the AASHTO and PCI prestress loss predictions were quite similar. Elastic shortening losses and initial prestress were almost identical. The small difference was due to inclusion of steel relaxation loss between casting and transfer in the PCI method. The AASHTO method predicted slightly higher steel relaxation losses. Concrete shrinkage and creep losses predicted by the different methods were similar. The difference in final effective prestress predicted by the PCI and AASHTO methods was not greater than 2 ksi for any individual beam.

Table 4.16 AASHTO Prestress Loss Predictions

Beam Name	f_{pj} (ksi)	Δf_{pES} (ksi)	f_{pi} (ksi)	Δf_{pR1} (ksi)	Δf_{pSR} (ksi)	Δf_{pCR} (ksi)	f_{pe} (ksi)	End Time (days)
0.270.5N.R	203	12.4	190	1.47	3.84	6.57	178	24
0.300.5N.R	225	13.9	211	1.63	3.84	7.38	198	24
1.270.5N.R	203	12.4	190	1.47	3.18	3.62	182	20
1.300.5N.R	225	13.9	211	1.63	3.36	4.35	202	21
1.270.5N.U	203	13.4	189	1.47	3.36	3.87	180	21
1.300.5N.U	225	13.9	211	1.63	3.36	4.35	202	21
3.270.5S.R	203	12.2	190	1.48	5.79	6.53	176	40
3.300.5S.R	225	13.7	211	1.64	5.99	7.65	196	42
3.270.5S.U	203	12.2	190	1.48	6.08	6.93	176	43
3.300.5S.U	225	13.7	211	1.64	6.43	8.35	195	47
4.270.5S.R	203	12.2	190	1.48	4.21	5.86	179	27
4.300.5S.R	225	13.7	211	1.64	4.35	6.80	198	28

4.3.2 Experimental Measurements of Prestress Losses

Prestress losses were experimentally measured in each beam. Vibrating wire gages were used to continually monitor internal strain changes in each beam. Compatibility between vibrating wire gages, concrete, and prestressing strands allowed changes in steel stress to be deduced from measured changes in strain. Prestress losses and effective prestress were determined in this manner. Crack initiation and crack reopening load tests were also used to measure prestress losses. Basic mechanics permitted effective prestress to be back calculated from crack initiation and crack reopening loads.

4.3.2.1 Measurement of Prestress Losses by Vibrating Wire Gages

One vibrating wire gage was placed in the live end of each beam. The gage was securely positioned between two of the three strands to ensure that its location relative to the height of the section would correspond to the eccentricity of the prestressing strands. Each strain reading was multiplied by 0.96, which was the batch factor supplied with the vibrating wire gages. Strain recordings began just before pouring concrete and continued until load testing. Initial recording intervals of one to five minutes were used until prestress transfer, upon which the recording interval was changed to one hour. In most cases, vibrating wire gage readings were recorded until the day of load testing or day before. For a few beams, the vibrating wire gages were disconnected a few days earlier to permit rearrangement of beams. Plots of the vibrating wire gage strain readings from the time of casting concrete to time of load testing are shown for each pour in Appendix D. Changes in vibrating wire gage strain measured at transfer and recorded during the time between transfer and load testing are reported in Table 4.17. The changes in strain measured at release were similar to the strain plateau values from surface strain profiles (see Appendix B). Each vibrating wire gage was also equipped with a thermistor that provided a measurement of temperature corresponding to each strain reading. The manufacturer recommended a temperature correction factor for vibrating wire gage strain readings. The temperature correction was used for the plots in Appendix D. However, the ambient lab temperature and concrete temperatures equilibrated by the time of prestress transfer, so the temperature correction was not necessary for prestress loss calculations.

Table 4.17 Vibrating Wire Gage Strains

Beam Designation	Change in Strain at Release (με)	Change in Strain after Release (με)
0.270.5N.RA	462	480
0.300.5N.RA	435	578
1.270.5N.RA	405	431
1.300.5N.RA	433	479
1.270.5N.UA	400	490
1.300.5N.UA	487	534
3.270.5S.RA	454	450
3.300.5S.RA	477	490
3.270.5S.UA	440	446
3.300.5S.UA	471	493
4.270.5S.RA	489	651
4.300.5S.RA	532	710

Two methods were used to reduce vibrating wire gage data. The first method was suggested by Ahlborn, et al. (2000). Equation 4.14 below may be used to express the stress in the concrete at the level of the prestressing strands just after transfer.

$$\Delta\varepsilon_{VWG,\mathrm{Re}lease}E_{ci} + \sigma_{c,Before\,\mathrm{Re}lease} = -\frac{f_{pi}A_{ps}}{A_n} - \frac{f_{pi}A_{ps}e_n^{\,2}}{I_n} + \frac{M_o e_n}{I_n} \qquad 4.14$$

Where:

$\Delta\varepsilon_{vwg,Release}$ = change in vibrating wire gage strain during release (in./in.)

E_{ci} = initial concrete modulus of elasticity (ksi)

$\sigma_{c,BeforeRelease}$ = stress in concrete before release (ksi)

f_{pi} = stress in prestressing strands just after transfer (ksi)

A_{ps} = cross sectional area of prestressing strands (in.^{2})

A_n = net section area (in.^{2})

e_n = net section strand eccentricity (in.)

I_n = net section moment of inertia (in.^{4})

M_o = self weight moment (k in.)

The equation above was solved for the initial prestress, yielding Equation 4.15.

$$f_{pi} = \left(\frac{1}{\frac{A_{ps}}{A_n} + \frac{A_{ps} e_n^{\,2}}{I_n}} \right) \left(\frac{M_o e_n}{I_n} - \Delta\varepsilon_{VWG,\mathrm{Release}} E_{ci} - \sigma_{c,Before\,\mathrm{Release}} \right) \qquad 4.15$$

The equation above is the product of a geometric constant and the sum of three stress components. If a "tension positive" sign convention is used, the vibrating wire gage strain will be negative since it is compressive. Therefore, stress from self weight moment and vibrating wire gage reading are additive, while any tensile concrete stress will effectively reduce the initial prestress. Ahlborn, et al. suggested the use of $\sigma_{c,BeforeRelease}$ to account for tensile stresses in concrete before prestress transfer that result from thermal effects and restrained shrinkage. An upper bound initial prestress may be calculated by assuming there is no stress in the concrete before transfer. A lower bound may be calculated by assuming the stress in the concrete before transfer is equal to the initial tensile strength, which would be indicated by pre-release cracks (Ahlborn 2000).

Equation 4.15 was used to calculate the initial prestress (immediately after transfer) in the test beams. Because of a lack of test data, initial concrete modulus of elasticity and tensile strength were calculated as a function of the initial measured compressive strength found in Table 4.1. The self weight moment was individually calculated for each beam, incorporating the effects of vibrating wire gage location and casting orientation. It is important to note that the initial prestress calculations had no relation to the jacking stress, and were highly dependent on concrete material properties. Prestress losses after transfer were calculated by multiplying the change in vibrating wire gage strain after release by the modulus of elasticity of the prestressing strands. The final effective prestress was found by subtracting prestress losses between transfer and load testing from the initial calculated prestress. The results of this method are presented in Table 4.18. The upper and lower bound estimates of initial and effective prestress are shown. The effective concrete age shown in the last column represents the age of the concrete when the last vibrating wire gage strain reading was recorded. The results were quite dispersed. In several cases, the calculated upper bound intial prestress was very close to the jacking stress, which is not reasonable. In one case, the upper bound effective prestress exceeded the jacking stress.

Table 4.18 Prestress Losses Measured by VWG Upper/Lower Bound Method

Beam Designation	Upper Bound f_{pi} (ksi)	Lower Bound f_{pi} (ksi)	Upper Bound f_{pe} (ksi)	Lower Bound f_{pe} (ksi)	Effective Concrete Age (days)
0.270.5N.RA	206	156	193	142	24
0.300.5N.RA	195	145	179	128	24
1.270.5N.RA	189	136	177	124	20
1.300.5N.RA	201	148	187	134	21
1.270.5N.UA	176	123	162	109	21
1.300.5N.UA	213	160	198	145	21
3.270.5S.RA	224	167	210	154	40
3.300.5S.RA	234	177	220	163	42
3.270.5S.UA	206	149	193	136	43
3.300.5S.UA	221	164	206	150	47
4.270.5S.RA	217	166	198	147	27
4.300.5S.RA	235	184	214	163	28

A second, simpler method was used to interpret vibrating wire gage data, which will be referred to as the basic method. In this method, the vibrating wire gages were effectively zeroed just before prestress transfer, ignoring the changes in strain before transfer. The stress in the prestressing strands just before transfer was assumed to be the stress reading in load cells before concrete was poured. Both elastic shortening and time dependent losses were calculated by multiplying the change in vibrating wire gage strain by the modulus of elasticity of prestressing strands. The initial prestress was found by subtracting elastic shortening losses from the jacking stress, and effective prestress was calculated by subtracting all losses from the jacking stress. The long term losses calculated by this method are the same as those calculated by the previous method. The results of the basic vibrating wire gage prestress loss method are shown in Table 4.19. The effective prestress calculated by the basic method was greater than the lower bound effective prestress in all beams, and was less than the upper bound effective prestress in half of the beams. In the other six beams, the basic method effective prestress was greater than the upper bound.

Table 4.19 Prestress Losses Measured by the Basic VWG Method

Beam Designation	f_{pj} (ksi)	Elastic Shortening Loss (ksi)	f_{pi} (ksi)	Time Dependent Losses (ksi)	f_{pe} (ksi)	Effective Concrete Age (days)
0.270.5N.RA	200	13.1	187	13.6	174	24
0.300.5N.RA	223	12.4	210	16.5	194	24
1.270.5N.RA	207	11.5	195	12.2	183	20
1.300.5N.RA	225	12.4	212	13.7	199	21
1.270.5N.UA	207	11.4	195	13.9	181	21
1.300.5N.UA	225	13.9	211	15.3	195	21
3.270.5S.RA	203	13.3	190	13.2	177	40
3.300.5S.RA	225	14.0	211	14.3	196	42
3.270.5S.UA	203	12.9	190	13.1	177	43
3.300.5S.UA	225	13.8	211	14.5	196	47
4.270.5S.RA	202	14.3	188	19.1	169	27
4.300.5S.RA	226	15.6	210	20.8	190	28

4.3.2.2 Measurement of Prestress Losses by Crack Initiation Tests

The effective prestress in each beam at the time of load testing was determined by crack initiation testing. This type of test was conducted by loading a beam until cracking was observed at the bottom of the section. Crack initiation indicated that the stress in the concrete had exceeded the tensile strength. Basic theory of mechanics permitted back calculation of effective prestress by Equation 4.16.

$$f_{pe} = \left(\frac{1}{\dfrac{A_{ps}}{A_g} + \dfrac{A_{ps} e_g y_g}{I_g}} \right) \left(\frac{M_o y_t}{I_t} + \frac{M_{applied} y_t}{I_t} - f_t \right) \qquad 4.16$$

Where:

f_{pe} = effective prestress (ksi)

A_{ps} = cross sectional area of prestressing strands (in.^{2})

A_g = gross section area (in.^{2})

e_g = gross section strand eccentricity (in.)

y_g = distance from gross section centroid to location of strain measurements (in.)

I_g = gross section moment of inertia (in.^{4})

y_t = distance from transformed section centroid to location of strain measurements (in.)

I_t = transformed section moment of inertia (in.^{4})

M_o = self weight moment (k in.)

$M_{applied}$ = applied moment at crack initiation (k in.)

f_t = tensile strength of concrete from split cylinder tests (ksi)

The concrete tensile strength used for effective prestress calculations was found by averaging all split cylinder test results for a given pour. Average split cylinder test results are provided in Table 4.7. It is important to note that the actual tensile strength of the concrete in the beam would be more closely predicted by modulus of rupture tests, which suggest a higher tensile strength. If the concrete tensile strength was based on modulus of rupture tests, the experimentally determined effective prestress would have been slightly lower.

Crack initiation was detected by measuring concrete surface strain near the bottom of the section. A DEMEC gage with accompanying gage points was used to measure strain in the same manner implemented in transfer length determination. Gage points were affixed to each beam so that three strain measurements could be recorded on each side of the beam. On a given beam side, one strain reading was recorded directly under the load point while the other two readings were measured 100 mm adjacent to the location of the load. In pour zero, the gage points were placed as close to the bottom of the section as possible, so y_t in Equation 4.16 was the distance from the bottom of the section to the centroid of the transformed section. In pours one, three, and four, the gage points were placed at the level of the strands, so y_t in Equation 4.16 was equal to the transformed eccentricity of the prestressing strands. Strain readings were recorded between each load increment. Load increments were 5 kips initially, but were reduced to 2 kips when the applied load approached the anticipated cracking load. A plot of load vs. strain, such as the one shown in Figure 4.12, was maintained during each test. Crack initiation was signaled when any one of the six strain series exhibited a nonlinear increase, which was often accompanied by a decrease in strain at another point. As an example, the cracking load for the test depicted in Figure 4.12 was taken as 28 kips. In most tests, the crack was still not visible at this load, and the load was increased further until the crack could be marked. Crack initiation plots for all 23 flexural tests are provided in Appendix E. Once crack initiation was detected by surface strain measurements, the applied load was increased until a crack was visible to the naked eye. The crack was traced with a marker on the underside of the beam. The beam was then unloaded.

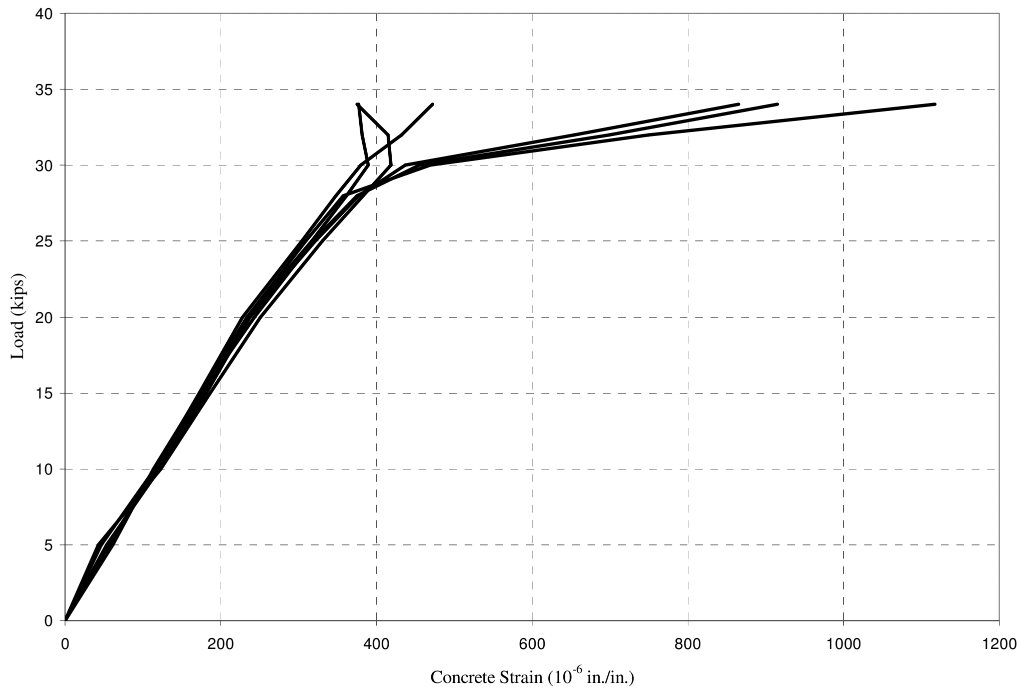

Figure 4.12 Crack Initiation Plot for 1.270.5N.RA

Results from crack initiation tests are shown in Table 4.20. The applied cracking loads shown in the second column were determined from crack initiation plots. The applied moment is the cracking moment resulting from the applied load. Two load tests were performed for each beam, so the effective prestress calculation for each beam end was averaged to obtain one value of effective prestress for each beam. The difference between effective prestress measured at opposite ends of a single beam exceeded 15 ksi in only two beams. In four beams, this difference was less than 3 ksi. It is important to note that the assumed cracking load was a major factor in the calculation effective prestress. A 1 kip change in cracking load produced changes in effective prestress as large as 8 ksi.

Table 4.20 Prestress Losses Measured by Crack Initiation

Beam Designation	$P_{applied}$ (k)	$M_{applied}$ (k in.)	f_{pe} (ksi)	$f_{pe,average}$ (ksi)
0.270.5N.RA 0.270.5N.RB	25 29	1125 1196	184 196	190
0.300.5N.RB	28	1260	208	208
1.270.5N.RA 1.270.5N.RB	28 30	1155 1164	169 170	169
1.300.5N.RA 1.300.5N.RB	34 34	1116 1320	161 196	179
1.270.5N.UA 1.270.5N.UB	25 25	1031 970	148 138	143
1.300.5N.UA 1.300.5N.UB	25 30	1125 1164	163 170	167
3.270.5S.RA 3.270.5S.RB	36 34	1397 1473	159 170	164
3.300.5S.RA 3.300.5S.RB	42 38	1630 1646	191 193	192
3.270.5S.UA 3.270.5S.UB	38 36	1475 1559	170 181	176
3.300.5S.UA 3.300.5S.UB	42 38	1630 1646	191 193	192
4.270.5S.RA 4.270.5S.RB	44 38	1584 1568	186 184	185
4.300.5S.RA 4.300.5S.RB	38 38	1568 1710	184 204	194

4.3.2.3 Measurement of Prestress Losses by Crack Reopening Tests

Effective prestress was also measured by crack reopening tests. These tests were performed by reloading each beam until the previously observed crack had reopened. The stress in the bottom of the section was assumed to be zero when the crack reopened. Equation 4.16 was used to calculate effective prestress. The applied moment in these calculations was the moment required to reopen the crack, and tensile strength of the concrete was taken as zero since the bottom of the section was already cracked.

The load at which a crack reopened was determined with crack detection gages such as the one pictured in Figure 3.15. Each crack detection gage was comprised of a brass bracket with plastic contact points that could be affixed to concrete. An axial strain gage was attached to the back of the bracket. For pour zero tests, the strain gage was calibrated so that relative displacement of the two contact points could be measured. In all other tests, the strain in the gage was directly measured. Beams were reloaded to the initial cracking load while measuring the strain in crack detection gages. The point at which the load vs. strain plot became nonlinear indicated crack reopening. A single crack detection gage with a one second recording interval was used for pour zero tests. This recording interval was too long and resulted in exclusion of critical data points. The interval was reduced to one tenth of a second for pour one tests. This resulted in smooth plots of load vs. strain, but the load at which the crack reopened was still vague because of a gradual transition from linear to nonlinear behavior. In beams from pours three and four, a second crack detection gage was placed adjacent to the crack, but not over the crack. Strain from both gages was plotted, and the load at which the two plots diverged was assumed to be the cracking load. An example of a crack reopening plot is shown in Figure 4.13. Crack reopening plots for all tests are provided in Appendix E.

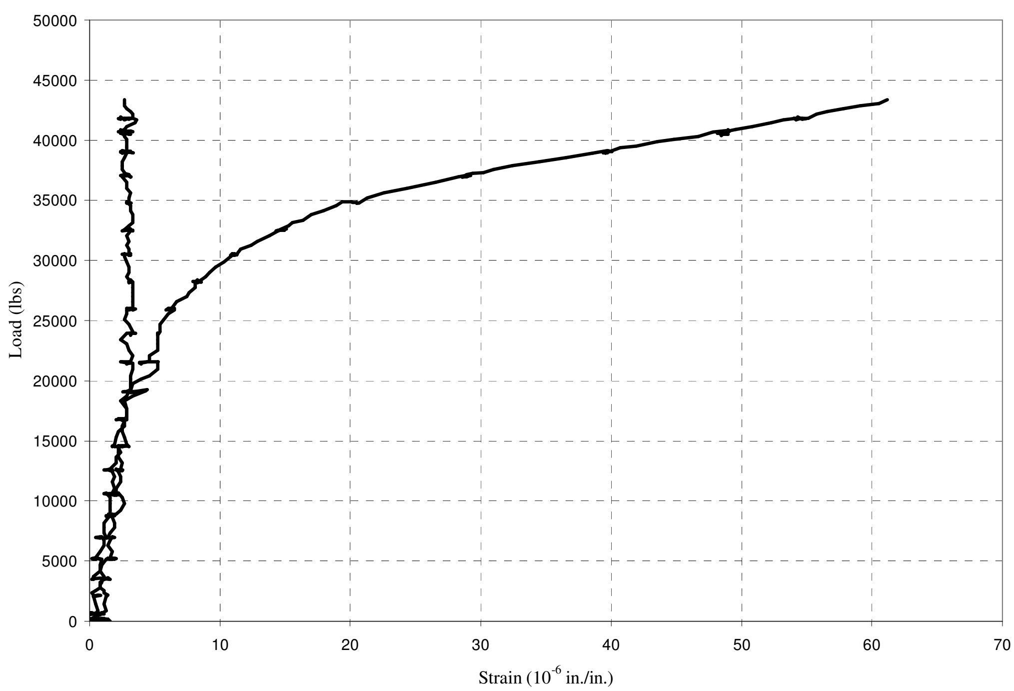

Figure 4.13 Crack Reopening Plot for 3.300.5S.RB

Results from crack reopening tests are shown in Table 4.21. These results were significantly dispersed. The difference in effective prestress calculated at opposite ends of a single beam ranged from 8 to 65 ksi. Crack reopening loads were difficult to decipher from load vs. strain plots. Misinterpretation of a crack reopening load by 1 kip caused changes in effective prestress as large as 8 ksi, as was the case with crack initiation load interpretation.

Table 4.21 Prestress Losses Measured by Crack Reopening

Beam Designation	$P_{applied}$ (k)	$M_{applied}$ (k in.)	f_{pe} (ksi)	$f_{pe,average}$ (ksi)
0.270.5N.RA 0.270.5N.RB	16 22	720 908	134 168	151
0.300.5N.RB	19	855	159	159
1.270.5N.RA 1.270.5N.RB	20 24	825 932	153 172	163
1.300.5N.RA 1.300.5N.RB	25 24	820 932	152 172	162
1.270.5N.UA 1.270.5N.UB	18 21	743 815	138 151	145
1.300.5N.UA 1.300.5N.UB	20 21	900 815	167 151	159
3.270.5S.RA 3.270.5S.RB	15 24	582 1040	89 155	122
3.300.5S.RA 3.300.5S.RB	26 26	1009 1126	150 167	159
3.270.5S.UA 3.270.5S.UB	27 22	1048 953	156 142	149
3.300.5S.UA 3.300.5S.UB	28 27	1087 1169	161 173	167
4.270.5S.RA 4.270.5S.RB	26 24	936 990	139 147	143
4.300.5S.RA 4.300.5S.RB	26 26	1073 1170	159 173	166

4.3.3 Comparison and Discussion of Prestress Loss Methods

The prestress losses predicted by PCI and AASHTO models were almost identical, so experimentally determined prestress losses will be compared to the AASHTO prediction only. Table 4.22 compares the prestress losses measured by the basic vibrating wire gage method to AASHTO predictions. The basic vibrating wire gage method was unique because it was based on the same assumptions implemented in the theoretical models:

1. The stress in the prestressing strands just before transfer was assumed to be the jacking stress.
2. Only elastic shortening and long term time dependent losses were considered.

The vibrating wire gage losses (elastic shortening and time dependent) were greater than theoretical losses for some beams, but less than theoretical losses for other beams. In some beams, a low measurement of elastic shortening loss was combined with a high measurement of time dependent losses, and vice versa. In other beams, the experimental measurements were greater than theoretical predictions for both elastic shortening and time dependent losses.

Table 4.22 Comparison of Basic Vibrating Wire Gage and AASHTO Prestress Losses

Beam Name	Elastic Shortening Loss (ksi)			Time Dependent Losses (ksi)		
	AASHTO	Basic VWG	VWG/ AASHTO	AASHTO	Basic VWG	VWG/ AASHTO
0.270.5N.R	12.4	13.1	1.06	11.9	13.6	1.15
0.300.5N.R	13.9	12.4	0.90	12.9	16.5	1.29
1.270.5N.R	12.4	11.5	0.93	8.27	12.2	1.48
1.300.5N.R	13.9	12.4	0.89	9.35	13.7	1.47
1.270.5N.U	13.4	11.4	0.85	8.71	13.9	1.60
1.300.5N.U	13.9	13.9	1.00	9.35	15.3	1.63
3.270.5S.R	12.2	13.3	1.09	13.8	13.2	0.96
3.300.5S.R	13.7	14.0	1.02	15.3	14.3	0.94
3.270.5S.U	12.2	12.9	1.05	14.5	13.1	0.90
3.300.5S.U	13.7	13.8	1.01	16.4	14.5	0.88
4.270.5S.R	12.2	14.3	1.17	11.6	19.1	1.65
4.300.5S.R	13.7	15.6	1.13	12.8	20.8	1.63
Average Ratio			1.01			1.30

All experimental measurements of prestress losses are summarized and compared to theoretical predictions in Table 4.23. Only the AASHTO theoretical values are presented, the reason for which was explained previously. Each experimental value of effective prestress is presented as its ratio to the AASHTO value. The effective prestress measured by the basic vibrating wire gage method correlated well with theoretical effective prestress. The vibrating wire gage losses measured by the upper/lower bound method were dispersed. The upper bound effective prestress was less than the AASHTO effective prestress in five of the six beams with normal strands, and greater than the AASHTO value in all of the beams with special strands.

This is most likely due to larger changes in vibrating wire gage strain resulting from higher strand stress levels. The lower bound effective prestress values were much less than values predicted by theoretical models and measured by the basic vibrating wire gage method. The lower bound values were based on a concrete stress before release that exceeded the tensile strength. The fact that no tensile cracking was observed before release suggests why these values are so low. The effective prestress calculated from crack initiation was within seven percent of the theoretical prediction in three fourths of the beams. However, the crack initiation effective prestress was significantly less than the theoretical prediction in the other beams. Effective prestress predicted by crack reopening was significantly less than the theoretical prediction for all beams. In some cases, the crack reopening effective prestress was even less than the lower bound vibrating wire gage calculation. It is important to note that prestress losses predicted by the PCI and AASHTO methods and measured by the basic vibrating wire gage method do not account for possible losses between pouring concrete and prestress transfer, with the exception of steel relaxation in the PCI method. In contrast, effective prestress values measured by the upper/lower bound vibrating wire gage method and the crack initiation/reopening methods include all possible sources of prestress loss, and are independent of the jacking stress.

Table 4.23 Summary of Prestress Loss Results

Beam Name	$f_{pe,AASHTO}$ (ksi)	$f_{pe,EXPERIMENTAL}/f_{pe,AASHTO}$				
		Vibrating Wire Gage (Basic)	Vibrating Wire Gage Upper Bound	Vibrating Wire Gage Lower Bound	Crack Initiation	Crack Reopening
0.270.5N.R	178	0.97	1.08	0.80	1.07	0.85
0.300.5N.R	198	0.98	0.90	0.65	1.05	0.80
1.270.5N.R	182	1.01	0.97	0.68	0.93	0.89
1.300.5N.R	202	0.98	0.93	0.66	0.89	0.80
1.270.5N.U	180	1.01	0.90	0.61	0.79	0.80
1.300.5N.U	202	0.97	0.98	0.72	0.83	0.79
3.270.5S.R	176	1.00	1.19	0.87	0.93	0.69
3.300.5S.R	196	1.00	1.12	0.83	0.98	0.81
3.270.5S.U	176	1.01	1.10	0.78	1.00	0.85
3.300.5S.U	195	1.01	1.06	0.77	0.99	0.86
4.270.5S.R	179	0.95	1.11	0.82	1.04	0.80
4.300.5S.R	198	0.96	1.08	0.82	0.98	0.84
Average Ratio		0.99	1.04	0.75	0.95	0.81

4.3.4 Prestress Losses Before Prestress Transfer

Low measurements of effective prestress by the lower bound vibrating wire gage method and crack initiation/reopening tests suggested that prestress losses may have occurred during the time between pouring concrete and transfer of prestress. One possible source of prestress loss was temperature variations associated with curing concrete. When concrete was poured around prestressing strands, the heat produced by hydration of Portland cement caused an increase in strand temperature and an associated thermal expansion. The length of the strands was fixed between abutments (constant strain), so the strands may have incurred a decrease in tension. If bonding occurred at an elevated temperature, a loss of prestress was "locked" into the beams. After bonding occurred, any additional change in temperature would have caused a change in steel stress because the coefficients of thermal expansion in concrete and steel differed (Barr, et al. 2005). Another possible source of prestress loss was shrinkage. In theory, no shrinkage occurred during the moist cure. However, some shrinkage may have occurred because of imperfections of the moist cure. In addition, shrinkage likely occurred during the time between end of cure and prestress transfer in pours one and three. Because beams were restrained from shrinkage strain before transfer, this strain was assumed to occur instantaneously at the time of transfer.

These effects were investigated in pour four. Dead end strand stress, vibrating wire gage strain, and internal temperature were monitored from the beginning of the concrete pour until just before transfer. In addition to the two beams, a small concrete prism was cast with an embedded vibrating wire gage so that strains in unrestrained concrete could be measured. The variation of dead end strand stress is shown in Figure 4.14. This stress was recorded by load cells at the dead end abutments. The vibrating wire gage strain is shown in Figure 4.15. These strain measurements include the recommended temperature correction factor. The assumed coefficients of thermal expansion were 12.2 and 10.4 $\mu\varepsilon/^{o}C$ for steel and concrete, respectively. The internal temperatures measured by vibrating wire gage thermistors are shown in Figure 4.16. In each plot, time zero corresponds to the beginning of the concrete pour. Bond was assumed to occur sometime between eight and sixteen hours after pouring. This was also the time of peak concrete temperatures. Formwork was removed at three days, and the prestressing strands were flame cut at six days.

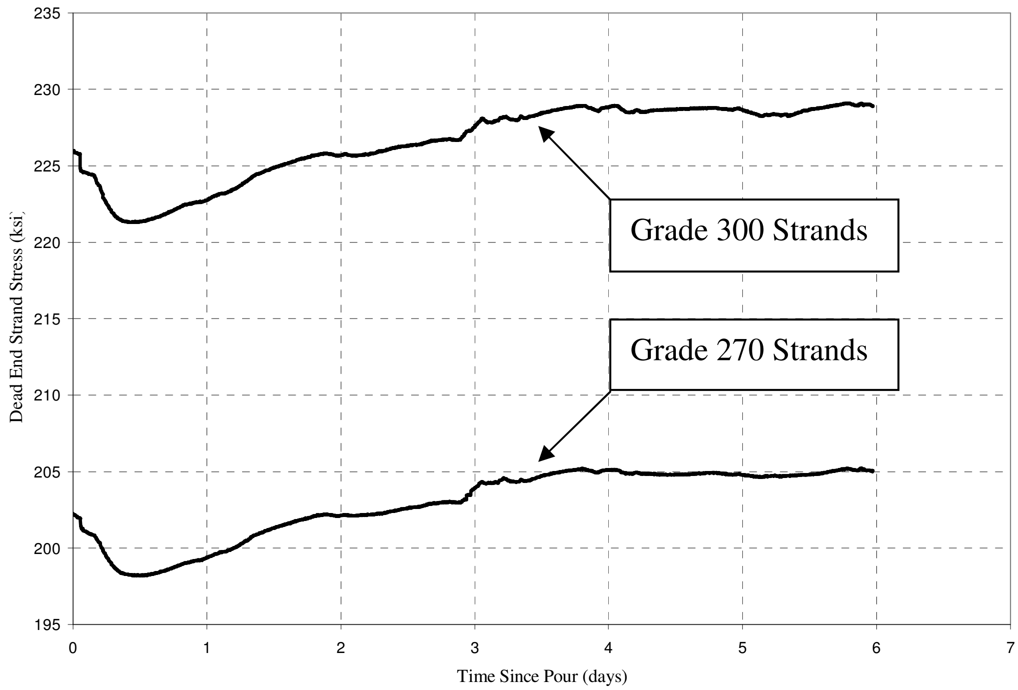

Figure 4.14 Dead End Strand Stress Between Casting and Transfer

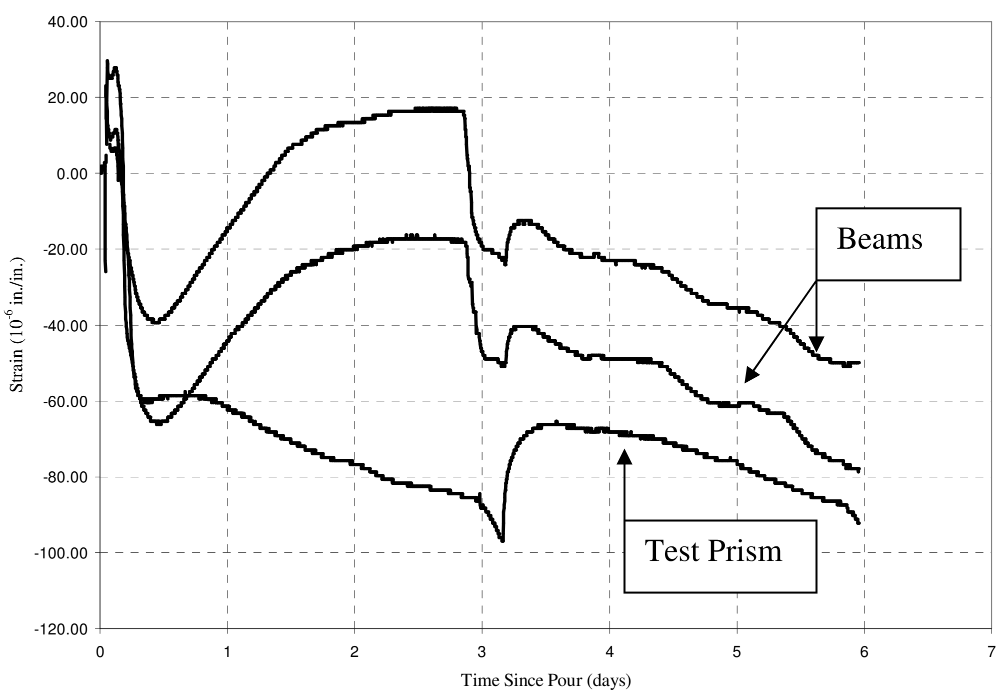

Figure 4.15 Vibrating Wire Gage Strain Between Casting and Transfer

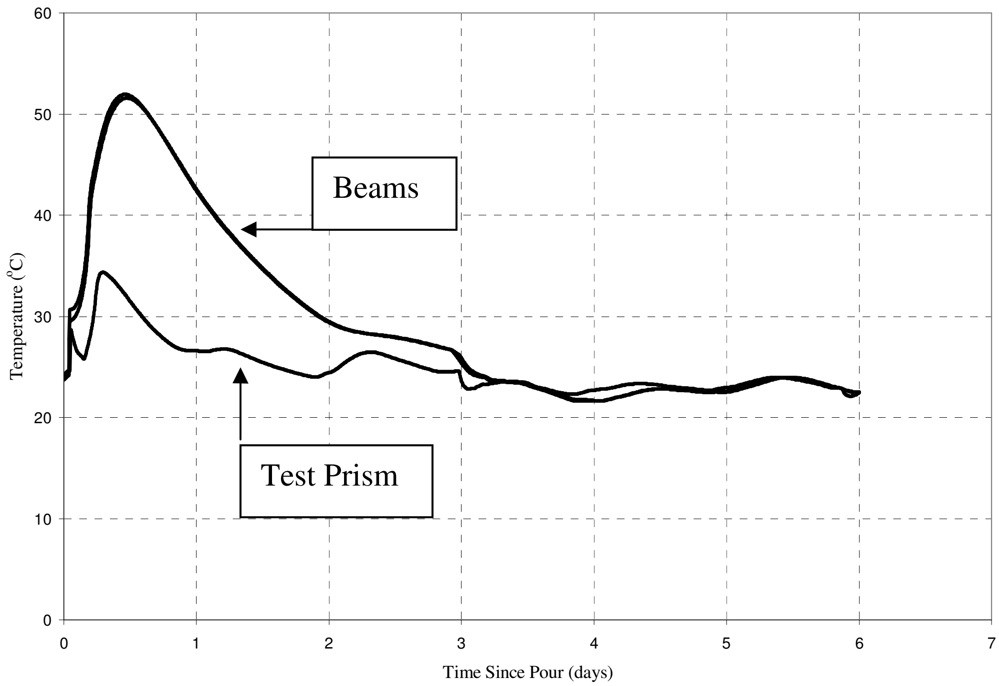

Figure 4.16 Internal Temperature Between Casting and Transfer

In the first twelve hours, beam temperatures increased sharply. This caused expansion of prestressing strands and resulted in a decrease in dead end stress. Vibrating wire gage strains were initially tensile, but became compressive. The compression most likely occurred because thermal concrete expansion was restrained by formwork. Bonding between concrete, vibrating wire gages, and prestressing strands was assumed to occur in the vicinity of twelve hours after pour. In the time between one half day and three days, temperatures gradually returned to the ambient temperature of the lab. Vibrating wire gage strains indicated compression in the test prism and tension in the beams. The prism experienced compression because of thermal contraction that was only slightly restrained by formwork. The beam experienced tension because the tensioned strands between the beams and abutments provided significant partial restraint to thermal contraction. Obviously, some beam contraction occurred because the dead end strand stress increased. Forms were removed three days after the pour, and vibrating wire gage readings indicated compressive strains in beams and the prism. This suggests that bond and confinement between concrete and wooden formwork were restraining additional thermal contraction. This idea is supported by the slight increase in dead end strand stress at day three.

In the time between removal of formwork and prestress transfer, vibrating wire gage strains were compressive. Temperatures were relatively constant, so the compression must have been a result of shrinkage. Because these strains were relatively small, no major change in dead end strand stress was observed.

Several of the events occurring between pouring of concrete and transfer of prestress could have caused decreases in strand stress. A significant loss of prestress could have resulted from fully restrained thermal expansion of strands before bonding occurred. After bonding occurred, additional stress may have been lost because of thermal contraction not restrained by external strand segments. Any restrained thermal contraction, as well as shrinkage, could have decreased strand stress instantaneously when the strands were cut. These sources of prestress loss are not addressed in current code provisions and were not included in the prestress losses measured by the basic vibrating wire gage method.

5. SUMMARY, CONCLUSIONS, AND RECOMMENDATIONS

5.1 Summary

Twelve pretensioned prestressed concrete beams were cast and tested in the Virginia Tech Structures and Materials Laboratory. The research was conducted as a portion of a larger project sponsored by the Virginia Department of Transportation. This thesis pertained to two specific objectives. The first objective was to determine the effect of casting position, if any, on the development of prestressing strand. The second objective was to compare experimental measurements of effective prestress to code provisions for prediction of prestress losses.

The effect of casting orientation, or top strand effect, was assessed by comparing transfer length and development length test results between beams with normal and inverted casting orientations. The formwork for four of the test beams was assembled upside down so that more than 12 in. of fresh concrete was placed below prestressing strands. The depth of fresh concrete below strands was 15 or 17 in. in inverted beams (depending on section size) whereas the depth of concrete below strands in normal beams was 2 in. Transfer lengths in the end regions of each beam were determined from surface strain measurements before and after the release of prestress. Development lengths were determined through iterative load tests near the ends of each beam.

Prestress losses were experimentally measured in each beam by vibrating wire gage strain readings and flexural crack initiation and reopening tests. One vibrating wire gage was placed in each beam at the level of the prestressing strands and allowed concrete strains to be measured from the time of pouring until load testing. The effective prestress in each beam was calculated from the load required to initiate flexural cracking and reopen the initial crack. Measured prestress losses were compared to theoretical predictions calculated according to PCI and AASHTO models.

5.2 Conclusions and Recommended Code Provisions

Transfer lengths were measured at each end of each test beam. The following conclusions were drawn from transfer length tests:

1. All transfer lengths measured in beams with normal casting orientation were conservatively shorter than current ACI and AASHTO code provisions.
2. The inverted casting position caused a 70 percent average increase in transfer length. It is recommend that code provisions for transfer length be increased to 90 strand

diameters when twelve or more inches of fresh concrete are cast below prestressing strand. All measured transfer lengths were shorter than 90 strand diameters, or 45 in. for 0.5 in. diameter strands.

3. Surface strain measurements and the 95 percent average maximum strain plateau method provided an effective means of determining transfer length.

Development lengths were determined through iterative load testing. While not as conclusive as transfer length tests, some important conclusions were drawn from development length tests.

1. The development lengths in beams with normal casting orientation were shorter than current ACI and AASHTO provisions.
2. The development lengths in beams with inverted casting orientation were equal to or longer than code provisions. It is recommend that the AASHTO development equation in Article 5.11.4.2 be increased by 40 percent when twelve or more inches of fresh concrete are cast below prestressing strand. This is equivalent to the factor in Article 5.11.2.1.2, which increases the development length of deformed bars by 40 percent when twelve or more inches or fresh concrete are cast below (AASHTO 2006). Similarly, it is recommended that the ACI development length equation in Section 12.9.1 be increased by 30 percent when twelve or more inches of fresh concrete are cast below. This is equal to the factor in Section 12.2.4 for the development length of deformed bars with twelve or more inches of fresh concrete cast below (ACI 2005).
3. Determination of development length through iterative load testing was indirect and sometimes inconclusive. While the target variable in these tests was embedment length, several other uncontrollable variables affected test results.

Prestress losses were predicted by theoretical models and experimentally measured. The following conclusions were drawn from prestress loss predictions and measurements:

1. Prestress losses predicted by the provisions of the PCI Committee on Prestress Losses and AASHTO refined method were very similar.
2. The prestress losses measured by the basic vibrating wire gage method were greater than PCI and AASHTO loss predictions. On average, the initial measured losses

were one percent greater than the theoretical predictions, while the long term measured losses were 30 percent greater than the theoretical predictions.

3. The upper/lower bound method for vibrating wire gage data reduction was unreliable. It produced results that were in discord with the basic vibrating wire gage method. Increases in vibrating wire gage strain at release caused increased measurements of initial prestress according to the upper/lower bound method. However, an increase in vibrating wire gage strain at release suggested greater elastic shortening losses, which reduced initial prestress according to the basic vibrating wire gage method.
4. Measurement of effective prestress by load testing was highly dependent on the ability to accurately determine the loads required to initiate and reopen cracks. Cracking loads were generally easier to isolate than crack reopening loads.
5. The effective prestress values measured by the flexural crack initiation and reopening tests were lower than the effective prestress values predicted by code provisions. This suggested that prestress losses occurred between pouring of concrete and transfer of prestress because of thermal and shrinkage effects. While the industrial fabrication of prestress concrete members differs from the fabrication methods used in this project, it is still recommend that code provisions be modified to consider such losses.

5.3 Recommendations for Further Research

Little research has been conducted to determine the effect of casting position on the transfer and development length of prestressing strand. The test results from this project indicated quantitative increases in transfer length of prestressing strand when a significant amount of concrete was cast below. However, the increases in development length were more qualitative than quantitative. Further research is necessary to determine the quantitative effect of casting position on development length.

In addition, no attempt was made in this project to determine if varying heights of fresh concrete below a strand could affect its transfer and development length. Further testing is necessary to determine if increases in transfer and development length are a function of the depth of fresh concrete cast below prestressing strand.

Further research is also necessary to determine if the bond properties of the strands used in this project are similar to properties of strands from other producers. It is recommended that bond quality of the grade 270 and grade 300 strands be investigated through pull out tests. Types of recommended strand bond testing include the North American Strand Producers (NASP) Bond Test and the Moustafa Bond Test.

Test results suggested that prestress losses occurred between the time of pouring concrete and prestress transfer. Such losses are not accounted for in current code provisions for estimation of prestress losses. More research is recommended to determine if these losses do in fact occur, and to quantify them if so.

REFERENCES

Ahlborn, T. M., French, C. E., & Shield, C. K. (2000). "High Strength Concrete Prestressed Bridge Girders: Long Term and Flexural Behavior." *Report No. MN/RC-2000-32*, Minnesota Department of Transportation, St. Paul, Minnesota.

American Association of State and Highway Transportation Officials (AASHTO). (2006). *AASHTO LRFD Bridge Design Specifications*, Third Edition, Washington, D.C.

American Concrete Institute (ACI). (2005). *Building Code Requirements for Structural Concrete and Commentary*, Committee 318, Farmington Hills, Michigan.

ASTM A416/A416M-05 (2006). "Standard Specification for Steel Strand, Uncoated Seven-Wire for Prestressed Concrete." American Society for Testing and Materials, West Conshohocken, Pennsylvania.

Baran, E., Shield, C. K., & French, C. E. (2005). "A Comparison of Methods for Experimentally Determining Prestress Losses in Pretensioned Prestressed Concrete Girders." *Ned H. Burns Symposium on Historic Innovations in Prestressed Concrete*, American Concrete Institute, Farmington Hills, Michigan.

Barnes, R. W., Grove, J. W., & Burns, N. H. (2003). "Experimental Assessment of Factors Affecting Transfer Length." *ACI Structural Journal*, 100(6), 740-748.

Barr, P. J., Stanton, J. F., & Eberhard, M. O. (2005). "Effects of Temperature Variations on Precast, Prestressed Concrete Bridge Girders." *Journal of Bridge Engineering*, 10(2), 186-194.

Buckner, C. D. (1995). "A Review of Strand Development Length for Pretensioned Concrete Members." *PCI Journal*, 40(2), 84-105.

Buckner, C. D. (1994). "An Analysis of Transfer and Development Lengths for Prestensioned Concrete Structures." *Report No. FHWA-RD-94-049*, Federal Highway Administration, Washington, D.C.

Cousins, T. E., Johnston, D. W., & Zia, P. (1990). "Transfer and Development Length of Epoxy Coated and Uncoated Prestressing Strand." *PCI Journal*, 35(4), 92-103.

Guyon, Y. (1960). *Prestressed Concrete*, John Wiley & Sons, New York.

Hanson, N. W. & Kaar, P. H. (1959). "Flexural Bond Tests of Pretensioned Prestressed Beams." *Research and Development Bulletin D28*, Portland Cement Association, Skokie, Illinois, 783-802.

Hill, A. T. Jr. (2006). "Material Properties of Grade 300 and Grade 270 Prestressing Strands and Their Impact on the Design of Bridges." M.S. Thesis, Virginia Polytechnic Institute and State University, Blacksburg, Virginia.

Jeanty, P. R., Mitchell, D, and Mirza, M. S. (1988). "Investigation of 'Top Bar' Effects in Beams." *ACI Structural Journal*, 85(3), 251-257.

Kolozs, R. T. (2000). "Transfer and Development Lengths of Fully Bonded 0.5 in. Prestressing Strand in Standard AASHTO Type 1 Pretensioned High Performance Lightweight Concrete (HPLC) Beams." M.S. Thesis, The University of Texas at Austin.

Nassar, A. J. (2002). "Investigation of Transfer Length, Development Length, Flexural Strength, and Prestress Loss Trend in Fully Bonded High Strength Lightweight Prestressed Girders." M.S. Thesis, Virginia Polytechnic Institute and State University, Blacksburg, Virginia.

Nilson, A. H. (1987). *Design of Prestressed Concrete*, Second Edition, John Wiley & Sons, New York.

Precast/Prestressed Concrete Institute (PCI) Committee on Prestress Losses (1975). "Recommendation for Estimating Prestress Losses." *PCI Journal*, 20(4), 43-75.

Russell, B. W., & Burns, N. H. (1996). "Measured Transfer Lengths of 0.5 and 0.6 in. Strands in Pretensioned Concrete." *PCI Journal*, 41(5), 44-65.

Shahawy, M. (2001). "A Critical Evaluation of the AASHTO Provisions for Strand Development Length of Prestressed Concrete Members." *PCI Journal*, 46(4), 94-117.

Simmons, M. B. (1995). "Transfer and Development in Pretensioned, Prestressed Concrete Girders Using ½ in. Diameter Strand." Dissertation, Auburn University, Auburn, Alabama.

Tadros, M. K., Al-Omaishi, N., Seguirant, S. P., & Gallt, J. G. (2003). "Prestress Losses in Pretensioned High-Strength Concrete Bridge Girders." NCHRP Report 496, Transportation Research Board, Washington, D.C.

Wan, B., Harries, K. A., and Petrou, M. F. (2002). "Transfer Length of Strands in Prestressed Concrete Piles." *ACI Structural Journal*, 99(5), 577-585.

APPENDIX A Concrete Material Test Data

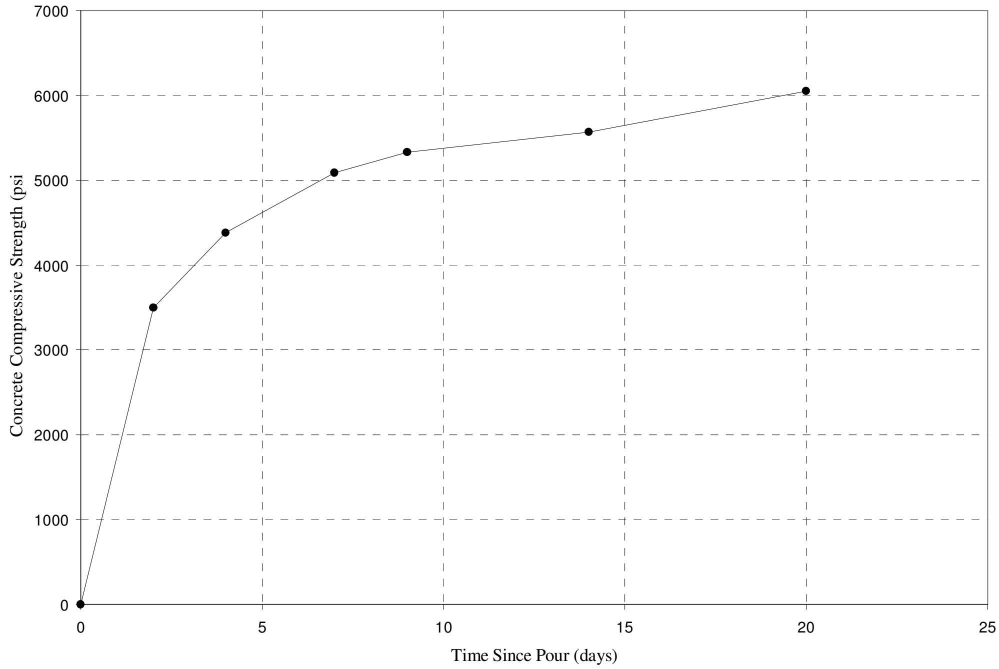

Figure A.1 Pour One Concrete Strength Gain

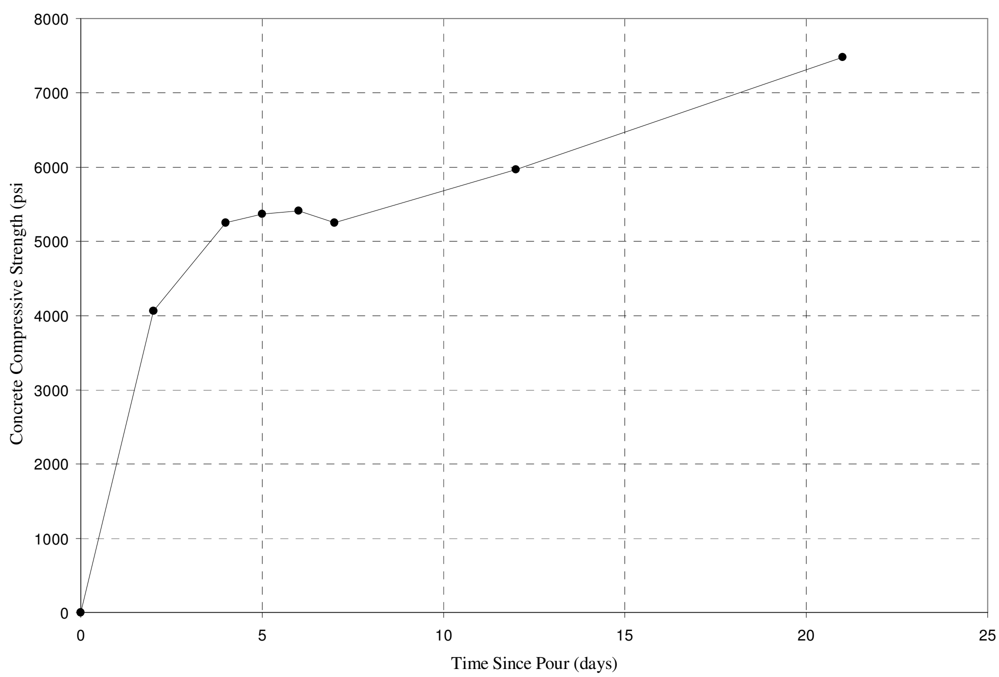

Figure A.2 Pour Three Concrete Strength Gain

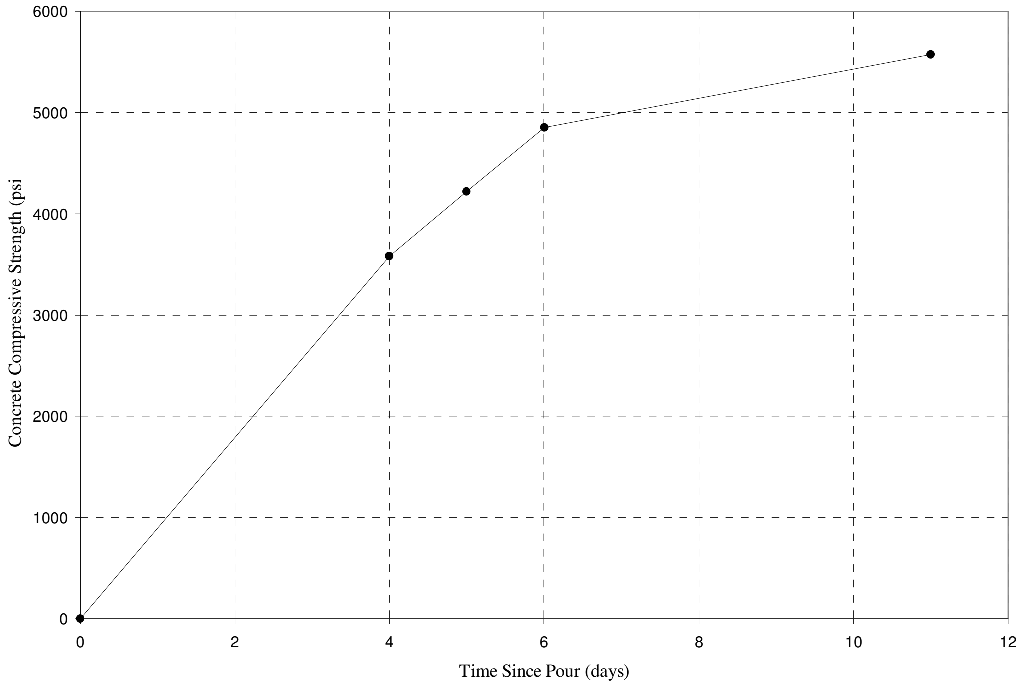

Figure A.3 Pour Four Concrete Strength Gain

Table A.1 Initial Concrete Cylinder Test Results

Pour	Time (days)	f'_c (psi)	E_c (ksi)
Zero	3	4770	
	3	4970	
One	2	3500	
	4	4380	
	7	5090	
	9	5330	
	14	5570	
	20	6050	
Three	2	4060	
	4	5250	
	5	5370	
	6	5410	
	7	5250	
	12	5970	4120
	21	7480	
Four	4	3580	
	5	4220	
	6	4850	2960
	11	5570	

Table A.2 Final Concrete Cylinder Test Results

Pour	Time (days)	f'_c (psi)	f_t (psi)	E_c (ksi)
Zero	24	6370 6760	581 617	4180
	25	6530 6570	557 637	2910
	30	7160 6170 6210	696 587 557	1600
One	20	6130 5970	736 637	4160
	21	6370 6530	517 557	1990
	22	6760 6680	716 716	1650
	23	6370 6680 6290	716 716	1690
Three	41	8040 7960	746 746	5350
	42	8440 7960	676 676	4980
	43	8440 7960	676 676 776	4870
	47	8160 8440	766 846	4950
	48	8160 8360	716 746	5450
Four	27	5770 6540 6760	696 736	3480
	28	6050 6290 6920	696 736	3730
	31	5970 6050	647	3460
	32	5970 6210	637	3400

APPENDIX B Strain Profiles for Transfer Length

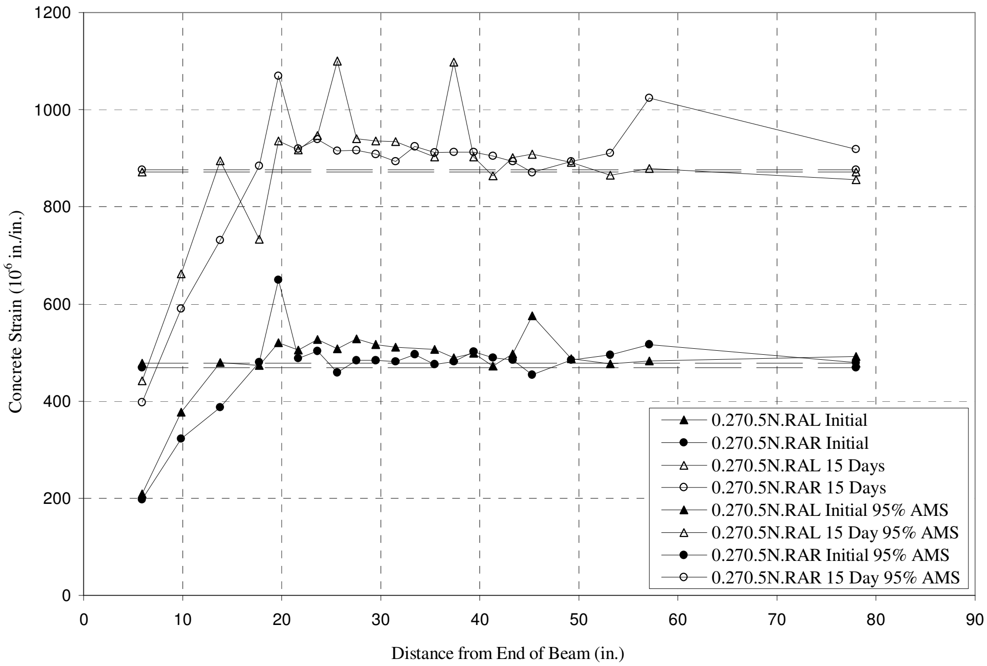

Figure B.1 Strain Profile for 0.270.5N.RA

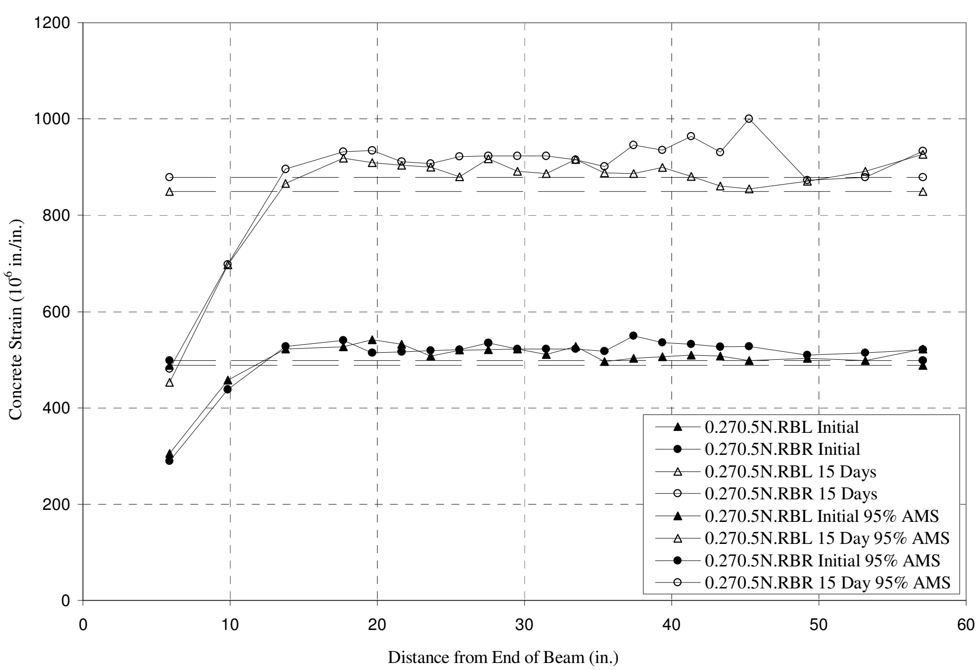

Figure B.2 Strain Profile for 0.270.5N.RB

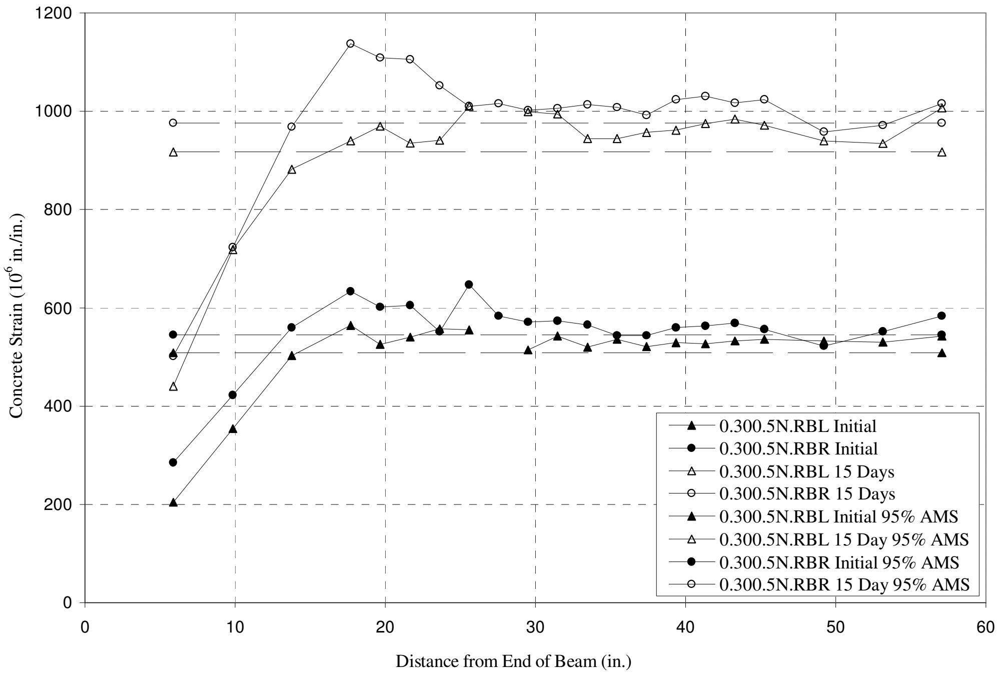

Figure B.3 Strain Profile for 0.300.5N.RA

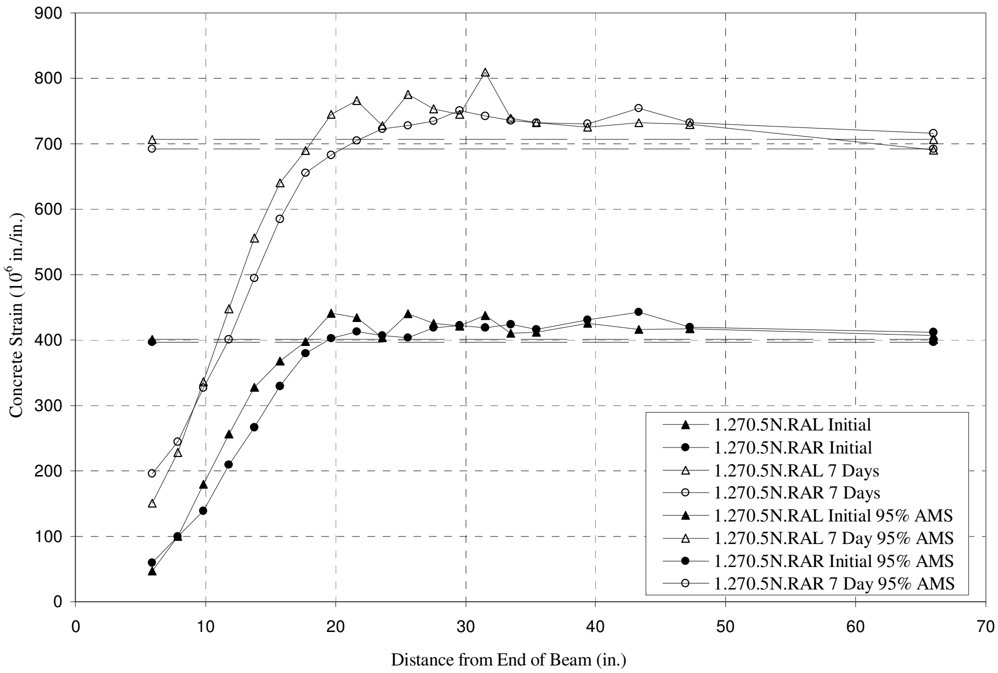

Figure B.4 Strain Profile for 1.270.5N.RA

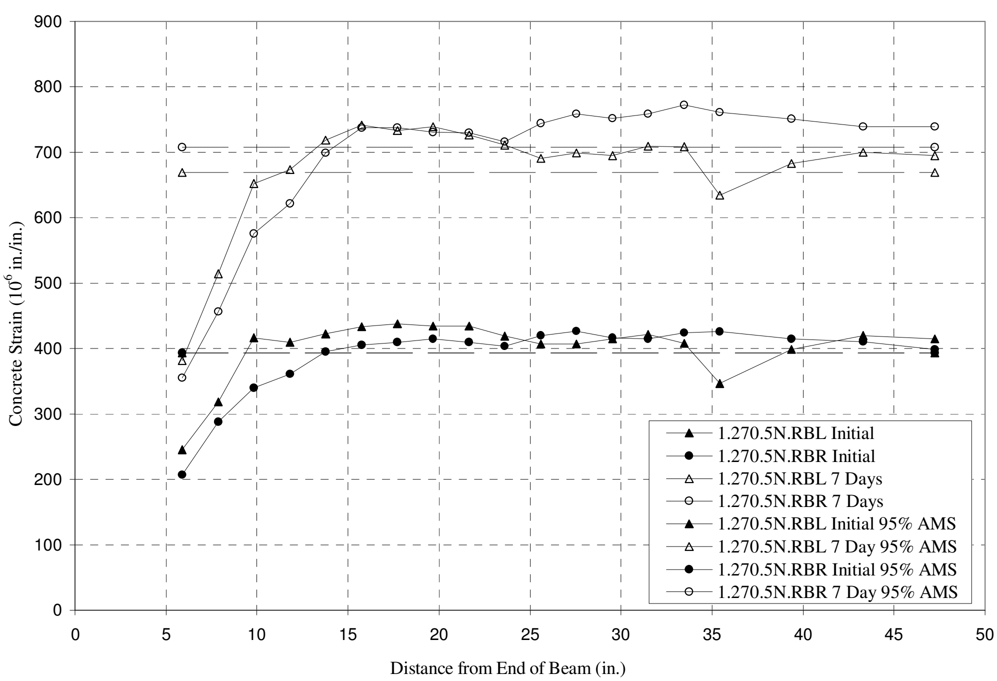

Figure B.5 Strain Profile for 1.270.5N.RB

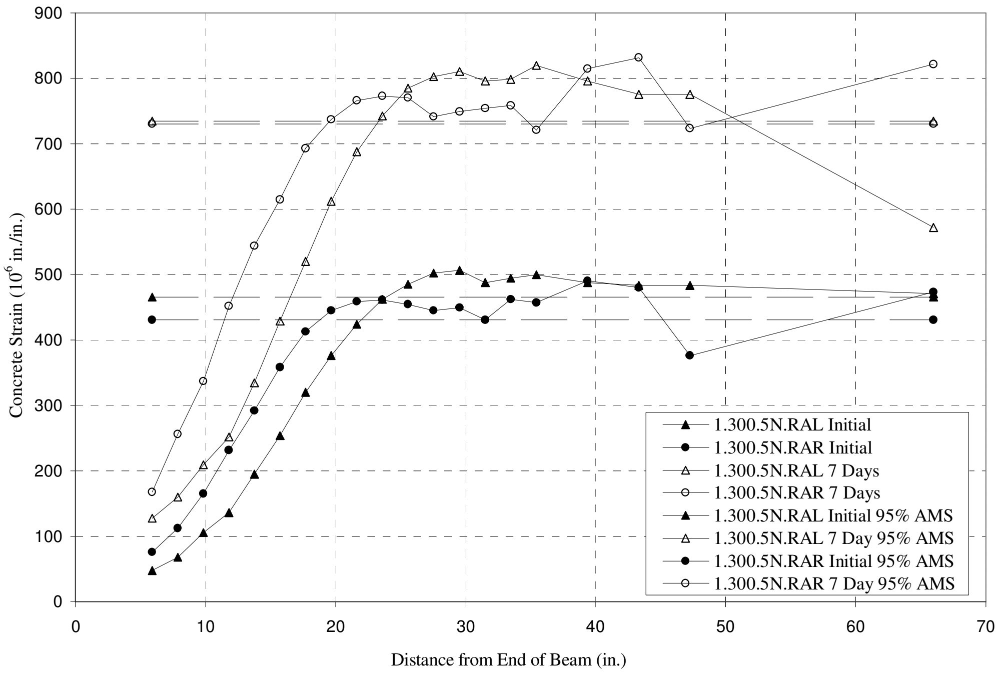

Figure B.6 Strain Profile for 1.300.5N.RA

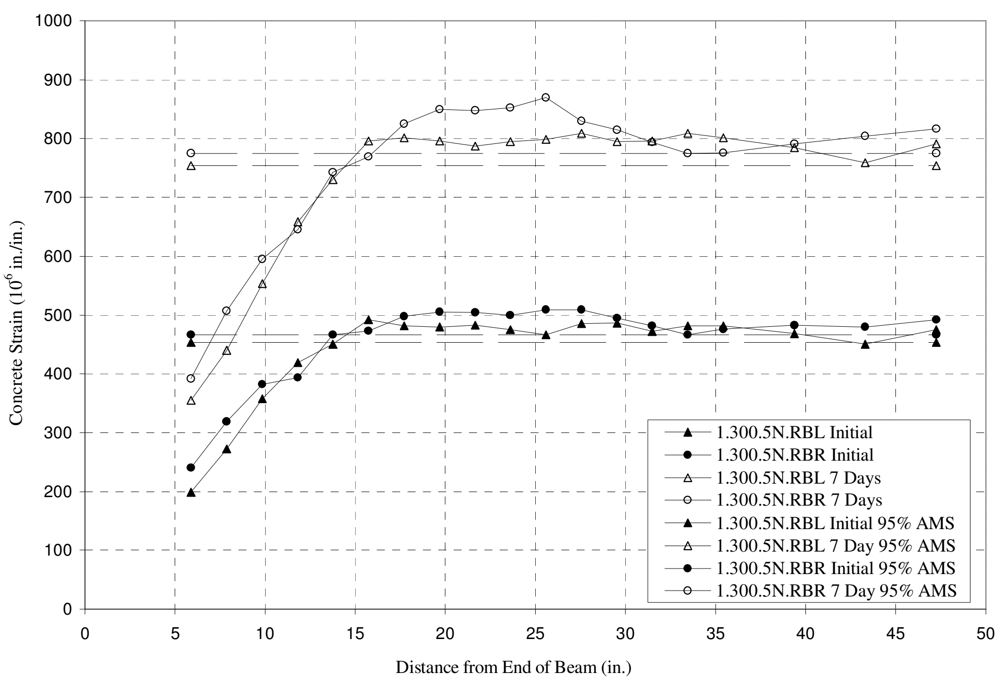

Figure B.7 Strain Profile for 1.300.5N.RB

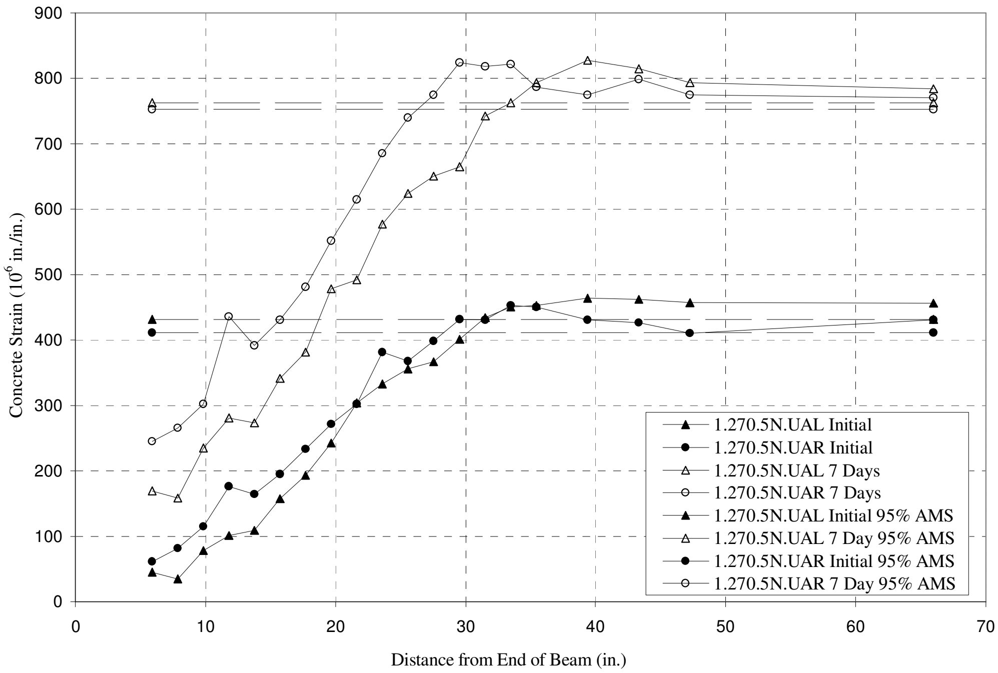

Figure B.8 Strain Profile for 1.270.5N.UA

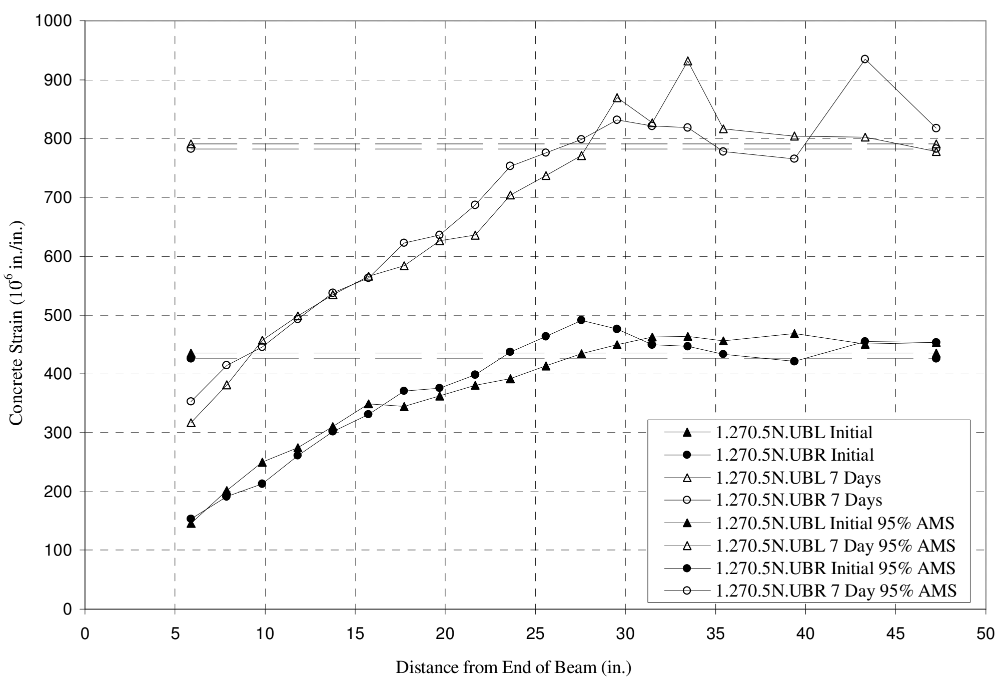

Figure B.9 Strain Profile for 1.270.5N.UB

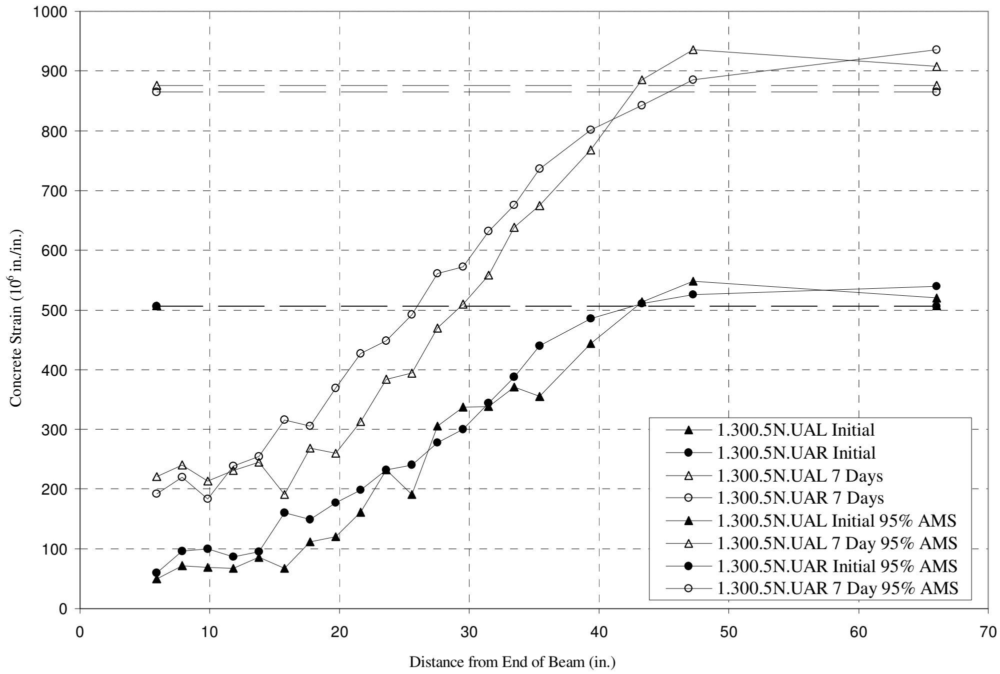

Figure B.10 Strain Profile for 1.300.5N.UA

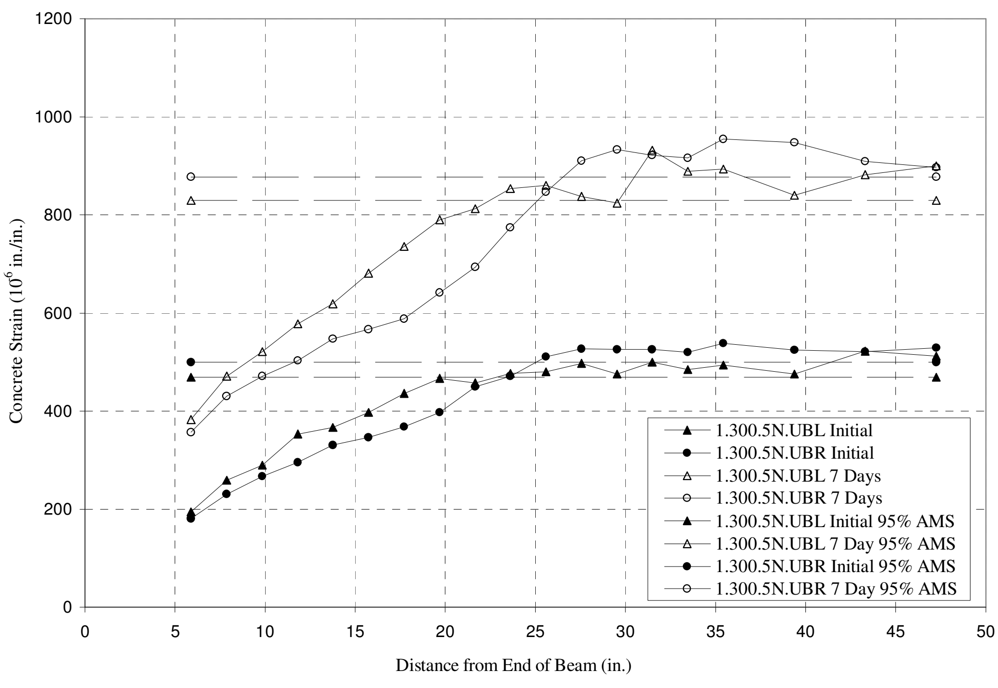

Figure B.11 Strain Profile for 1.300.5N.UB

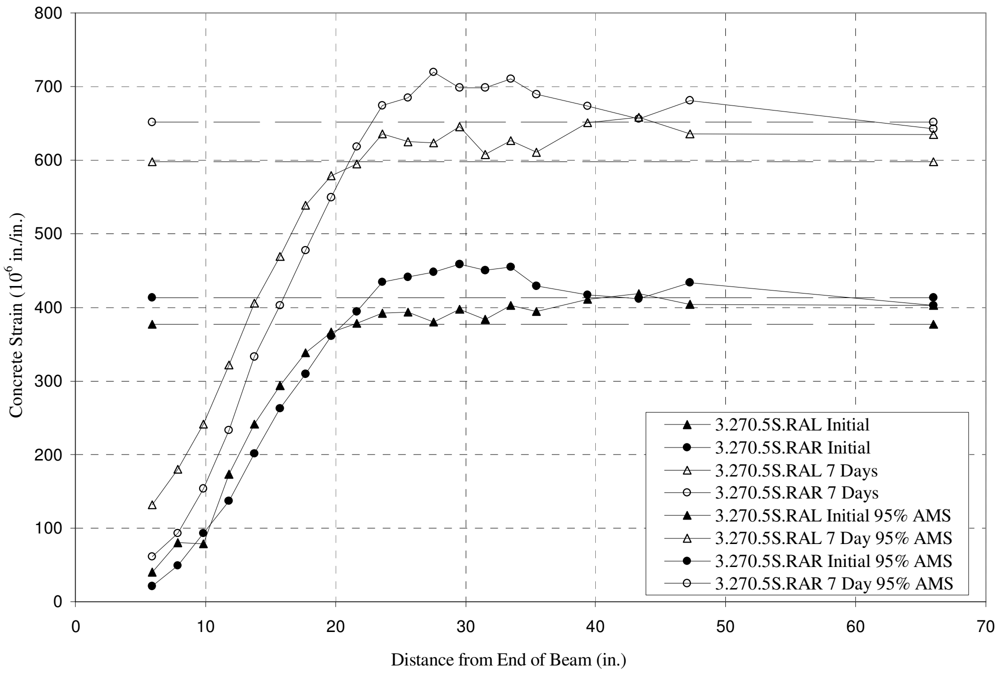

Figure B.12 Strain Profile for 3.270.5S.RA

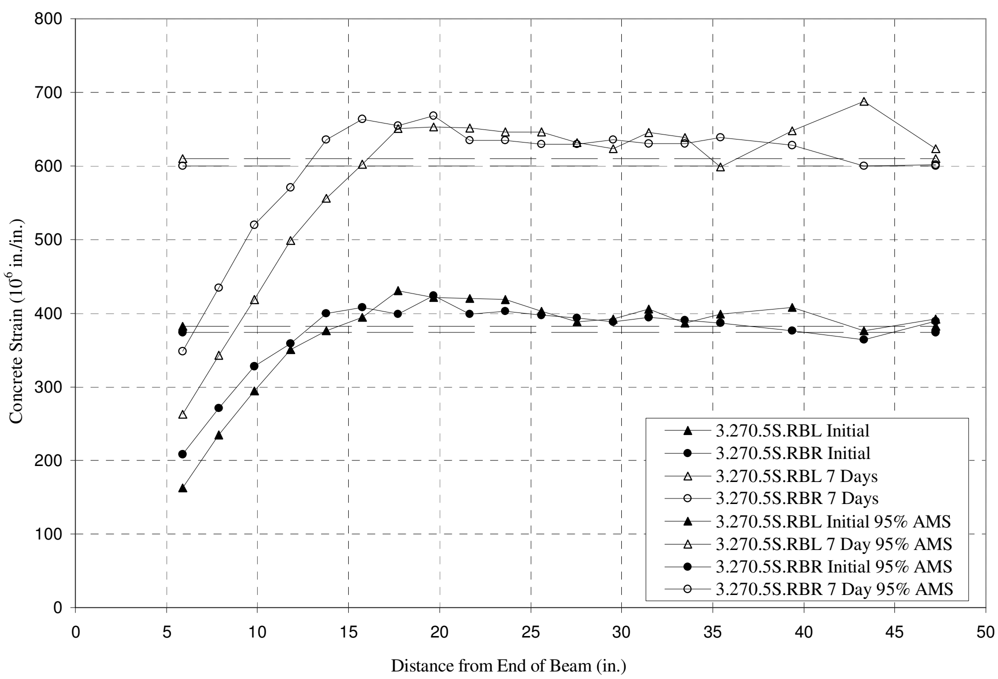

Figure B.13 Strain Profile for 3.270.5S.RB

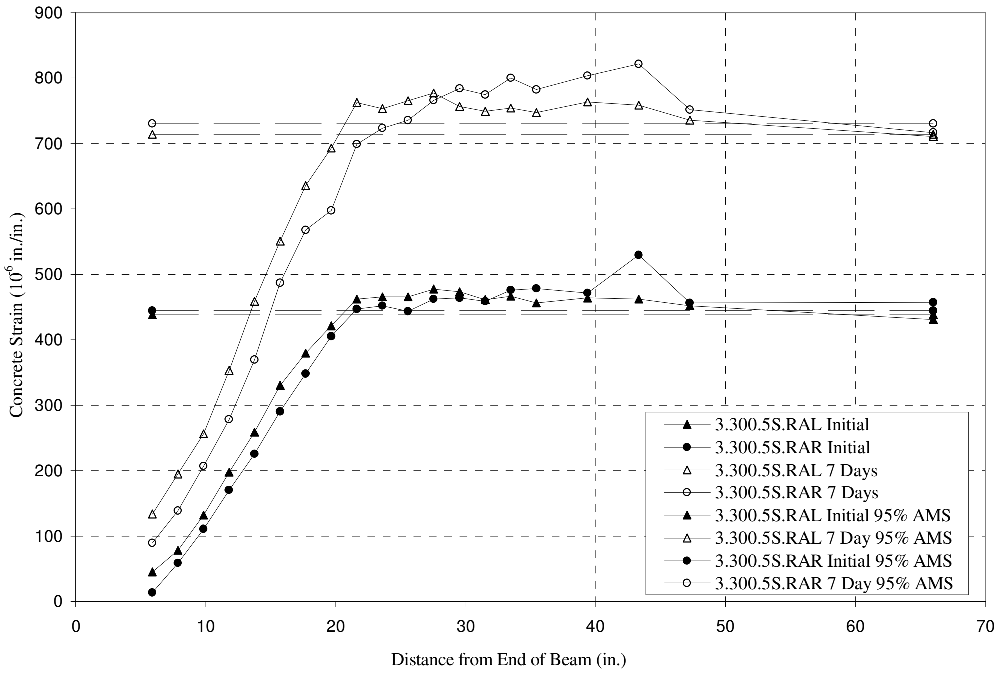

Figure B.14 Strain Profile for 3.300.5S.RA

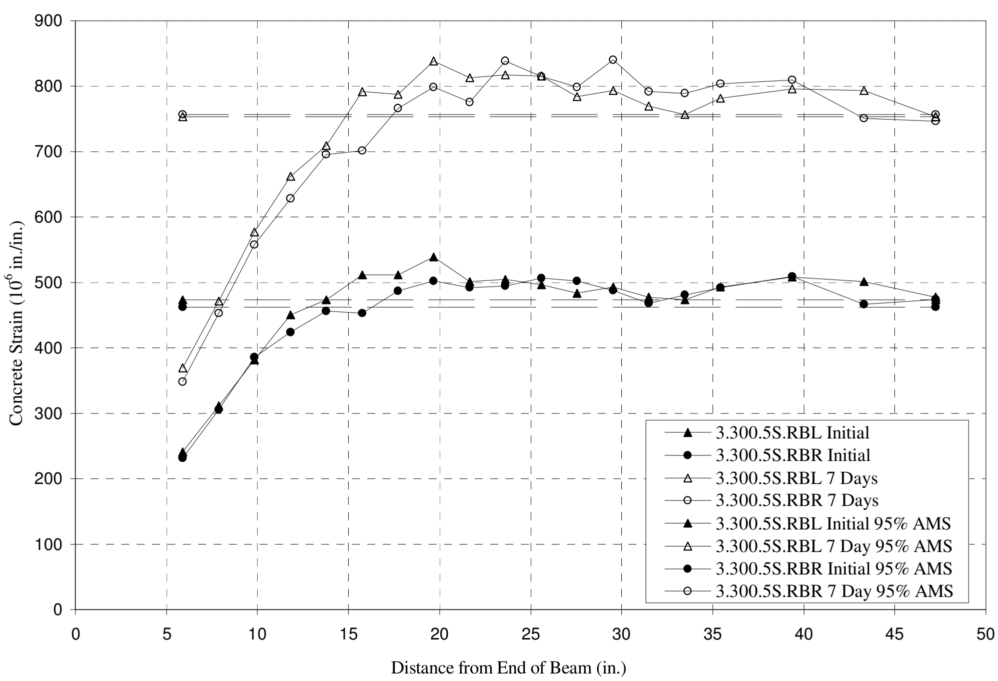

Figure B.15 Strain Profile for 3.300.5S.RB

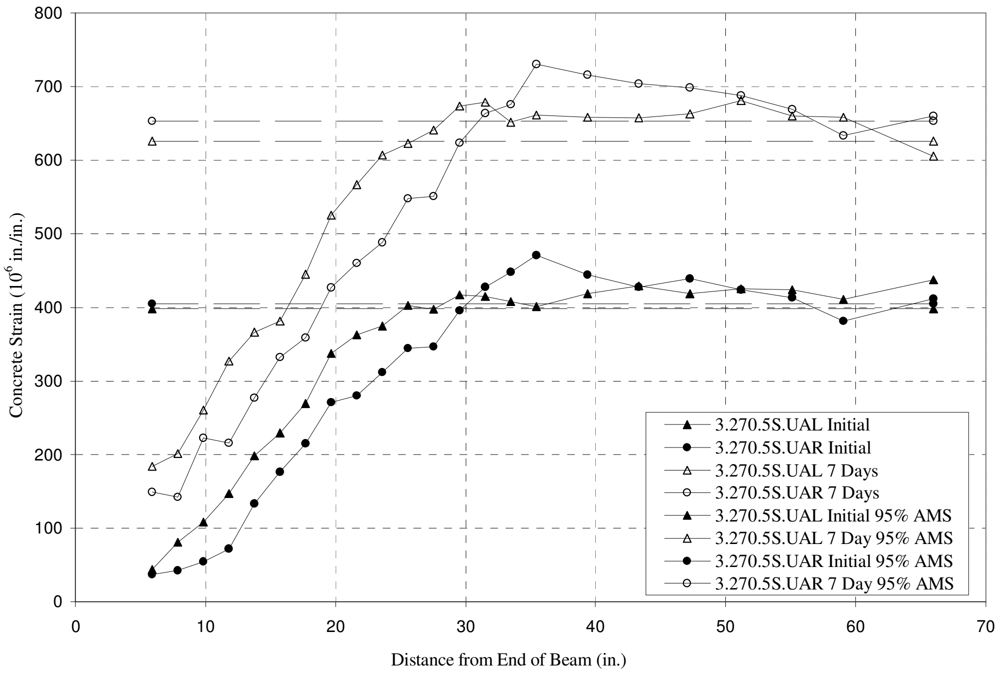

Figure B.16 Strain Profile for 3.270.5S.UA

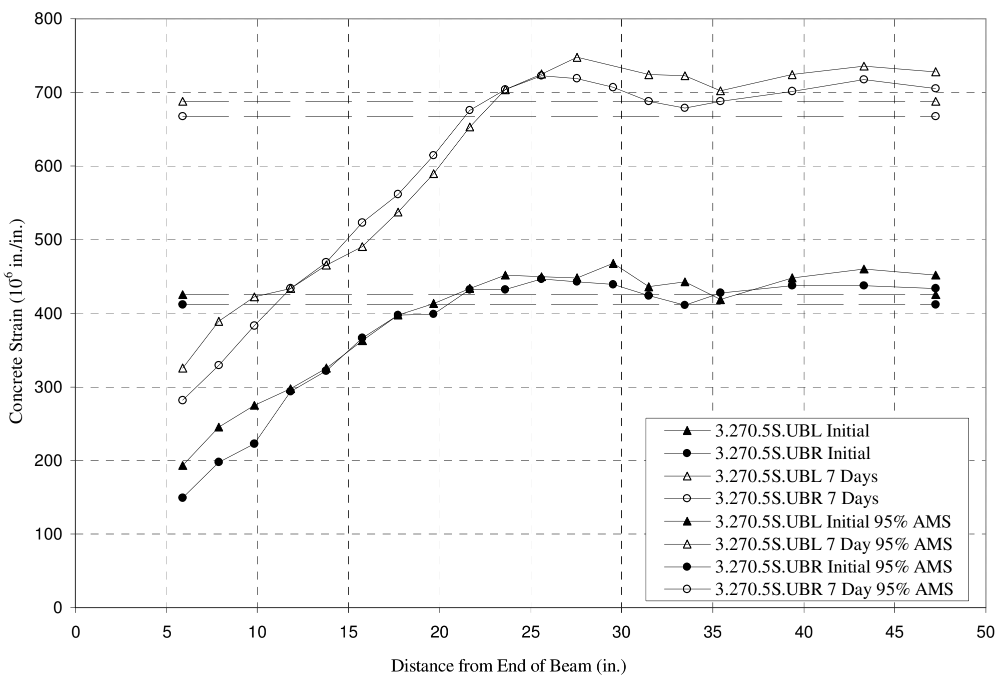

Figure B.17 Strain Profile for 3.270.5S.UB

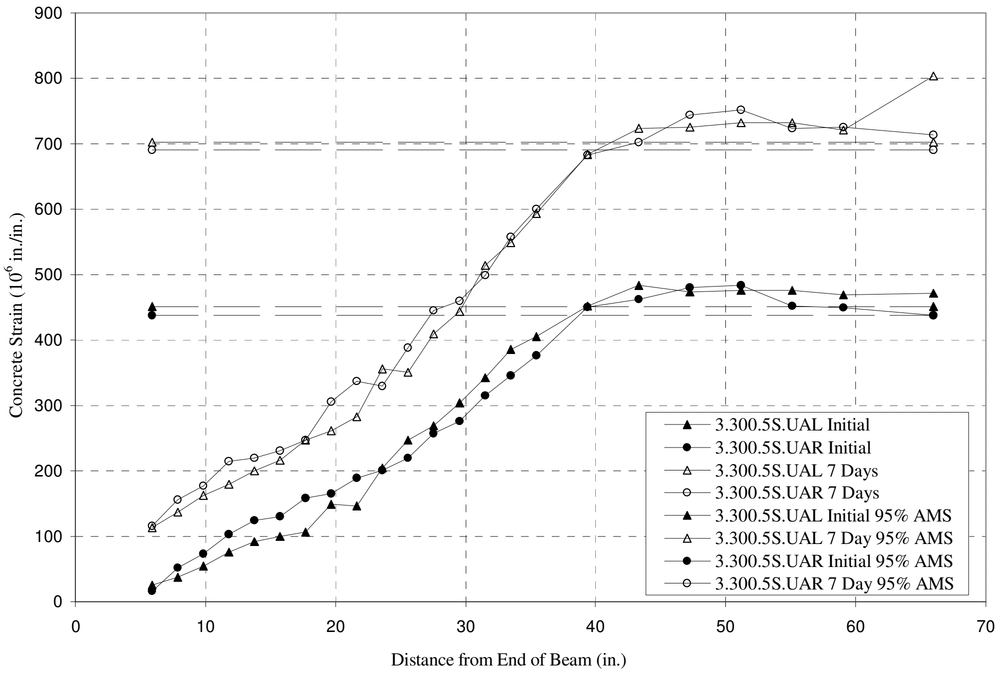

Figure B.18 Strain Profile for 3.300.5S.UA

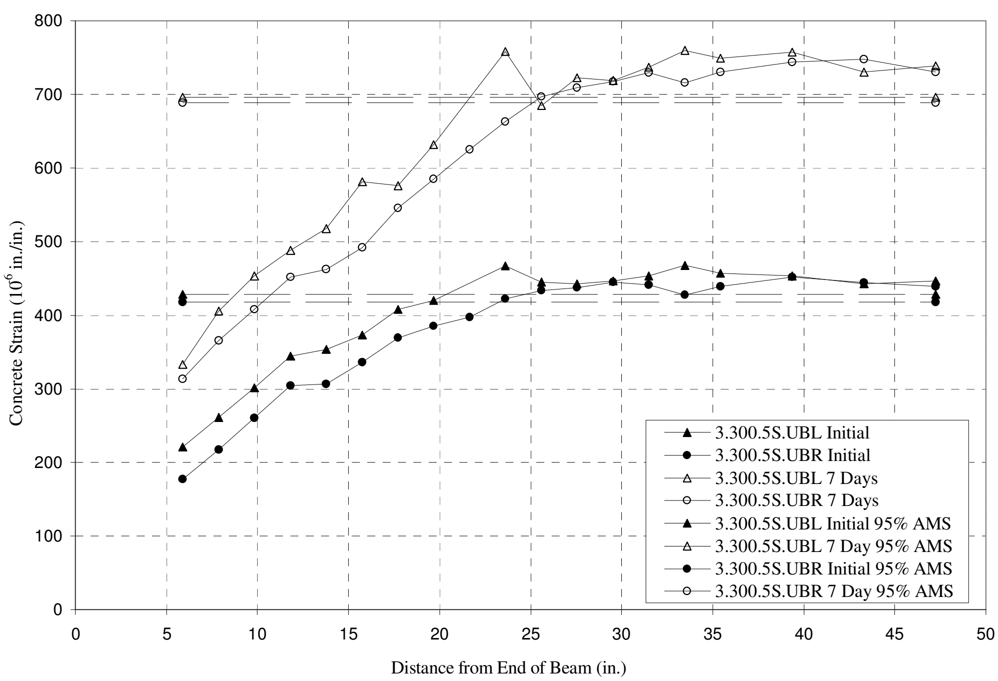

Figure B.19 Strain Profile for 3.300.5S.UB

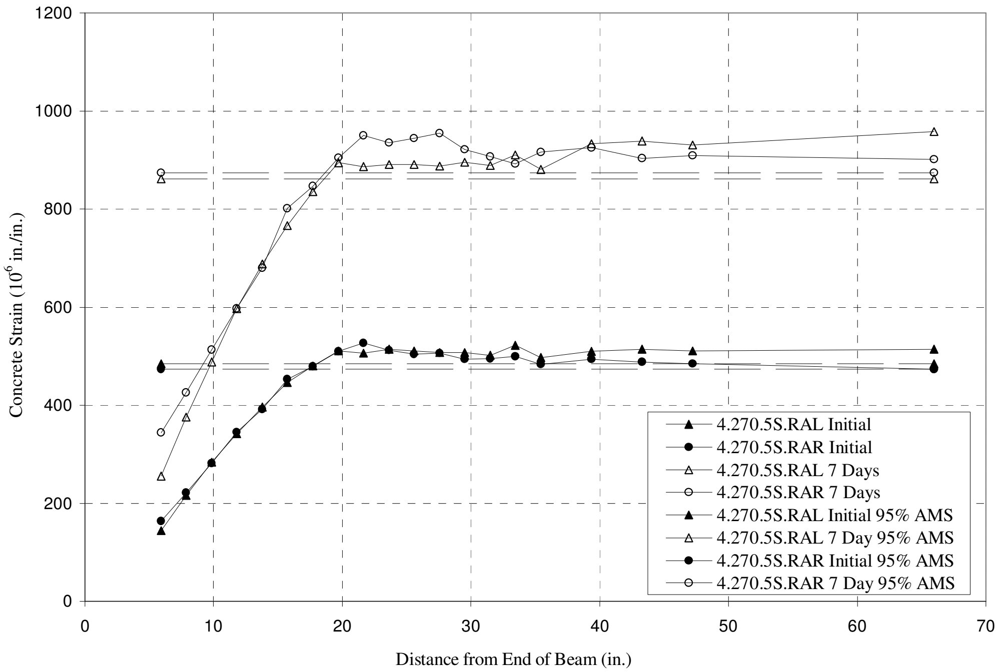

Figure B.20 Strain Profile for 4.270.5S.RA

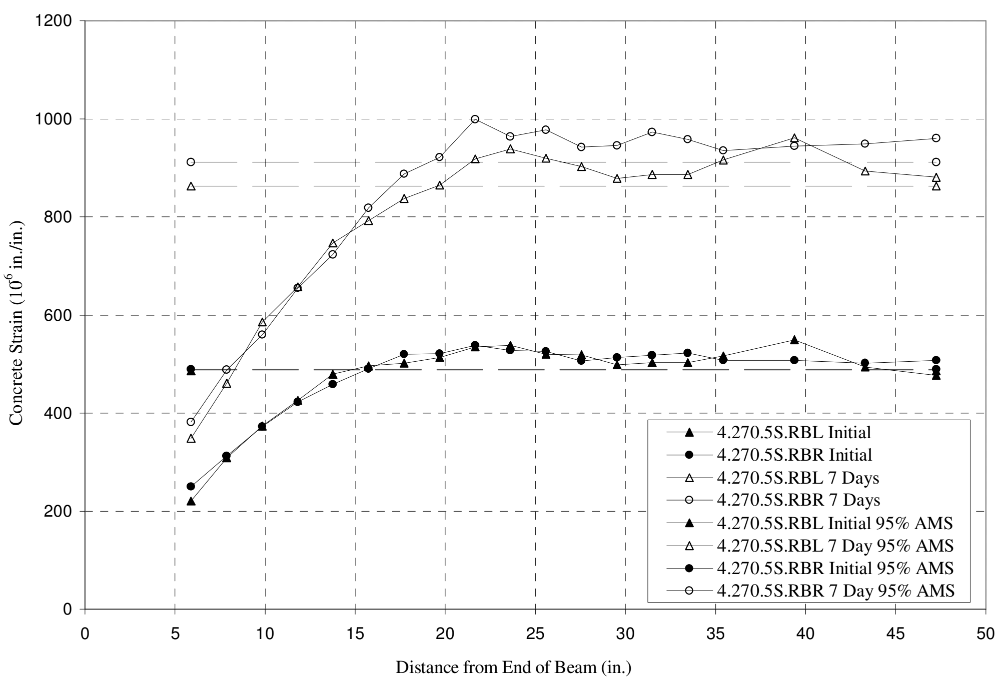

Figure B.21 Strain Profile for 4.270.5S.RB

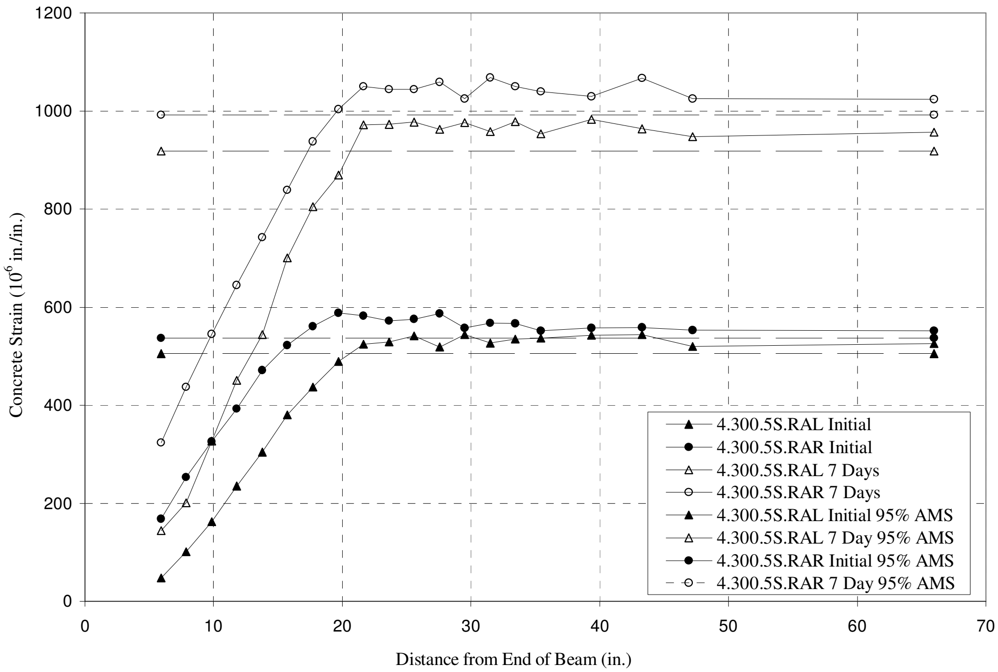

Figure B.22 Strain Profile for 4.300.5S.RA

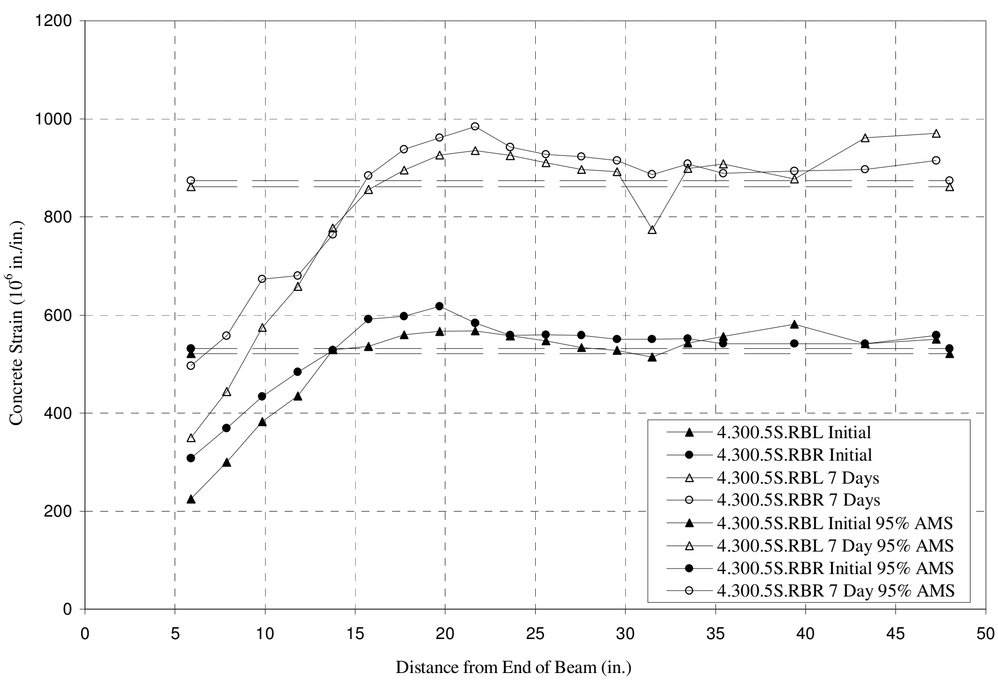

Figure B.23 Strain Profile for 4.300.5S.RB

APPENDIX C Moment vs. Deflection and Moment vs. Strand Slip Plots

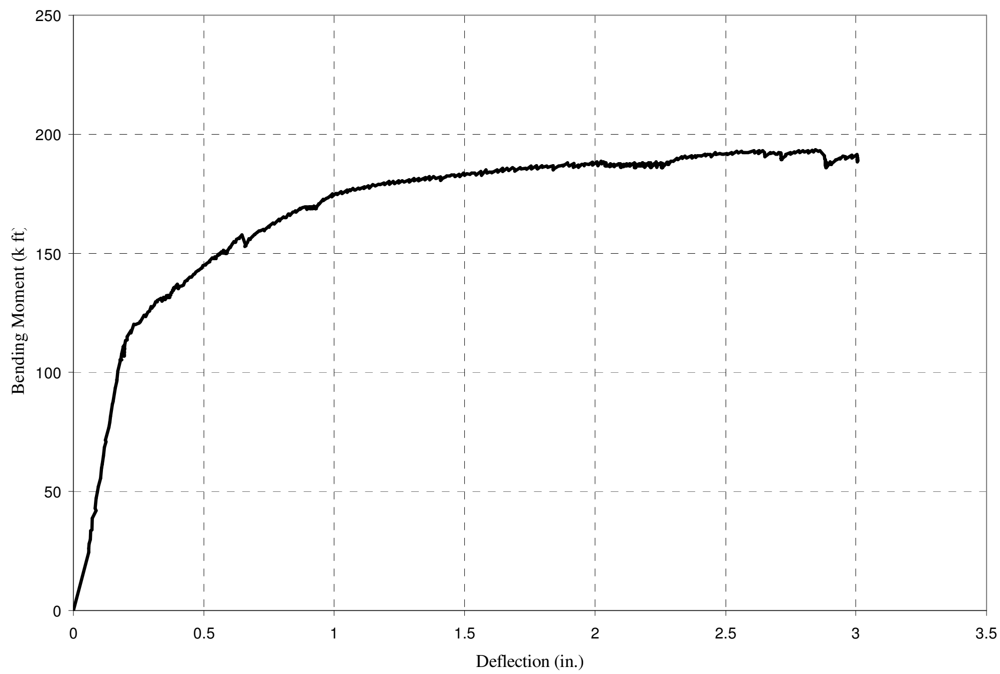

Figure C.1 Moment vs. Deflection for 0.270.5N.RA

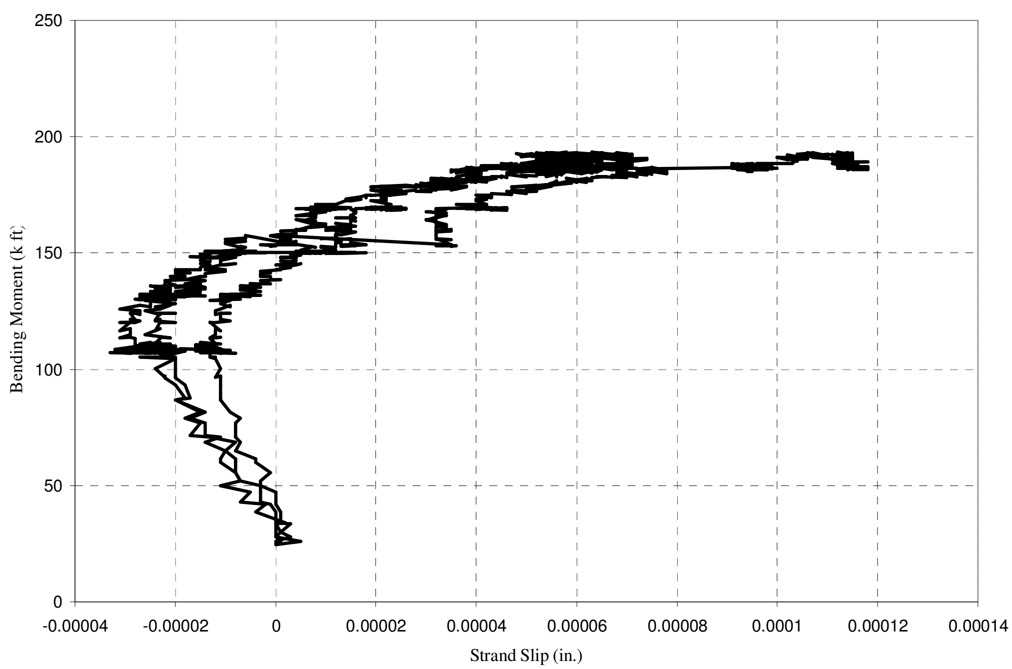

Figure C.2 Moment vs. Strand Slip for 0.270.5N.RA

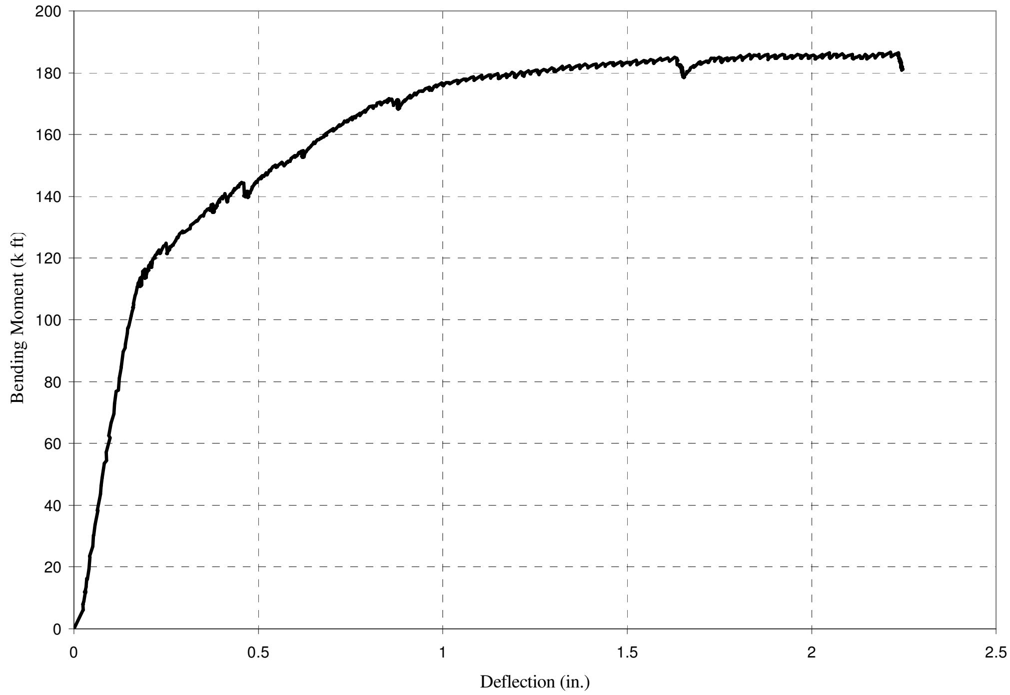

Figure C.3 Moment vs. Deflection for 0.270.5N.RB

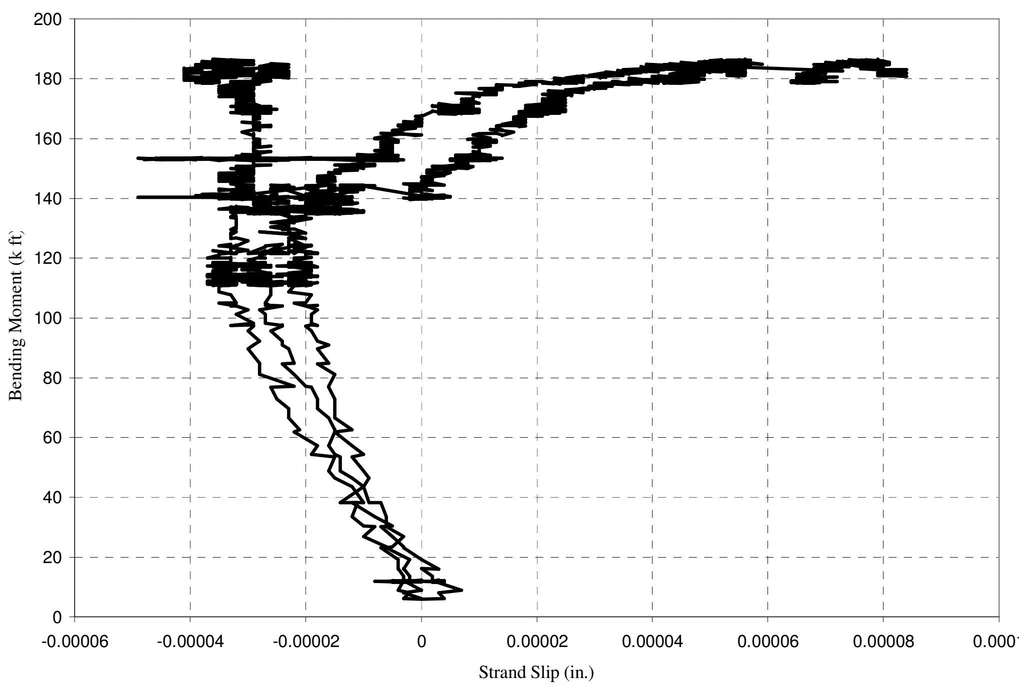

Figure C.4 Moment vs. Strand Slip for 0.270.5N.RB

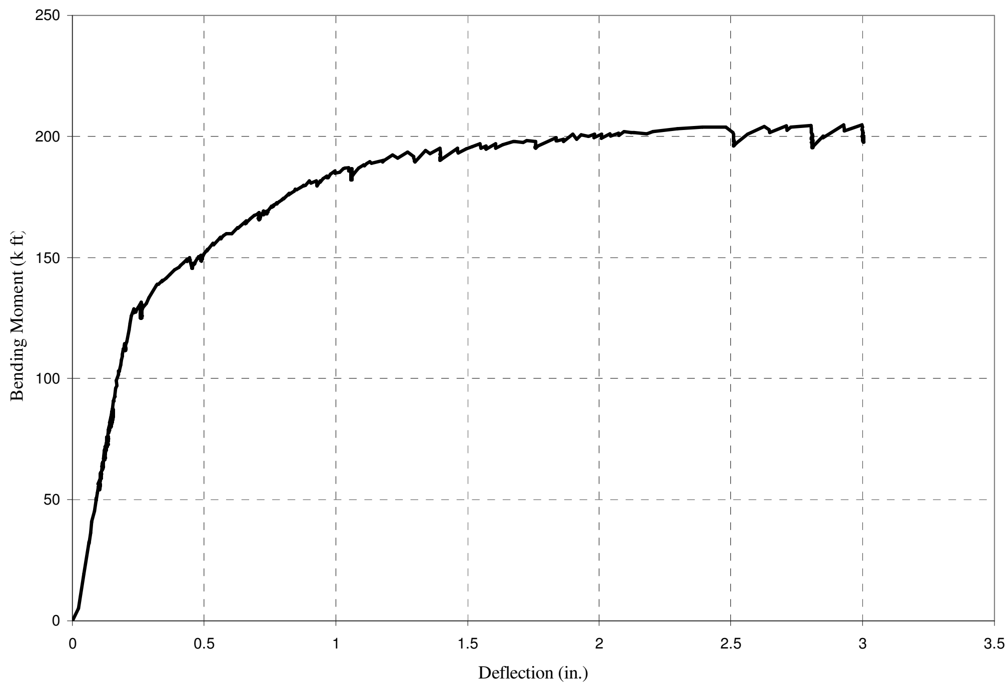

Figure C.5 Moment vs. Deflection for 0.300.5N.RB

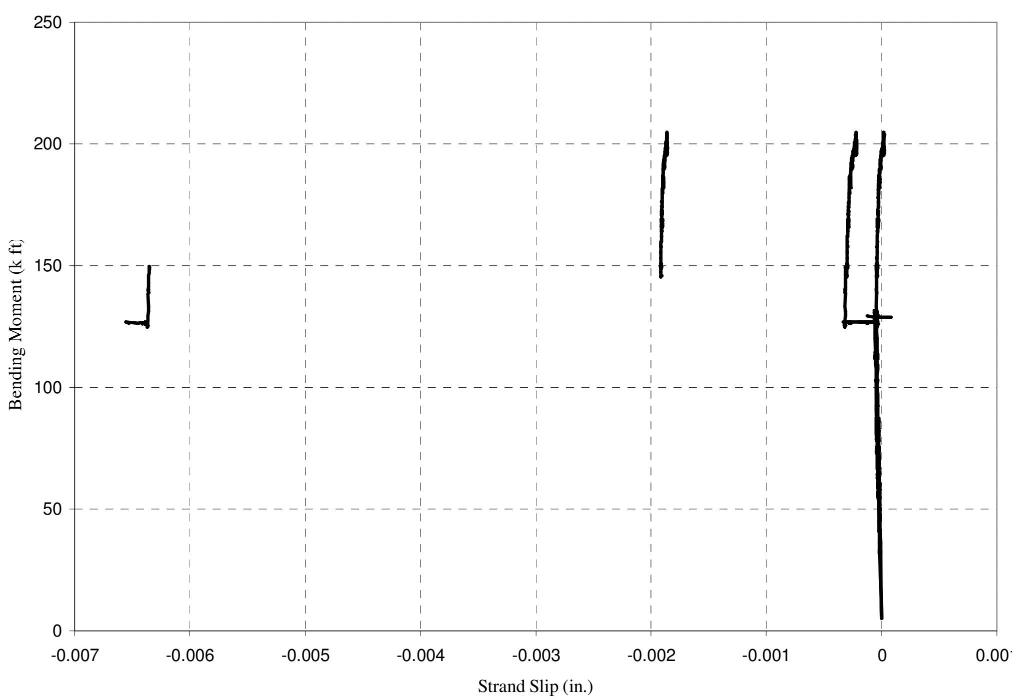

Figure C.6 Moment vs. Strand Slip for 0.300.5N.RB

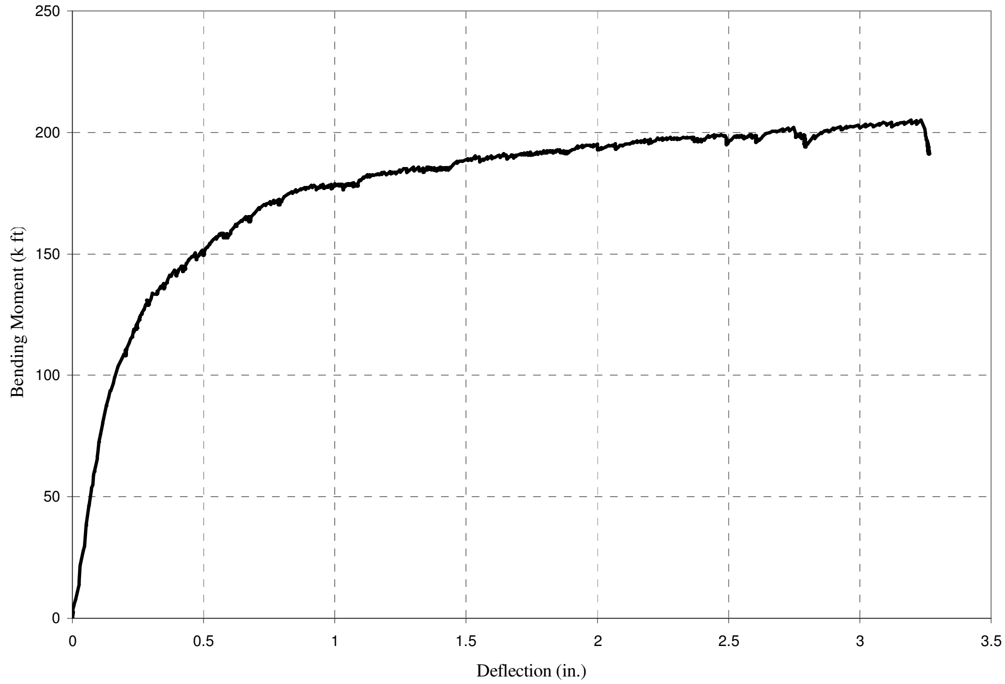

Figure C.7 Moment vs. Deflection for 1.270.5N.RA

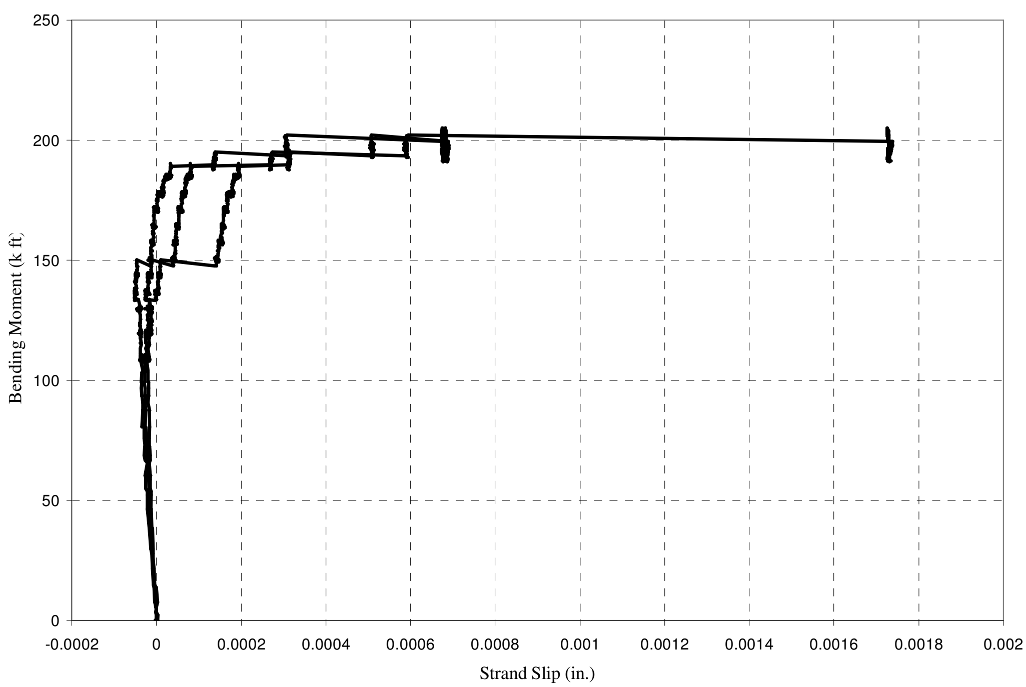

Figure C.8 Moment vs. Strand Slip for 1.270.5N.RA

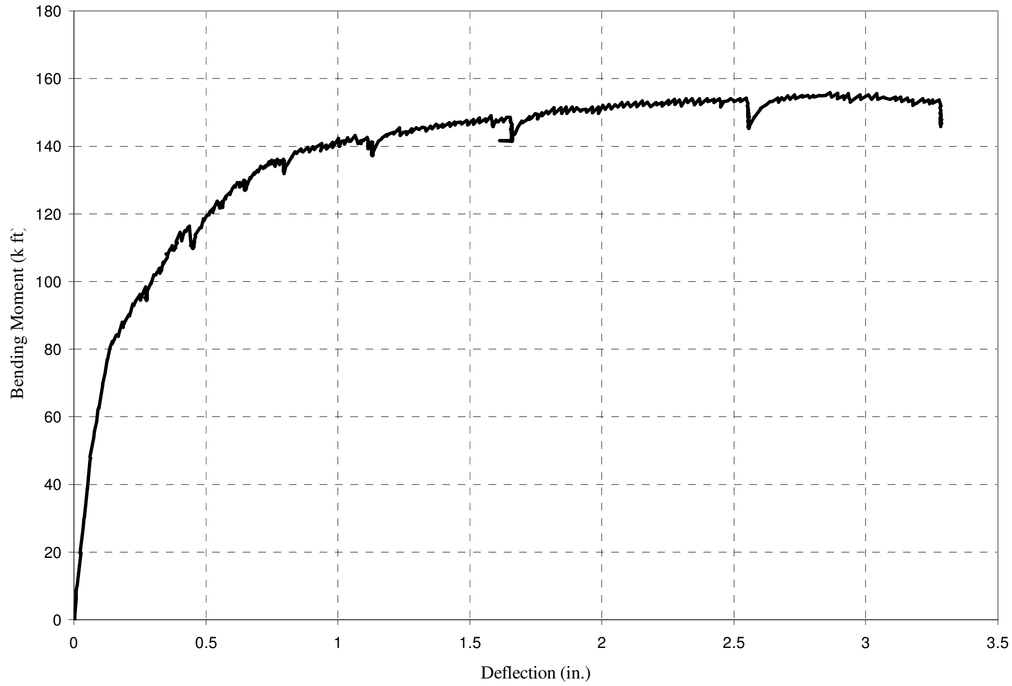

Figure C.9 Moment vs. Deflection for 1.270.5N.RB

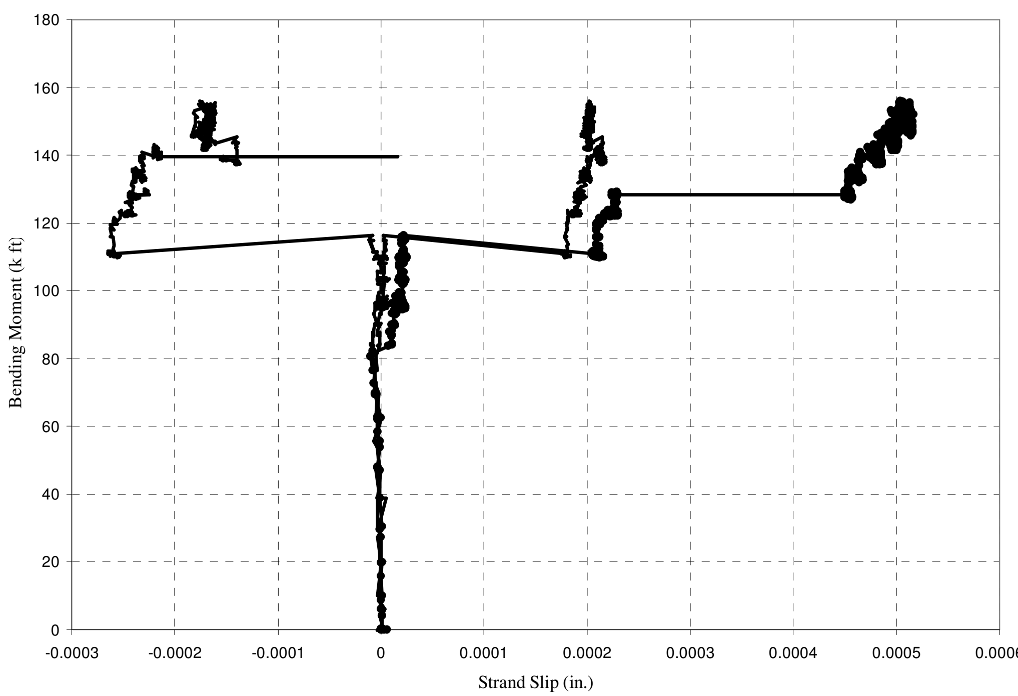

Figure C.10 Moment vs. Strand Slip for 1.270.5N.RB

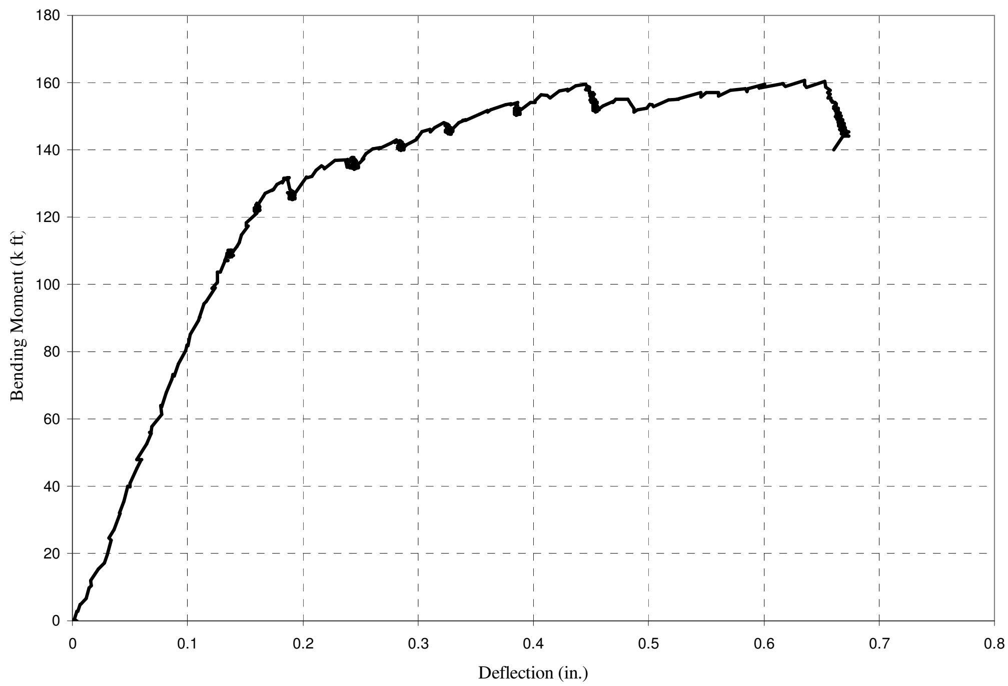

Figure C.11 Moment vs. Deflection for 1.300.5N.RA

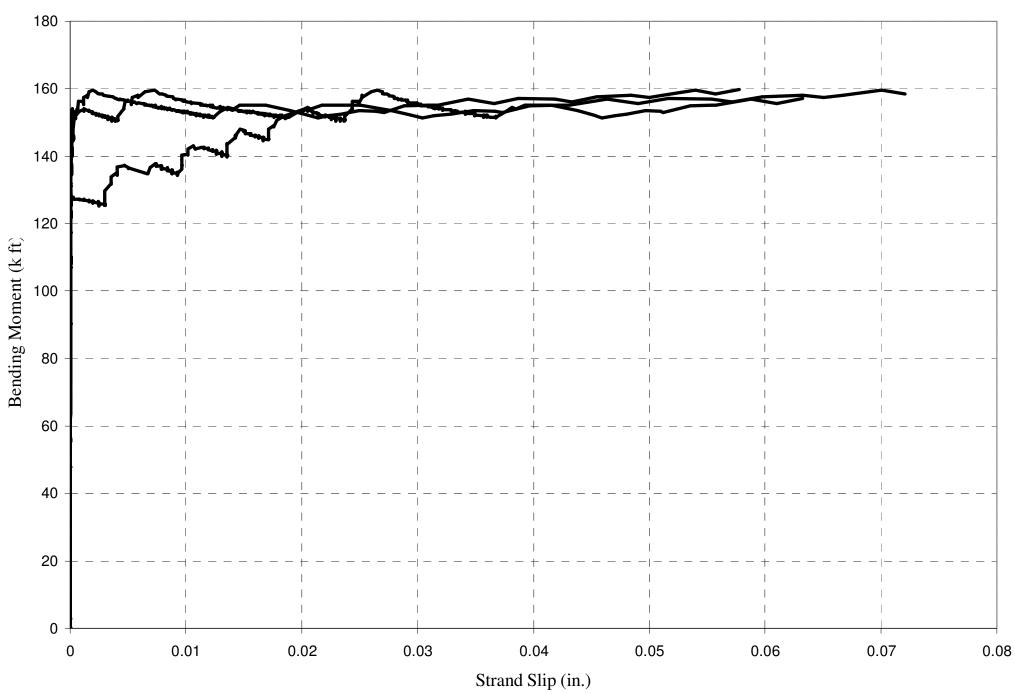

Figure C.12 Moment vs. Strand Slip for 1.300.5N.RA

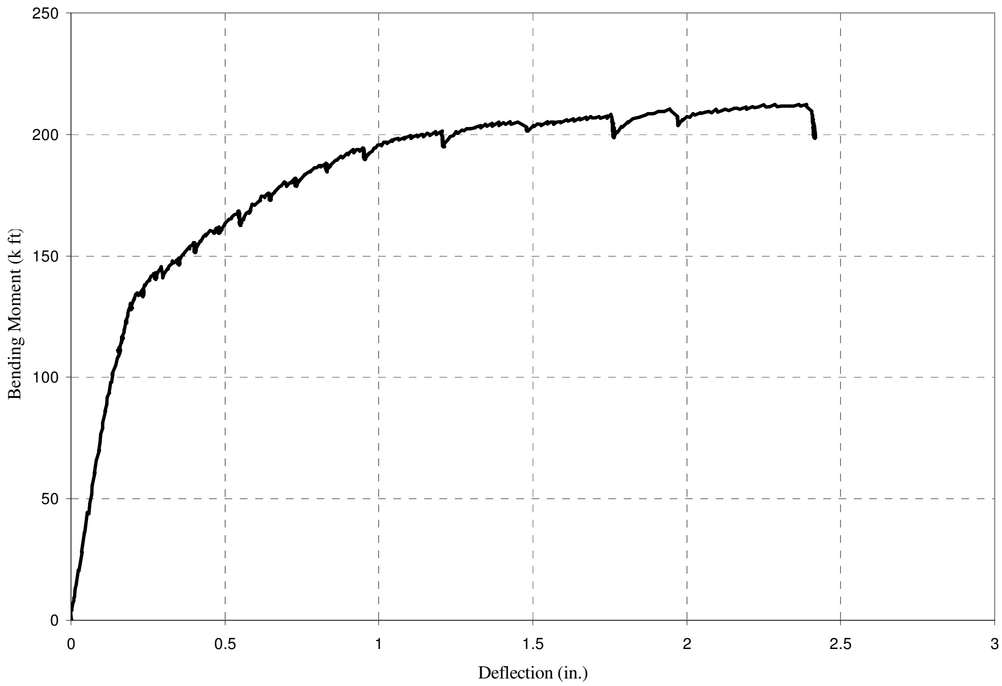

Figure C.13 Moment vs. Deflection for 1.300.5N.RB

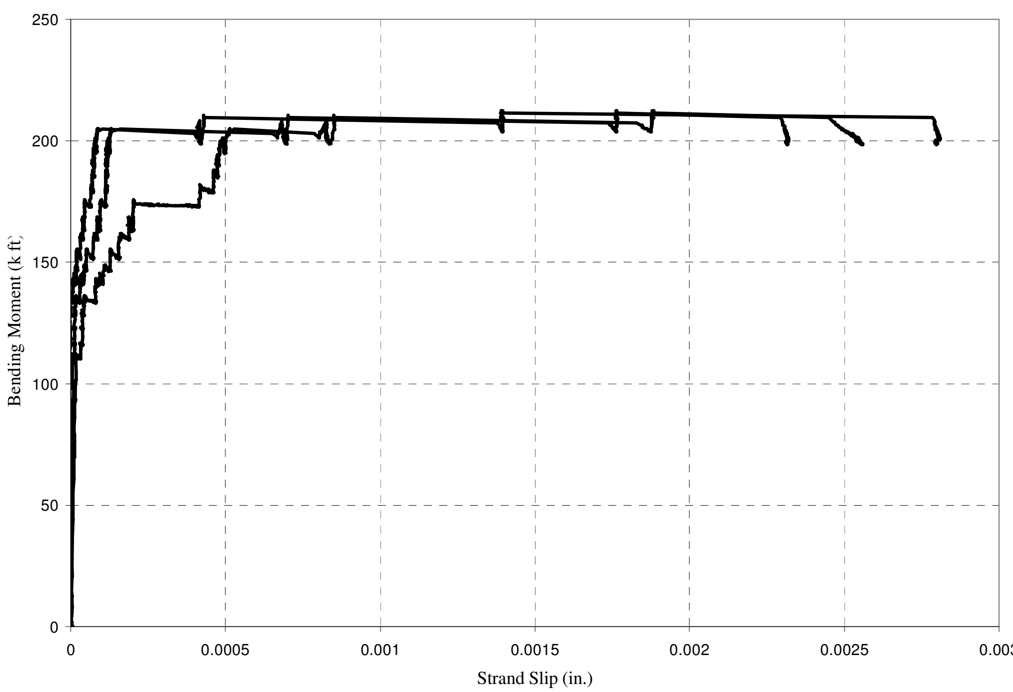

Figure C.14 Moment vs. Strand Slip for 1.300.5N.RB

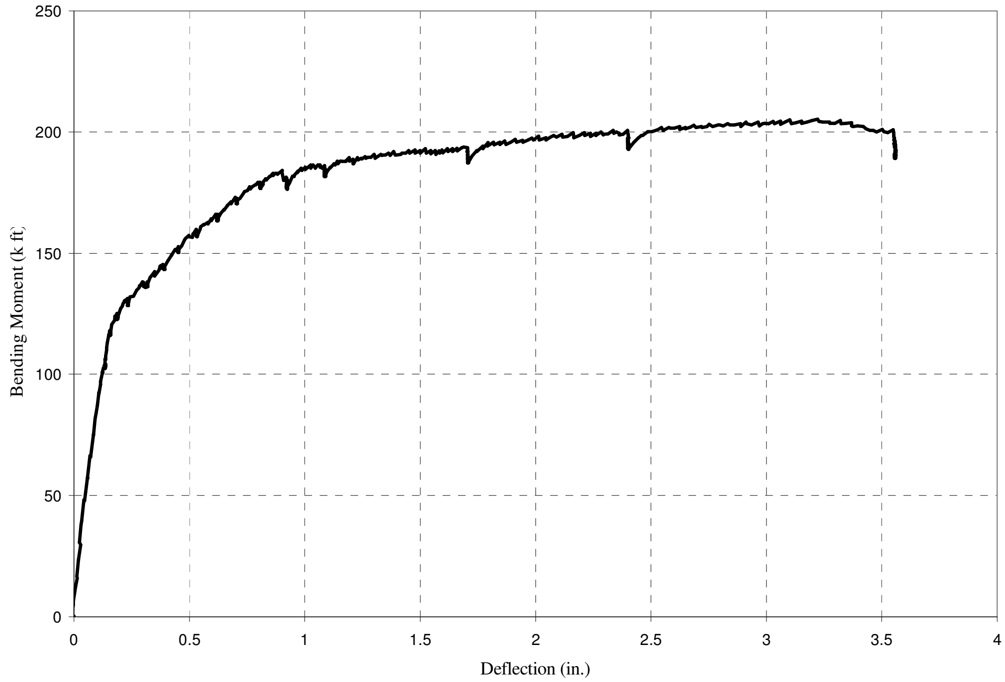

Figure C.15 Moment vs. Deflection for 1.270.5N.UA

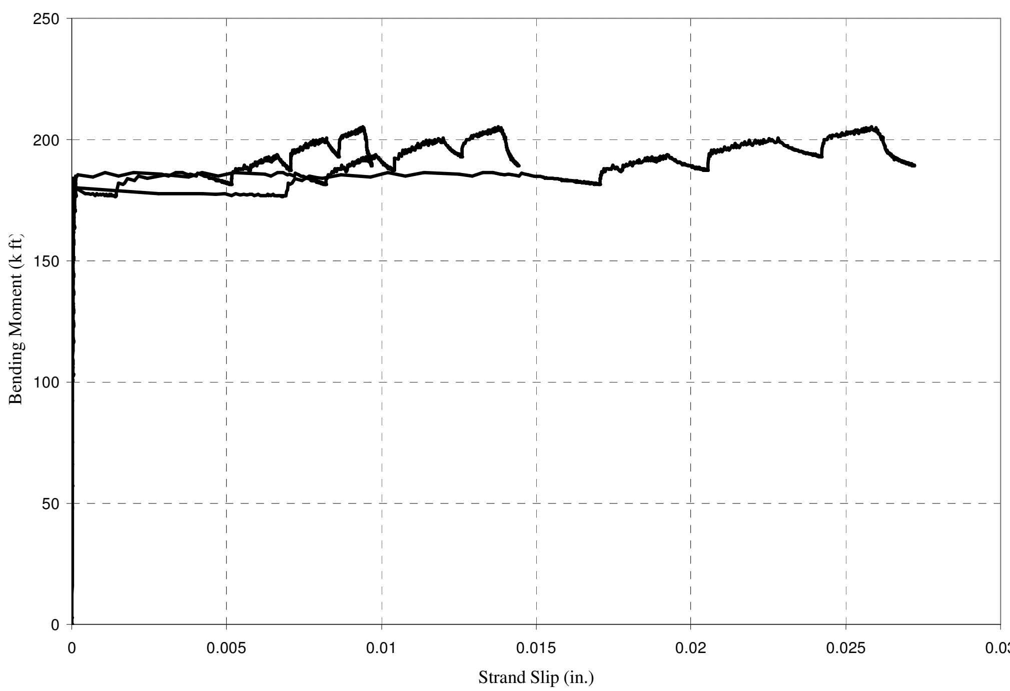

Figure C.16 Moment vs. Strand Slip for 1.270.5N.UA

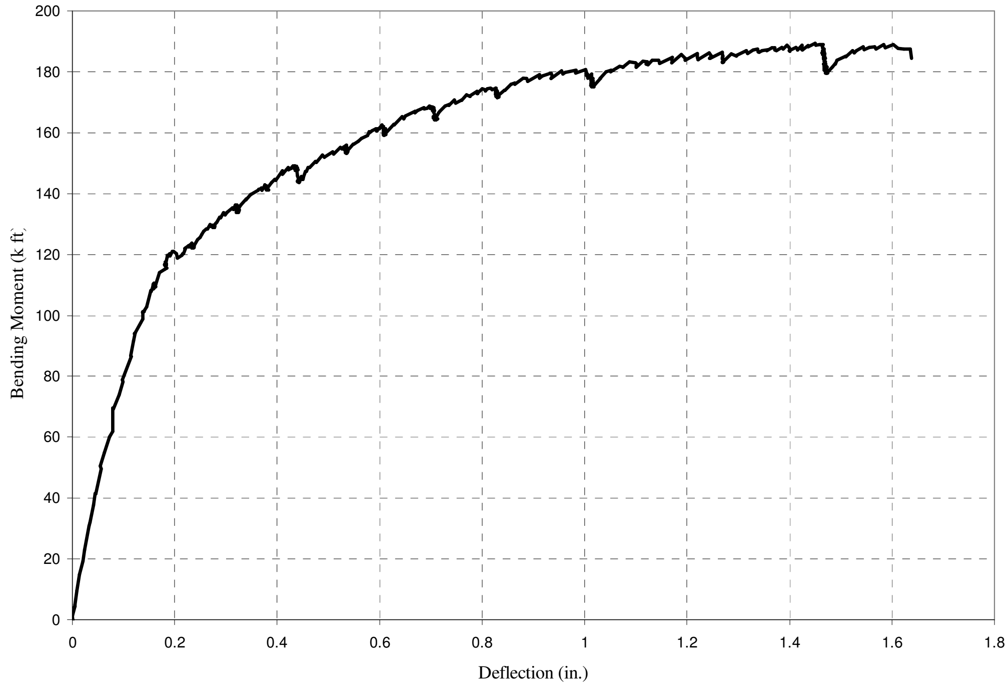

Figure C.17 Moment vs. Deflection for 1.270.5N.UB

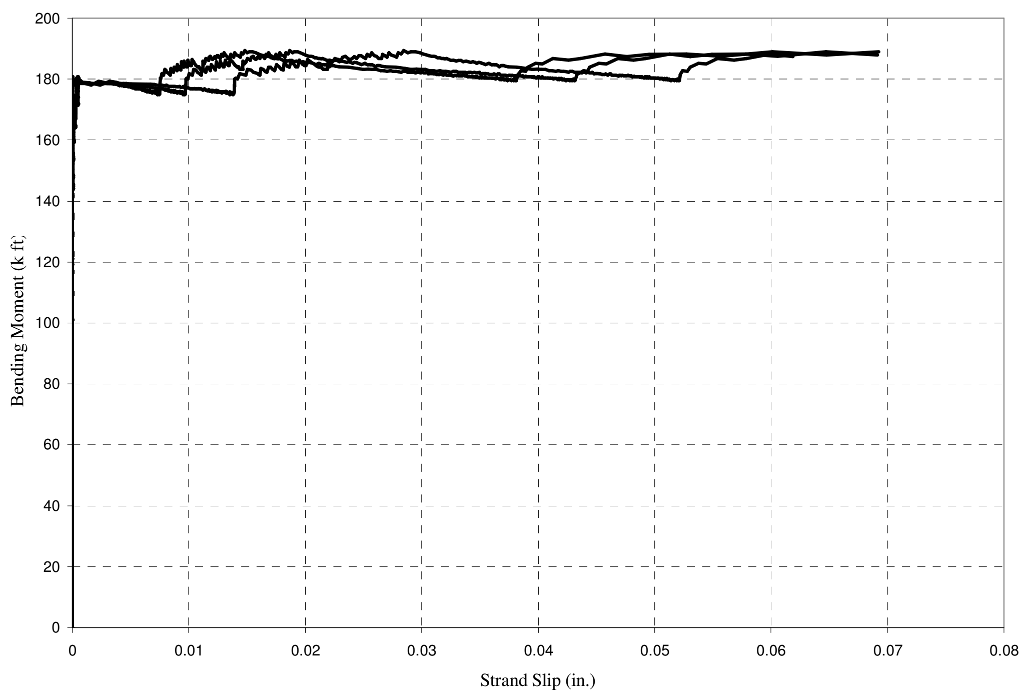

Figure C.18 Moment vs. Strand Slip for 1.270.5N.UB

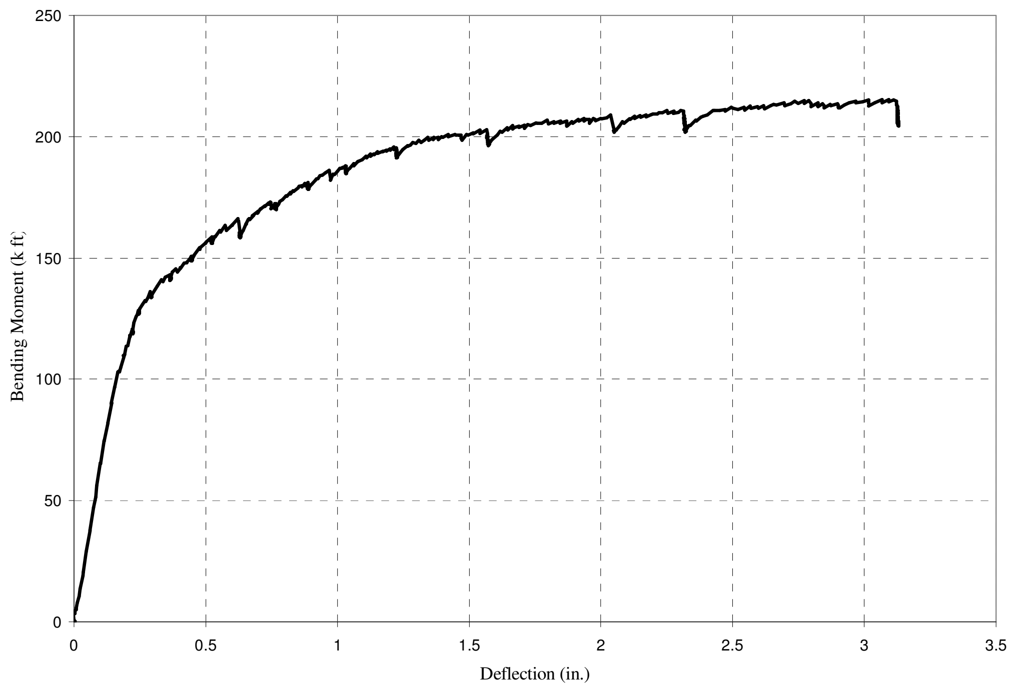

Figure C.19 Moment vs. Deflection for 1.300.5N.UA

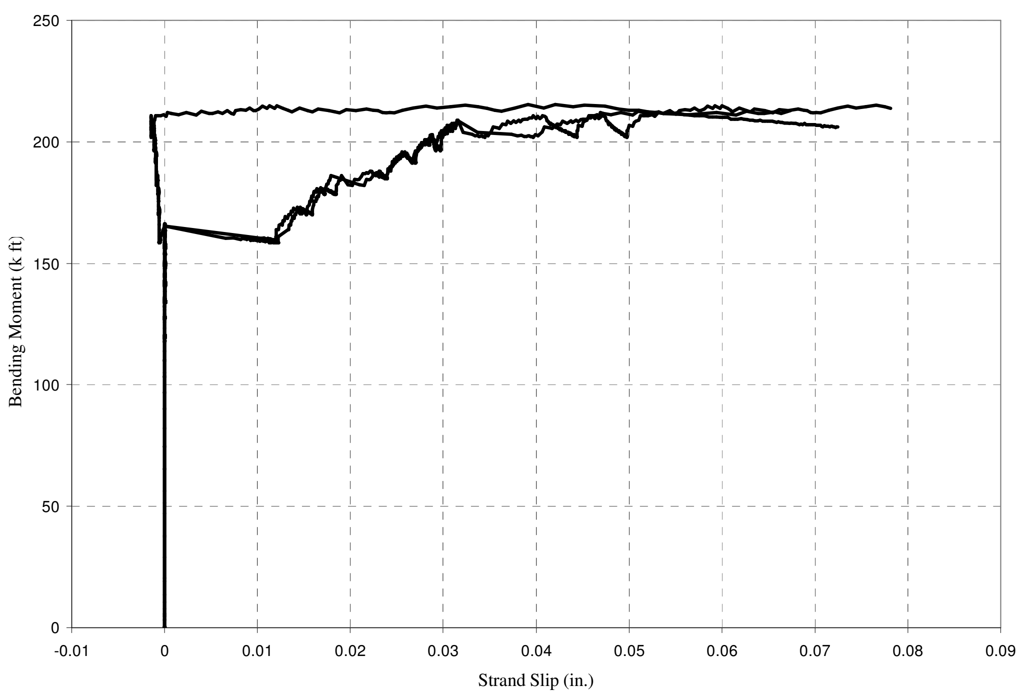

Figure C.20 Moment vs. Strand Slip for 1.300.5N.UA

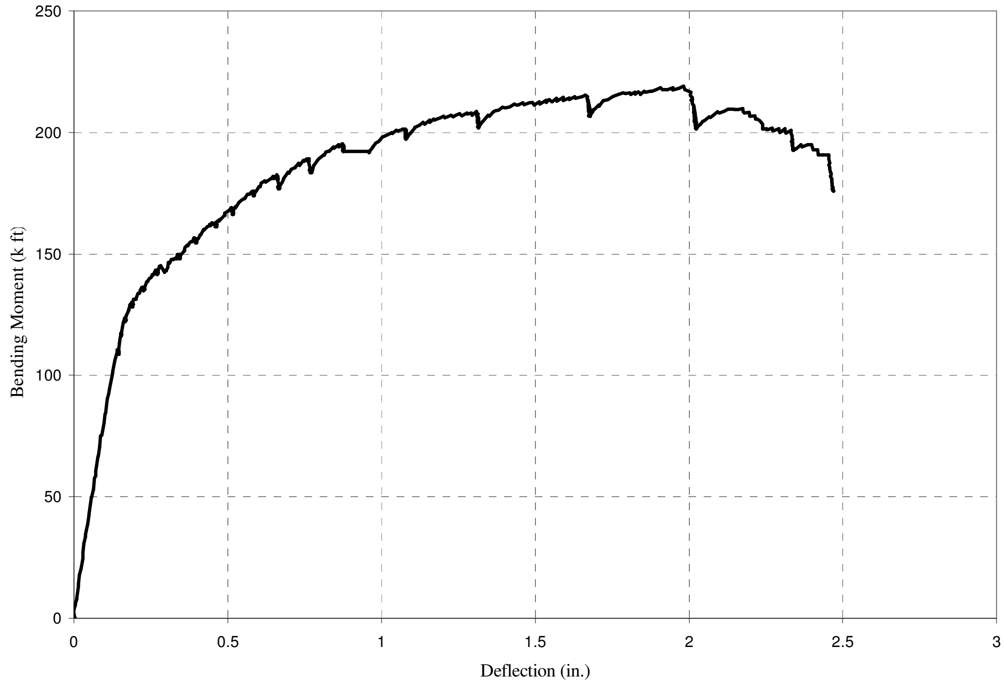

Figure C.21 Moment vs. Deflection for 1.300.5N.UB

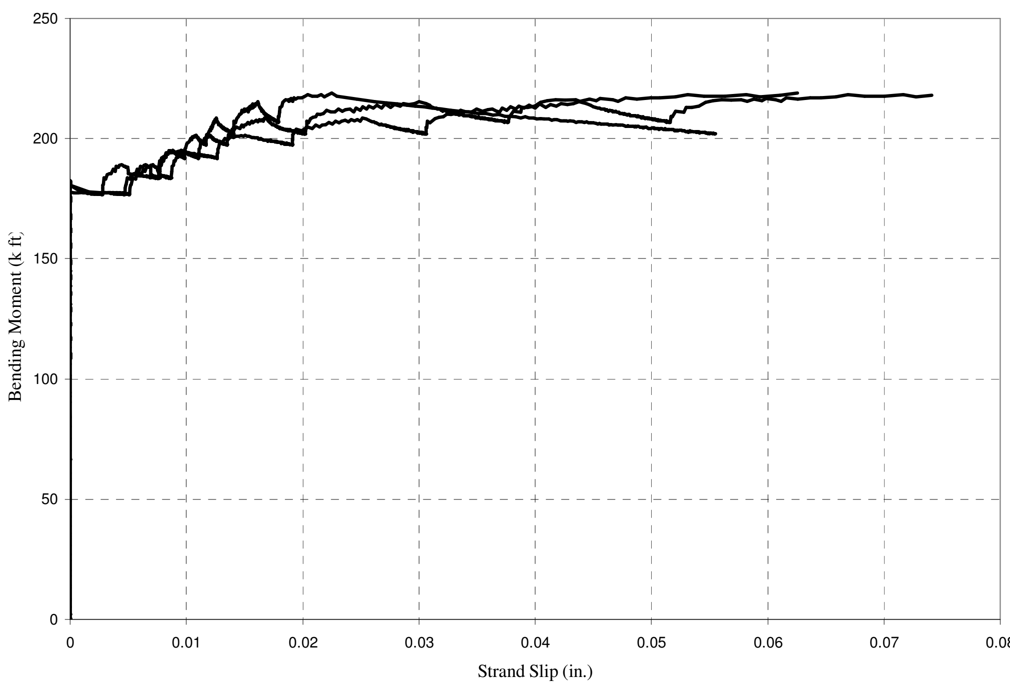

Figure C.22 Moment vs. Strand Slip for 1.300.5N.UB

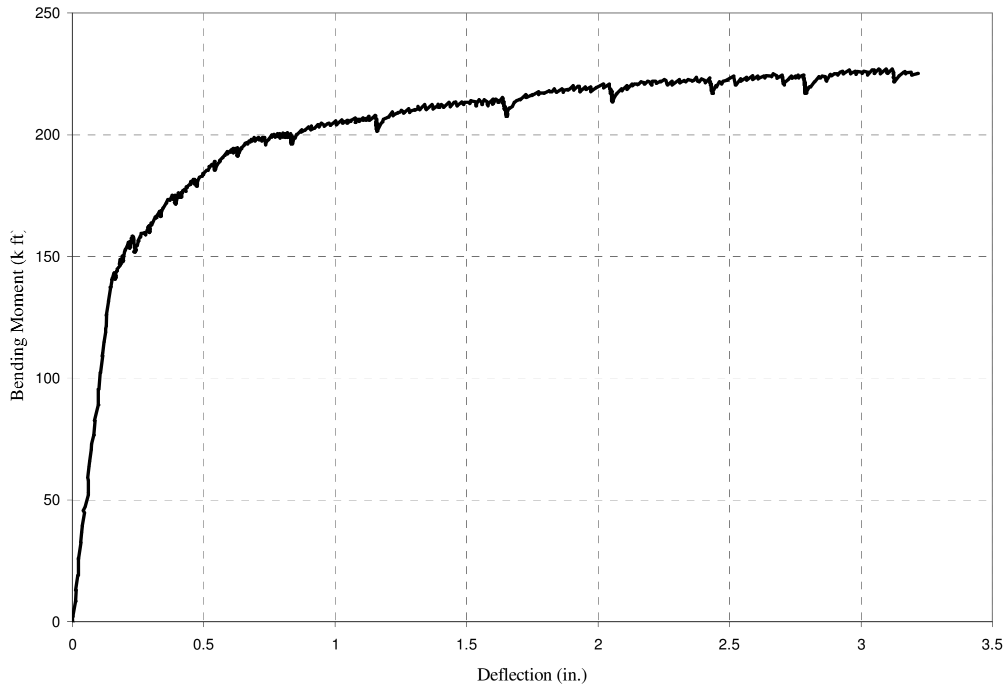

Figure C.23 Moment vs. Deflection for 3.270.5S.RA

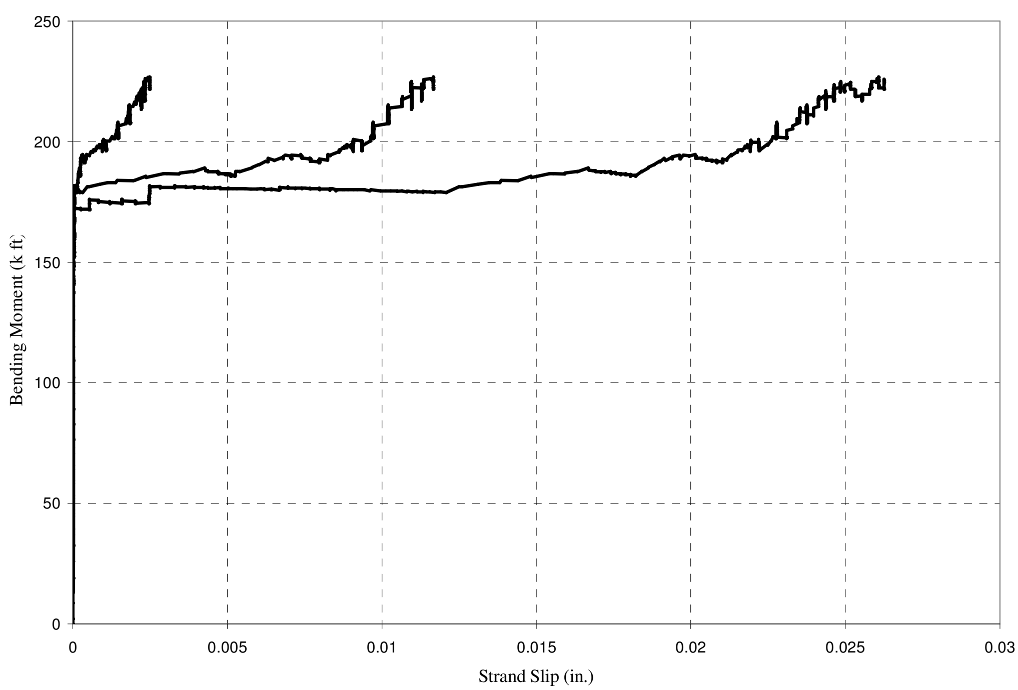

Figure C.24 Moment vs. Strand Slip for 3.270.5S.RA

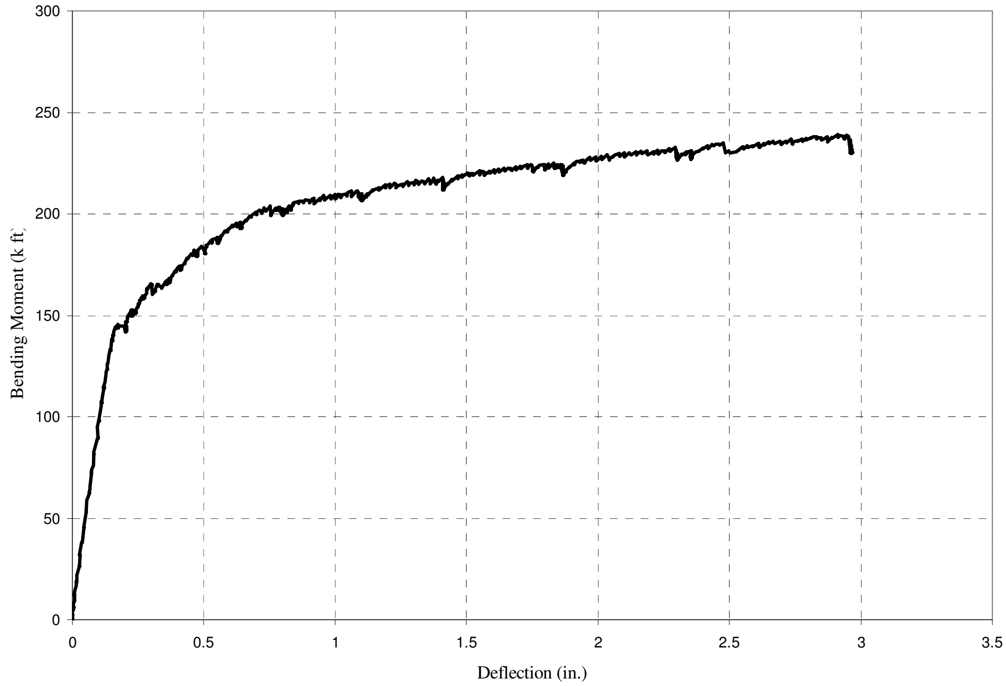

Figure C.25 Moment vs. Deflection for 3.270.5S.RB

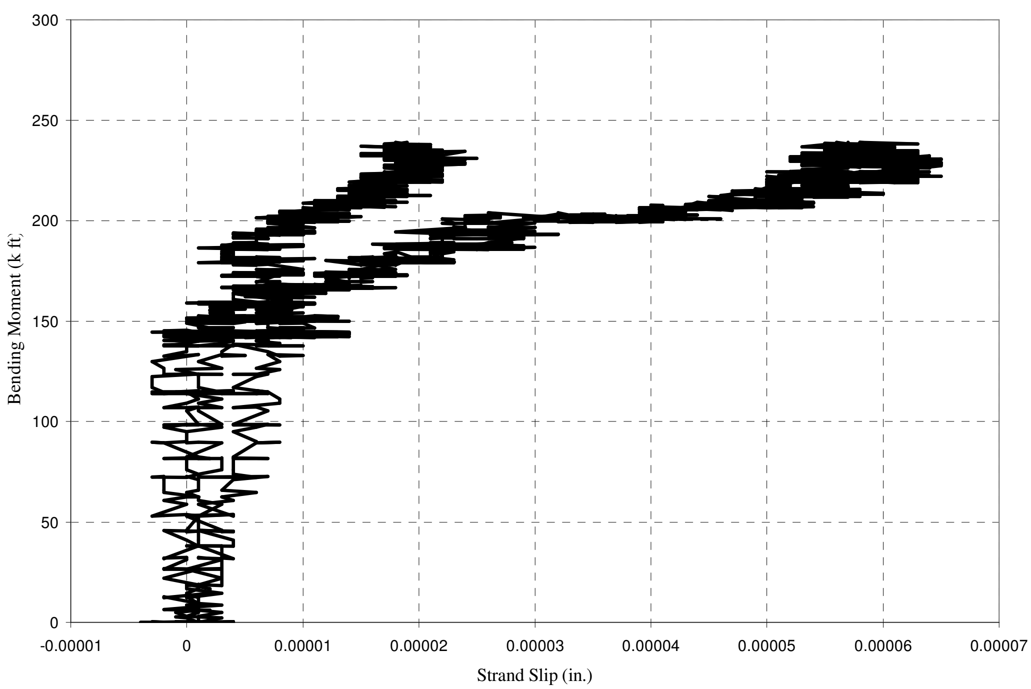

Figure C.26 Moment vs. Strand Slip for 3.270.5S.RB

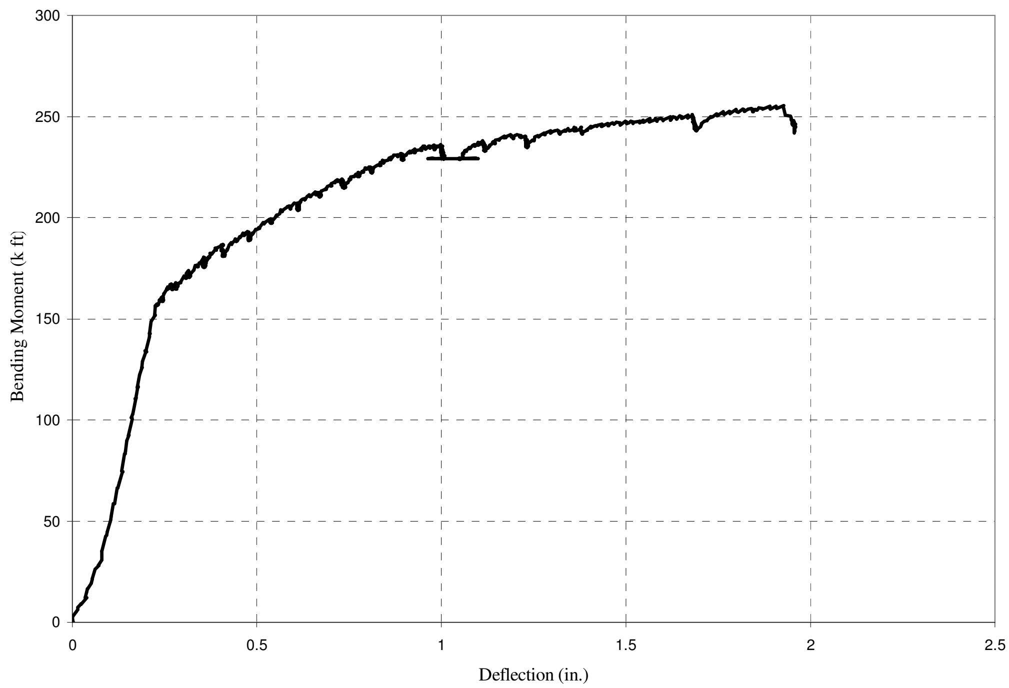

Figure C.27 Moment vs. Deflection for 3.300.5S.RA

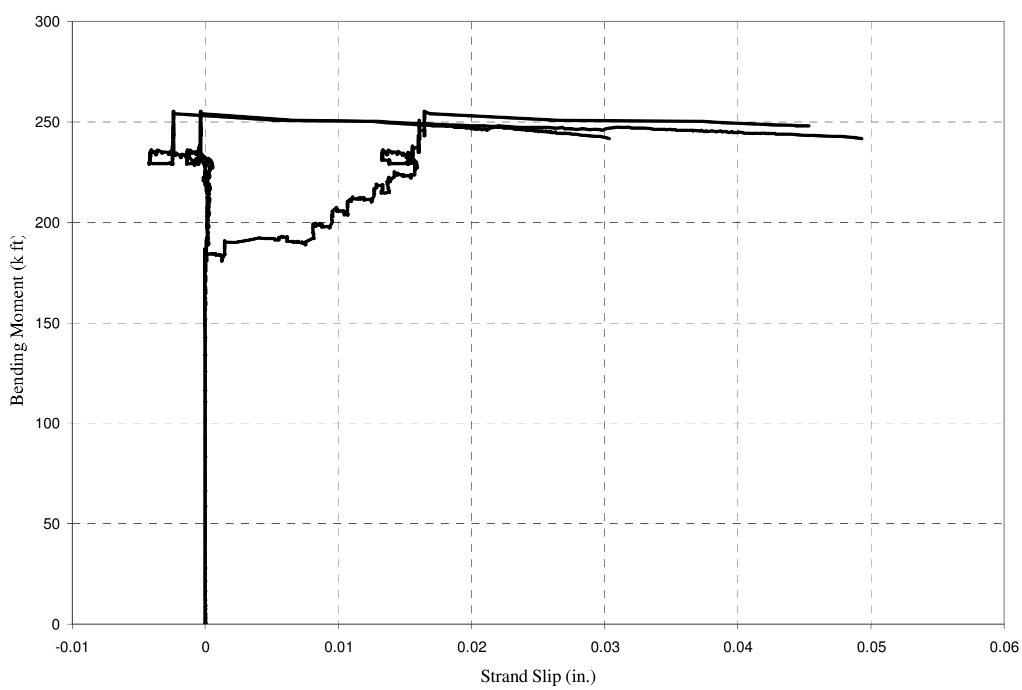

Figure C.28 Moment vs. Strand Slip for 3.300.5S.RA

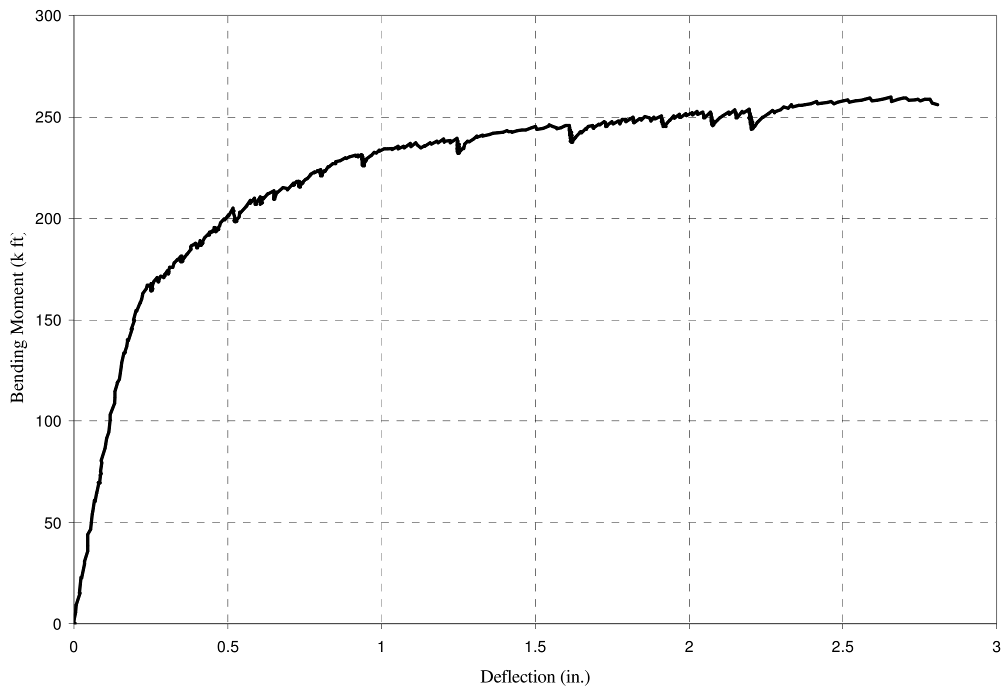

Figure C.29 Moment vs. Deflection for 3.300.5S.RB

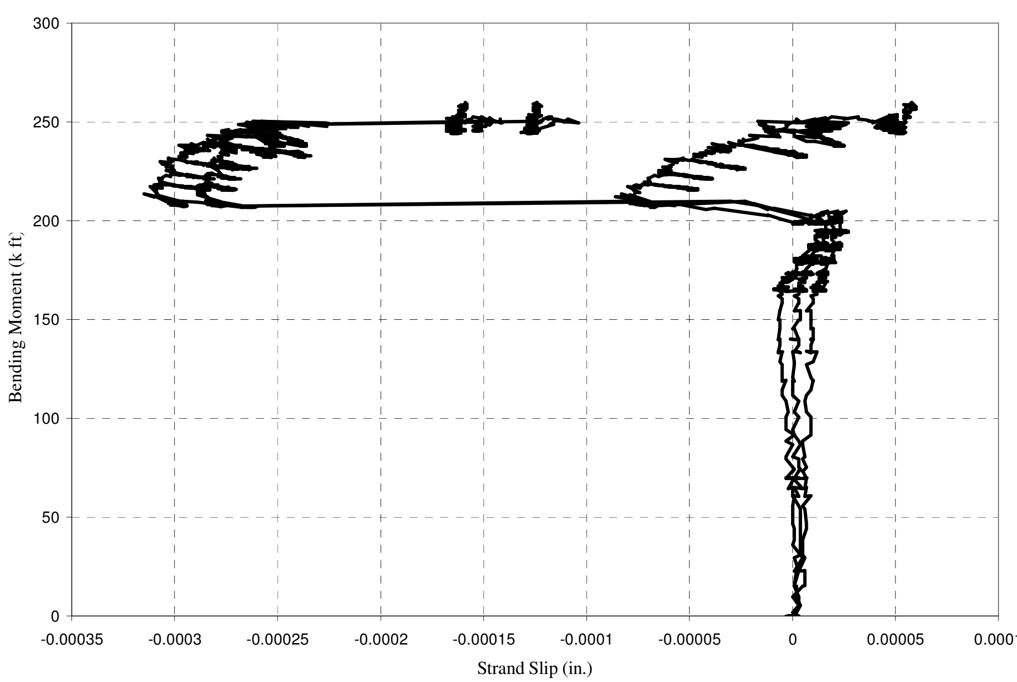

Figure C.30 Moment vs. Strand Slip for 3.300.5S.RB

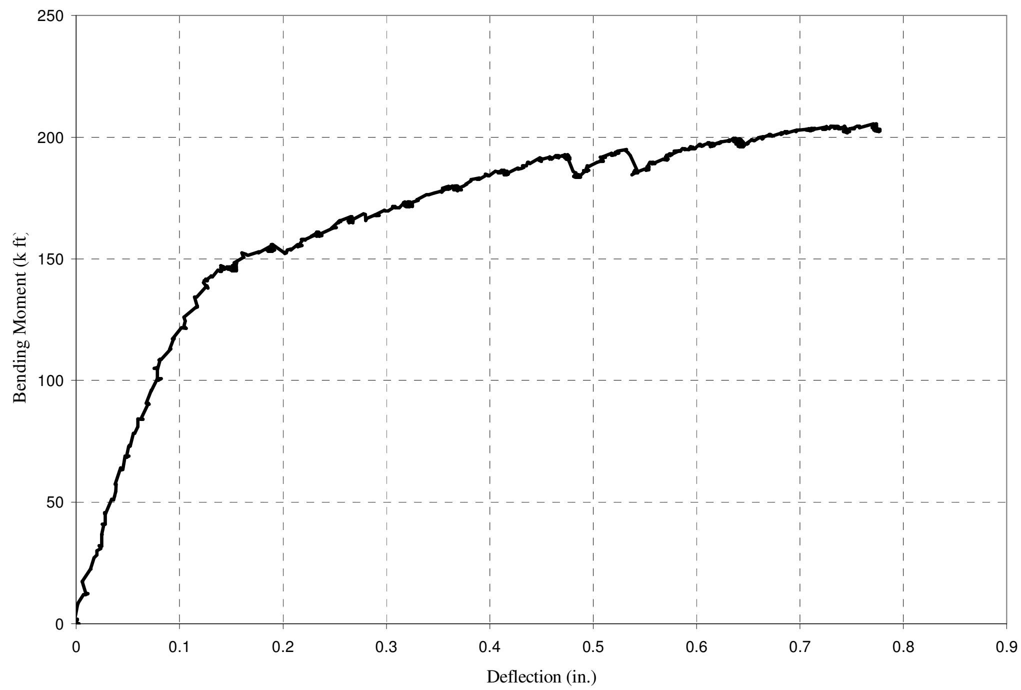

Figure C.31 Moment vs. Deflection for 3.270.5S.UA

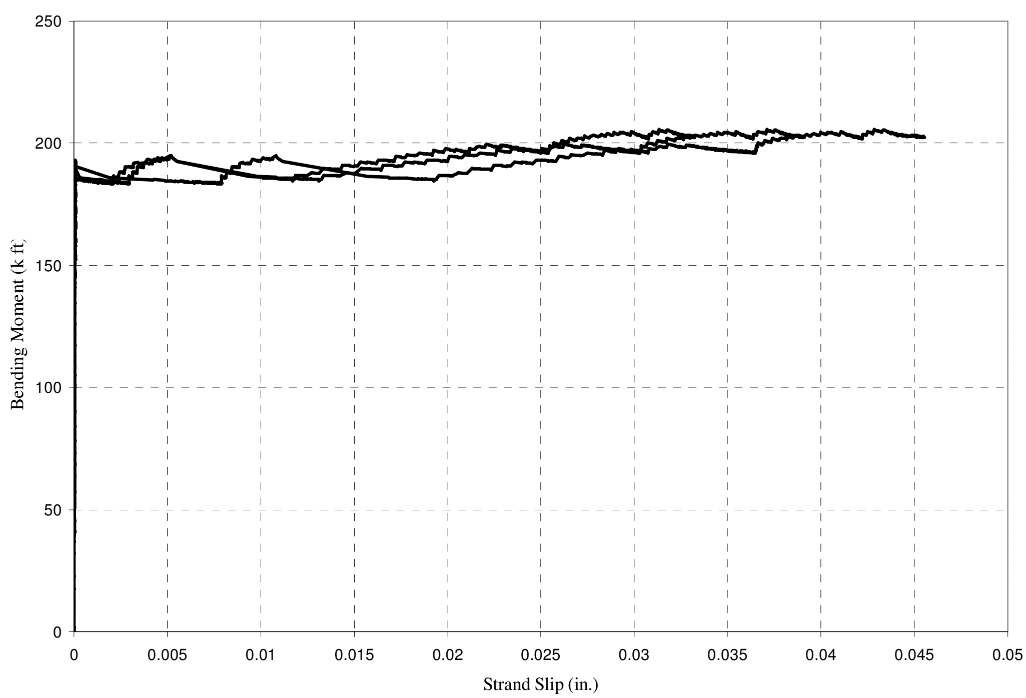

Figure C.32 Moment vs. Strand Slip for 3.270.5S.UA

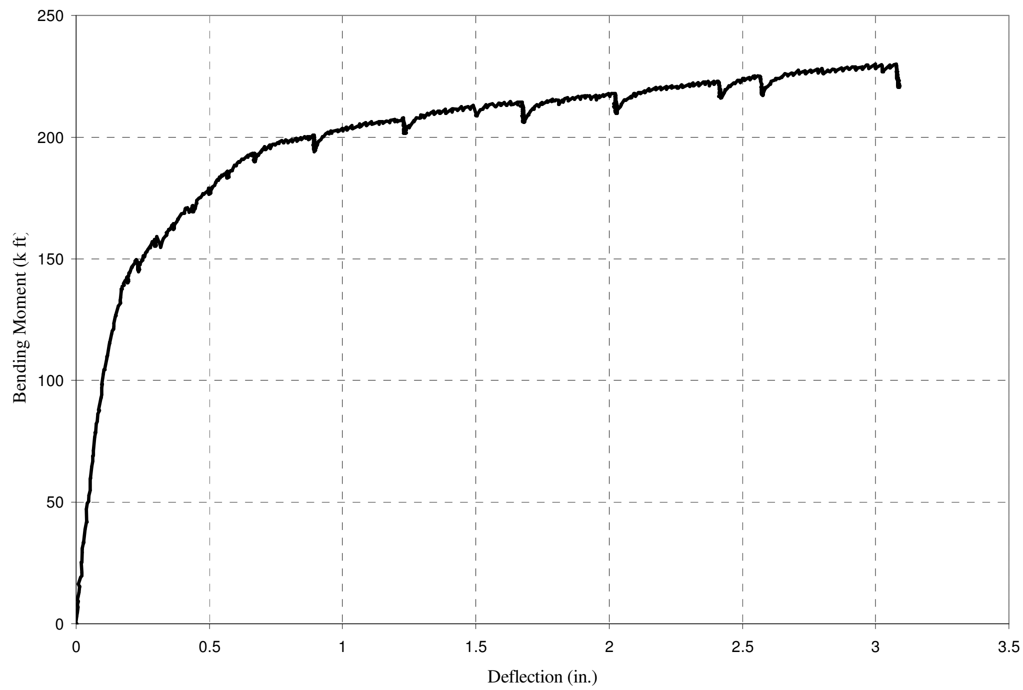

Figure C.33 Moment vs. Deflection for 3.270.5S.UB

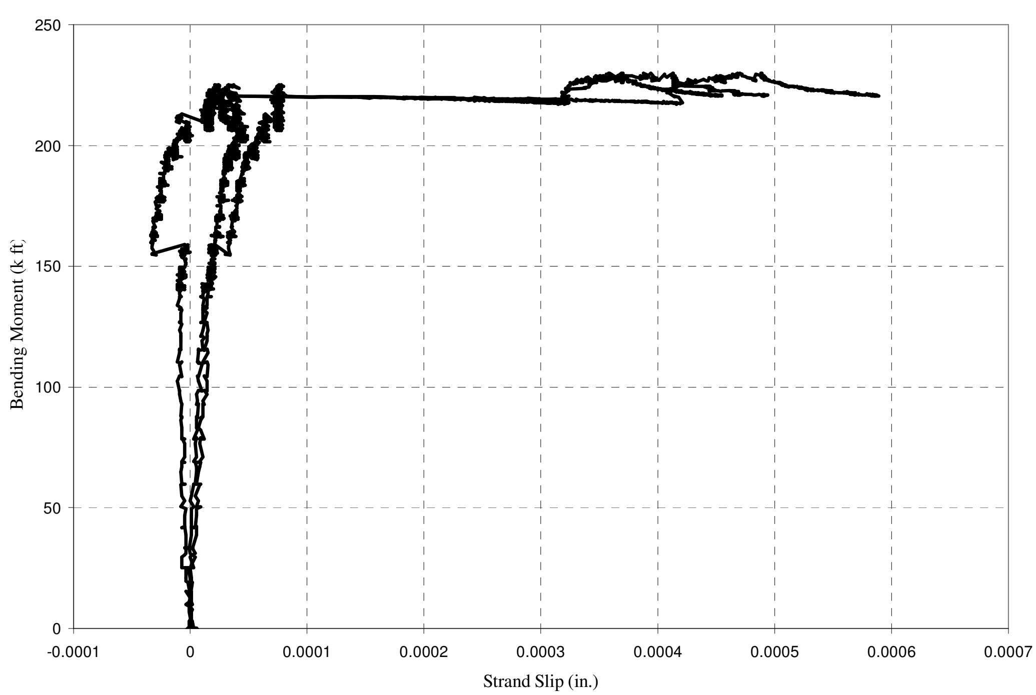

Figure C.34 Moment vs. Strand Slip for 3.270.5S.UB

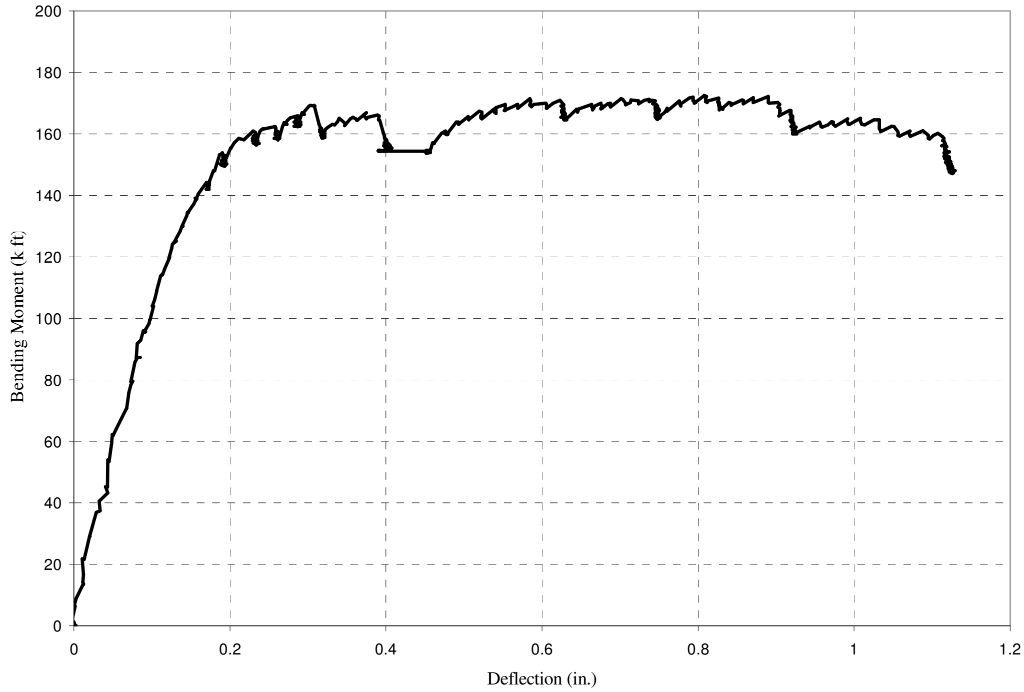

Figure C.35 Moment vs. Deflection for 3.300.5S.UA

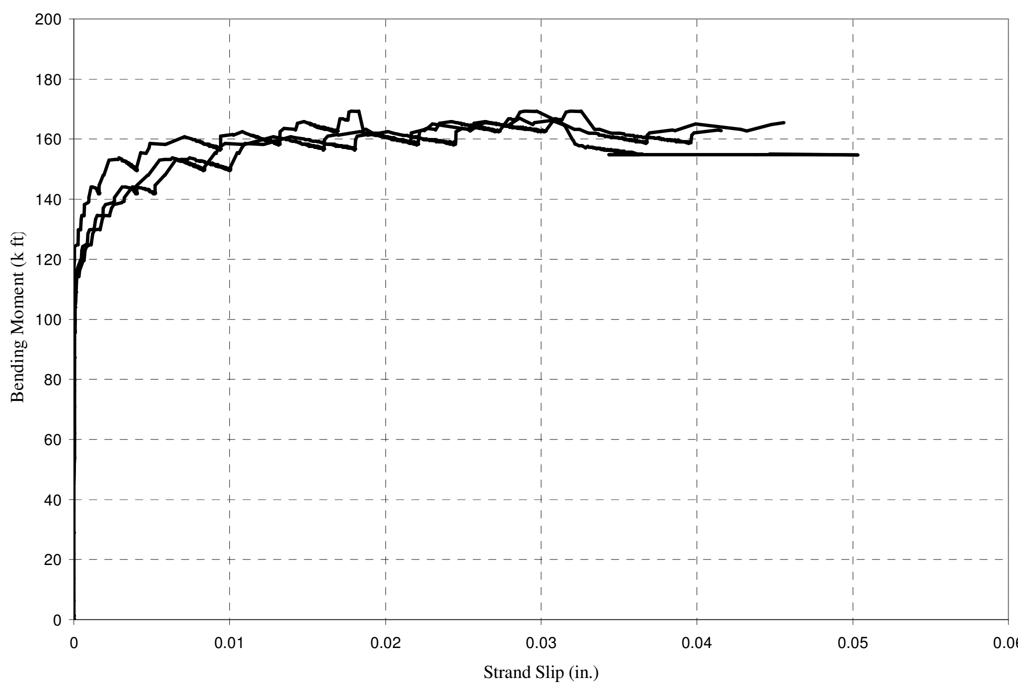

Figure C.36 Moment vs. Strand Slip for 3.300.5S.UA

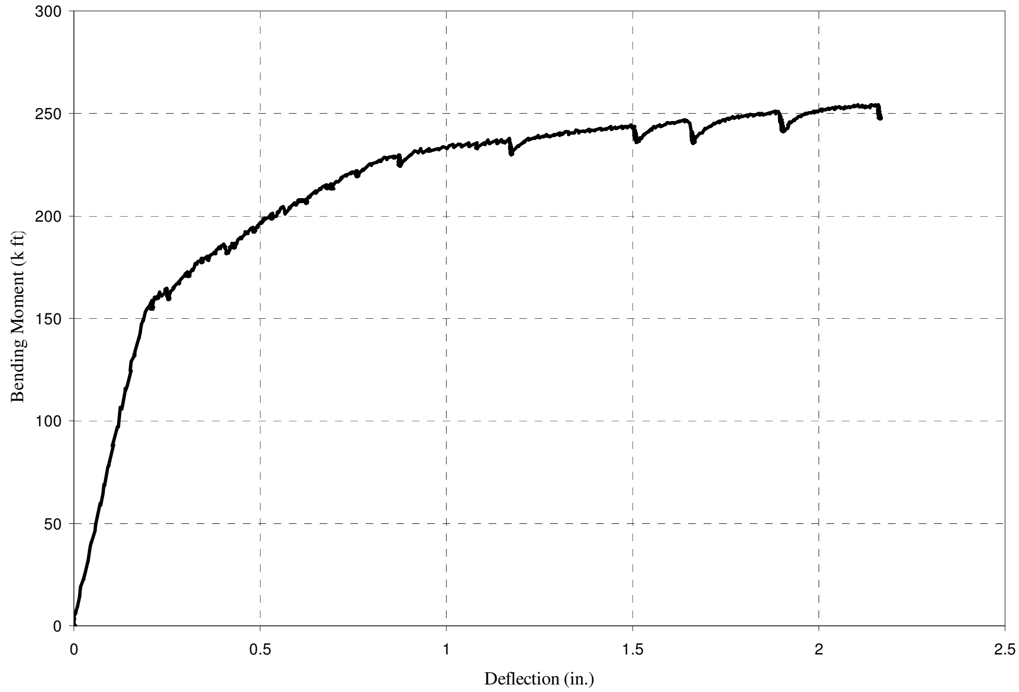

Figure C.37 Moment vs. Deflection for 3.300.5S.UB

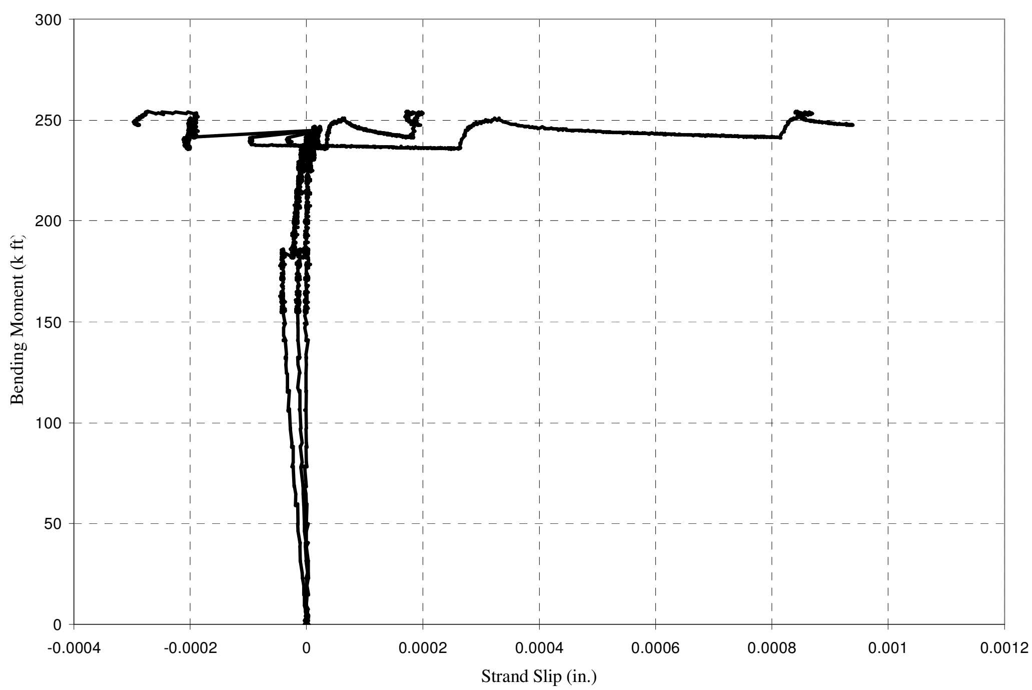

Figure C.38 Moment vs. Strand Slip for 3.300.5S.UB

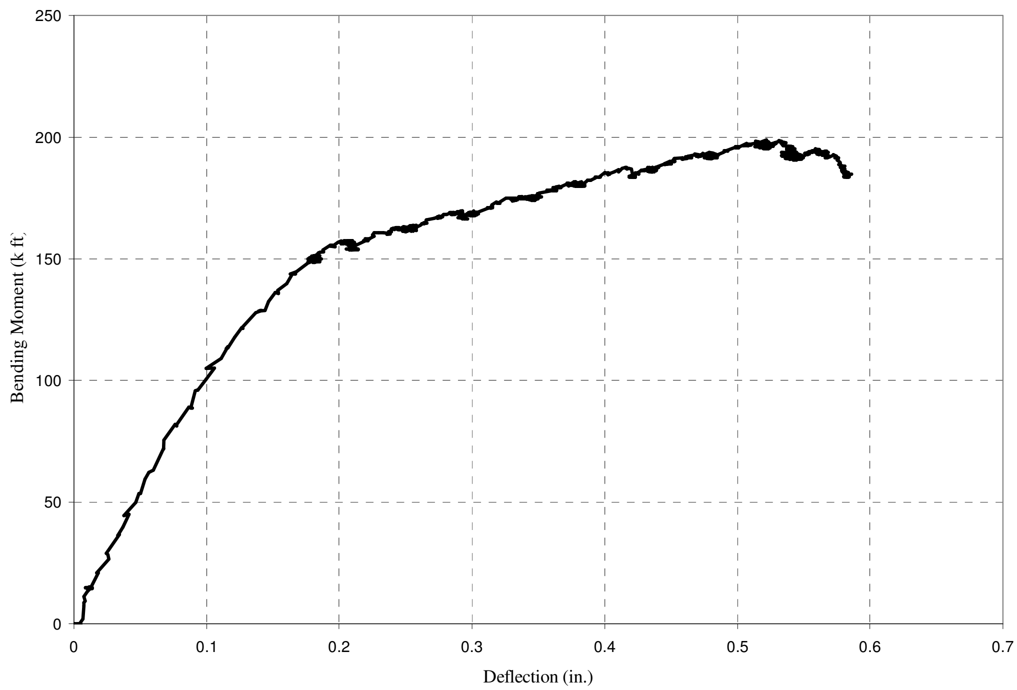

Figure C.39 Moment vs. Deflection for 4.270.5S.RA

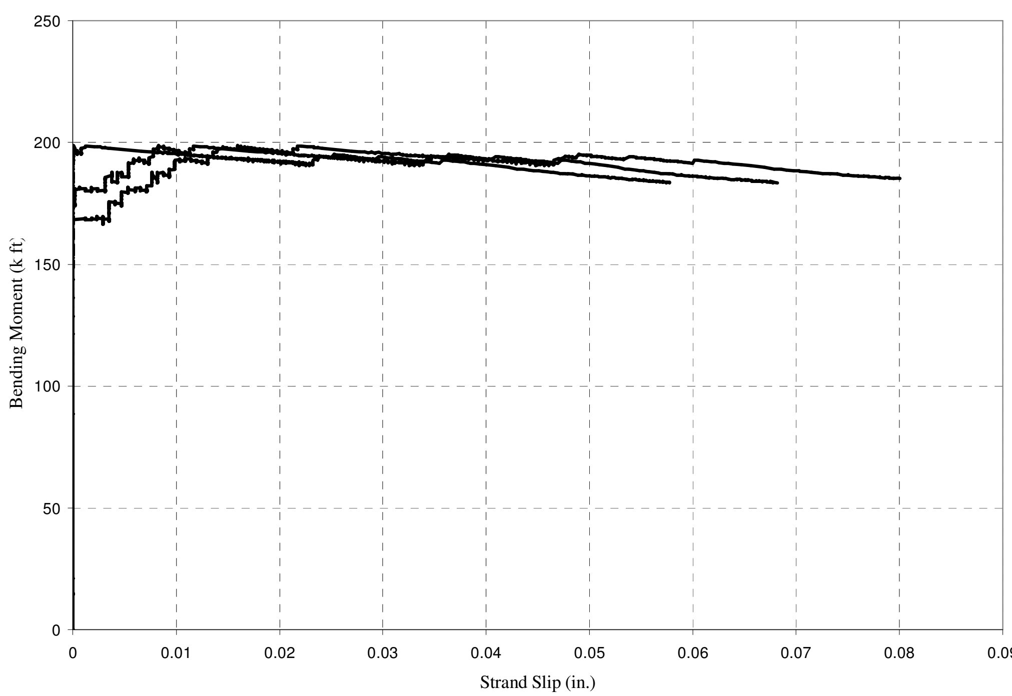

Figure C.40 Moment vs. Strand Slip for 4.270.5S.RA

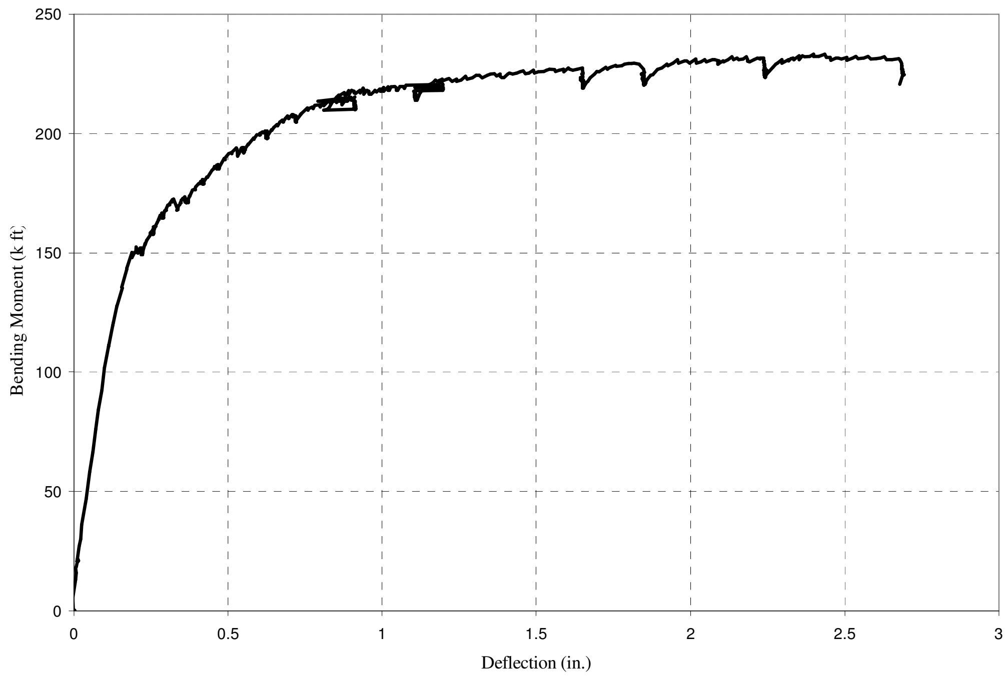

Figure C.41 Moment vs. Deflection for 4.270.5S.RB

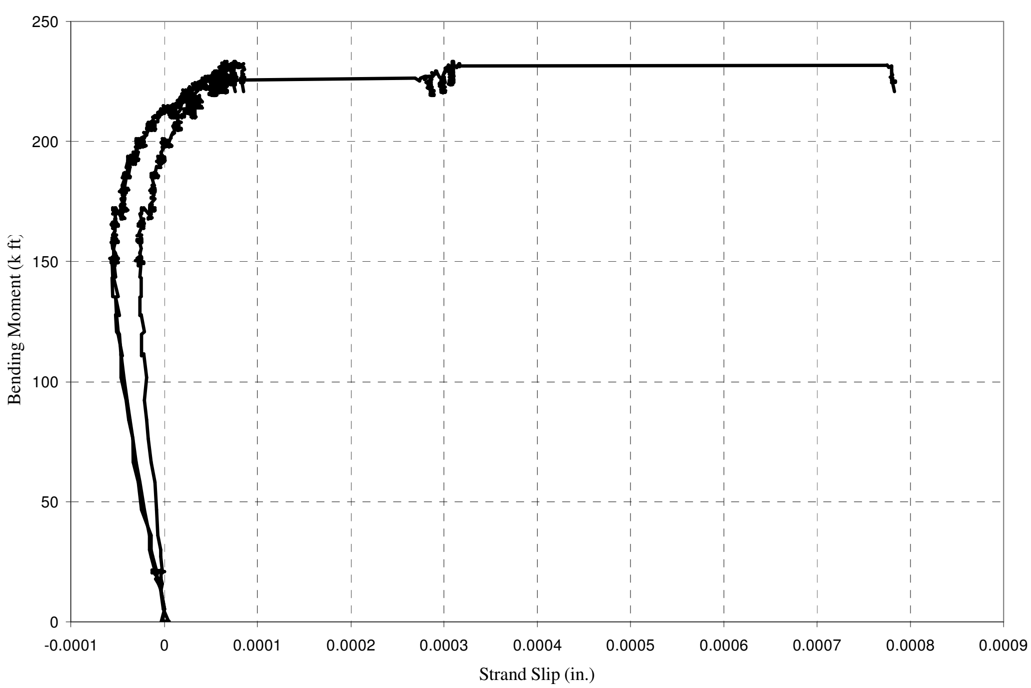

Figure C.42 Moment vs. Strand Slip for 4.270.5S.RB

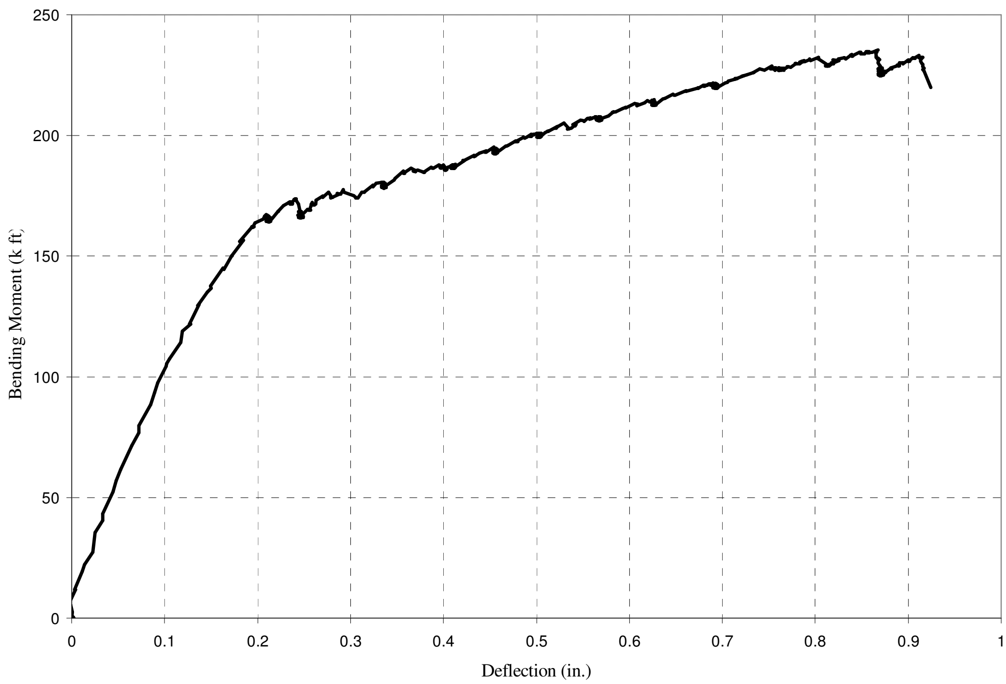

Figure C.43 Moment vs. Deflection for 4.300.5S.RA

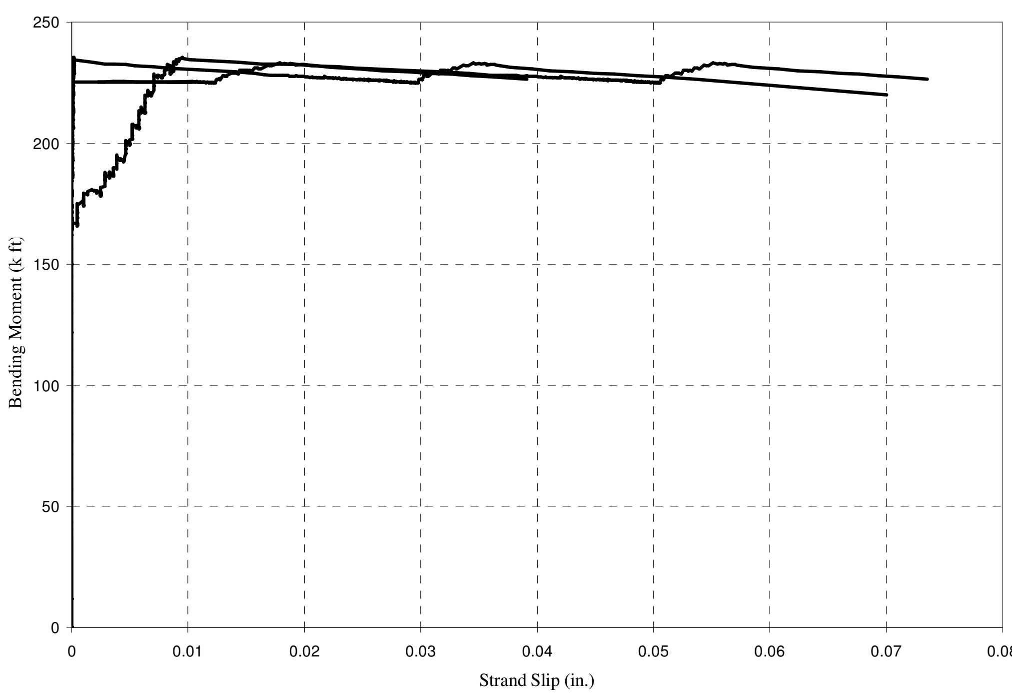

Figure C.44 Moment vs. Strand Slip for 4.300.5S.RA

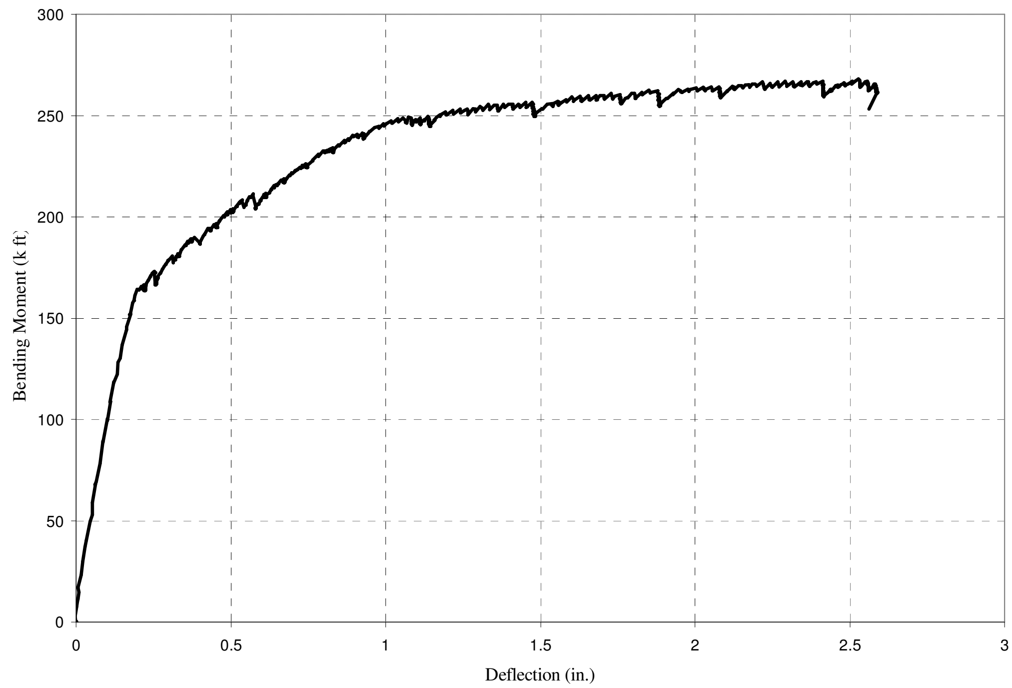

Figure C.45 Moment vs. Deflection for 4.300.5S.RB

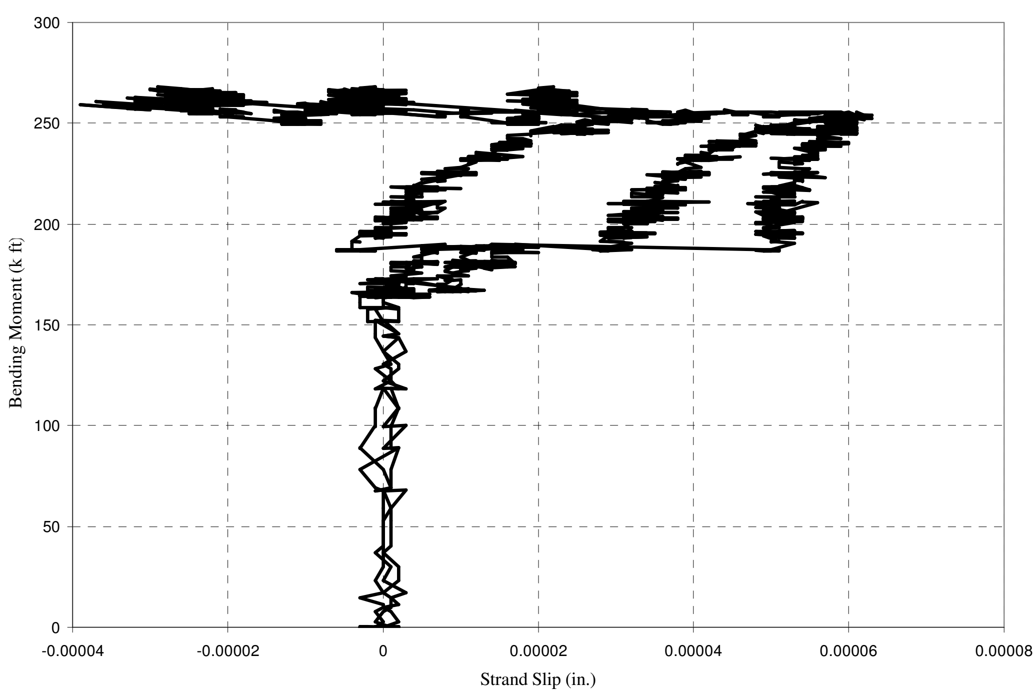

Figure C.46 Moment vs. Strand Slip for 4.300.5S.RB

APPENDIX D Vibrating Wire Gage Strain Plots

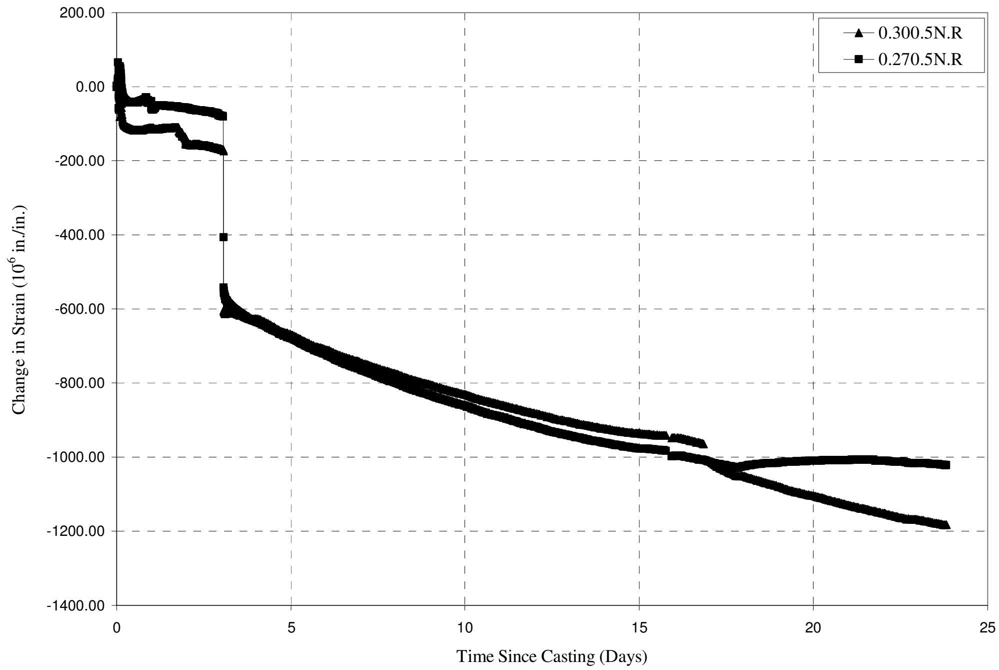

Figure D.1 Pour Zero Vibrating Wire Gage Strains

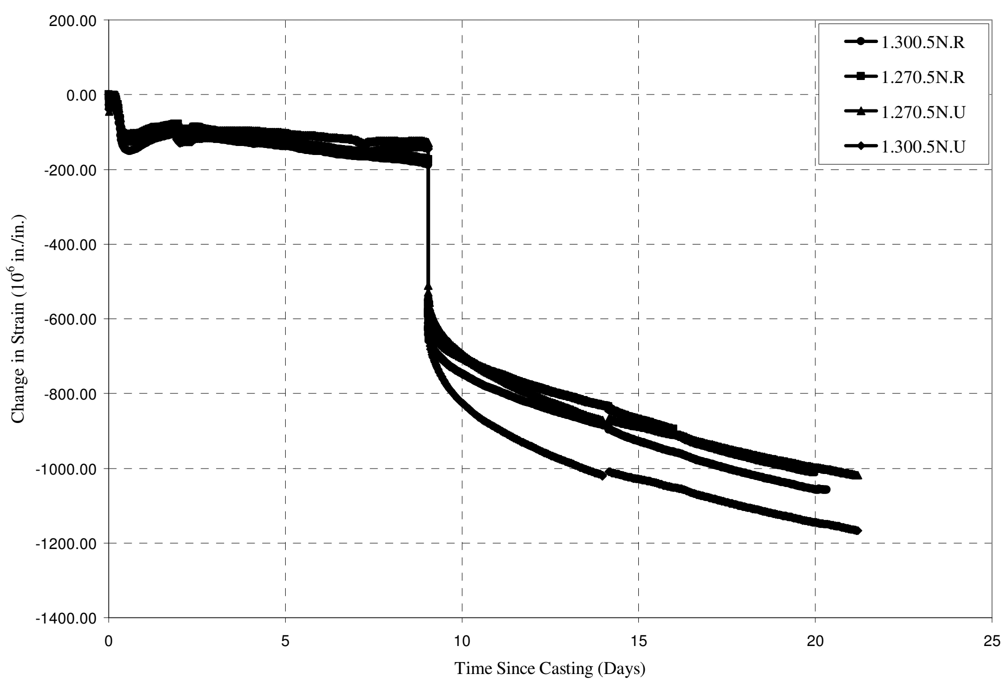

Figure D.2 Pour One Vibrating Wire Gage Strains

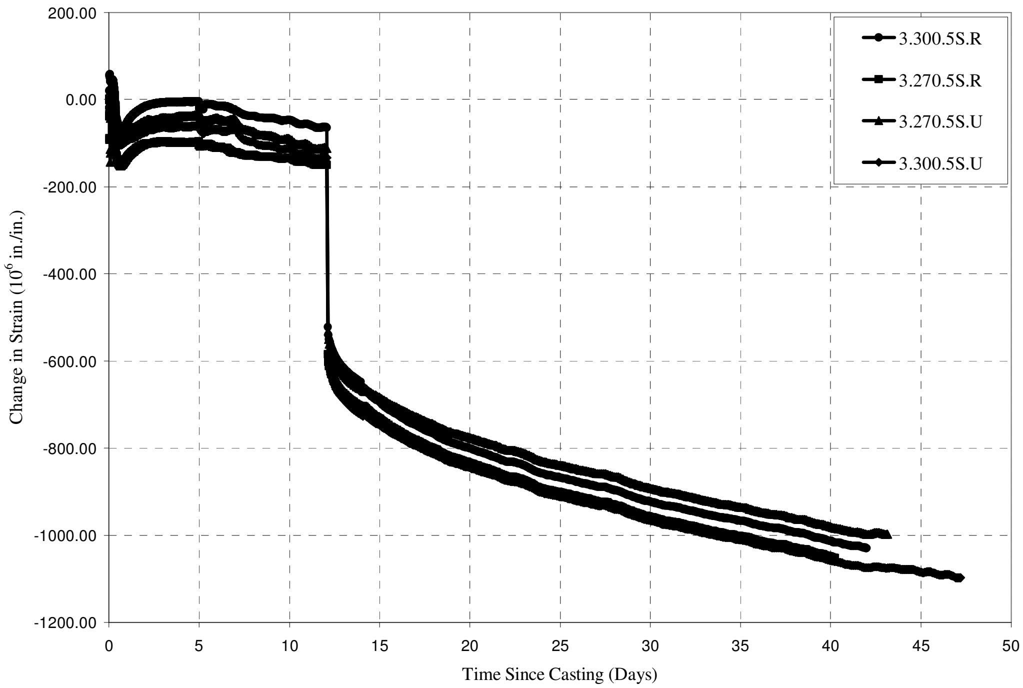

Figure D.3 Pour Three Vibrating Wire Gage Strains

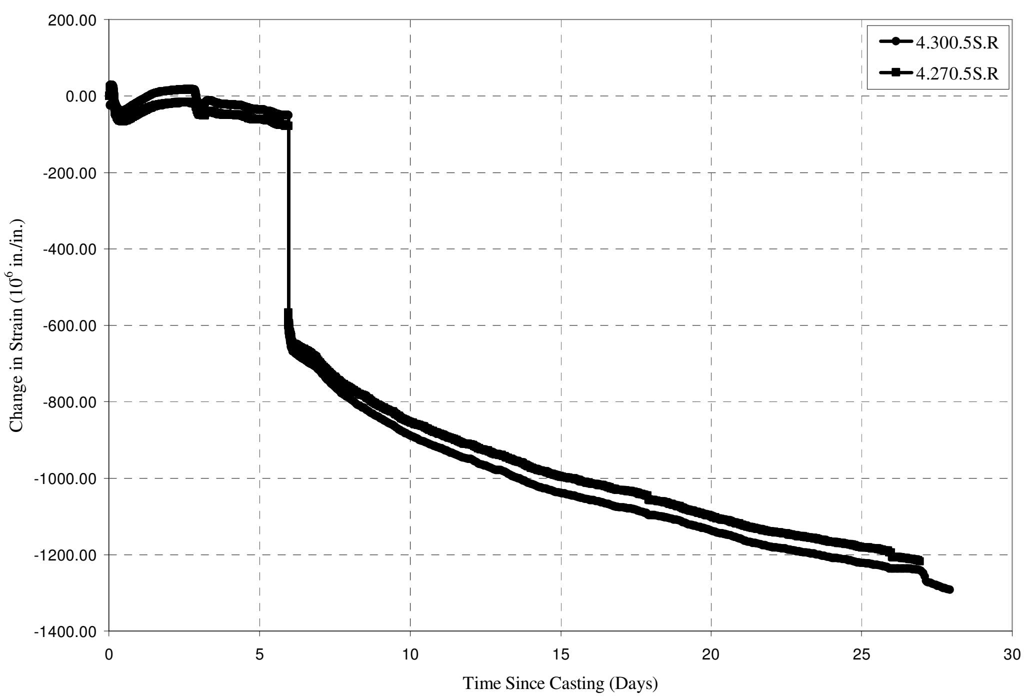

Figure D.4 Pour Four Vibrating Wire Gage Strains

APPENDIX E Crack Initiation and Crack Reopening Plots

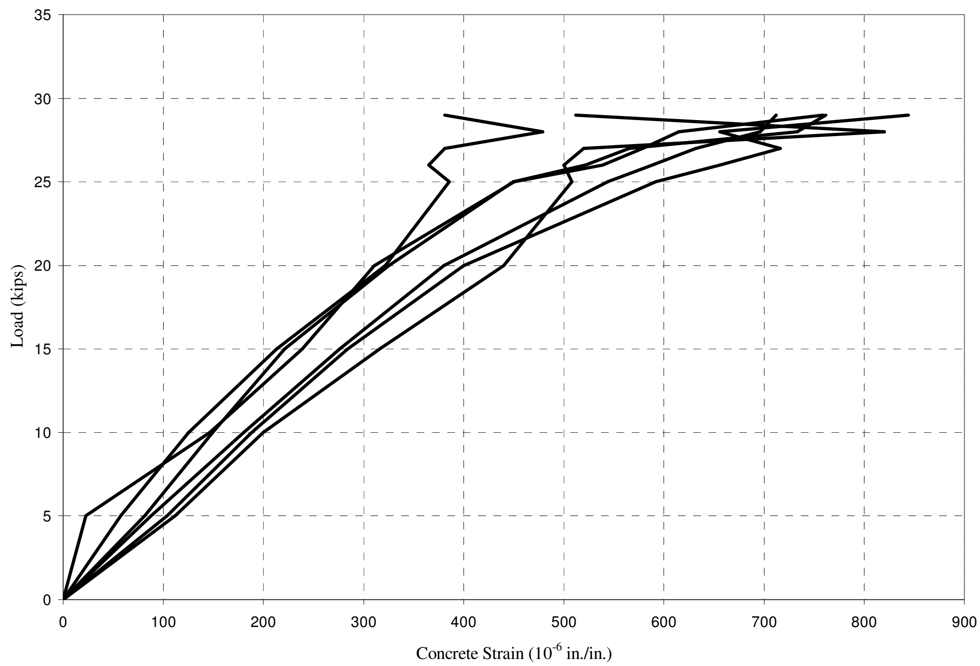

Figure E.1 Crack Initiation for 0.270.5N.RA

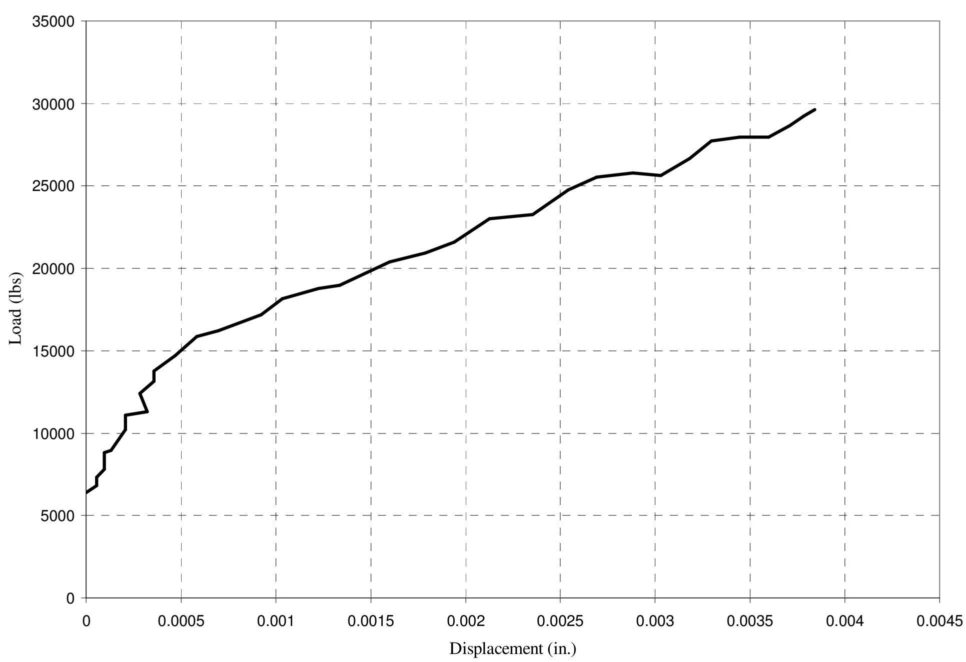

Figure E.2 Crack Reopening for 0.270.5N.RA

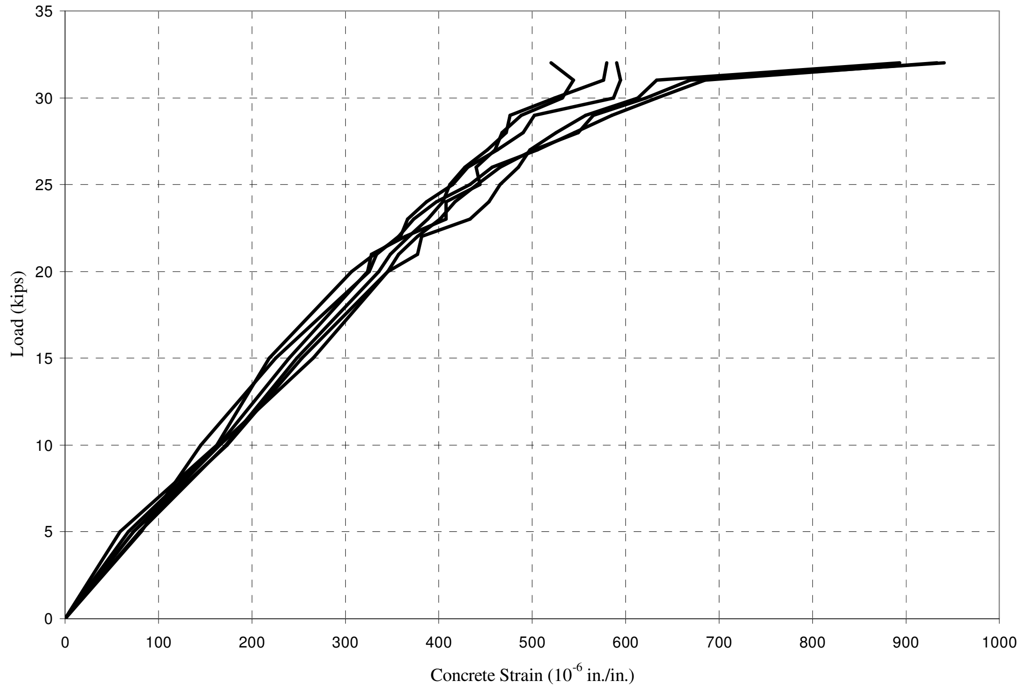

Figure E.3 Crack Initiation for 0.270.5N.RB

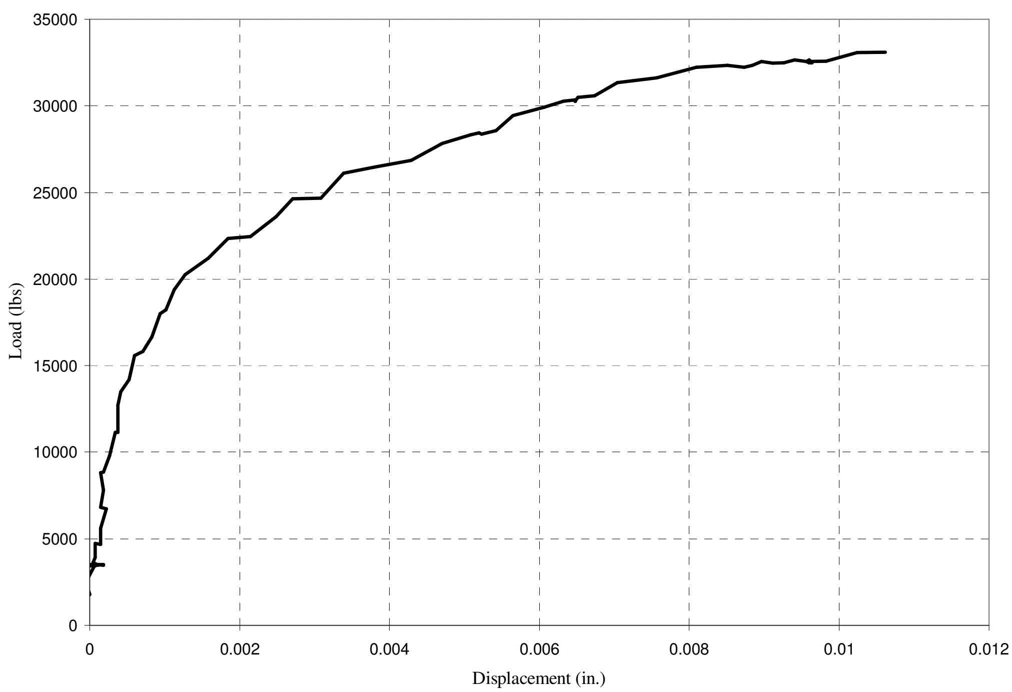

Figure E.4 Crack Reopening for 0.270.5N.RB

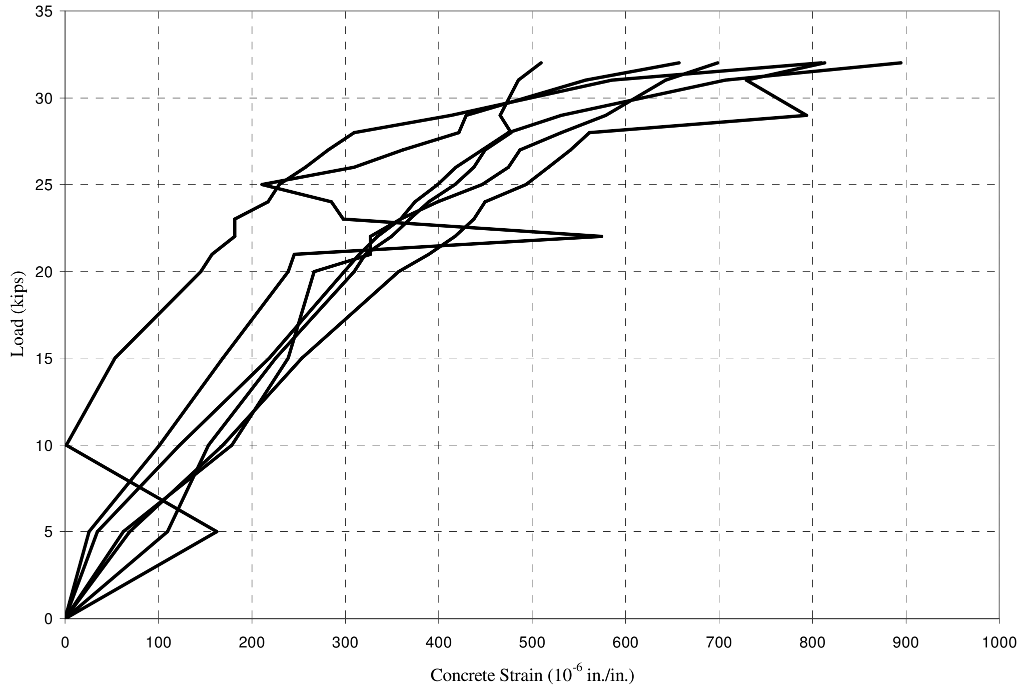

Figure E.5 Crack Initiation for 0.300.5N.RB

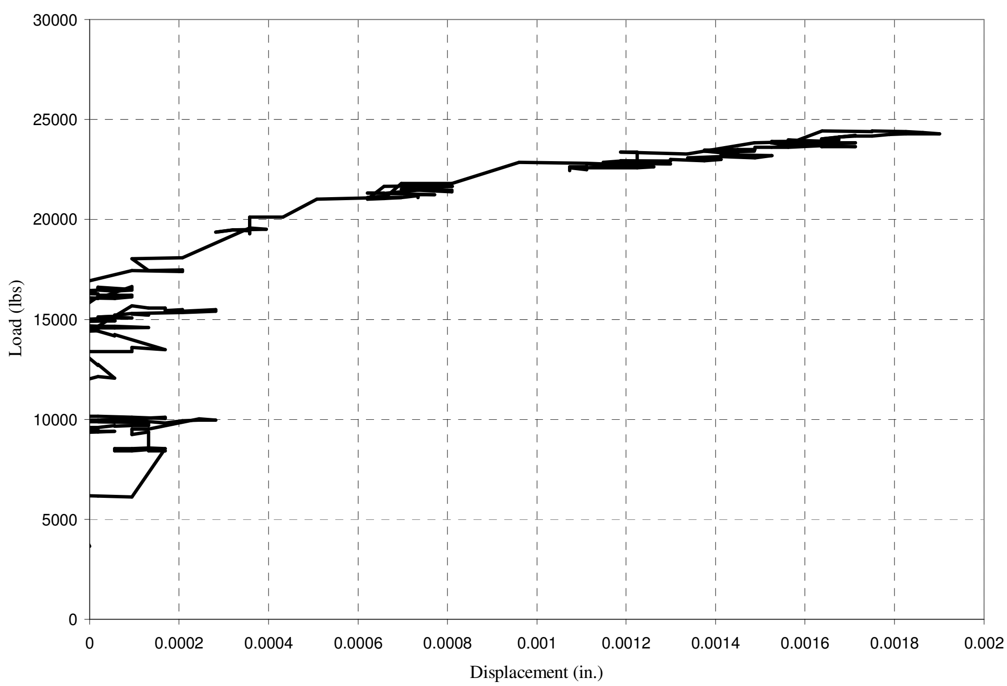

Figure E.6 Crack Reopening for 0.300.5N.RB

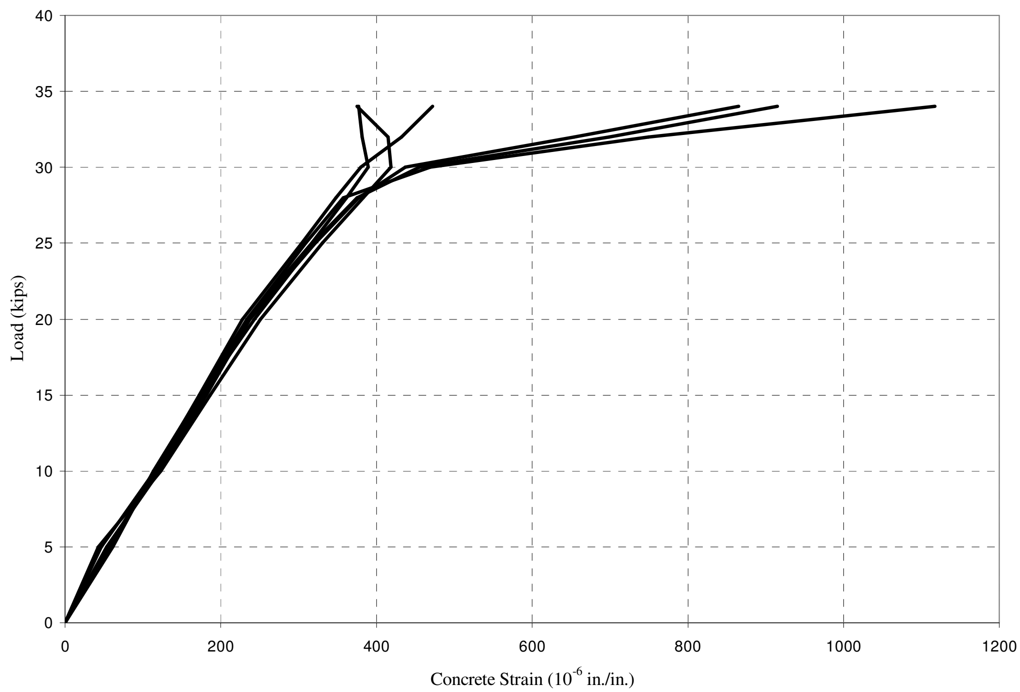

Figure E.7 Crack Initiation for 1.270.5N.RA

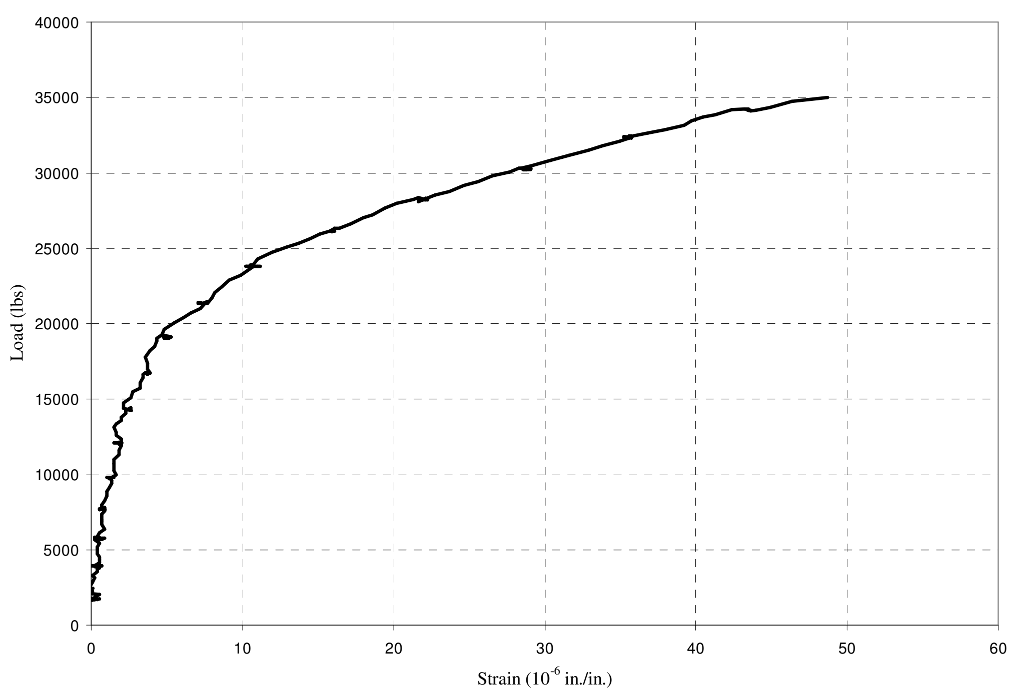

Figure E.8 Crack Reopening for 1.270.5N.RA

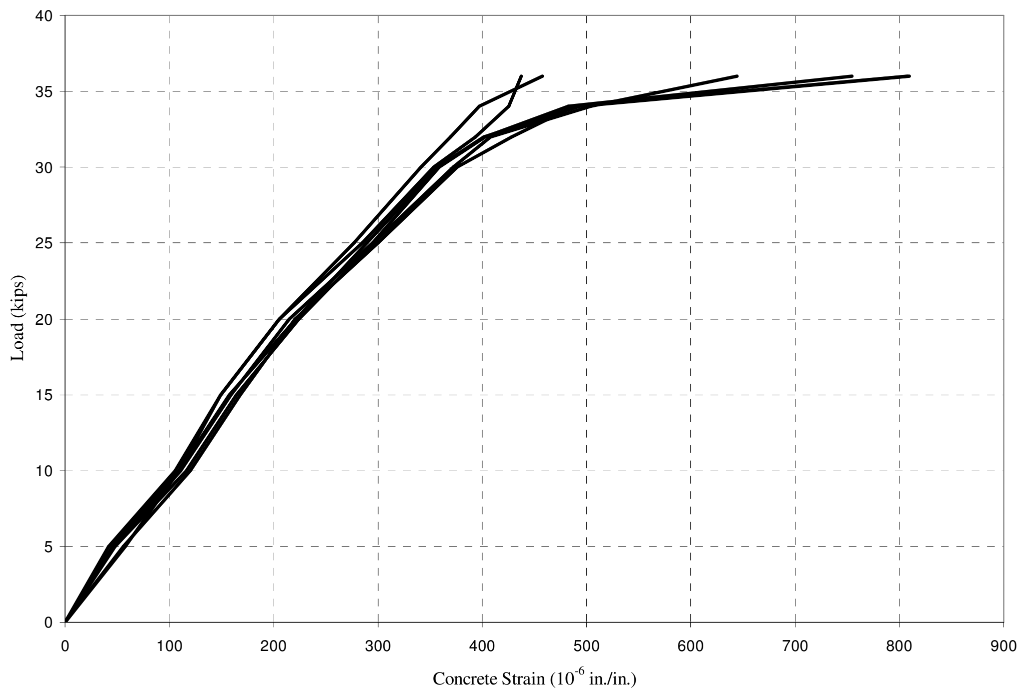

Figure E.9 Crack Initiation for 1.270.5N.RB

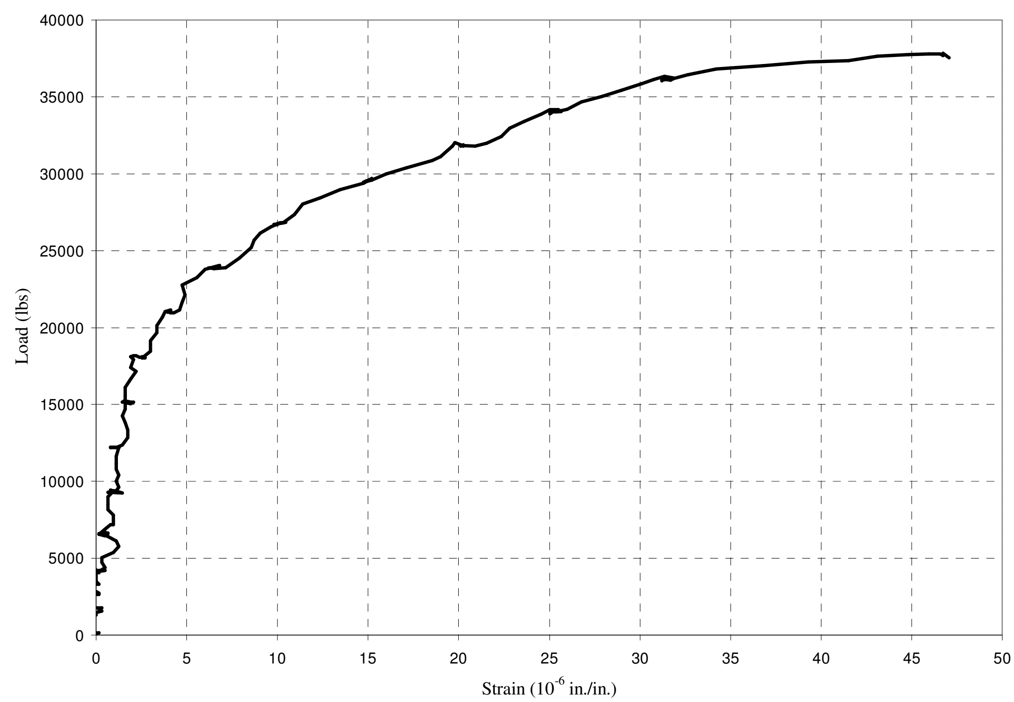

Figure E.10 Crack Reopening for 1.270.5N.RB

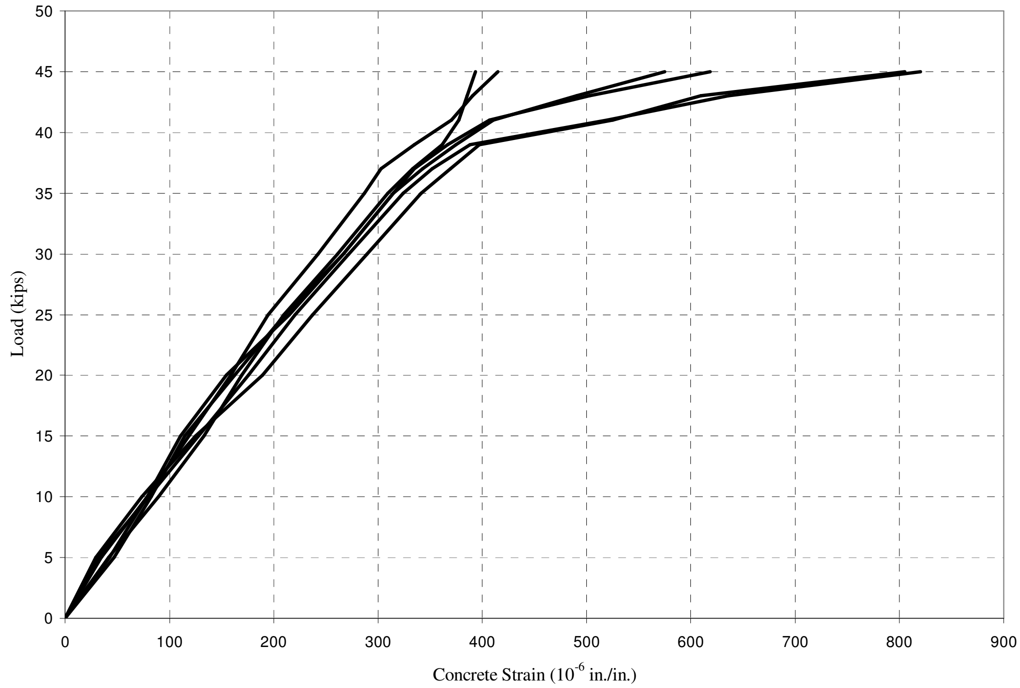

Figure E.11 Crack Initiation for 1.300.5N.RA

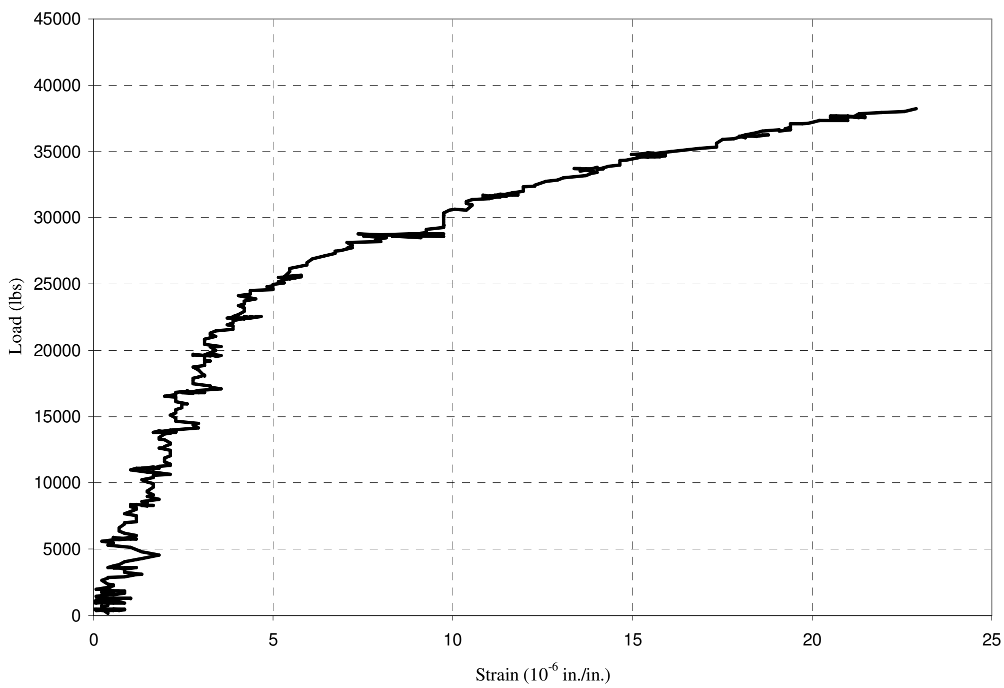

Figure E.12 Crack Reopening for 1.300.5N.RA

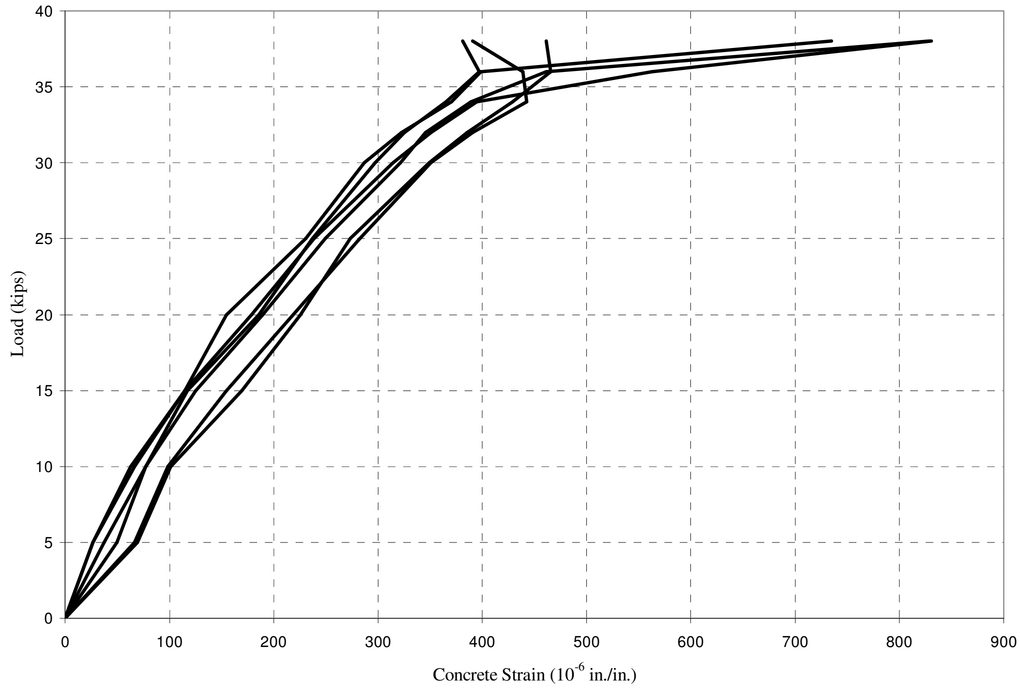

Figure E.13 Crack Initiation for 1.300.5N.RB

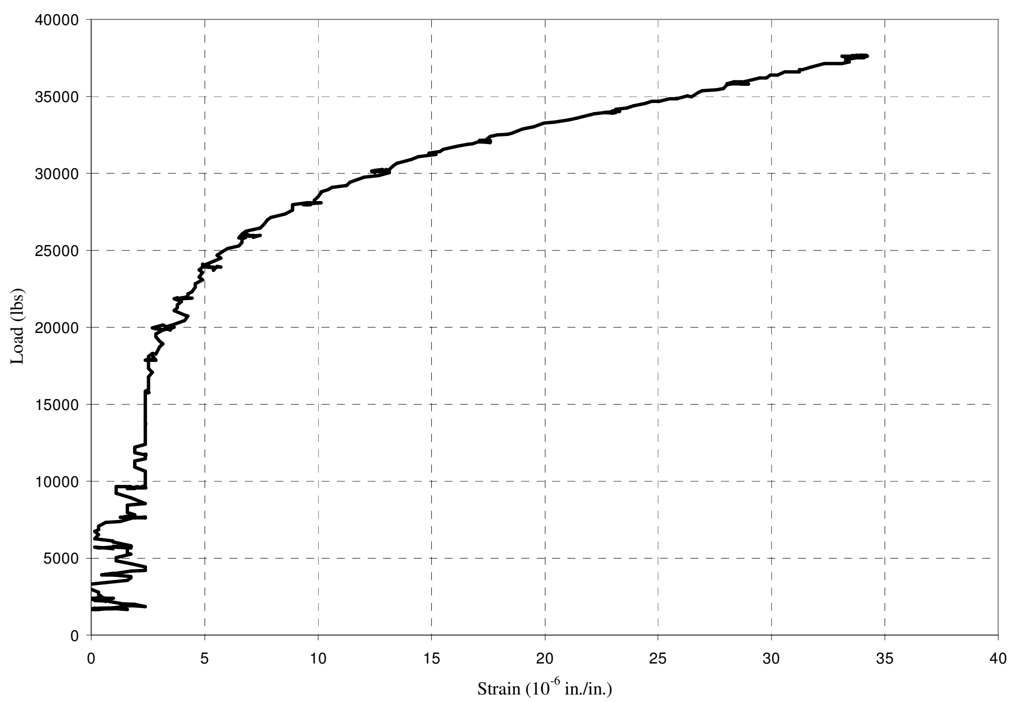

Figure E.14 Crack Reopening for 1.300.5N.RB

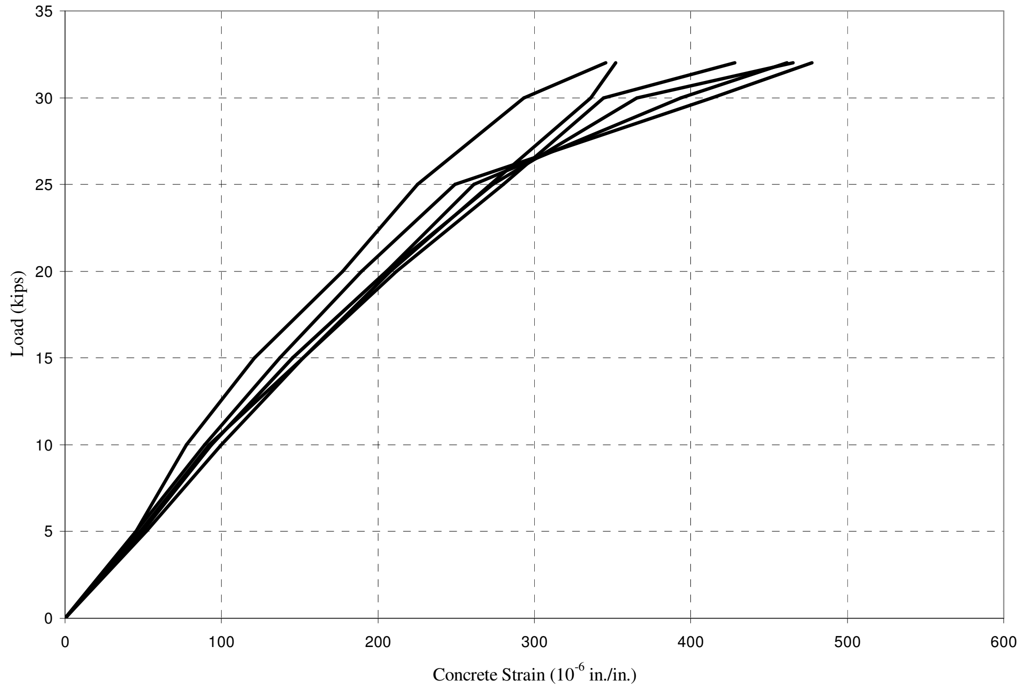

Figure E.15 Crack Initiation for 1.270.5N.UA

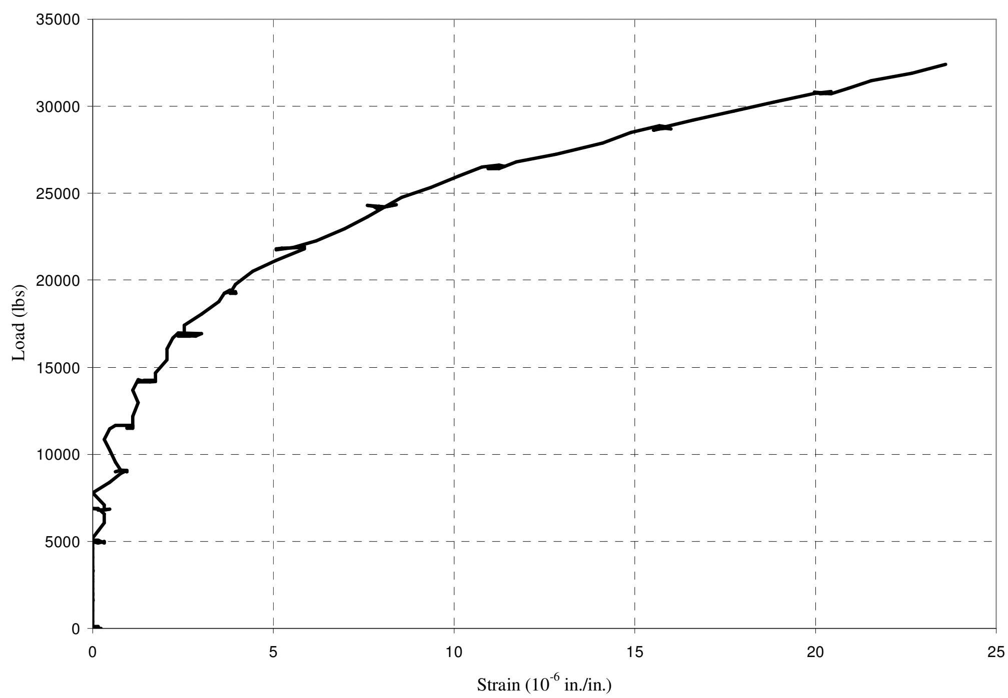

Figure E.16 Crack Reopening for 1.270.5N.UA

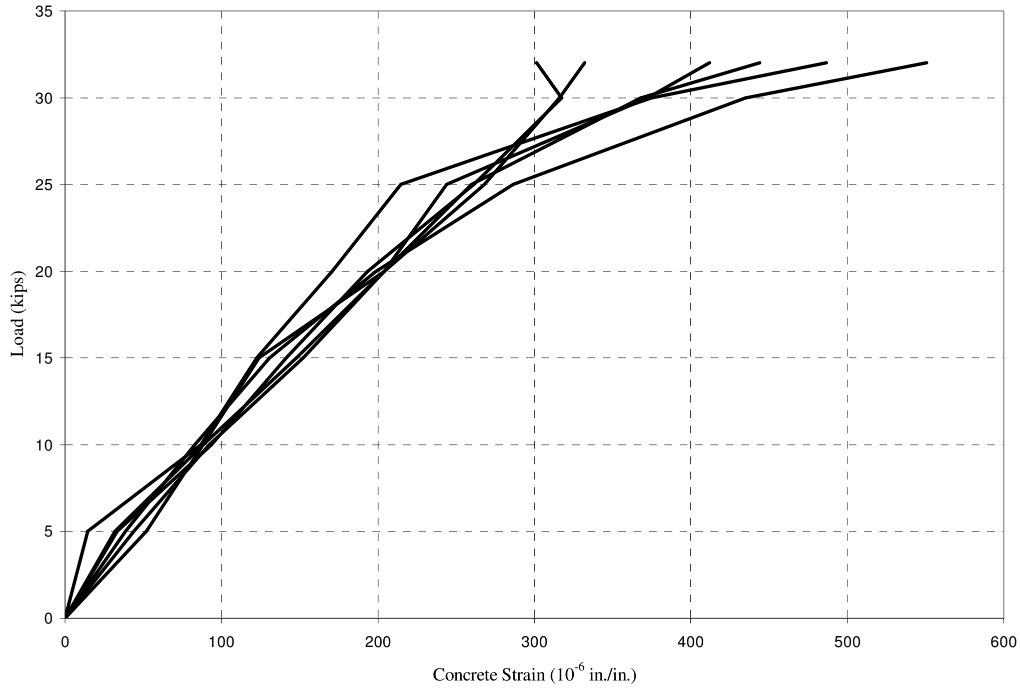

Figure E.17 Crack Initiation for 1.270.5N.UB

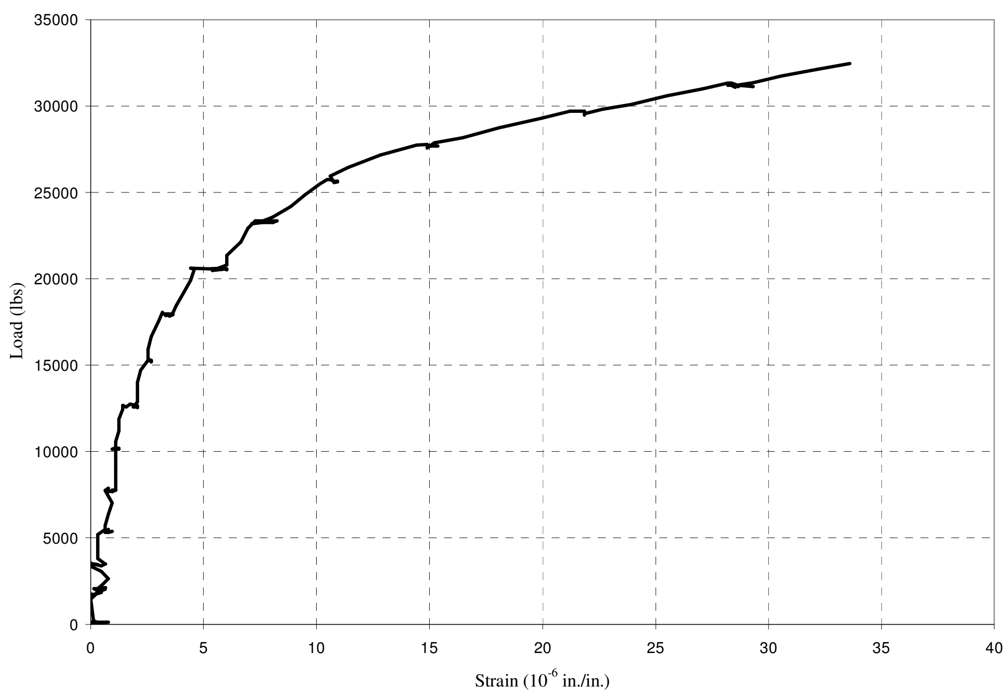

Figure E.18 Crack Reopening for 1.270.5N.UB

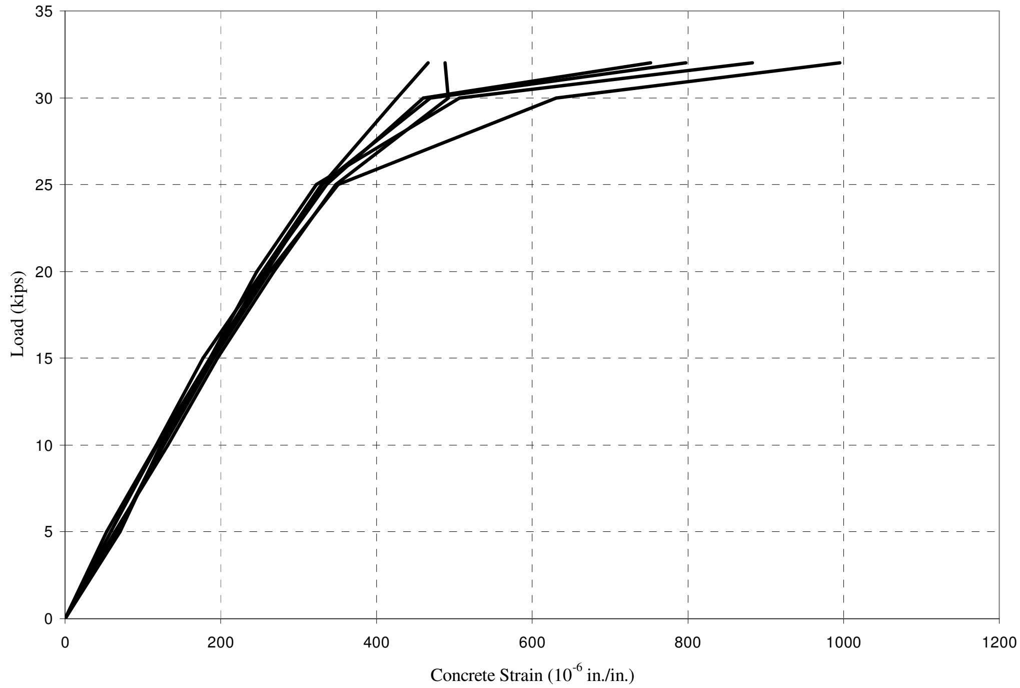

Figure E.19 Crack Initiation for 1.300.5N.UA

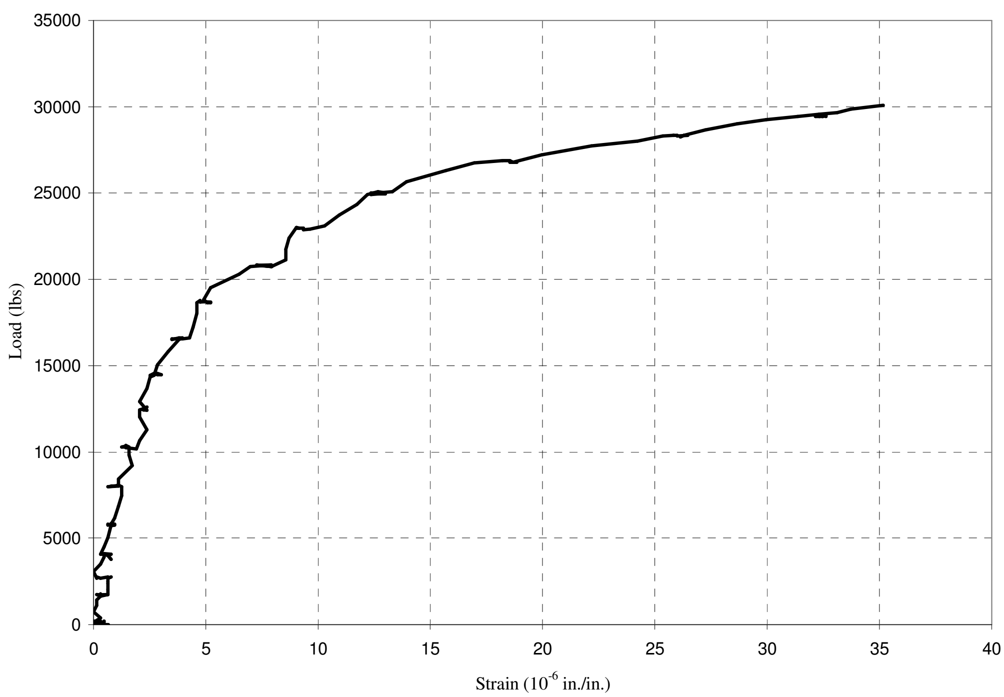

Figure E.20 Crack Reopening for 1.300.5N.UA

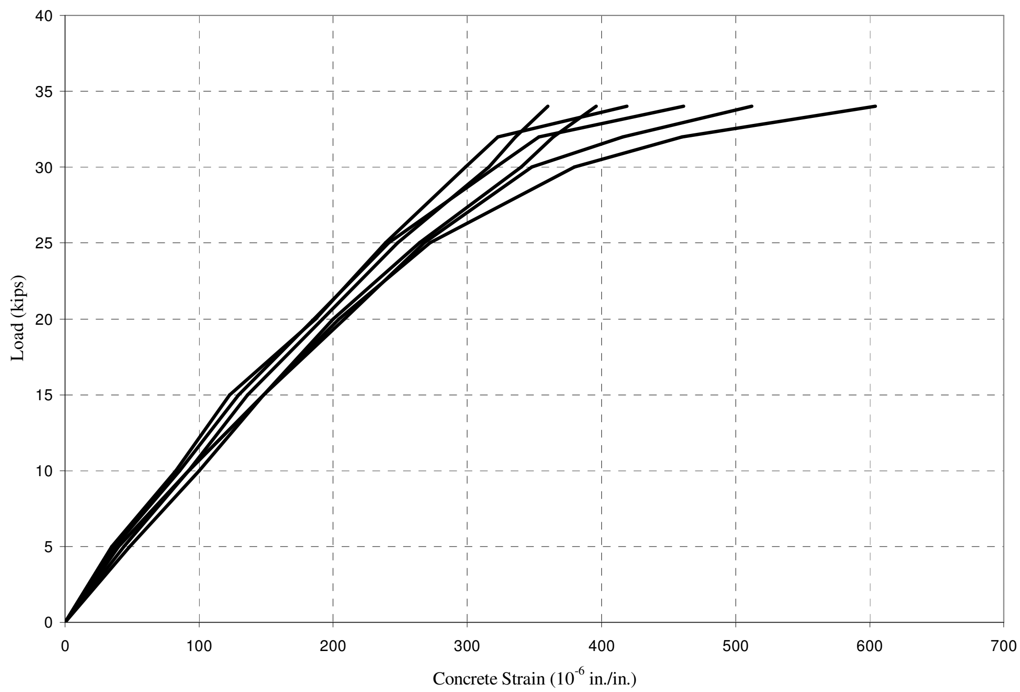

Figure E.21 Crack Initiation for 1.300.5N.UB

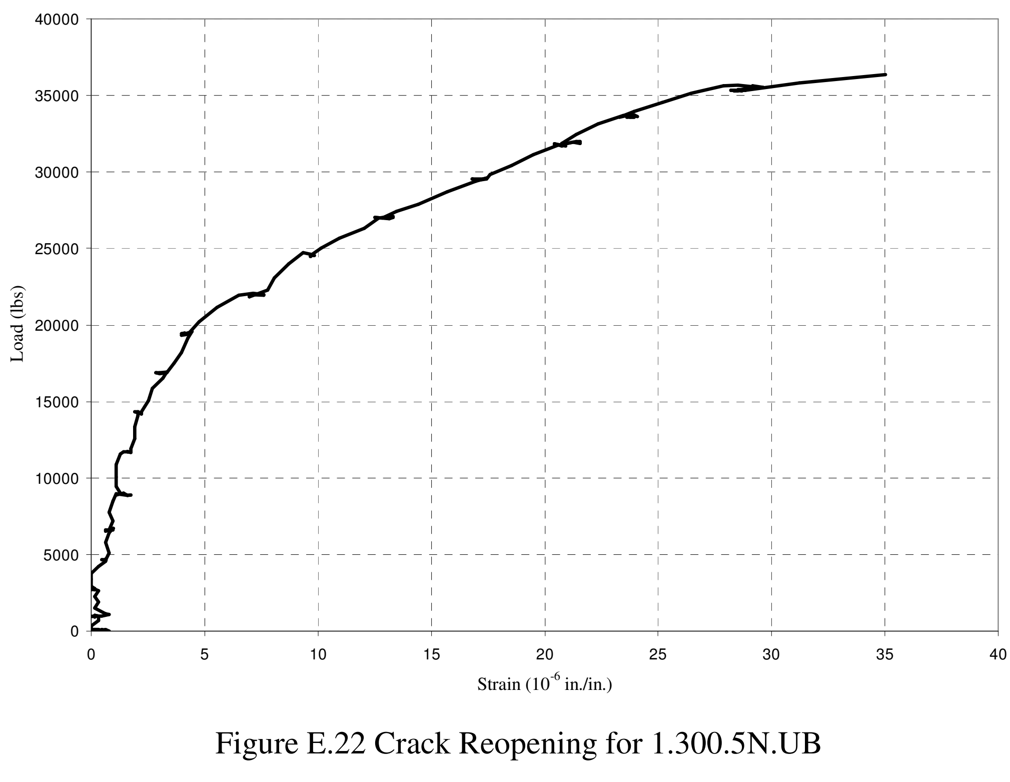

Figure E.22 Crack Reopening for 1.300.5N.UB

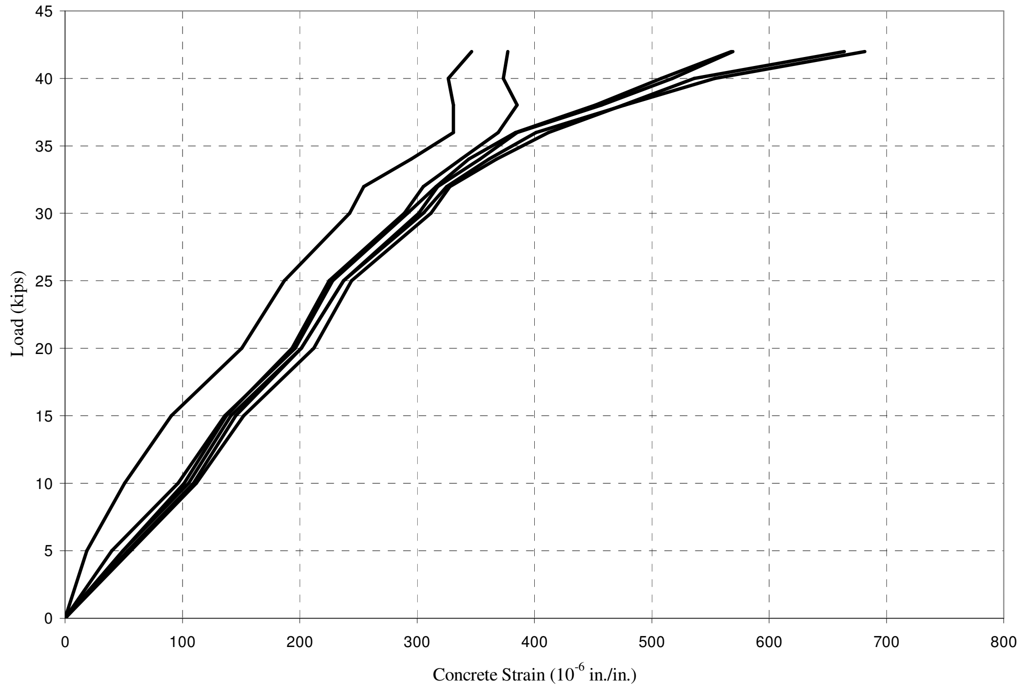

Figure E.23 Crack Initiation for 3.270.5S.RA

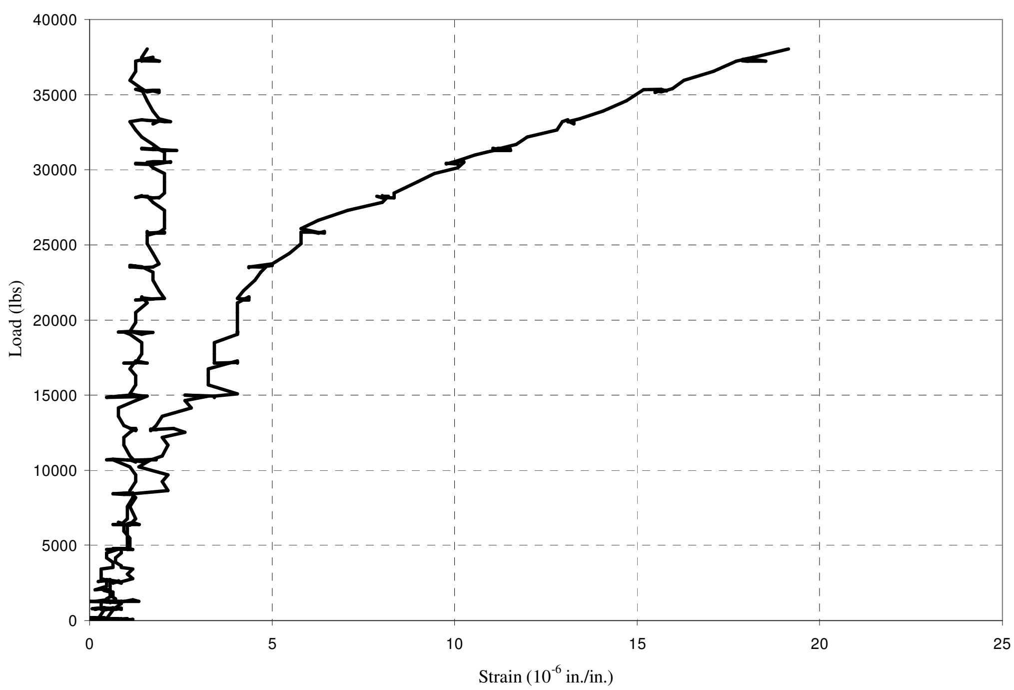

Figure E.24 Crack Reopening for 3.270.5S.RA

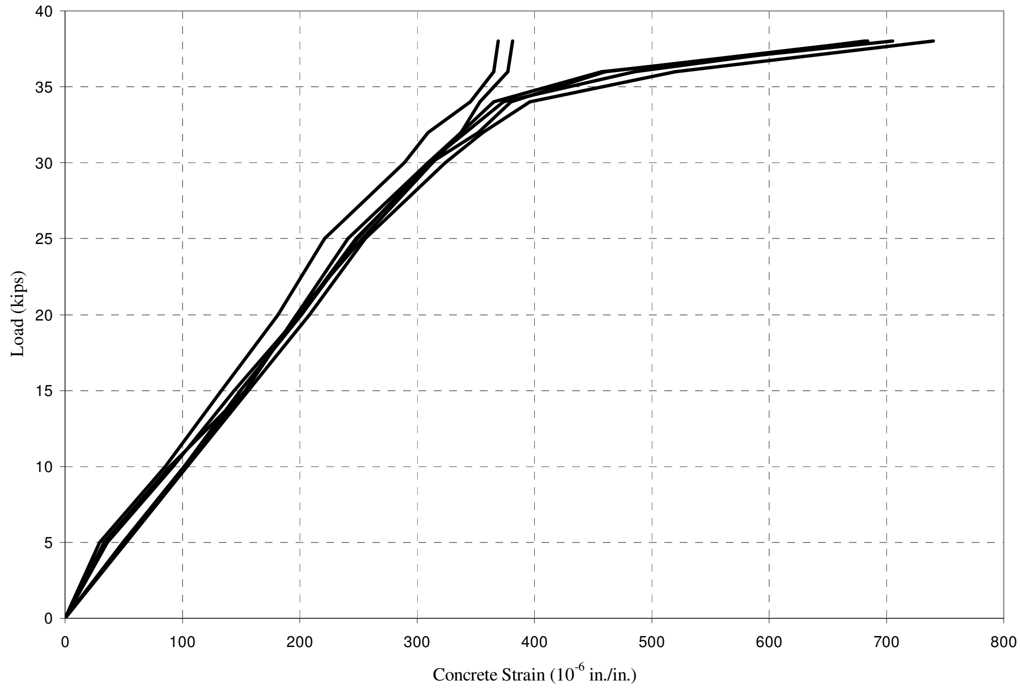

Figure E.25 Crack Initiation for 3.270.5S.RB

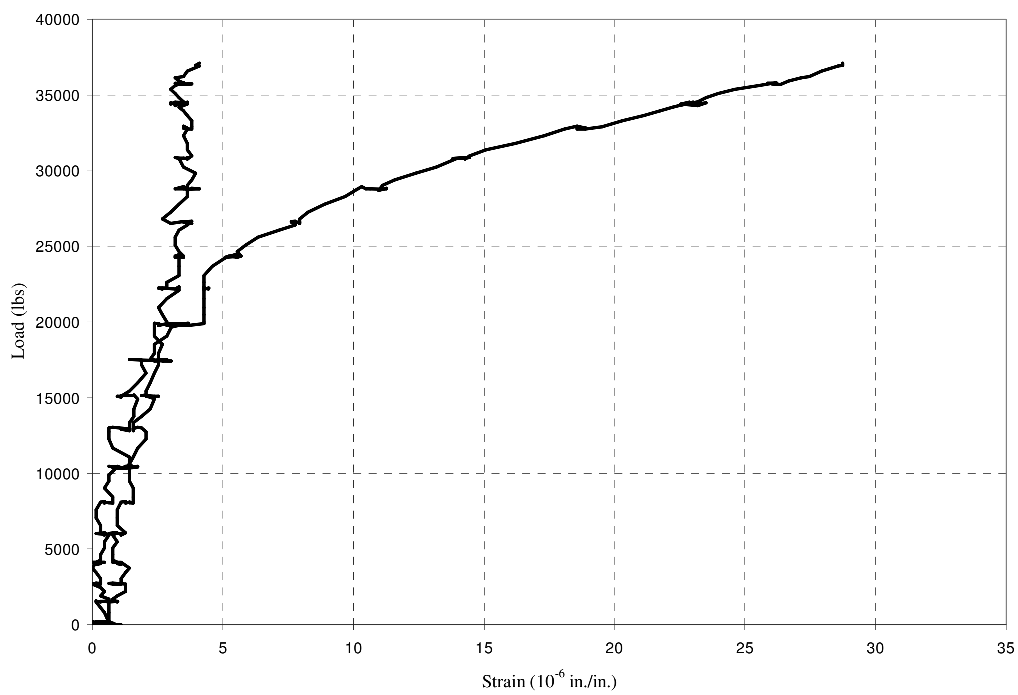

Figure E.26 Crack Reopening for 3.270.5S.RB

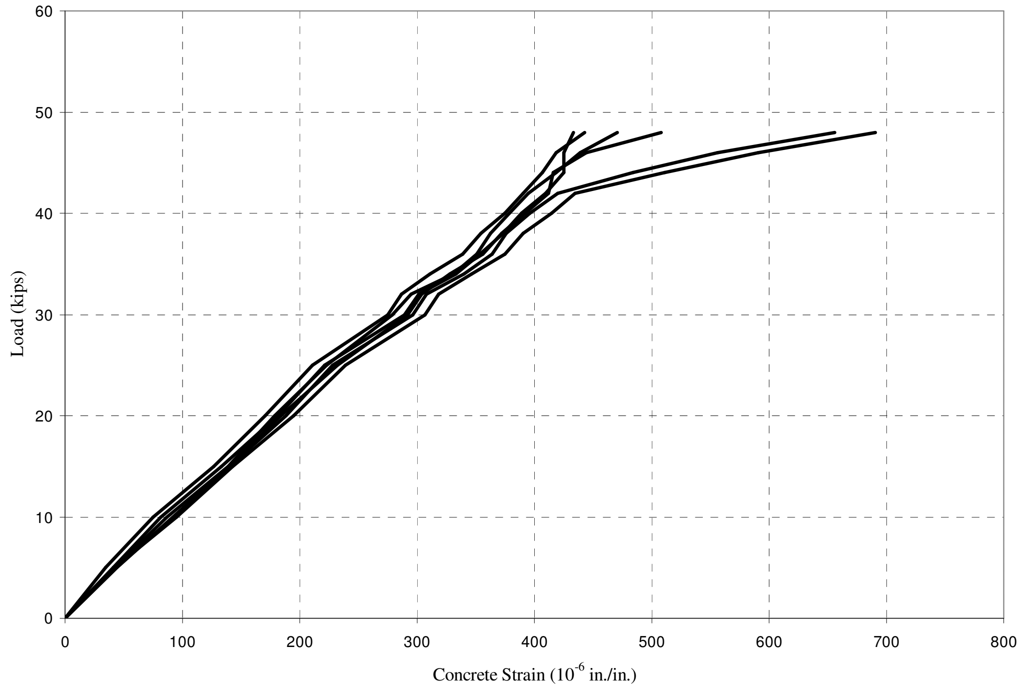

Figure E.27 Crack Initiation for 3.300.5S.RA

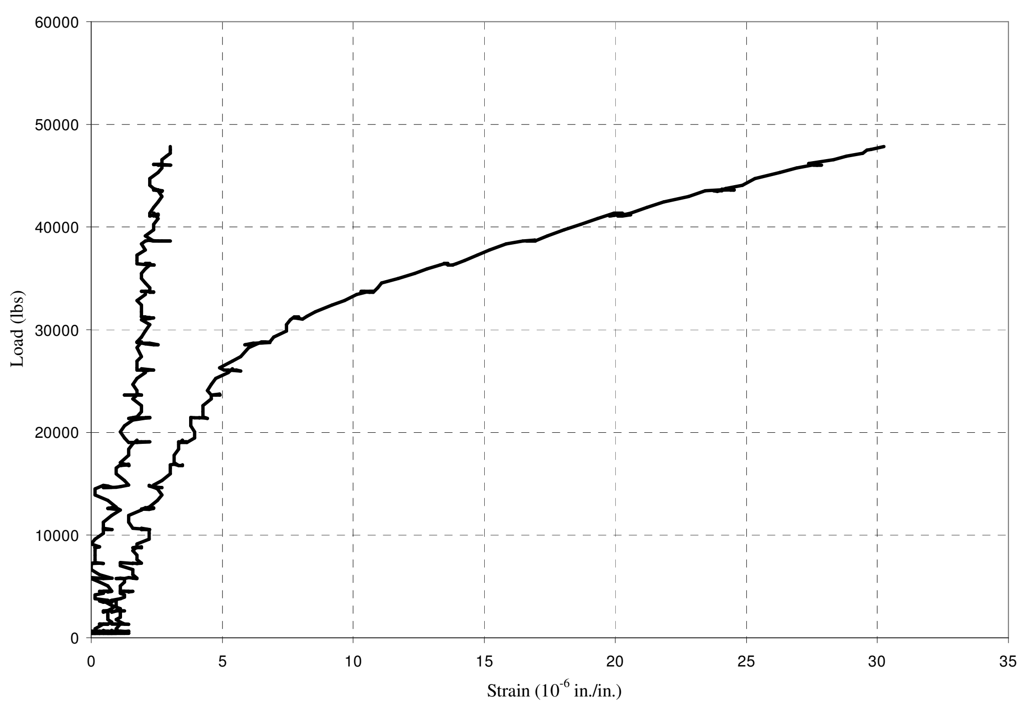

Figure E.28 Crack Reopening for 3.300.5S.RA

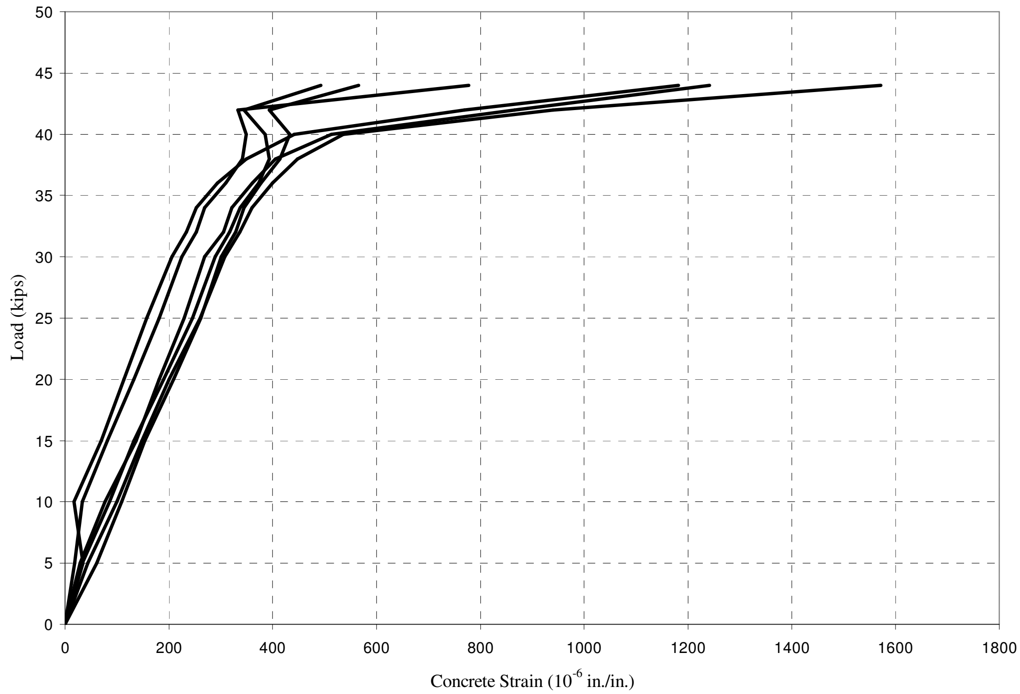

Figure E.29 Crack Initiation for 3.300.5S.RB

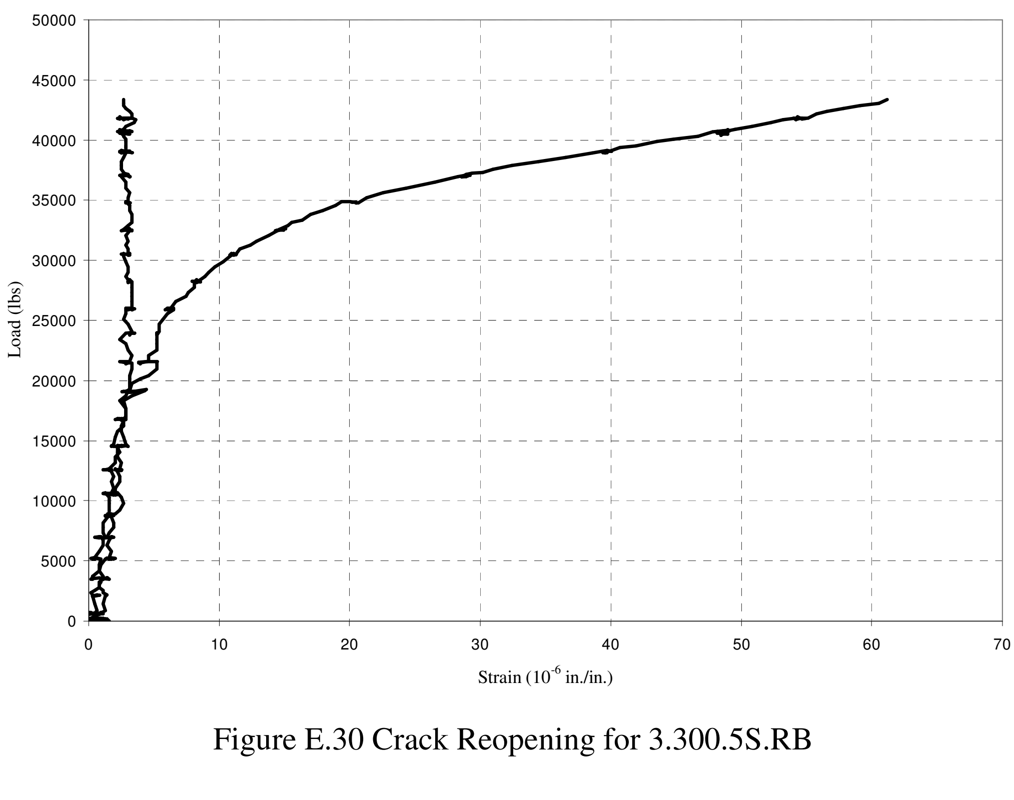

Figure E.30 Crack Reopening for 3.300.5S.RB

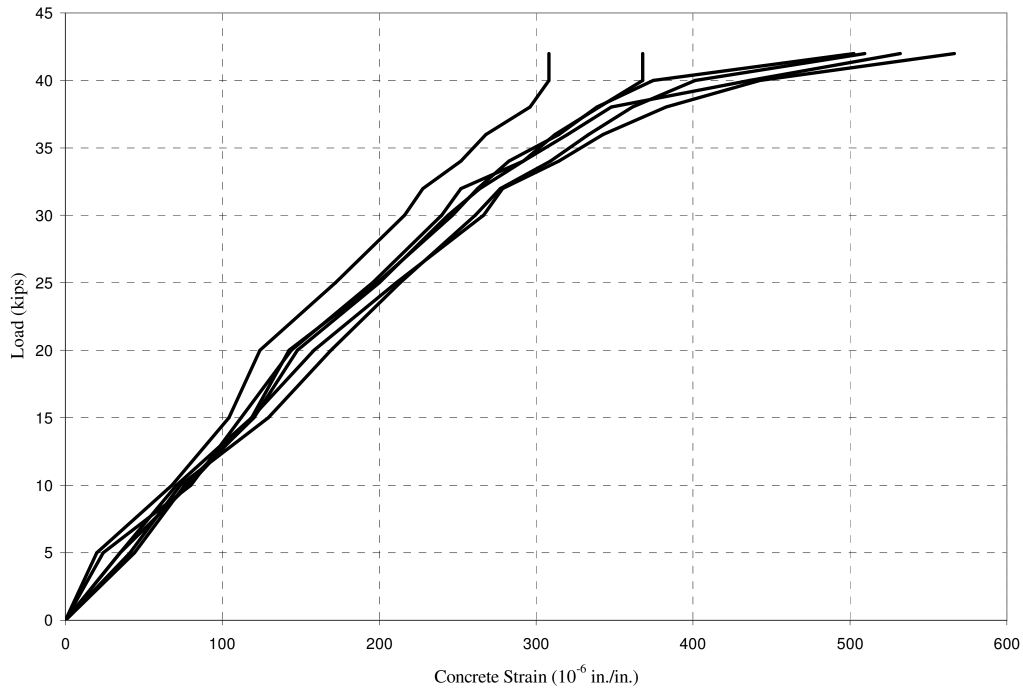

Figure E.31 Crack Initiation for 3.270.5S.UA

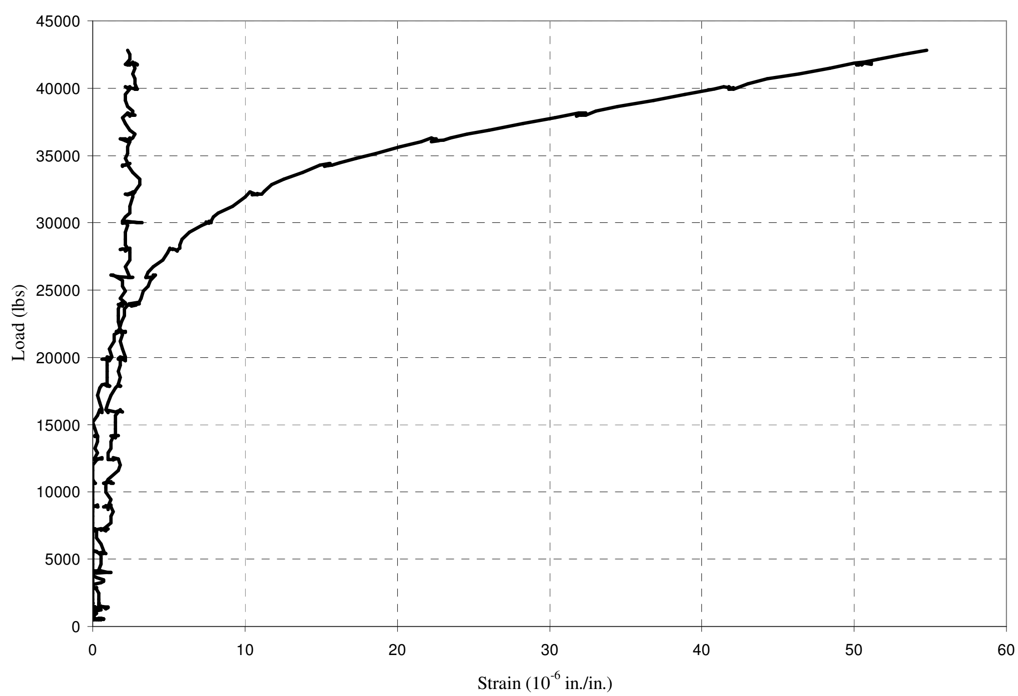

Figure E.32 Crack Reopening for 3.270.5S.UA

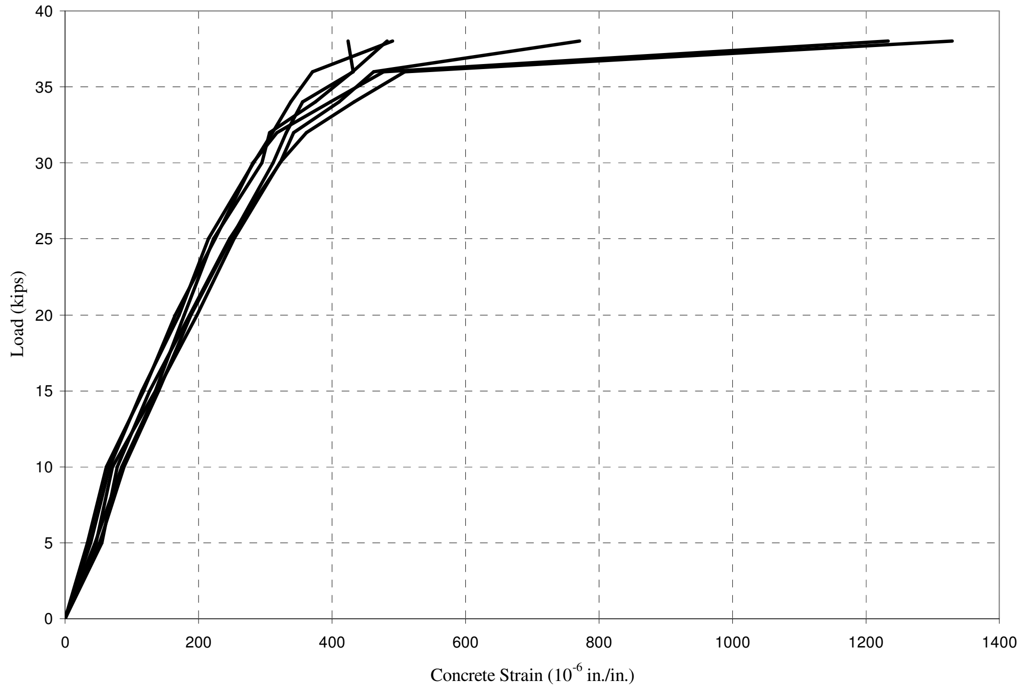

Figure E.33 Crack Initiation for 3.270.5S.UB

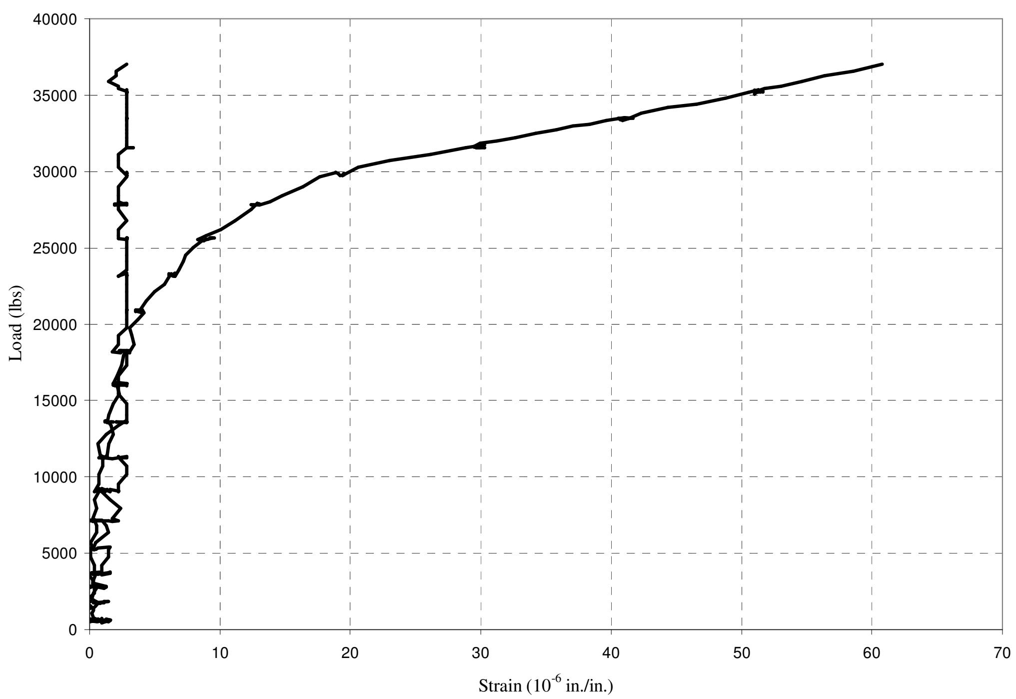

Figure E.34 Crack Reopening for 3.270.5S.UB

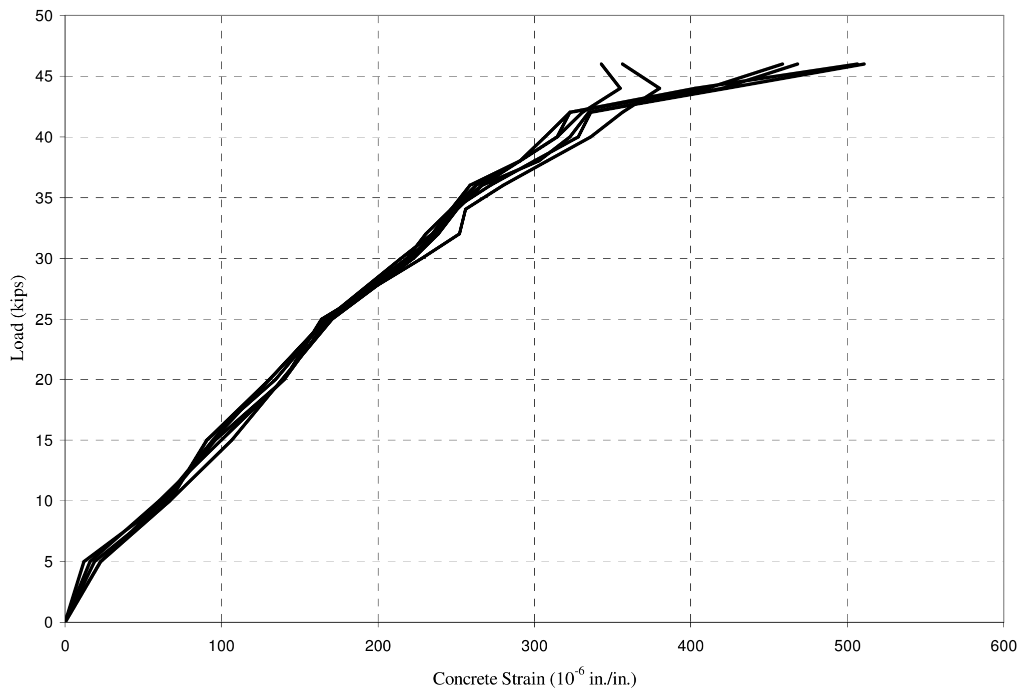

Figure E.35 Crack Initiation for 3.300.5S.UA

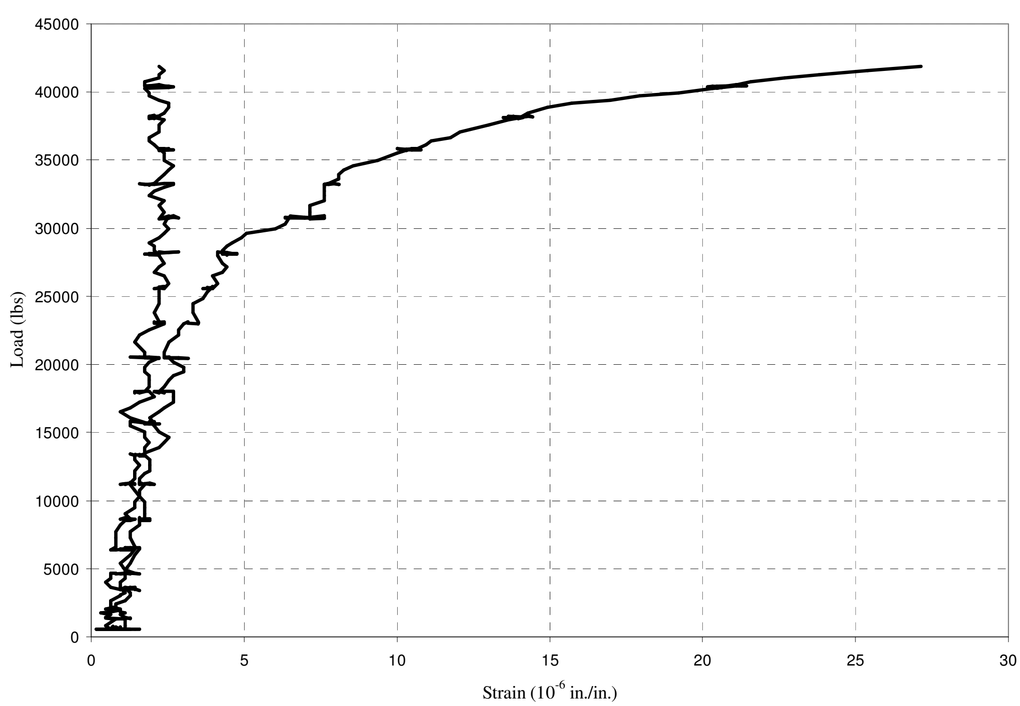

Figure E.36 Crack Reopening for 3.300.5S.UA

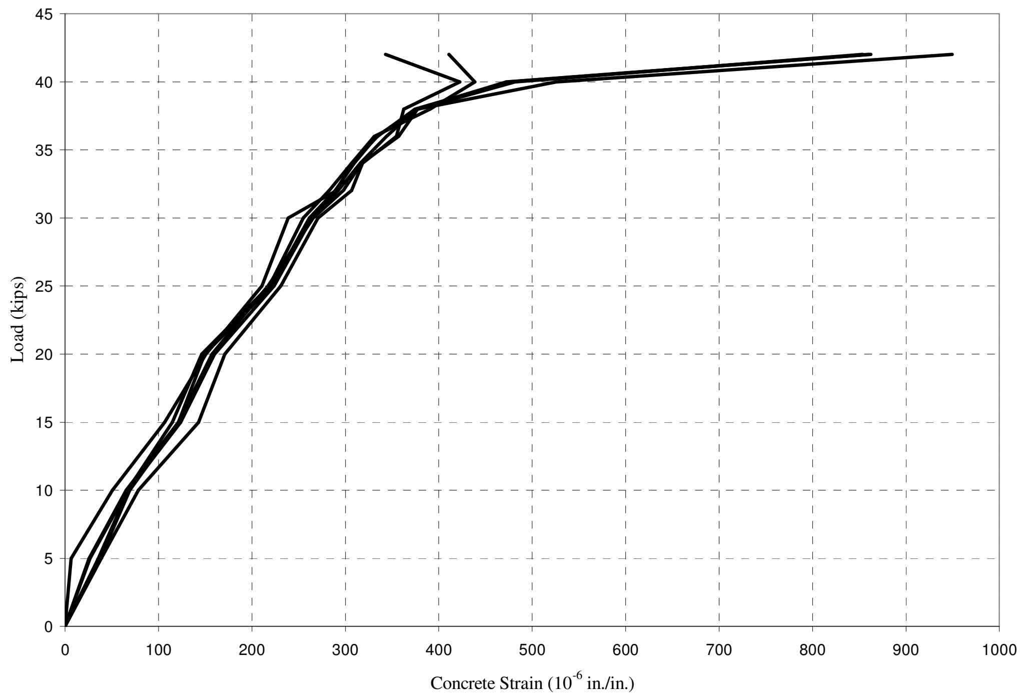

Figure E.37 Crack Initiation for 3.300.5S.UB

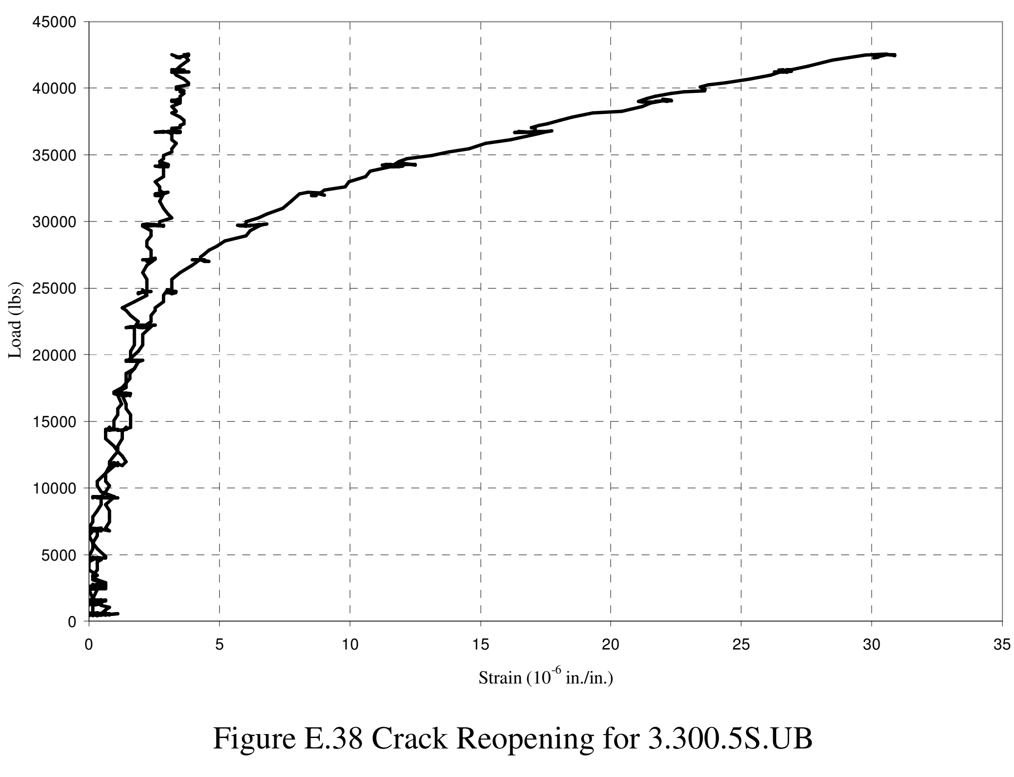

Figure E.38 Crack Reopening for 3.300.5S.UB

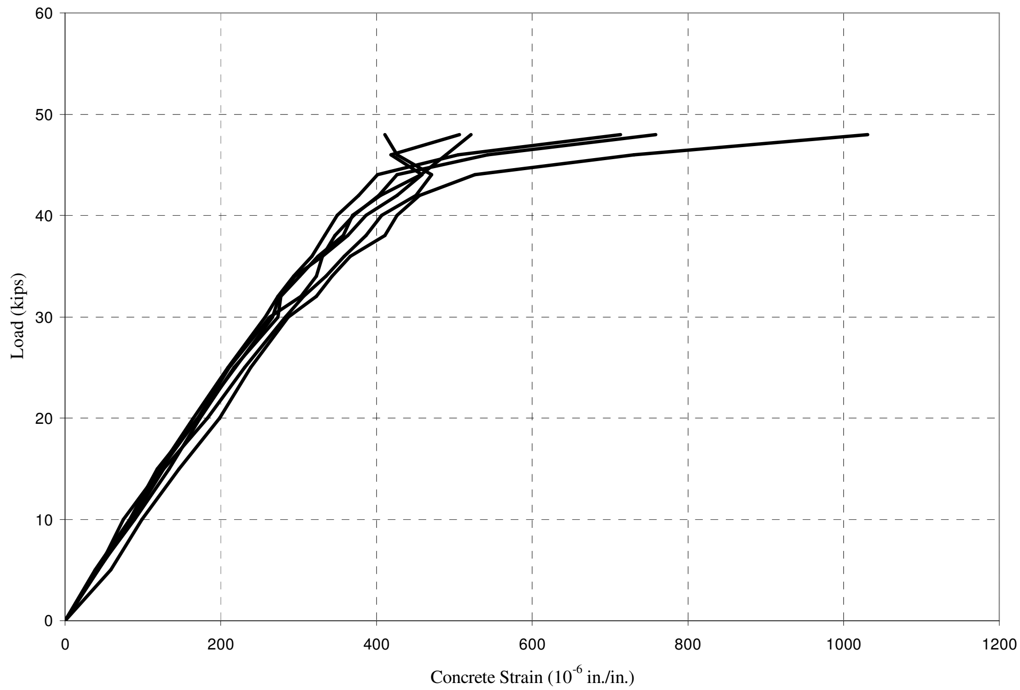

Figure E.39 Crack Initiation for 4.270.5S.RA

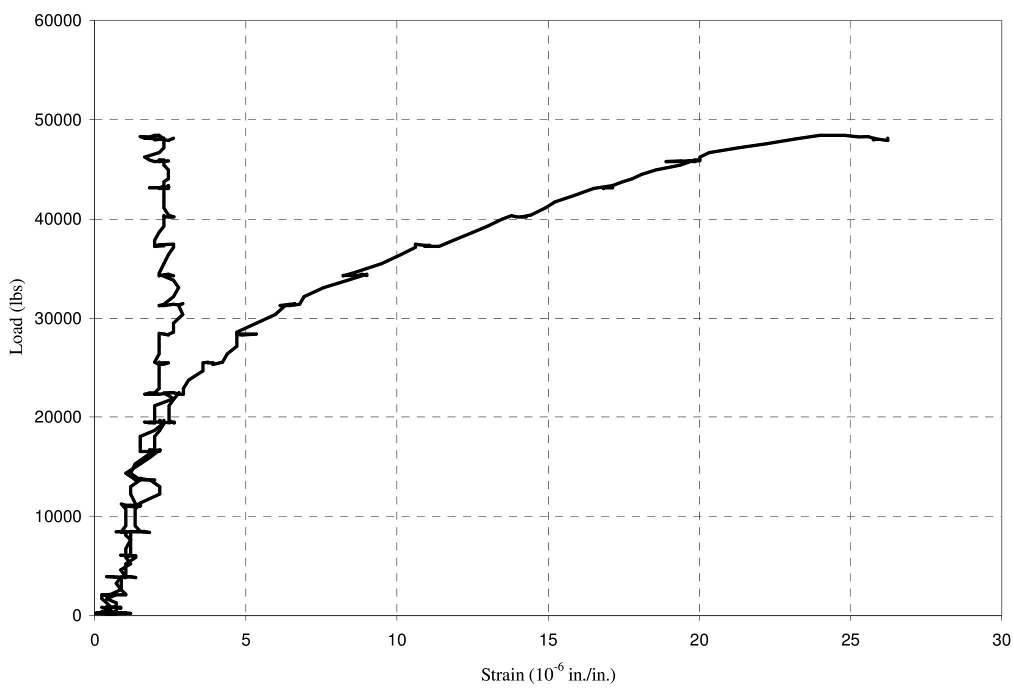

Figure E.40 Crack Reopening for 4.270.5S.RA

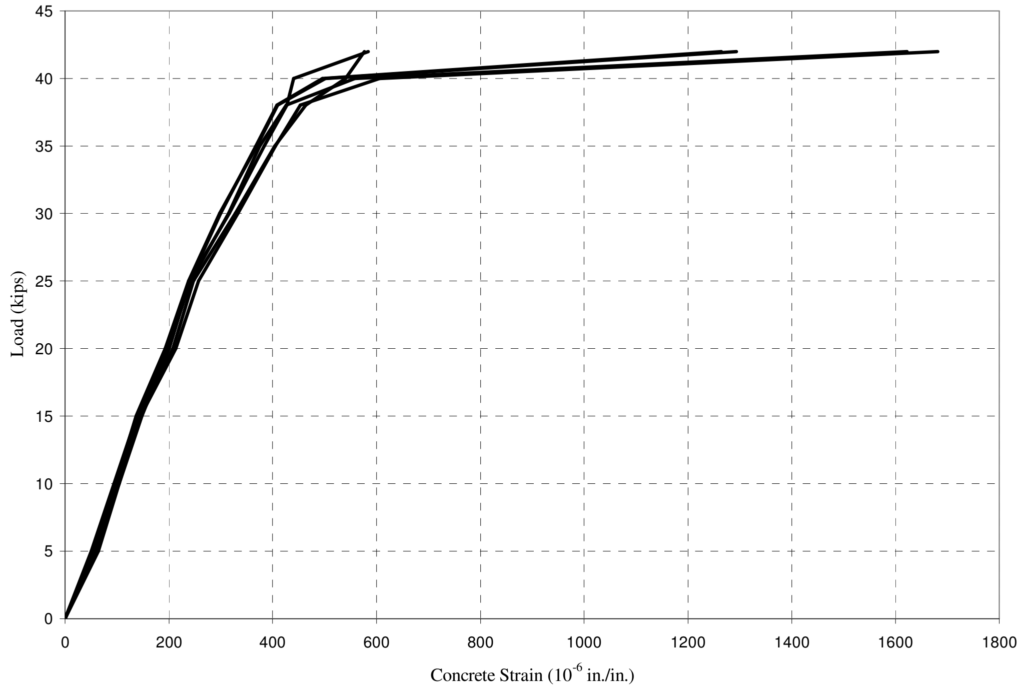

Figure E.41 Crack Initiation for 4.270.5S.RB

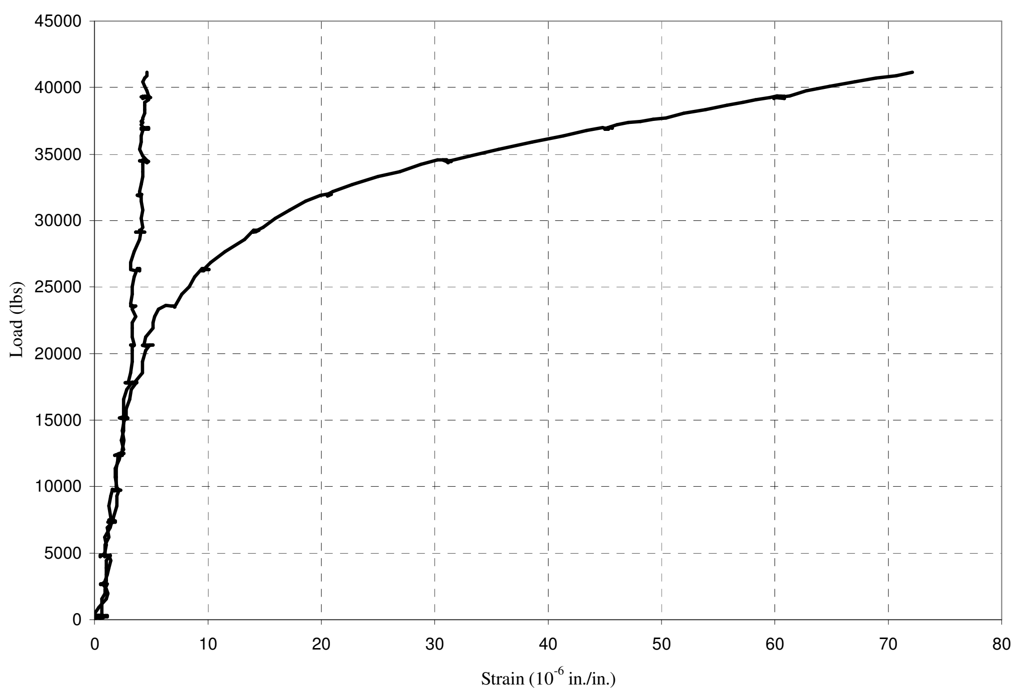

Figure E.42 Crack Reopening for 4.270.5S.RB

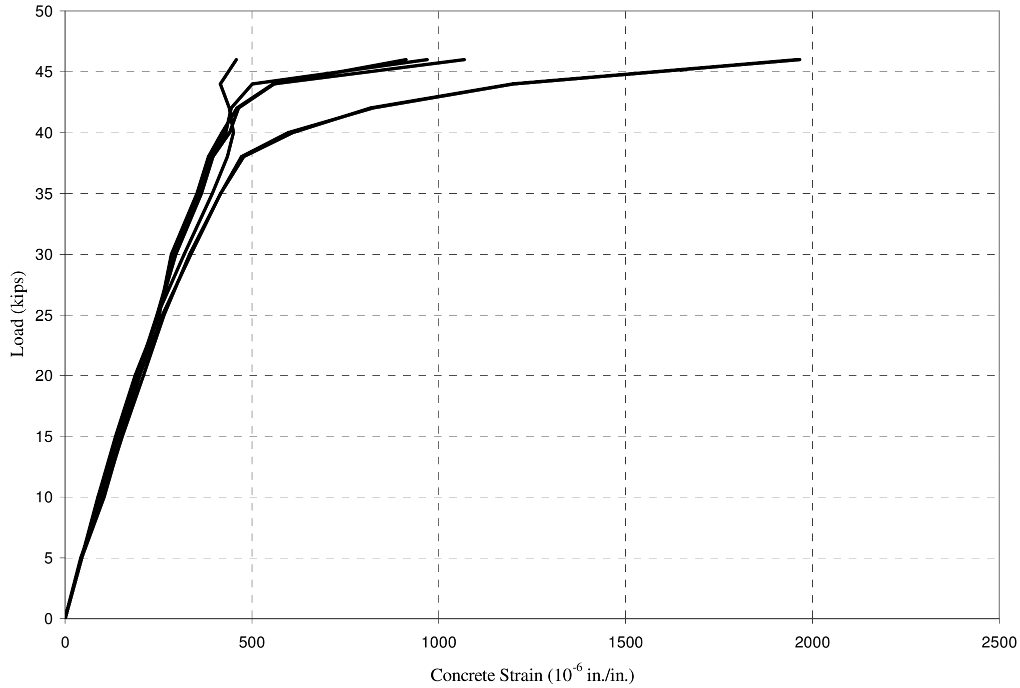

Figure E.43 Crack Initiation for 4.300.5S.RA

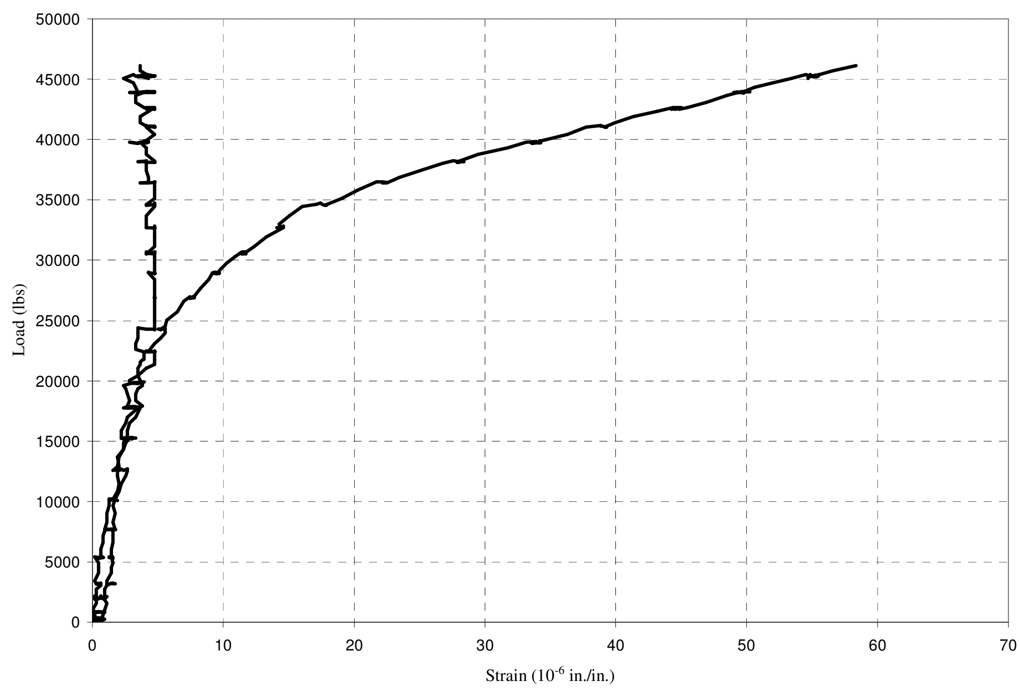

Figure E.44 Crack Reopening for 4.300.5S.RA

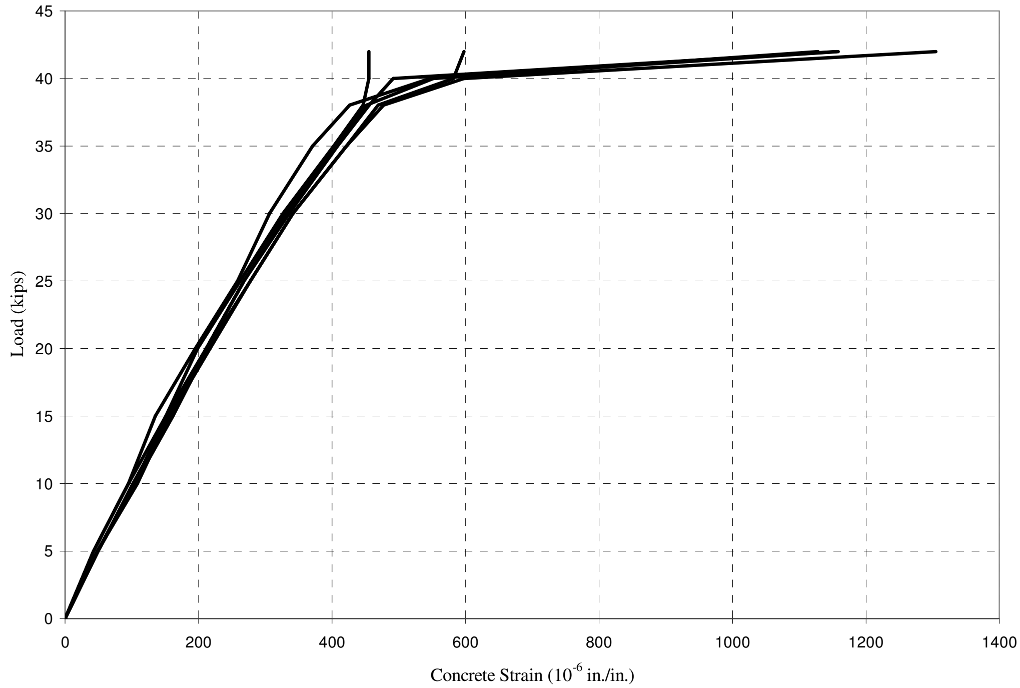

Figure E.45 Crack Initiation for 4.300.5S.RB

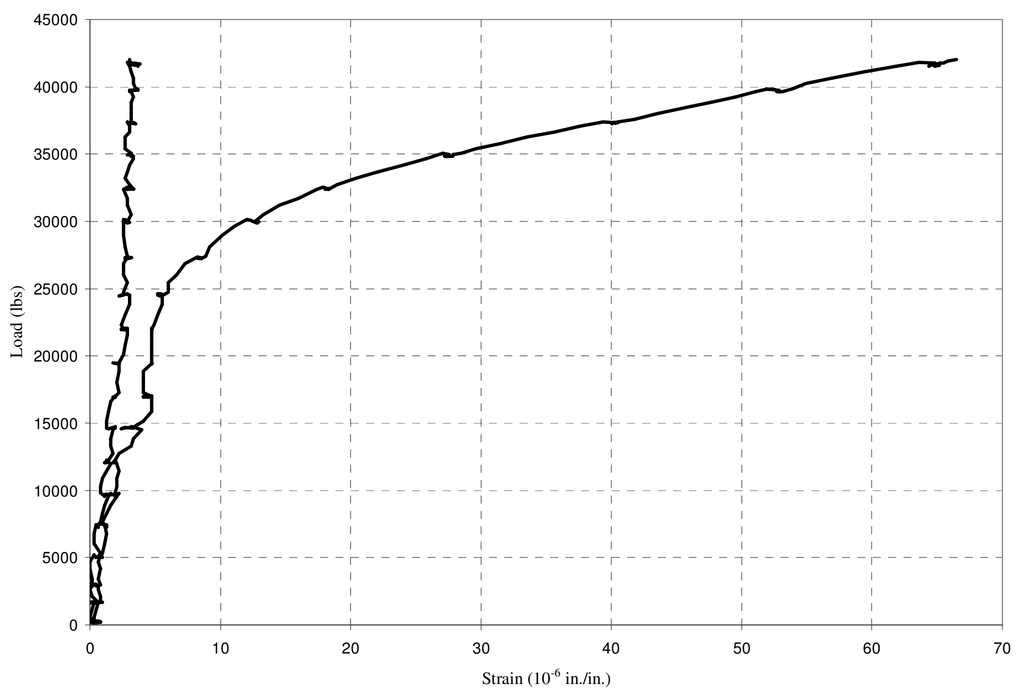

Figure E.46 Crack Reopening for 4.300.5S.RB